National Library of Canada
Acquisitions and Bibliographic Services Branch
395 Wellington Street
Ottawa, Ontario
K1A 0N4

Bibliothèque nationale du Canada
Direction des acquisitions et des services bibliographiques
395, rue Wellington
Ottawa (Ontario)
K1A 0N4

Your file Votre référence

Our file Notre référence

NOTICE

The quality of this microform is heavily dependent upon the quality of the original thesis submitted for microfilming. Every effort has been made to ensure the highest quality of reproduction possible.

If pages are missing, contact the university which granted the degree.

Some pages may have indistinct print especially if the original pages were typed with a poor typewriter ribbon or if the university sent us an inferior photocopy.

AVIS

La qualité de cette microforme dépend grandement de la qualité de la thèse soumise au microfilmage. Nous avons tout fait pour assurer une qualité supérieure de reproduction.

S'il manque des pages, veuillez communiquer avec l'université qui a conféré le grade.

La qualité d'impression de certaines pages peut laisser à désirer, surtout si les pages originales ont été dactylographiées à l'aide d'un ruban usé ou si l'université nous a fait parvenir une photocopie de qualité inférieure.

Canada

A Study of Vibration Response Characteristics of the Human Hand-Arm System

Raghu Gurram

A Thesis

in

The Department

of

Mechanical Engineering

Presented in Partial Fulfillment of the Requirements
for the Degree of Doctor of Philosophy at
Concordia University
Montreal, Quebec, Canada

September 1993

ISBN 0-315-97636-5

Name RAGHU GURRAM

Dissertation Abstracts International is arranged by broad, general subject categories. Please select the one subject which most nearly describes the content of your dissertation. Enter the corresponding four-digit code in the spaces provided.

Mechanical Engineering.
SUBJECT TERM

0548
SUBJECT CODE

U·M·I

Subject Categories

THE HUMANITIES AND SOCIAL SCIENCES

COMMUNICATIONS AND THE ARTS
Architecture 0729
Art History 0377
Cinema 0900
Dance 0378
Fine Arts 0357
Information Science 0723
Journalism 0391
Library Science 0399
Mass Communications 0708
Music 0413
Speech Communication 0459
Theater 0465

EDUCATION
General 0515
Administration 0514
Adult and Continuing 0516
Agricultural 0517
Art 0273
Bilingual and Multicultural 0282
Business 0688
Community College 0275
Curriculum and Instruction 0727
Early Childhood 0518
Elementary 0524
Finance 0277
Guidance and Counseling 0519
Health 0680
Higher 0745
History of 0520
Home Economics 0278
Industrial 0521
Language and Literature 0279
Mathematics 0280
Music 0522
Philosophy of 0998
Physical 0523
Psychology 0525
Reading 0535
Religious 0527
Sciences 0714
Secondary 0533
Social Sciences 0534
Sociology of 0340
Special 0529
Teacher Training 0530
Technology 0710
Tests and Measurements 0288
Vocational 0747

LANGUAGE, LITERATURE AND LINGUISTICS
Language
- General 0679
- Ancient 0289
- Linguistics 0290
- Modern 0291

Literature
- General 0401
- Classical 0294
- Comparative 0295
- Medieval 0297
- Modern 0298
- African 0316
- American 0591
- Asian 0305
- Canadian (English) 0352
- Canadian (French) 0355
- English 0593
- Germanic 0311
- Latin American 0312
- Middle Eastern 0315
- Romance 0313
- Slavic and East European 0314

PHILOSOPHY, RELIGION AND THEOLOGY
Philosophy 0422
Religion
- General 0318
- Biblical Studies 0321
- Clergy 0319
- History of 0320
- Philosophy of 0322

Theology 0469

SOCIAL SCIENCES
American Studies 0323
Anthropology
- Archaeology 0324
- Cultural 0326
- Physical 0327

Business Administration
- General 0310
- Accounting 0272
- Banking 0770
- Management 0454
- Marketing 0338

Canadian Studies 0385
Economics
- General 0501
- Agricultural 0503
- Commerce-Business 0505
- Finance 0508
- History 0509
- Labor 0510
- Theory 0511

Folklore 0358
Geography 0366
Gerontology 0351
History
- General 0578
- Ancient 0579
- Medieval 0581
- Modern 0582
- Black 0328
- African 0331
- Asia, Australia and Oceania 0332
- Canadian 0334
- European 0335
- Latin American 0336
- Middle Eastern 0333
- United States 0337

History of Science 0585
Law 0398
Political Science
- General 0615
- International Law and Relations 0616
- Public Administration 0617

Recreation 0814
Social Work 0452
Sociology
- General 0626
- Criminology and Penology 0627
- Demography 0938
- Ethnic and Racial Studies 0631
- Individual and Family Studies 0628
- Industrial and Labor Relations 0629
- Public and Social Welfare 0630
- Social Structure and Development 0700
- Theory and Methods 0344

Transportation 0709
Urban and Regional Planning 0999
Women's Studies 0453

THE SCIENCES AND ENGINEERING

BIOLOGICAL SCIENCES
Agriculture
- General 0473
- Agronomy 0285
- Animal Culture and Nutrition 0475
- Animal Pathology 0476
- Food Science and Technology 0359
- Forestry and Wildlife 0478
- Plant Culture 0479
- Plant Pathology 0480
- Plant Physiology 0817
- Range Management 0777
- Wood Technology 0746

Biology
- General 0306
- Anatomy 0287
- Biostatistics 0308
- Botany 0309
- Cell 0379
- Ecology 0329
- Entomology 0353
- Genetics 0369
- Limnology 0793
- Microbiology 0410
- Molecular 0307
- Neuroscience 0317
- Oceanography 0416
- Physiology 0433
- Radiation 0821
- Veterinary Science 0778
- Zoology 0472

Biophysics
- General 0786
- Medical 0760

EARTH SCIENCES
Biogeochemistry 0425
Geochemistry 0996
Geodesy 0370
Geology 0372
Geophysics 0373
Hydrology 0388
Mineralogy 0411
Paleobotany 0345
Paleoecology 0426
Paleontology 0418
Paleozoology 0985
Palynology 0427
Physical Geography 0368
Physical Oceanography 0415

HEALTH AND ENVIRONMENTAL SCIENCES
Environmental Sciences 0768
Health Sciences
- General 0566
- Audiology 0300
- Chemotherapy 0992
- Dentistry 0567
- Education 0350
- Hospital Management 0769
- Human Development 0758
- Immunology 0982
- Medicine and Surgery 0564
- Mental Health 0347
- Nursing 0569
- Nutrition 0570
- Obstetrics and Gynecology 0380
- Occupational Health and Therapy 0354
- Ophthalmology 0381
- Pathology 0571
- Pharmacology 0419
- Pharmacy 0572
- Physical Therapy 0382
- Public Health 0573
- Radiology 0574
- Recreation 0575
- Speech Pathology 0460
- Toxicology 0383

Home Economics 0386

PHYSICAL SCIENCES
Pure Sciences
Chemistry
- General 0485
- Agricultural 0749
- Analytical 0486
- Biochemistry 0487
- Inorganic 0488
- Nuclear 0738
- Organic 0490
- Pharmaceutical 0491
- Physical 0494
- Polymer 0495
- Radiation 0754

Mathematics 0405
Physics
- General 0605
- Acoustics 0986
- Astronomy and Astrophysics 0606
- Atmospheric Science 0608
- Atomic 0748
- Electronics and Electricity 0607
- Elementary Particles and High Energy 0798
- Fluid and Plasma 0759
- Molecular 0609
- Nuclear 0610
- Optics 0752
- Radiation 0756
- Solid State 0611

Statistics 0463

Applied Sciences
Applied Mechanics 0346
Computer Science 0984
Engineering
- General 0537
- Aerospace 0538
- Agricultural 0539
- Automotive 0540
- Biomedical 0541
- Chemical 0542
- Civil 0543
- Electronics and Electrical 0544
- Heat and Thermodynamics 0348
- Hydraulic 0545
- Industrial 0546
- Marine 0547
- Materials Science 0794
- Mechanical 0548
- Metallurgy 0743
- Mining 0551
- Nuclear 0552
- Packaging 0549
- Petroleum 0765
- Sanitary and Municipal 0554
- System Science 0790

Geotechnology 0428
Operations Research 0796
Plastics Technology 0795
Textile Technology 0994

PSYCHOLOGY
General 0621
Behavioral 0384
Clinical 0622
Developmental 0620
Experimental 0623
Industrial 0624
Personality 0625
Physiological 0989
Psychobiology 0349
Psychometrics 0632
Social 0451

ABSTRACT

A study of Vibration Response Characteristics of the Human Hand-Arm System

Raghu Gurram, Ph.D.
Concordia University, 1993

Prolonged exposure to vibration transmitted to the operators of hand-held power tools has been related to symptoms of vibration white finger (VWF) disease, also known as "Raynaud's Phenomenon of Occupational Origin". Many subjective and objective epidemiological, and clinical studies have established the prevalence rates and vibration related symptoms, such as VWF disease, loss of muscle strength, injuries to bones and joints, and disorders of central nervous system. The mechanism leading to these disorders, however, remains almost unknown. The biodynamic response characteristics of the hand-arm system, subject to handle vibration are investigated through: (i) measurement and synthesis of driving point mechanical impedance; (ii) study of hand-grip pressure distribution to gain an insight to a probable mechanism leading to VWF disease; (iii) study of electromyography of finger flexor muscles to enhance an understanding of the vibration induced loss of muscle and grip strength; and (iv) study of vibration transmissibility of the hand-arm system and the protection offered by so-called "anti-vibration" gloves.

The biodynamic response of the hand-arm system is investigated for sinusoidal as well as stochastic excitations in the three orthogonal directions of vibration. Linear and nonlinear analytical models with constant and grip force dependent parameters are developed to characterize the dynamic response of the hand-arm system. A comparison of the model response to the measured data revealed that the nonlinear analytical models with grip force dependent

parameters can accurately predict the hand-arm vibration response for different hand-grip forces over a wide frequency range of tool vibration. Further, the measured data reported in the literature are synthesized to propose a range of idealized values of driving point impedance in all the three directions of vibration.

The hand response to impinged and transmitted vibration is investigated through measurement and analysis of distribution of dynamic forces at the hand-handle interface, and electrical activity of the finger flexor muscles. A sensing grid comprising of flexible pressure sensors was fabricated to measure the interface pressure under static and dynamic conditions. The pressure distribution is related to impaired blood flow, and thus to the probable mechanism leading to the onset of VWF disease. The primary injury mechanisms are further investigated using electromyography (EMG) of the finger flexor muscles, the muscle group responsible for exerting the grip force on the handle. Analysis of the results showed that EMG of muscle group under vibration is as high as 6 times the EMG measured under static grip condition. A methodology is proposed to measure the hand-transmitted vibration and to assess the performance of the anti-vibration gloves. Analytical models are developed to characterize the vibration transmissibility of the hand-arm and the protective gloves. The study concluded that anti-vibration gloves attenuate vibration only in a limited frequency band.

ACKNOWLEDGMENTS

I would like to thank my thesis supervisors Dr. Subhash Rakheja and Dr. Gerard J. Gouw for their support and guidance during all the stages of this thesis dissertation.

I wish to thank Dr. S. Ma, Dr. A.J. Brammer and Mr. P. E. Boileau for their contributions at different stages of the research work.

I also want to thank my colleagues and fellow students who participated as subjects and contributed to this effort. I especially want to acknowledge Dale Rathwell, Danius Juras, Ron Rehel, Manuel Afonso, Danny Prairie and Roger Clement for helping conduct laboratory experiments, and Alain Piché for providing computer assistance.

The Financial support provided by the Institut de recherche en santé et en sécurité du travail du Québec (IRSST) in form of *Bourse Thématique de Mérite Exceptionel en Ingénierie* is gratefully acknowledged.

Finally, I wish to thank my wife, Padmaja, for her constant motivation, patience, understanding and many sacrifices. I dedicate this thesis to her.

TABLE OF CONTENTS

CHAPTER 2
BIODYNAMIC RESPONSE OF THE HAND-ARM SYSTEM

CHAPTER 3
DEVELOPMENT OF ANALYTICAL HAND-ARM VIBRATION MODELS

CHAPTER 4
DRIVING-POINT MECHANICAL IMPEDANCE OF THE HUMAN HAND-ARM SYSTEM: SYNTHESIS AND MODEL DEVELOPMENT

CHAPTER 5
HAND GRIP PRESSURE DISTRIBUTION UNDER STATIC AND DYNAMIC LOADS

CHAPTER 6
RESPONSE OF FINGER FLEXOR MUSCLES TO HAND TRANSMITTED VIBRATION

CHAPTER 7
VIBRATION TRANSMISSIBILITY CHARACTERISTICS OF THE HAND-ARM AND GLOVES

CHAPTER 8
CONCLUSIONS AND RECOMMENDATIONS FOR FUTURE WORK

LIST OF FIGURES

LIST OF TABLES

LIST OF ABBREVIATIONS

ANOVA	Analysis of variance
c, c_i	Damping coefficient
c_{0i}, c_{1i}, c_{2i}	Nonlinear damping coefficients
C_i^e	Equivalent damping constant
DOF	Degrees-of-freedom
EMG	Electromyogram
f	Frequency
F	F-ratio
F_g	Grip force
F_{Di}	Dissipative forces
F_{Ki}	Restoring forces
F_{Oi}	Excitation forces
G_{FV}	Cross spectral density of force and velocity
G_w	Power spectral density of velocity
GPD	Grip pressure distribution
HAV	Hand-arm vibration
Hz	Hertz
ISO	International Standards Organization
k, k_i, K	Stiffness coefficient
K_{2i}	Cubic spring constant
K_i^e	Equivalent spring constant
kg	Kilogram
kPa	kilo Pascal
m	Meter

mm	Millimeter
m_i	Mass
mV	Millivolt
MVC	Maximum voluntary contraction
n	A counter
N	Newton
P	Excitation force
rms	Root Mean Square
s	Second
TR	Transmissibility ratio
$U(\bar{\chi})$	Objective function
VWF	Vibration white finger
x	Displacement response
X_h	Direction of vibration
Y_h	Direction of vibration
z	Relative displacement
$\|z\|$	Magnitude of Impedance
Z_h	Direction of vibration
ø	Impedance phase angle in degrees
σ	Standard deviation
p	Probability of error
ε	Random error
ω	Circular frequency
α	A constant

CHAPTER 1

INTRODUCTION AND SCOPE OF THE THESIS RESEARCH

1.1 General

Raynaud's phenomenon, named after Maurice Raynaud, may be defined as an episodic spasm or intermittent constriction of peripheral vessels of an extremity that results in change of color of skin. Raynaud's phenomenon or blanching of the digits is commonly precipitated by exposure to cold, and it may occur in association with several other factors and diseases. Vibration as a cause of Raynaud's phenomena was first reported in the literature in 1911 and 1920.

Operators of hand-held power tools, such as chain saws, grinders, chisels, and drills, are exposed to comprehensive levels of vibration arising from the tool - workpiece interactions. These high amplitude vibrations predominate in a wide frequency range, 10 - 2000 Hz, and are often limited to the hand-arm of the operators. Prolonged exposure to such vibration has been related to several occupational health disorders, specifically tingling, numbness, and blanching of fingers. The close association between white finger attacks and the vibration entering the hands was responsible for the introduction of the term "*Vibration Induced White Finger*" (VWF), which is also known as "*Traumatic Vasospastic Disease*" (TVD). The VWF disease is also known as "Raynaud's Phenomenon of Occupational Origin" in order to separate it from the similar symptoms due to non-occupational reasons. The complex of VWF and associated pathology is now termed as the vibration syndrome or, more

precisely, the hand-arm vibration syndrome, to distinguish it from the disorders caused by occupational exposure to the whole body vibration.

The symptoms of hand-arm vibration (HAV) syndrome develop in a gradual manner, and may involve a number of years of occupational exposure to hand transmitted vibration. The most serious among the diseases caused by prolonged exposure to hand-transmitted vibration is perhaps the vibration white finger (VWF) disease. The first symptoms of VWF disease are related to intermittent tingling and numbness of the fingers. With continued exposure, the tingling is followed by an attack of finger blanching confined, in the first instance, to a finger tip, which subsequently propagates to the base of the finger. While cold acts as the provocative agent, factors such as central body temperature, metabolic rate and emotional state, etc. are also involved. An attack usually lasts 15 - 60 minutes but in advanced cases it may extend from 1 to 2 hours. The recovery phase is signaled by the appearance of a red flush, usually seen in the palm. With further vibration exposure nutritional changes take place in the finger pulps leading to the formation of small areas of skin necrosis at the finger tips.

In view of the severity of the hand-arm vibration diseases, caused by prolonged exposure to hand-held power tool vibration, numerous efforts have been mounted to study the hand-arm vibration syndrome. These studies have been directed towards enhancing an understanding of the bio-dynamic response of the hand-arm, hand-arm syndrome etiology, dose-response standards, and to develop methods to control transmission of vibration to the hand.

In this chapter the relevant literature on epidemiological studies, studies on symptoms and effects of prolonged exposure to hand-arm vibration, and studies on characterization of hand-transmitted vibration are briefly reviewed, to formulate the scope of the dissertation research.

1.2 Symptoms and Effects of Prolonged Exposure to Hand-transmitted Vibration

Effects of occupational exposure to hand-transmitted vibration have been the focus of many epidemiological and clinical investigations (*Wasserman et al., 1977; Brammer et al., 1982*). The symptoms and effects of prolonged exposure to hand-transmitted vibration may be grouped as:

(i) Neural and vascular effects

(ii) Muscular effects

(iii) Bone and joint effects and

(iv) Effects on Central Nervous System (CNS).

The above mentioned effects are known to decrease the performance and productivity of the workers, and often the effected workers are forced to change occupation.

1.2.1 PERIPHERAL NEURAL AND VASCULAR EFFECTS

Workers using hand-held vibration tools frequently experience numbness and pain in the arms and hands. Such symptoms have been related to cause disturbances to the operator's sleep rhythm (*Pyykkö, 1975*). The earliest signs of peripheral vascular changes in the hand-arm system have been reported as the attacks of finger tip blanching. These initial attacks usually occur during exposure to cold (*Pyykkö, 1986; Taylor et al., 1982*), and the frequency and severity of episodes of white finger increase with continued exposure to

vibration. The developmental process whereby the digital vessels become sensitive to a cold stimulus is not entirely clear, and several hypotheses have been proposed (*Pelmear et al., 1992*). Subsequently, with progression of disease, the attacks of finger blanching may occur even in the warm weather. During VWF attacks, blood flow to the affected segments of the fingers is reduced or completely shut off by contraction of the muscles, resulting in severe pain (*Pyykkö, 1975*). The symptoms and signs are reported to be in response to pathological and physiological changes in the tissues of the fingers (*Pelmear et al., 1992*)

1.2.2 MUSCLE FORCE AND MUSCLE FATIGUE

The effects of hand-transmitted vibration on various muscles have been investigated using subjective and objective studies. The subjective complaints of deterioration of hand grip force and muscle strength in workers using vibrating tools have been mentioned in many of the studies. However, objective tests utilized measurement techniques to assess grip strength, pinch power and tapping ability. The response of biceps brachii, triceps brachii and flexor muscles to vibration excitation have been extensively investigated using electromyography (EMG) to assess the muscle fatigue (*Dupuis et al., 1979, 86*). *Teleky* (*1938*) reported degeneration in muscle tissue in the hand of workers using vibratory tools. *Banister et al.* (*1972*) and *Färkkilä* (*1980*) showed that the use of vibratory tools causes significant decrease in manipulative skill and grip strength. *Taylor et al.* (*1975*) reported that repeated ischemic attacks in advanced cases, lead to impairment of temperature sensation. Further symptoms such as inability to do fine work have been observed among the operators of vibrating tools. Among Japanese chain saw operators with more than 2,000 hours of chain saw use, about 28 % reported symptoms of decreased

grip force and muscle strength (*Miyashita et al., 1983*). Similar symptoms were reported by 20 % of Finnish chain saw workers with more than 5,000 hours of chain saw use (*Färkkilä et al., 1982*). The pathophysiologic mechanisms involved in the reduced muscle strength are, yet again, not clear.

1.2.3 BONES AND JOINTS

Injuries to bones, such as cysts, vacuoles, decalcification have been related to exposure to hand-transmitted vibration. In a radiographic study conducted on 35 lumberjacks, *Kumlin et al.* (*1973*) have found cysts and vacuoles in 20% of lumberjacks in the metacarpal bones or phalanges or both. In a similar study on 165 lumberjacks *James et al.* (*1975*) have reported bone cysts and related injuries among 44 % of workers using vibrating tools. *Bovenzi et al. (1980*) conducted a study of several Italian shipyard workers operating vibratory tools to investigate the prevalence of bone injuries. The study reported that about 31% of 169 caulkers who worked with vibrating tools were reported to have bone cysts or vacuoles. *Gemne et al.* (*1987*) have conducted an extensive literature evaluation of the radiological documentation of bone and joint pathology in the hands and arms of power tool workers. They concluded that hand-arm vibration causes an excessive prevalence of bone cysts and vacuoles.

1 2.4 CENTRAL NERVOUS SYSTEM (CNS)

Although the vibration syndrome has been characterized by vascular and peripheral nervous symptoms, evidences of nervous disorders, indicating involvement of central nervous system, among the operators of vibrating tools have also been reported (*Klimkova, 1966*). *Griffin* (*1980*) concluded that hand-arm vibration can impair CNS function through damage to the autonomic centers in the brain. The symptomatology alleged to be associated with vibration induced

disturbances of the central nervous system includes anxiety, depression, headache, palm sweating, irritability and emotional instability (*Habu, 1984*). In view of the subjective nature of the study, however, these signs and symptoms were not specific to a single stressor such as vibration.

1.3 Vibration White Finger

The time between the first use of vibrating tools and the first appearance of episodic finger blanching is designated as the latent period. The latent period appears to vary from less than 1 year to many years depending upon various factors such as intensity of vibration, duration of exposure, hand grip force, push-pull force, hand-arm posture and protective gear. Based on clinical observation and subjective surveys, *Taylor et al.* (1968) have proposed a grading system to monitor and express clinically the severity of VWF. Based upon clinical observations and subjective evaluations the VWF symptoms were classified in six different stages, as illustrated in Table 1.1. Of the various stages of VWF indicated, stages 2, 3 and 4 were related to interference with work and social activities. Subjects with symptoms in these stages are usually advised to change their occupation. The Taylor-Pelmear grading system, however, did not address the neurological disorders associated with different stages of VWF symptoms (*Pelmear et al., 1992*). Therefore, a need for reclassification was recognized based on the concept that the peripheral neural and vascular involvements in the hand-arm system may be distinct and that the disabilities related to one may progress independently of the other (*Brammer et al., 1987a*). Subsequently, a group of researchers at a workshop in Stockholm, Sweden, in 1986 have proposed an alternate staging system for the vascular and sensorineural effects (*Brammer et al., 1987b; Gemne et al., 1987; Pelmear et al., 1992*). Tables 1.2 and 1.3 illustrate the scales for classification of cold-

induced Raynaud's Phenomenon and the sensorineural effects of the hand-arm vibration (HAV) syndrome, respectively.

TABLE 1.1
Stages of Vibration Induced White Finger (*Taylor and Pelmear, 1975*)

VWF Stage	Conditions of digits	Interferences with Work and Social Activities
0	No blanching of digits	No complaints
0T	Intermittent tingling	No interference with activities
0N	Intermittent numbness	No interference with activities
1	Blanching of one or more fingertips with or without tingling and numbness	No interference with activities
2	Blanching of one or more fingertips with numbness, usually occurring during winter	Slight interference with domestic and social activities
3	Extensive blanching. Frequent episodes in summer as well as winter	Definite interference at work, at home and with social activities. Restrictions on hobbies
4	Extensive blanching of most fingers	Occupation changed to avoid further vibration exposure because of severity of signs and symptoms

1.3.1 PROPOSED MECHANISM LEADING TO VIBRATION WHITE FINGER

Although many studies have clearly identified the nature of symptoms characterizing the hand-arm vibration syndrome, these studies have provided very little in sight to the syndrome etiology. In vibration induced white finger, the

TABLE 1.2
Scales for Classification of cold-induced Raynaud's Phenomenon associated with HAV Syndrome (Gemne et al., 1987)

Stage	Grade	Description
0		No attacks
1	Mild	Occasional attacks affecting only the tips of one or more fingers
2	Moderate	Occasional attacks affecting distal and middle phalanges of one or more fingers
3	Severe	Frequent attacks affecting all phlanges of most fingers
4	Very Severe	As in stage 3, with trophic skin changes in finger tips

TABLE 1.3
Scales for classification of sensorineural affects of HAV syndrome (Brammer et al., 1987b)

Stage	Symptom
0SN	Exposed to vibration but no symptoms
1SN	Intermittent numbness, with or without tingling
2SN	Intermittent or persistent numbness; reduced sensory perception
3SN	Intermittent or persistent numbness; reduced tactile, perception and/or manipulative dexterity

vibration has been identified as the etiological factor, and cold is the provocative factor (*Agate et al., 1946*). After a period of latency, the blood vessels begin to respond more intensively to external stimuli like cold (Pyykkö, 1974). Through the sympathetic nervous system, cold causes the vasoconstriction in the vessels of the arm and the hand. The blood flow then decreases considerably, far below the normal levels, due to hypertrophy in the vessel walls (*Folkow , 1972*) and at a point the intraluminal pressure falls below that of the critical closing pressure of the vessel (*Roddie et al., 1957*). An attack of VWF may thus occur due to the resulting collapse of the finger vessels. The mechanism causing hypertrophy of the vessel wall is, however, still unknown.

1.4 Epidemiological Studies

Numerous epidemiological studies have been carried out in several countries to identify the population of workers affected by occupation exposure to vibration and to assess the impact of the workplace vibration environment. An extensive study conducted in the U.S. estimated that of 8 million vibration exposed workers approximately 7 million are exposed to whole body vibration and 1 million are exposed to hand arm vibration (*Wasserman et al., 1974*). In Canada an estimate made by the National Research Council of Canada indicated that approximately 200,000 workers are exposed to hand arm vibration (*Brammer, 1984*). Recent studies conducted in Great Britain also supported the findings of North America, and identified the population of workers exposed to occupational hand-arm vibration (*Bednal, 1987*). The results of the study, presented in Figure 1.1, reveal that approximately 700,000 workers are exposed to occupational hand-arm vibration in different industries in Great Britain. Epidemiological studies of workers using hand-held vibrating tools have been conducted in several countries all over the world. Traditionally cross-sectional

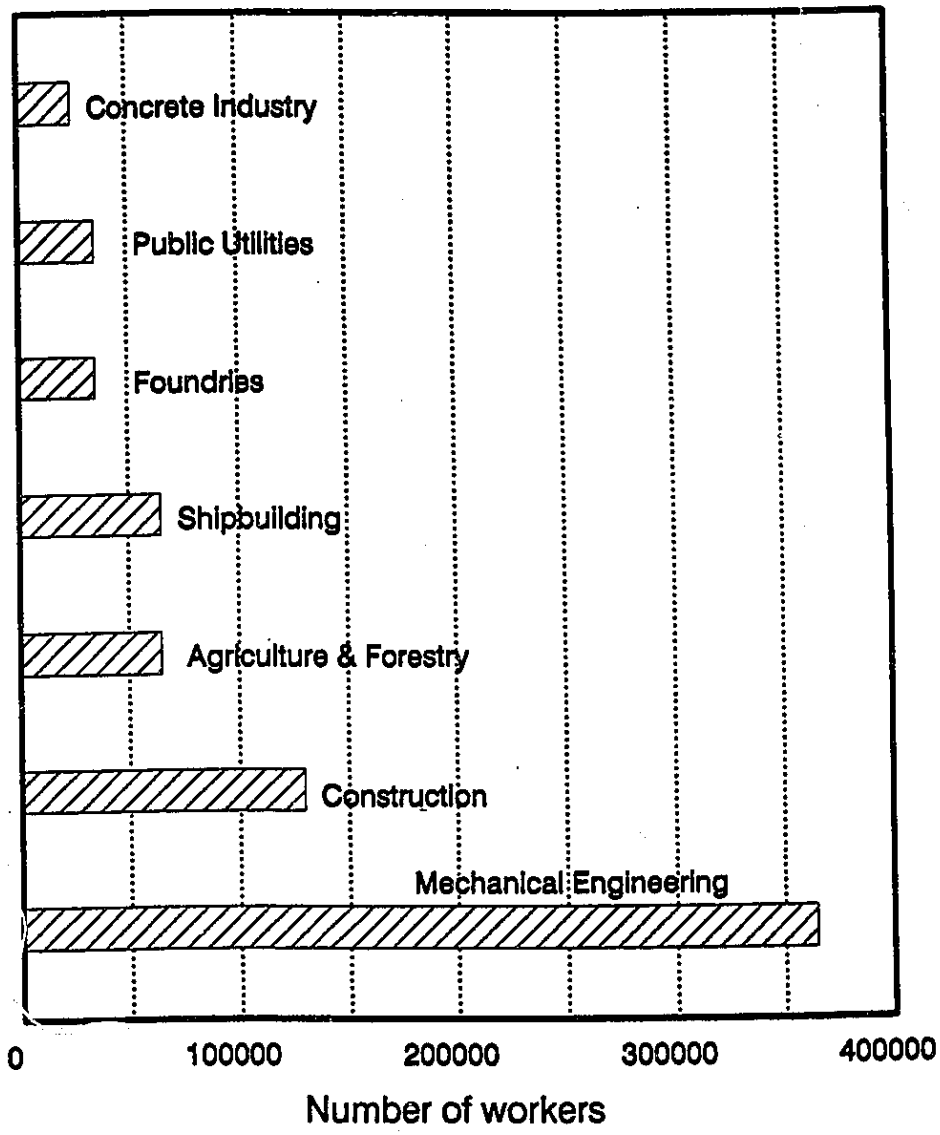

Figure 1.1 Manual workers exposed to hand-arm vibration in Great Britain (*Bednal, 1987*)

and longitudinal epidemiologic studies concentrated on three classes of power tools: (a) pneumatic tools (chippers, grinders, jack-hammers, reveters, drills); (b) electrically operated tools (sanders, pedestal grinders, swagers, impact hammers); and (c) chain saws. Many investigators have performed numerous field measurements to characterize the nature of vibration generated by different hand-held power tools, while in operation. The dominant frequency ranges of different tools are summarized in Table 1.4. The direction of vibration, X_h, Y_h and Z_h, refer to the coordinate system proposed in the International Standard, ISO 5349 (1986). Table 1.5 illustrates the unweighted root mean squared (*rms*) accelerations of the vibration levels measured on different power tools. The results of the studies, summarized in Tables 1.4 and 1.5, reveal that the magnitude of vibration encountered on different tools varies significantly, from 10 m/s^2 weighted to 2,014 m/s^2 unweighted, depending upon the tool, application, speed, feed, location of point of measurement, etc.. The range of dominant frequencies of vibration, however, appears to be clustered in the 40 - 150 Hz range, irrespective of the tool and the operating conditions. While the measured acceleration levels differ considerably for different tools, the magnitude of acceleration is evidently very high irrespective of the type of tool or the operating conditions. All the epidemiological studies reported the prevalence of HAV syndrome among the population of workers exposed to hand-arm vibration, independent of the level and nature of vibration exposure. The prevalence of VWF symptoms among the operators using different tools are illustrated in Table 1.5. The National Institute of Occupational Safety and Health (NIOSH, Ohio), in the U.S., has established a linear relationship between measured acceleration levels and the prevalence of vascular symptoms (*NIOSH, 1989*). While the epidemiologic studies do not provide a relationship between the vibration levels and the occurrence of HAV syndrome among the power tool

operators, these studies provide ample evidence that the use of vibration producing tools is associated with the development of HAV syndrome.

TABLE 1.4.
Frequency Range and Directions of Dominant Vibrations Generated by Different Power Tools

Type of Tool (Reference)	Dominant Frequency (Hz)	Dominant Direction of Vibration*
Heavy duty sander (*Radwin, 1986*)	70-150	X_h, Y_h, Z_h
Orbital sander (*Radwin, 1986*)	60 - 100	X_h, Y_h, Z_h
Vertical polisher (*Radwin, 1986*)	70 - 125	X_h, Y_h, Z_h
Bush cleaner (*Daikoku et al., 1989*)	100 - 150	X_h
Garden tool (*Daikoku et al., 1989*)	63 - 80	X_h
Chain saw (*Reynolds et al., 1982*)	100 - 150	X_h, Y_h, Z_h
Chain saw (*Futatsuka et al., 1985*)	100 - 125	X_h, Y_h, Z_h
Chain saw (*Pelnar et al., 1982*)	63 - 125	X_h, Y_h, Z_h
Chain saw (*Hempstock et al., 1975*)	80 - 125	N/A
Pneumatic hammer(*Hempstock et al.,1975*)	40	N/A
Pneumatic hammer (*Farkkila et al., 1978*)	80	Z_h
Chipping hammer (*Reynolds et al., 1982*)	25 - 125	X_h, Y_h, Z_h
Pedestal grinder (*Hempstock et al., 1975*)	250	N/A
Horizontal grinder (*Reynolds et al., 1982*)	63	X_h, Y_h, Z_h
Vertical grinder (*Reynolds et al., 1982*)	40	X_h, Y_h, Z_h
Motorcycle handle (*Harrison et al., 1982*)	320	X_h
Motorcycle handle (*Harrison et al., 1982*)	125	Y_h, Z_h

* ISO - 5349, 1986; See Figure 1.2

TABLE 1.5
Acceleration Levels Measured on Different Tools and Associated VWF Rates Reported in Different Studies

Tool Type (Reference)	Reported Acceleration Level (m/s^2)*	Prevalence of VWF Symptoms (%)
Chipping hammer (*Taylor et al., 1984*)	2014	80
Riveter (*Oliver et al., 1979*)	1183	75
Chipping hammer (*Taylor et al., 1981*)	424	45
Pedestal grinder (*Agate et al., 1949*)	382	86
Chipping hammer (*Matsumoto, 1981*)	378	64
Jack-leg drill (*Chattergee et al., 1978*)	362	50
Jack-leg drill (*Robert et al., 1977*)	339	70
Jack-leg drill (*Matsumoto et al., 1979*)	335	80
Chipping hammer (*Behrens et al.,1984*)	251	47
Grinder (*Bovenzi et al., 1980*)	205	31
Pavement breaker (*Walker et al., 1985*)	195	10
Pedestal grinder (*Pelmear et al., 1975*)	125	96
Pedestal grinder (*Starck et al., 1983*)	122	100
Jack-leg drill (*Iwata ,1968*)	121	72
Chain saw (*Matsumoto et al., 1979*)	75	38
Jack-leg drill (*Brubaker et al., 1986*)	20#	45
Hand grinder (*Pelmear et al., 1975*)	20	35
Riveter (*Engström et al., 1986*)	10#	25

* Unweighted acceleration except as mentioned
\# Weighted acceleration as per ISO - 4 hour value

1.5 Factors Affecting the Hand Transmitted Vibration

Results of the field studies summarized in Tables 1.4 and 1.5, clearly illustrate that the characteristics of hand-held power tools vibration are strongly related to the tool and operating factors. *Griffin (1974)* identified a list of extrinsic and intrinsic variables that influence mechanical and subjective response of operators exposed to vibration. The extrinsic variables include grip strength, grip type, duration of exposure, clothing, and frequency, amplitude, and direction of vibration. The intrinsic variables include body size, body posture and muscle tension. *Reynolds et al. (1977)* reported that the influence of extrinsic variables on hand-induced vibration is of major importance compared to that of the intrinsic variables. The determination of total vibration exposure and dosage necessitates quantitative measures of vibration amplitudes entering the hand in a wide frequency range, and hand grip forces, as a function of time in all three directions for well defined body postures. In view of the complexities associated with quantification of all the factors for a sample of tools and workers, a need to identify the important factors that affect severity of exposure in a significant manner has been emphasized (*Taylor and Brammer, 1982*). Table 1.6 summarizes various physical, bio-dynamic and individual factors that influence the hand-transmitted vibration.

1.6 Vibration Exposure Guidelines

High levels of hand-transmitted vibration, high rates of prevalence of VWF symptoms among the exposed workers, and the severe health effects of hand-arm vibration, have all prompted efforts to develop standards to assess the vibration exposure levels. These efforts have achieved only moderate success since the etiology of VWF is not yet fully understood. Certain norms with regard to measurements, evaluations and reporting methods, however, have been

TABLE 1.6
Factors affecting Hand Transmitted Vibration (Taylor and Brammer, 1982)

Physical	Dominant vibration amplitudes entering hand. Dominant vibration frequencies entering hand. Years of employment involving vibration exposure. Total duration of exposure each day. Temporal pattern of exposure each working day. Dominant vibration direction relative to the hand. Non occupational exposure to hand-arm vibrations.
Bio-dynamic	Hand grip forces. Surface area, location and mass of parts of hands in contact with source of vibration. Posture.
Individual	Factors influencing source intensity and exposure duration (e.g. state of tool maintenance, operator control of tool, machine work rate and skill). Hand size and weight.

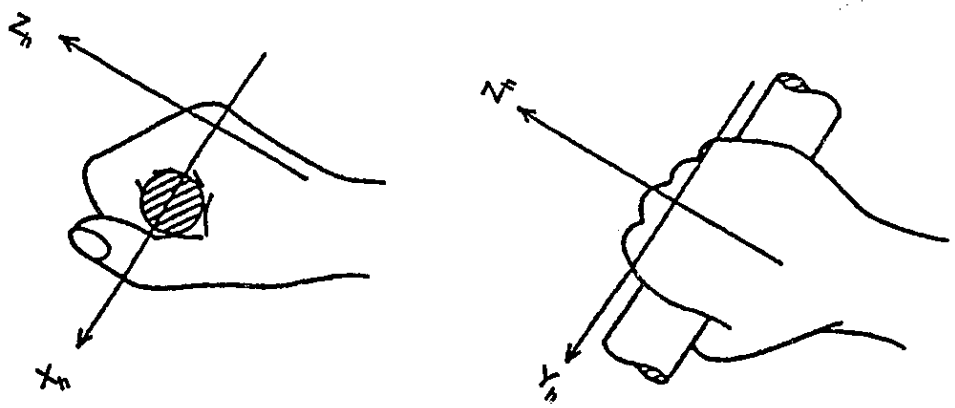

Figure 1.2 Reference coordinate system proposed in *ISO - 5349 (1986)*

established. The dose-response standards attempt to relate the overall vibration acceleration levels, frequency of vibration, and exposure duration to the occurrence of VWF symptoms. The International Standards Organization (ISO) has outlined a reference coordinate system shown in Figure 1.2 to be employed for the measurement and reporting of HAV data (*ISO 5349, 1986*). Various guidelines proposed by different organizations suggest that vibration exposure be expressed in terms of *rms* acceleration in m/s^2 in the 1/3 octave band spectrum with center frequencies of 6.3 Hz. and 1250 Hz. Figure 1.3 illustrates a comparison of threshold limits of *rms* acceleration levels recommended by the British Standards Institute (BSI), American National Standard Institute (ANSI), and American Conference of Government Industrial Hygienists (ACGIH), for different periods of exposure during a work day. Acceleration levels that fall below a recommended curve for a given exposure time are considered to be acceptable. The standards do not specify safe exposure levels in terms of acceleration and exposure duration. However, the standards are intended for providing guidance for protecting a majority of workers from serious impairment due to vibration related diseases. Using the results of several epidemiologic studies, *Brammer (1982, 1986)* proposed a dose-response relationship, as shown in Figure 1.4. The dose response curves describe the percentiles of population that may be expected to develop stage 1 HAV syndrome, as a function of weighted acceleration, and duration of exposure. For example, for 4 hour daily exposure of 20 m/s^2 acceleration it will take 2 years if the worker is in the 20 th percentile (3 years if in 40 th percentile) to reach stage 1. The data presented in Figure 1.4 serve well to initiate proactive measures, such as job rotation, by predicting in advance the occurrence of stage 1 of VWF disease.

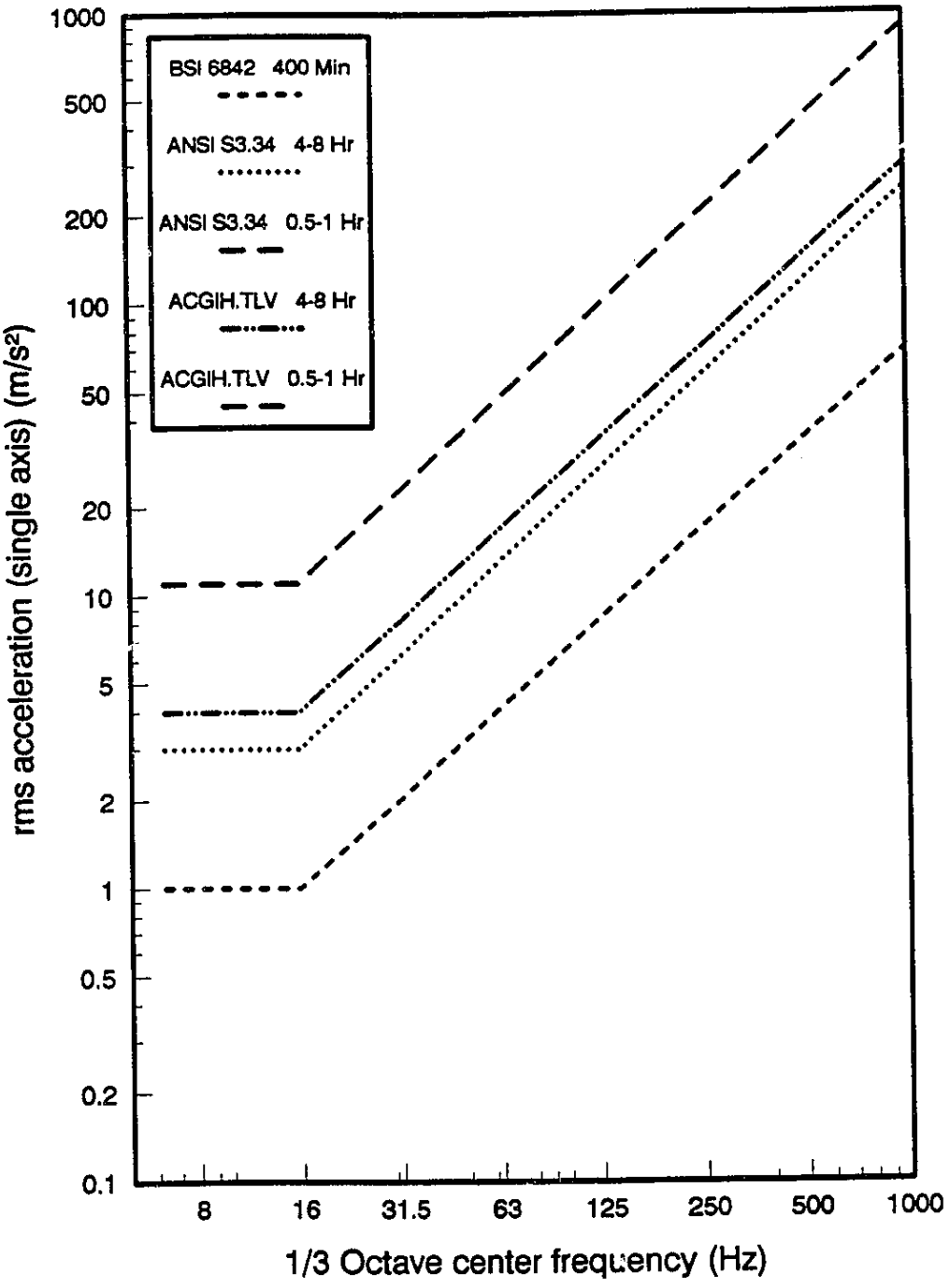

Figure 1.3 Hand-arm vibration standards recommended by different organizations

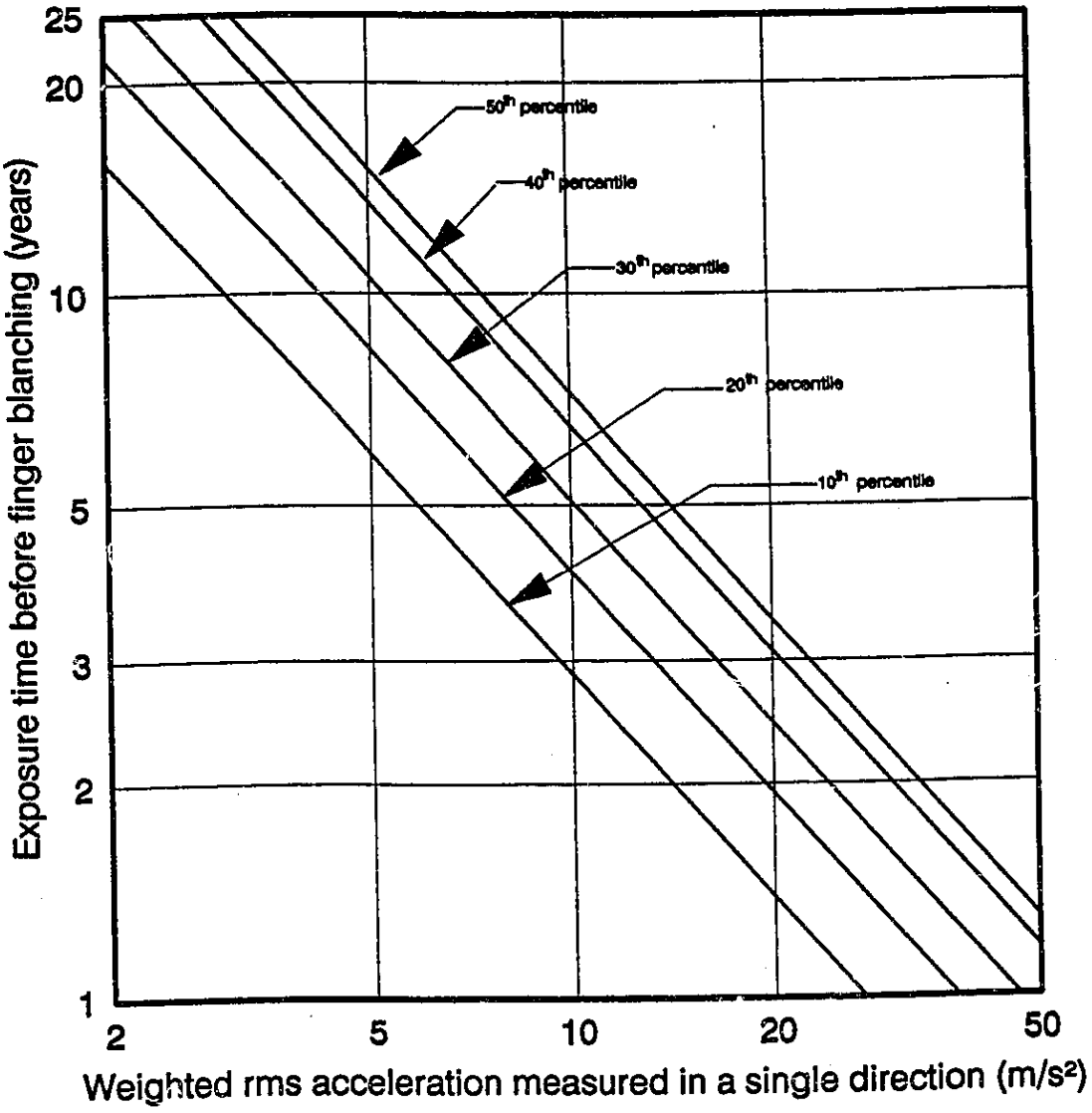

Figure 1.4 Exposure time for different percentiles of a population group exposed to vibration in three coordinate axes (*Brammer, 1986; ISO - 5349, 1986*)

1.7 Scope and Objectives of the Dissertation Research

Many subjective and objective studies have identified several vibration induced diseases among hand-held power tool operators. The workers are affected by vibration white finger (VWF) disease at the finger tips and hands, loss of grip and muscle strength, injuries to bones and joints. Such severe effects of vibration on the operators have prompted several clinical studies to identify the primary injury mechanisms, and engineering studies to design protective devices and vibration isolators.

In the past several decades epidemiologists have conducted extensive longitudinal and cross sectional studies. These studies have provided the vibration syndrome prevalence rates and typical offending tools and their vibration levels. The studies have not yielded the vibration levels that might not cause injuries to the hand-arm system as the syndrome was prevalent in all industries irrespective of levels of vibration generated by the tools used in that industry. Further, several epidemiological studies have reported the onset of VWF disease at the tips of index, middle and ring fingers. However, no investigation has been reported underlying the reasons for the onset of VWF disease at the tips of the fingers. Medical doctors have diagnosed the syndrome and established the means of quick identification of the diseases. However, the mechanism leading to hand-arm vibration syndrome still remains to be solved. A number of studies also indicated that occurrence of the initial stages of VWF may be related to impaired blood flow. Studies on the mechanism causing impaired blood flow, however, have not been reported. Clinical studies have further characterized the response of flexor carpi ulnaris muscles, flexor extensor muscle, biceps and triceps muscles to static and dynamic loads. However, the vibration response and activity of the finger-flexor muscles, a

muscle primarily responsible for exertion of grip force, have not been investigated. The importance of understanding the injury mechanism has been further recognized to identify the means to minimize the occurrence of VWF. The grip pressure distribution at the hand-handle interface would provide considerable insight to the pattern, location and magnitude of local pressures, and may help understand the onset and propagation of vibration white finger disease. Simultaneous investigation of the response of finger flexor muscles under different dynamic loading conditions provide more insight to the muscle dynamics of the hand-arm system.

The engineers have conducted extensive measurements at work places and in laboratories. These studies were only marginally successful due to the complex nature of the hand-arm system and involvement of multitude of factors influencing the transmission of vibration. This stalled progress in development of standardized measurement techniques and reporting methods. An example to this effect is that no standard procedure has been established for evaluation and reporting of vibration isolation performance of anti-vibration gloves. However, the attempts to model the HAV system and to design vibration isolation devices have met with some success. Studies on hand-arm vibration have proposed linear HAV models, based on laboratory measurements of impedance, compliance or accelerance in order to design protective devices and to carry out relative hand-tool vibration transmission analyses. The linear models are considered valid only for a selected set of test conditions, grip force, hand-handle orientation. The non-linear visco-elastic properties of the hand-arm system have been completely ignored. Consequently, the correlation between analytical and experimental results is often very poor. The need to develop accurate models, and models capable of describing hand-arm response for a

range of grip forces, has been identified. The International Standards Organization (*ISO/TC 108*) has recognized these issues and is currently engaged in standardizing the mechanical impedance data. Similarly the ISO and several other scientific bodies all over the world have been attempting to standardize the testing methods for performance evaluation of anti-vibration gloves (*CEN/231/3 N46 1992; ISO/108/4/3 N65 1992*). Various issues discussed above have contributed to some ambiguity and this thesis research attempts to investigate some of these issues unresolved thus far.

1.7.1 OBJECTIVES OF THE DISSERTATION RESEARCH

The primary objective of this dissertation research is to investigate the dynamic response characteristics of the hand-arm system under vibration, and to study the response behavior in relation to occurrence of operator fatigue and VWF. From the literature review, it is apparent that occurrence of VWF and muscle fatigue is related to: (i) characteristics of transmitted vibration; (ii) muscular activities; and (iii) the restrained blood flow in the arteries of the hand. The specific objectives of thesis are thus formulated to investigate these characteristics of the hand-arm system under different operating conditions in an attempt to identify the mechanism leading to the VWF, and to reduce the muscle fatigue and risks of VWF. The specific objectives of the dissertation research are:

(a) Develop a method of measuring the driving point impedance of the hand-arm system using stochastic and sinusoidal excitations.

(b) To investigate the influence of various operating conditions on the dynamic response of the hand-arm system.

(c) To develop linear and nonlinear HAV models and identify the model parameters as a function of the grip force.

(d) To derive idealized values of mechanical impedance of hand-arm system through data synthesis.

(e) To propose a method of measuring grip pressure distribution under static and dynamic loading conditions and identify the location of peak pressures.

(f) To investigate the influence of transmitted vibration on finger flexor muscles through measurement of EMG under static and dynamic loading conditions, and to enhance an understanding of the muscle fatigue caused by hand-transmitted vibration.

(g) To investigate the vibration transmissibility of the finger, knuckle and the wrist to develop the vibration transmission pattern in the human hand, and propose an effective method of evaluating the vibration transmission of anti-vibration gloves.

(h) To propose simple hand and hand-glove models using the vibration transmissibility data.

1.7.2 THESIS ORGANIZATION

This thesis research is divided into eight chapters. Relevant literature is discussed in appropriate chapters to highlight the research contributions.

Chapter 2 is devoted to discuss the method of measuring the driving point impedance of the hand-arm system using sinusoidal and stochastic excitations. The measured impedance data were examined for repeatability of results. Further, the data were utilized to discuss the influence of grip force, magnitude of excitation and type of excitation. Chapter 3 examines various existing techniques to develop hand-arm models and proposes methods of developing linear and nonlinear models using optimization techniques. Linear and non-linear models were developed so as to account for the influence of grip force on dynamic response of the hand-arm system. Chapter 4 synthesizes driving point mechanical impedance data in all the three orthogonal directions of vibration. The synthesized data were utilized to develop hand-arm impedance envelops indicating most probable range of impedance values. Further, hand-arm models are proposed by fitting the model response with the synthesized data in X_h-, Y_h-, and Z_h- directions.

Chapter 5 proposes a method of measuring hand grip pressure distribution using flexible thin film pressure sensors. The hand grip pressure distribution was acquired under static and dynamic loading conditions. The hand grip pressure data were examined to obtain the location of peak pressures so as to correlate peak pressures to the onset of VWF disease. Chapter 6 attempts to establish the influence of vibration related parameters on electrical activities of finger flexor muscles. Surface electrodes and standard EMG equipment were utilized to acquire the EMG of finger flexors. Chapter 7 is devoted to study the methods of obtaining hand vibration transmissibility and proposes a method of obtaining transmissibility of commercially available anti-vibration gloves using miniature accelerometers and laser based vibration sensors. The transmissibility data were further utilized to model the hand and

hand-glove system. The conclusions derived from the thesis research and suggestions for future investigations are presented in Chapter 8.

CHAPTER 2

BIODYNAMIC RESPONSE OF THE HAND-ARM SYSTEM

2.1 Introduction

The severe health risks posed by prolonged exposure to hand-held power tool vibration, supported by the findings of the epidemiological studies, have prompted a strong desire to enhance a thorough understanding of the vibration response characteristics of the human hand-arm. While subjective measures provide considerable information related to minimum threshold and equal sensation, inter-subject variation and poor repeatability of the subjective data pose difficulties in characterizing the hand-arm vibration response. Alternatively, the biodynamic response of the human hand-arm may be characterized using objective methods. The objective measurement of the response of the human tissues to vibration also poses difficulties due to lack of appropriate sensors and possibilities of injuries to the subjects during experimentation. Methods, based upon measurement of mechanical impedance, compliance or accelerance, have thus been proposed to objectively measure the vibration response of the human tissues using current design of sensors in a carefully controlled vibration environment. A number of studies have been conducted to characterize the dynamic response of the hand-arm system using transmissibility and impedance measurements (*Abrams et al., 1969; Suggs et al., 1977; Reynolds et al., 1984; Lundström et al., 1989*). The transmissibility measurements, however, have been considered valid for low frequency vibration due to the presence of high noise levels in the hand transmitted vibration (*Boileau et al., 1992; Aatola, 1989*). Driving point mechanical impedance of the human whole-body and hand-arm have been extensively investigated to

characterize the biodynamic response, since the driving point impedance is well suited to describe the overall dynamic response. The impedance may be related to the amount of mechanical energy transferred from power tools (*Reynolds et al., 1977*), and thus occurrence of occupational diseases due to prolonged use of the power tools.

Driving point impedance measurements of the hand-arm can be easily performed on live subjects to investigate the influence of various operating factors, such as different grip forces, methods of clasping handles. The primary limitation of the mechanical impedance method is that the vibration transmitted to the various parts of the upper limb cannot be quantified. The measured response may be considered to represent the total response of an equivalent mechanical system of the hand-arm system. The response data thus obtained may be utilized to develop analytical model of the hand-arm system.

The driving point impedance of the human hand-arm have been, invariably, measured using a simulated handle, subject to swept sinusoidal vibration. Few investigators have attempted to investigate the dynamic response of the hand-arm system using the vibration spectrum generated by a specific tool (*Bernard, 1990*). A unique spectrum of the random vibration generated by different tools, however, cannot be established to derive the mechanical impedance of the hand-arm system. The mechanical impedance of the hand-arm system, subject to random vibration, may thus be evaluated using white noise random excitations.

The driving point mechanical impedance characteristics of the hand-arm system have been reported for varied test conditions, such as grip forces,

magnitude of vibration excitation, thrust or feed forces (*Griffin et al., 1982; Reynolds et al., 1984*). Excessive discrepancies among the reported data, however, have necessitated more data sets to derive meaningful conclusions and a range of most probable values. The differences and similarities among various data sets are discussed in Chapter 4 to establish the range of most probable values of driving point mechanical impedance of the human hand-arm. In this section, the driving point impedance of the human hand-arm system is investigated using sinusoidal and stochastic excitations. The measurements are performed for different test conditions to establish the influence of various physical and biodynamic factors on the hand-arm impedance characteristics.

2.2 Measurement of Driving-Point Impedance of Human Hand-Arm

The mechanical driving point impedance is defined as the ratio of applied force to the resulting velocity measured at the driving point. The driving point impedance of the human hand-arm is derived from the measured force and velocity at the driving point, where the vibration impinges on the hand. The impedance is usually measured using sinusoidal excitation, but the concept can be extended to random excitations (*Burström et al., 1992; Hempstock et al., 1989; Witte et al., 1976; Weis et al., 1964*).

For sinusoidal vibration, the driving point impedance, is expressed as:

$$Z(j\omega) = \frac{F(j\omega)}{\dot{X}(j\omega)} \tag{2.1}$$

where, $Z(j\omega)$ is the complex driving point impedance, $F(j\omega)$ is the applied force and $\dot{X}(j\omega)$ is the velocity measured at the driving point. The impedance is frequently expressed in terms of the magnitude, $|Z(j\omega)|$, and phase, $\varphi(j\omega)$

between the applied force and driving point velocity. The driving point impedance of the human hand-arm, subject to random vibration excitation, is computed from auto- and cross- correlation functions of the force and velocity (*Thompson, 1988, Weis et al., 1964*). The mechanical impedance for random excitation may be obtained from the following relation:

$$Z(j\omega) = \frac{G_{FV}(j\omega)}{G_{VV}(j\omega)} \tag{2.2}$$

Where, $G_{FV}(j\omega)$ is the cross spectral density of the force and velocity, and $G_{VV}(j\omega)$ is the power spectral density of the velocity.

2.2.1 MEASUREMENT PROCEDURE

The vibration of a majority of hand-held power tools predominate in the 10 - 1000 Hz frequency range (*ISO 5349, 1986*). The mechanical driving point impedance characteristics of the hand-arm thus need to be measured using a simulated tool handle subject to vibration in the 10 - 1000 Hz frequency range. The experimental tool handle must be designed such that its frequency response is flat in this frequency range. A 38 mm diameter handle, split along its axial direction was designed and its fundamental resonance frequency was investigated through finite element analysis using the IDEAS software (*IDEAS, 1988*). The tool handle was attached to an electrodynamic vibration exciter driven by a power amplifier and a signal generator through a constant acceleration feedback loop. A resonance dwell test was performed under simulated tool vibrations along the three coordinates proposed in ISO-5349 (*1986*). The results of test and finite element analysis revealed that fundamental frequencies of the handle were well above 2000 Hz in all the three directions of

vibration. A force transducer was mounted between the handle and the vibration exciter to monitor the driving force as a function of frequency. The variations in apparent mass of the handle with excitation frequency were computed as:

$$M(j\omega) = \frac{F(j\omega)}{\ddot{X}(j\omega)} \tag{2.3}$$

Where $M(j\omega)$ is the apparent mass of the handle, and $\ddot{X}(j\omega)$ is the acceleration of the handle. The measurements revealed insignificant variations in the apparent mass of the handle.

The mass of the handle affects the measured impedance characteristics in a considerable manner due to relatively low mass of the hand-arm that rests on the handle. The measured force is thus corrected for the handle inertia using an analog circuit. Various studies reported in the literature reveal dependence of hand-arm impedance on the physical and biological parameters. Of these, the grip force affects the driving point impedance significantly (*Mishoe et al., 1977*). It is thus desirable to study the biodynamic response characteristics of the hand-arm for different values of constant grip force. Two strain gages, one to measure the bending strain caused by hand grip, and the other for temperature compensation, were mounted on the handle to monitor the total grip force. The strain gages, connected in a half-bridge configuration, were calibrated by applying known loads at a static position of the handle. The strain gage signal was constantly displayed to each test subject, through a digital voltmeter, to enable the subject to maintain nearly constant grip force during the test.

The instrumented handle was mounted on the vibration exciter such that the biodynamic response of the hand-arm can be measured in the X_h, Y_h, and Z_h directions recommended by ISO-5349 (*1986*). Figure 2.1 illustrates the hand-handle orientation for measurement of X_h, Y_h, and Z_h components of driving point mechanical impedance. Figure 2.2 illustrates the schematic of the test apparatus. The measured acceleration was integrated to attain the velocity of the driving point. The mass corrected force and the corresponding driving point velocity were recorded using a data acquisition system.

2.2.2 TEST VARIABLES

The driving point mechanical impedance of the human hand-arm is dependent upon the grip force, posture, and magnitude and frequencies of vibration. The measurements were performed for a range of these variables to quantify the relative significance of various physical and biological variables. Table 2.1 summarizes the range of variables used for the impedance measurements.

Impedance characteristics of four adult male subjects were measured in the frequency range of 10-1000 Hz. The attributes of subjects, such as age, weight and height are listed in the Table 2.2. The experiments were conducted at three different grip force levels of 10 N, 25 N and 50 N. The subjects, in standing posture, gripped the vibrating handle with their dominant right hand and were asked to maintain nearly constant grip force throughout the experiment by observing the total grip force displayed by the digital voltmeter. The subject's arm was maintained in a horizontal position with the elbow bent approximately 90 degrees. For the selected sweep rate of 6 octaves/minute, each experiment lasted approximately 75 seconds for sinusoidal excitation. For experiments

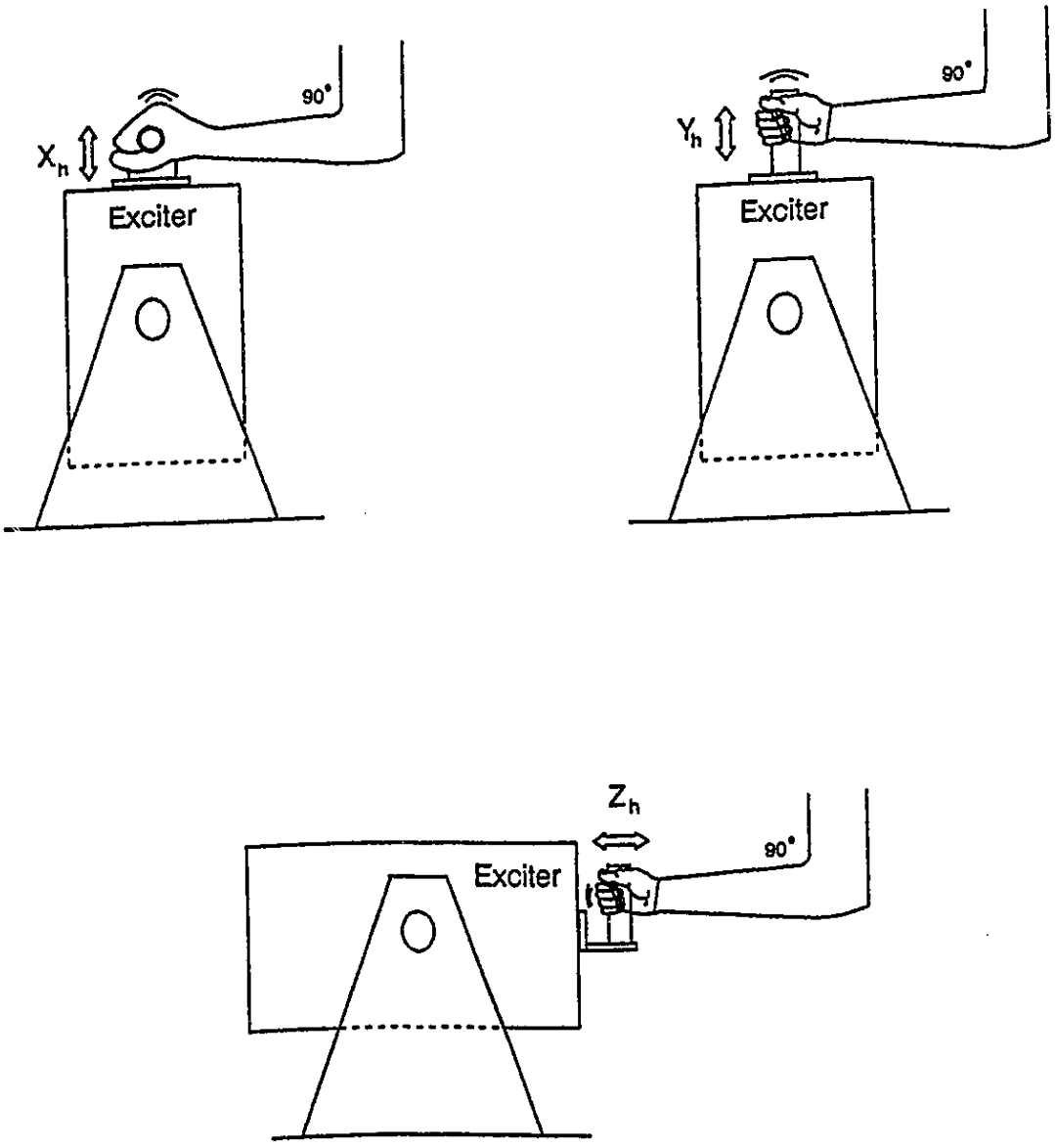

Figure 2.1: Hand-handle orientation in three orthogonal directs of vibration (ISO - 5349, 1986)

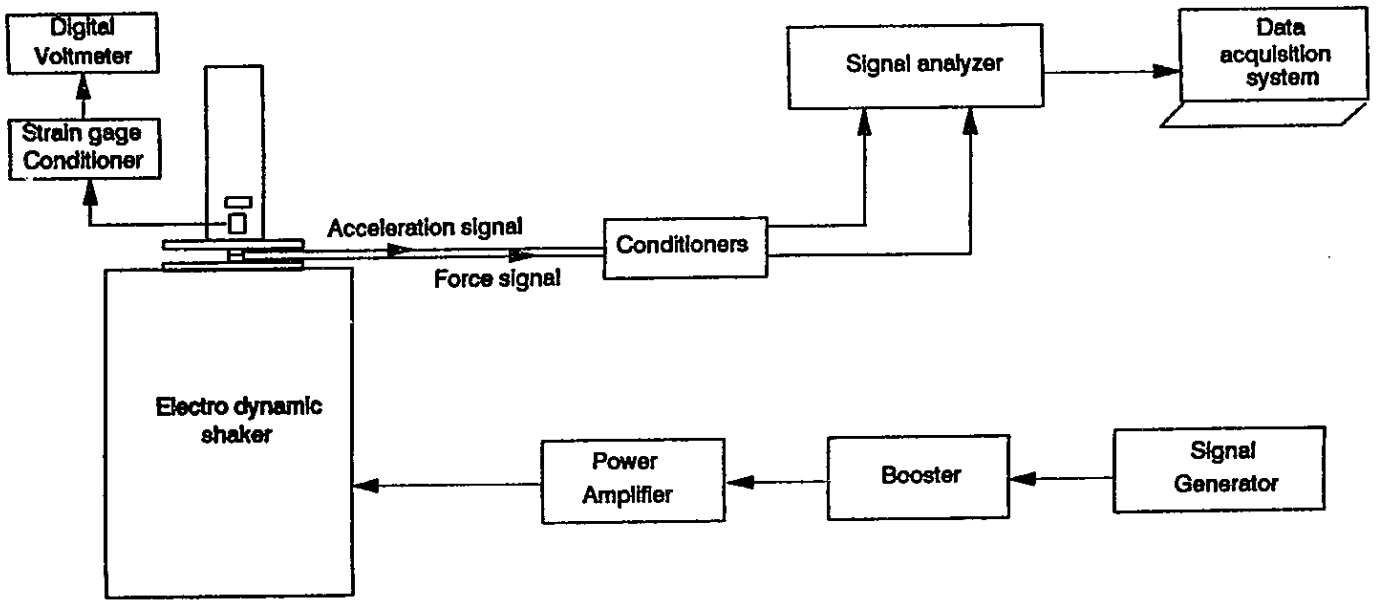

Figure 2.2: Schematic of the impedance measurement apparatus.

using white noise random excitation each test lasted approximately 60 seconds to achieve a minimum of 200 spectra averages.

TABLE 2.1
Summary of Experimental Parameters Investigated

Direction of vibration	X_h, Y_h, Z_h
Frequency range	10 - 1000 Hz
Excitation	
Sinusoidal	1.0, 2.0, and 3.0 g peak
Random	0.2 m/s^2, 0.5 m/s^2 and 0.7 m/s^2 *rms.*
Grip force	10 N, 25 N, and 50 N
Handle shape and size	Circular shape and 38 mm diameter
Number of subjects	4
Sex	Male
Elbow angle	90 degrees
Shoulder abduction	0 degree
Grip type	Palm grip from above the handle using dominant right hand
Body posture	Standing upright

2.3 Hand-Arm Impedance as a Function of Frequency and Grip Force

The human hand-arm impedance characteristics, reported in the literature, have shown a strong dependence of impedance on the grip force and the excitation frequency (*Mishoe et al., 1977*). It is thus desirable to describe the driving point impedance characteristics of the hand-arm through a function

TABLE 2.2
Attributes of the Test Subjects

Attribute	Subject #			
	1	2	3	4
Age (years)	30	31	41	32
Height (m)	1.65	1.75	1.89	1.78
Weight (kg)	65	75	85	77
Hand width (m)	0.09	0.10	0.10	0.10
Hand length (m)	0.18	0.19	0.20	0.19
Forearm length (m)	0.24	0.29	0.28	0.26
Upper arm length (m)	0.26	0.30	0.29	0.29

relating impedance to the hand grip force and frequency. Such a describing function will provide a quick and convenient tool to predict the human hand-arm impedance for different values of grip force and excitation frequency.

$$Z_e = K_{z0} + \sum_{i=1}^{14} K_{zi}\alpha_i \tag{2.4}$$

$$\varphi_e = K_{\varphi 0} + \sum_{i=1}^{14} K_{\varphi i}\alpha_i \tag{2.5}$$

Where Z_e and φ_e are the impedance and phase estimated as a function of the grip force and excitation frequency. K_{zi} and $K_{\varphi i}$ are the coefficients determined from the regression analysis. α_i are related to the magnitude of grip force, F_g and excitation frequency, f, in the following manner:

$$\alpha_1 = F_g; \alpha_2 = f; \alpha_3 = F_g^2; \alpha_4 = f^2; \alpha_5 = F_g f$$

$$\alpha_6 = F_g^2 f^2; \alpha_7 = F_g^3; \alpha_8 = f^3; \alpha_9 = F_g f^2; \alpha_{10} = F_g^2 f$$

$$\alpha_{11} = \exp(-f); \alpha_{12} = \exp(-1/f); \alpha_{13} = \exp(-1/f^2); \alpha_{14} = \exp(-1/F_g f)$$

2.4. Results and Discussion

The experiments were performed on four subjects for the range of test variables described in Table 2.1. The measured data were analyzed to yield driving point impedance characteristics of the hand-arm system. Each test was performed five times to verify the repeatability of the measurements. The resulting impedance data were smoothened by fitting closely approximated splines (*Pokorny et al., 1989*). The measured data was then analyzed to determine the influence of various test variables on the driving point impedance characteristics. The mean impedance data obtained at 1/3 octave center band frequencies for different combinations of experimental parameters in all the three directions of vibration are presented in Tables A1 - A18 in Appendix - I. A representative set of measured data for each axis of vibration are discussed to highlight the overall pattern and the influence of various test variables. The measured values of impedance magnitude and phase are further compared to those reported in the literature in Chapter 4.

2.4.1 INTER-SUBJECT AND INTRA-SUBJECT VARIATIONS

The measurements performed on each subject, for selected set of test variables, was first analyzed to determine the intra-subject variation. The driving point impedance curves, derived from five measurements performed on each subject and for each set of variables, were averaged, and corresponding standard deviations were computed as a function of excitation frequency. The

results, in-general, revealed higher inter-subject standard error or variations than the intra-subject variations. Similarly the deviations in impedance magnitude data were observed to be larger than the deviations recorded in the impedance phase data. The peak intra-subject standard error was observed in the range of 3% - 5%. The intra-subject standard error in impedance magnitude, however, were observed to be very small (1% - 2%) at frequencies above 500 Hz. The peak inter-subject standard error in impedance magnitude was observed to be high, in the 20% - 40% range. The peak intra-subject standard error in impedance phase was observed to be small and in the 1% - 3% range for all directions of vibration. The peak inter-subject standard error in impedance phase, however, was observed to be high in the 5% - 25% range.

The driving point impedance magnitude and phase, measured on all four subjects, subject to vibration along the X_h - direction, is illustrated in Figure 2.3. The impedance characteristics in the Figure are reported for 25 N constant grip force and 1.0 g peak constant acceleration. The results clearly illustrate large inter-subject variations in magnitude. The inter-subject variations in impedance phase, however, are relatively insignificant in the excitation frequency range of 140 - 1000 Hz. The peak standard error of the impedance magnitude measured on four subjects is approximately 50 Ns/m observed at 475 Hz. The peak standard error in the impedance phase data is observed as 12 degrees at 25 Hz. The peak standard error of the magnitude and phase computed as a percentage of the mean value, is observed as 23 % and 25 %, respectively at 40 Hz. However, the overall pattern among the data curves is similar.

Figure 2.4 illustrates impedance magnitude and phase characteristics of the 4 subjects measured using a grip force of 25 N and random excitations

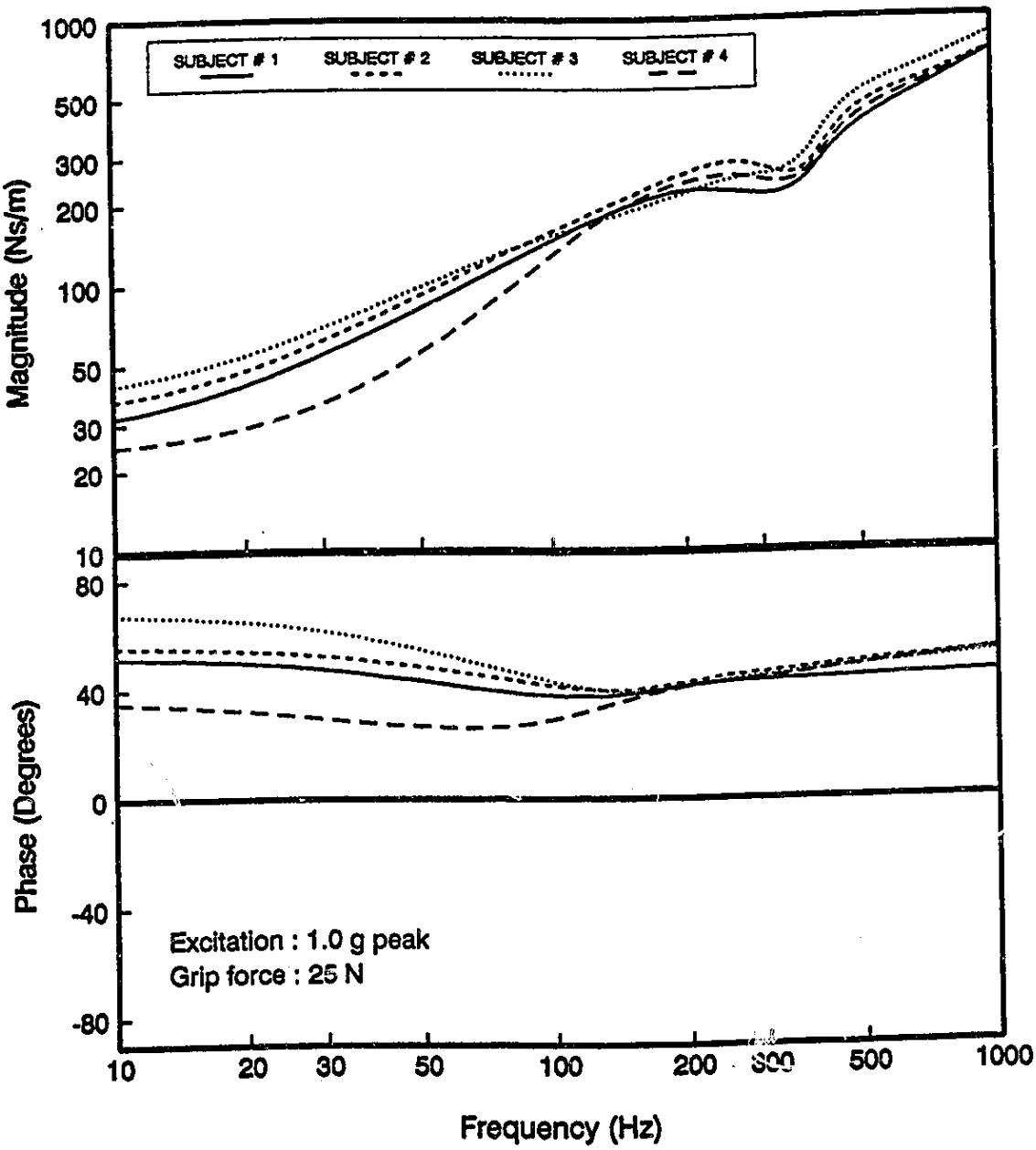

Figure 2.3: Driving point mechanical impedance of all four subjects under sinusoidal excitations (X_h- direction).

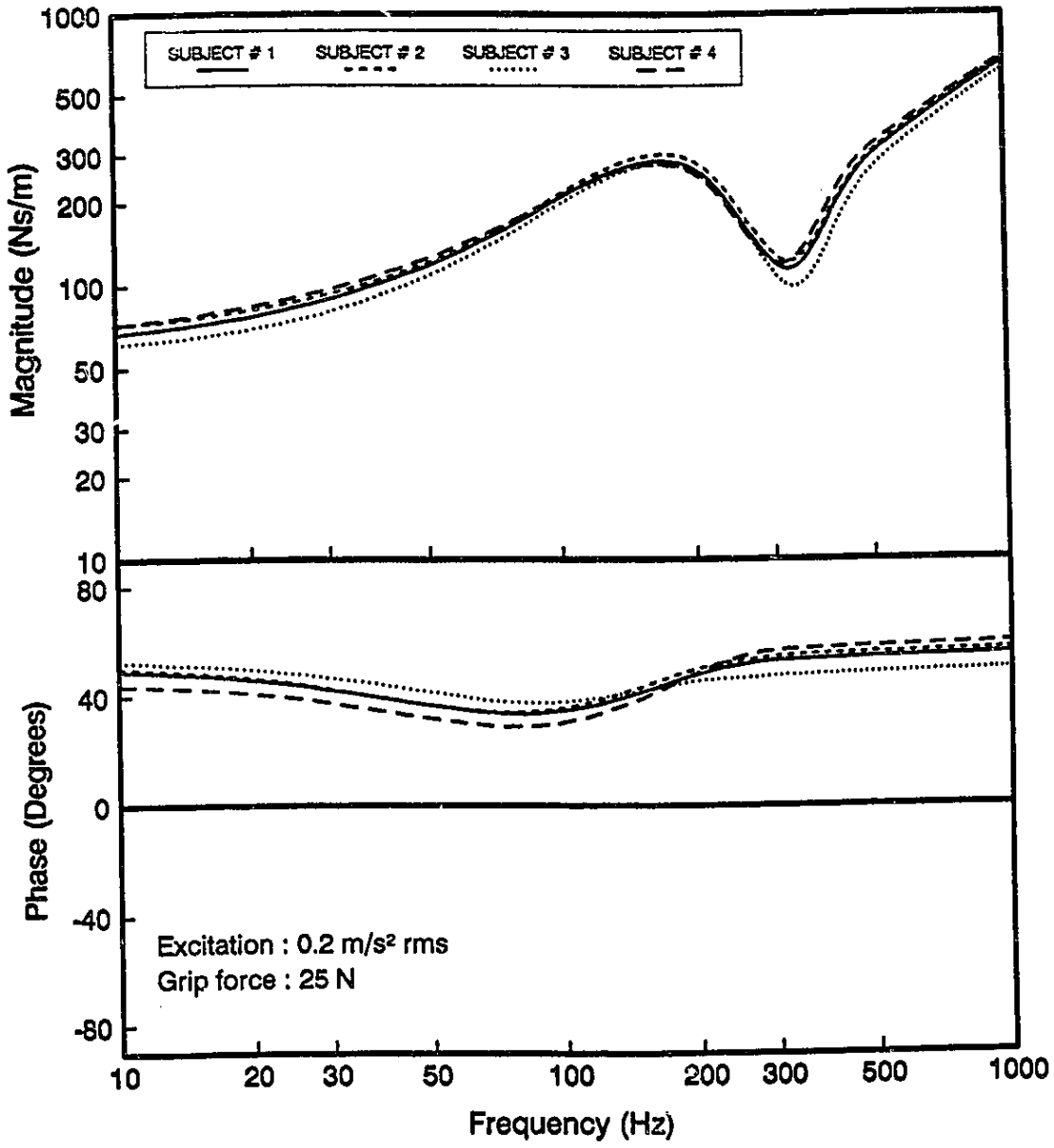

Figure 2.4: Driving point mechanical impedance of all four subjects under random excitation (X_h- direction).

(0.2 m/s^2). A comparison of figures 2.3 and 2.4 reveals that the inter-subject variation in impedance magnitude as well as phase, measured under random vibration, are considerably smaller than those measured under swept-sine vibrations. The peak standard errors in magnitude and phase are computed as 26 Ns/m and 3.6 degrees, respectively, at 1000 Hz. The comparison of Figures 2.3 and 2.4 further reveals that the impedance characteristics measured using random and swept-sine excitations are generally similar with identifiable resonances around 400 Hz. The impedance magnitude, under both types of excitations, increases with increasing frequency, for excitation frequencies below 300 Hz. The magnitude of impedance under random excitation tends to be somewhat larger than that measured under swept-sine vibration, at low frequencies. The magnitude of impedance measured using random excitations, however, is smaller than that measured using sinusoidal excitations above 400 Hz. The variations, in general, may be attributed to the different amplitudes and nature of excitations. The impedance phase angle in both the cases is observed in the range of 35 - 60 degrees.

2.4.2 INFLUENCE OF AMPLITUDE OF VIBRATION

Figures 2.5 and 2.6 illustrate the mean values of impedance obtained using 25 N grip force and different amplitudes of sinusoidal and random excitations along the X_h - direction. The impedance characteristics measured under sinusoidal excitation of 1.0 g, 2.0 g and 3.0 g peak acceleration are compared in Figure 2.5, while the impedance response characteristics under random excitations, 0.2, 0.5 and 0.7 m/s^2 rms acceleration are compared in Figure 2.6. The results reveal that amplitude of vibration, sinusoidal or random, affects the driving point impedance of the human hand-arm in a relatively insignificant manner. The peak variation in impedance magnitude, for the range

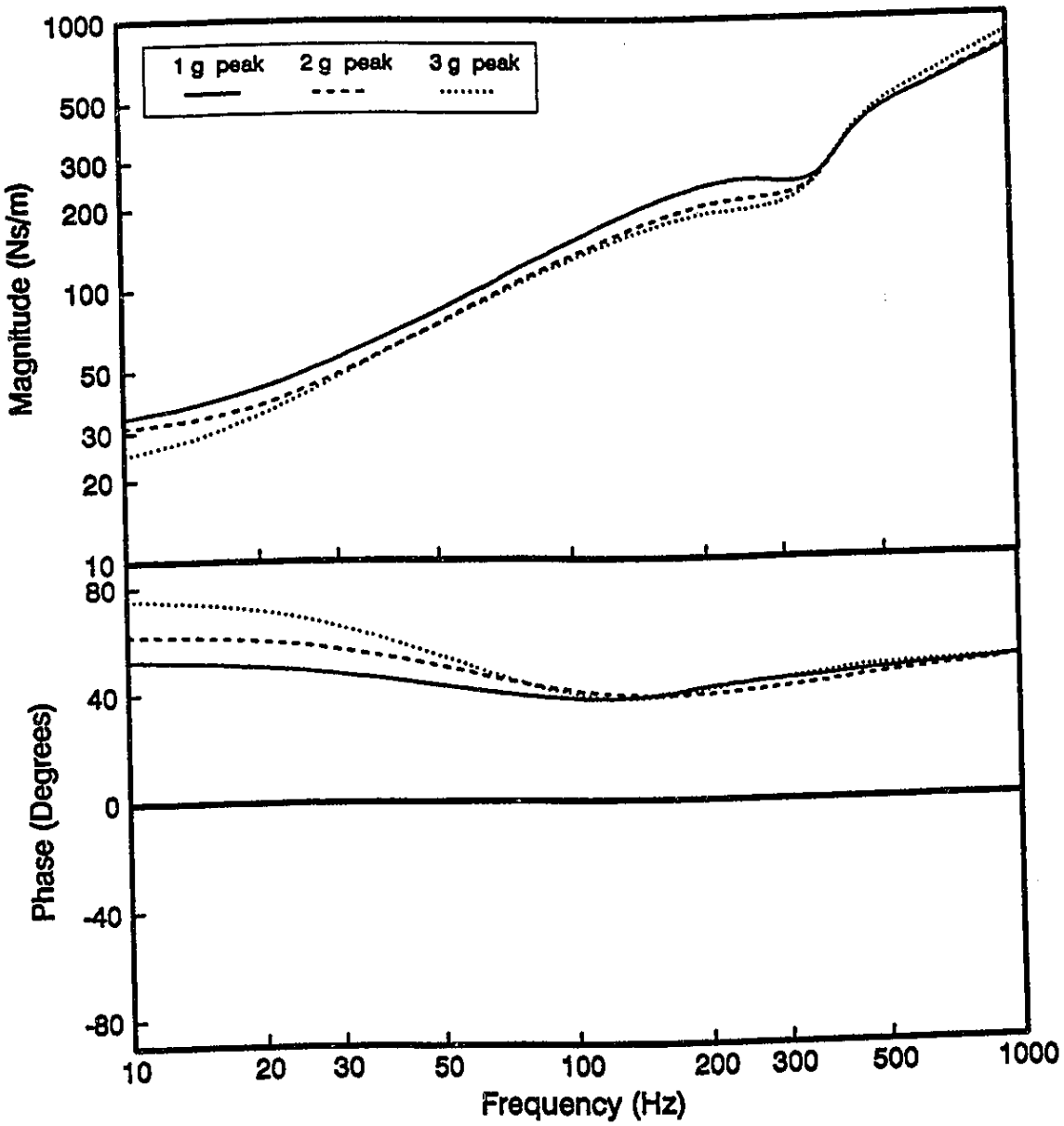

Figure 2.5: Mean values of mechanical impedance under sinusoidal excitations (X_h- direction; Grip force 25 N).

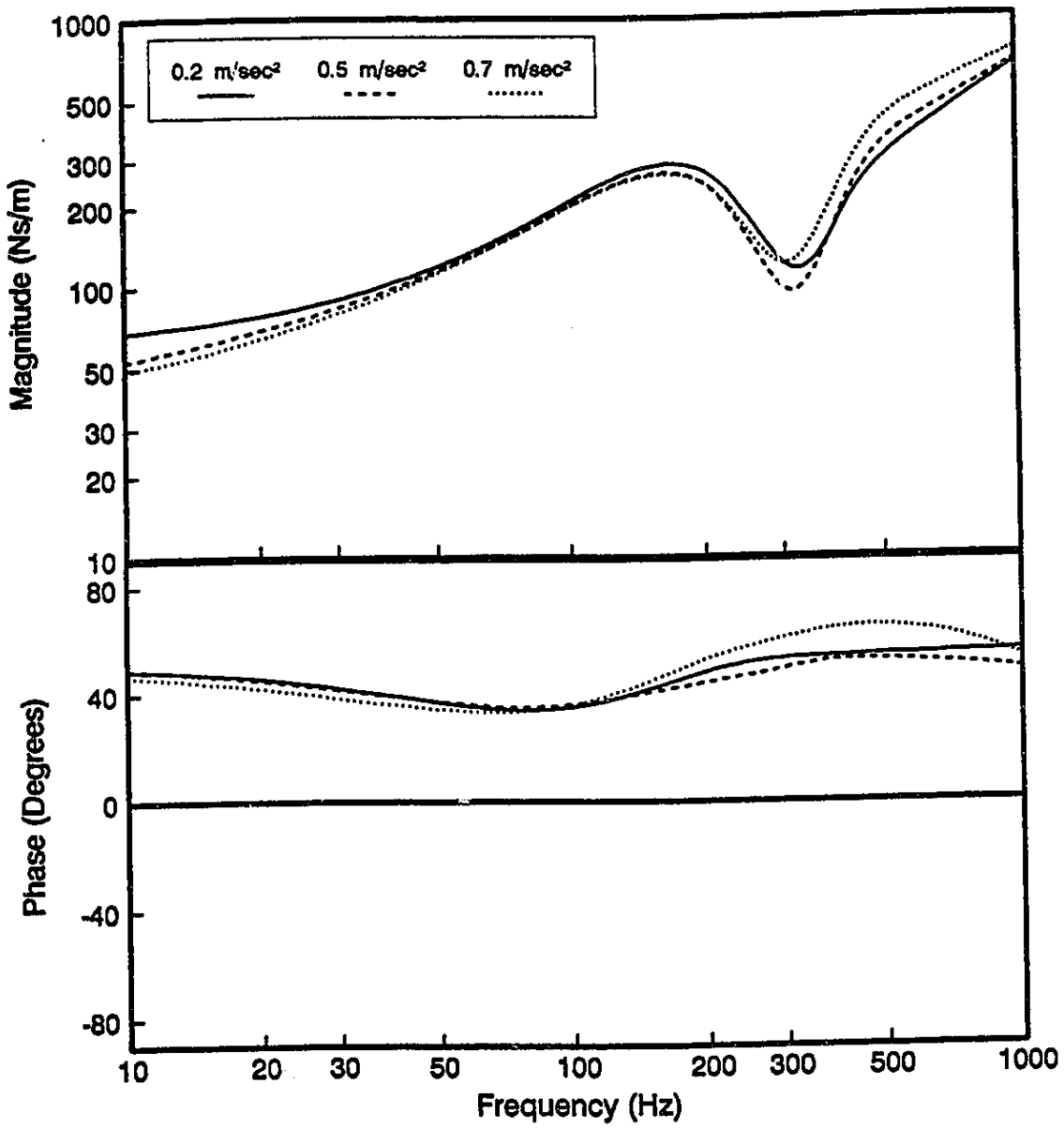

Figure 2.6: Mean values of mechanical impedance under random excitations (X_h- direction; Grip force 25 N).

of excitation levels considered in this study, is observed to be below 10%. While sinusoidal excitation yield variations in impedance phase at frequencies below 80 Hz only, the phase deviation under random excitations is insignificant. Similar conclusions may be deduced from the data presented in Tables A7 to A18 (Appendix - I) for Y_h- and Z_h- components of impedance magnitude and phase for different levels of random and sinusoidal vibration.

2.4.3 INFLUENCE OF GRIP FORCE

Figures 2.7 and 2.8 depict the influence of different grip forces on the measured impedance under sinusoidal (2.0 g peak acceleration) and random (0.7 m/s^2 rms acceleration) excitation levels, respectively. The magnitude of driving point impedance, in general, tends to increase with increase in the excitation frequencies. While a general pattern of variation in impedance phase with changes in grip force is not clearly evident, the variations in impedance phase are observed at frequencies below 100 Hz only. In an attempt to quantify the influence of variation in grip force on the driving point impedance, the average change in impedance magnitude and phase per unit change in grip force is computed in X_h - component impedance magnitude and phase per unit change in grip force is illustrated in Figure 2.9. The results presented in the Figure corresponds to impedance data obtained under 1.0 g peak acceleration, when the grip force is changed from 10 N to 25 N. Figure 2.9 reveals that the variations in impedance magnitude per unit change in grip force approach maximum value of 2 Ns/m/N near 150 Hz. The average change in the impedance magnitude per unit grip force in the 400 -1000 Hz frequency range may be considered as 1 Ns/m/N. The change in impedance phase per unit grip force is considerably smaller, as shown in the Figure. In the 50 - 500 Hz frequency range, the change in impedance phase per unit change in grip force is

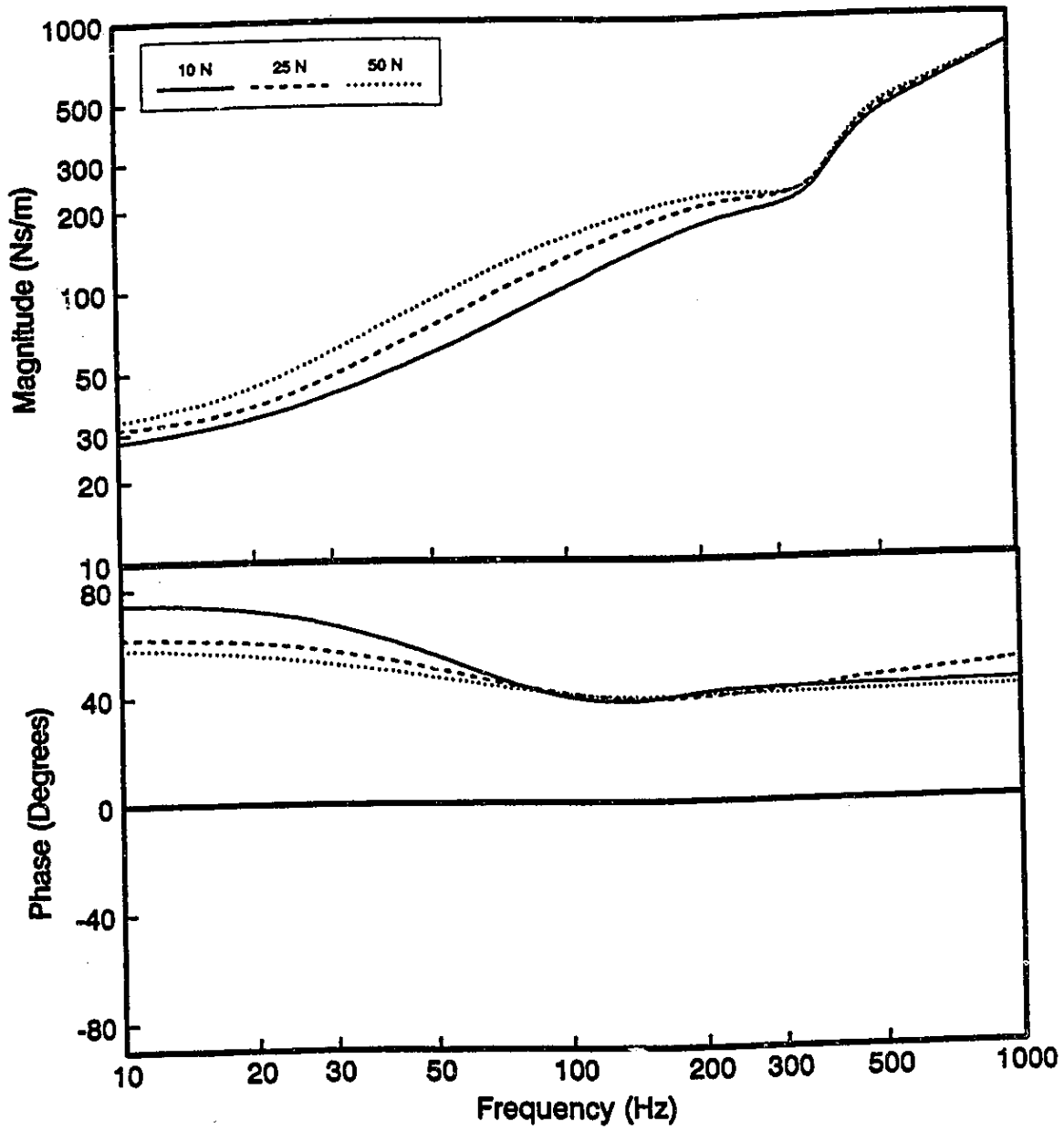

Figure 2.7: Mean values of mechanical impedance under sinusoidal excitations using three different magnitudes of grip force (X_h- direction; 2.0 g peak acceleration).

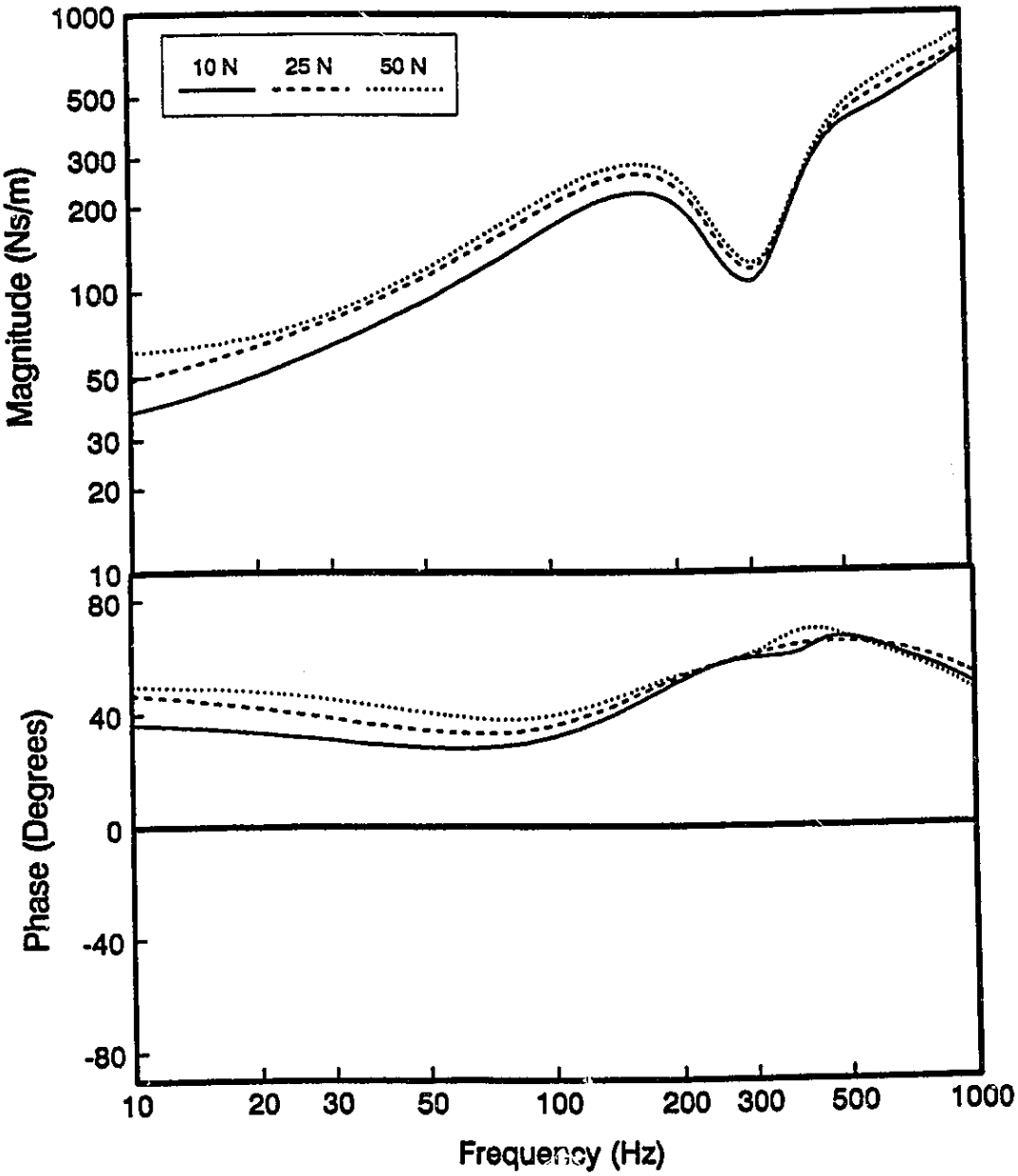

Figure 2.8: Mean values of mechanical impedance under random excitations using three different magnitudes of grip force (X_h- direction; 0.7 m/s^2 rms).

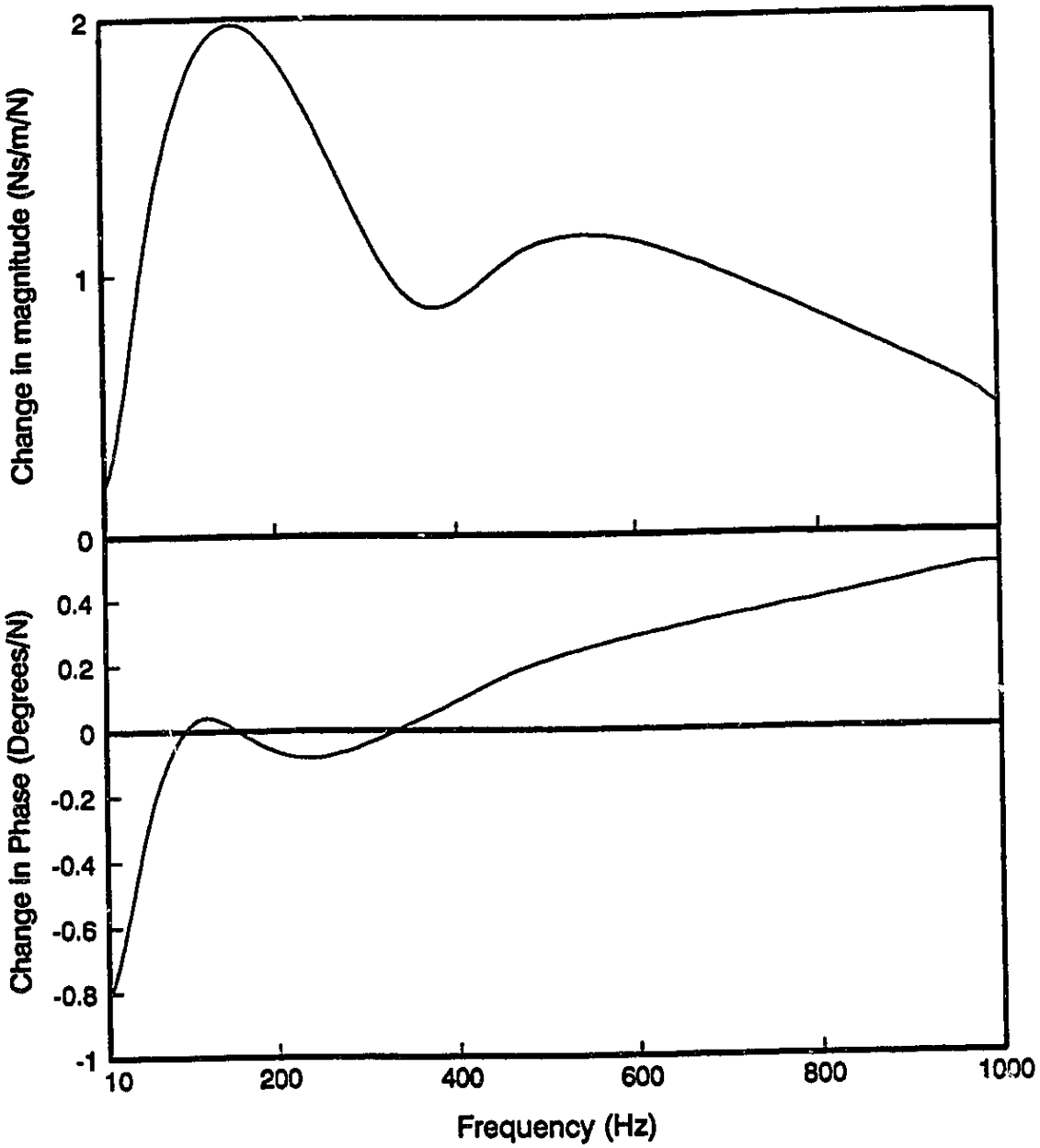

Figure 2.9: Change of impedance per unit change of grip force (X_h- direction; 1.0 g peak acceleration).

in the range of ± 0.2 degrees/N. At extremely low frequencies, the phase angle response variation is observed as -0.8 degrees/N at 10 Hz. At extremely high frequencies the change in phase is approaches approximately 0.5 degree/N. From Figure 2.9 it is apparent that the change in impedance magnitude and phase with change in the grip force is dependent upon the excitation frequency. The magnitude and phase of the X_h- component of impedance measured for different grip forces are presented in Tables A1 to A6 in Appendix - I. The Y_h- and Z_h- component of impedance magnitude and phase, presented in Tables A7 to A18 (Appendix - I), exhibit similar dependence upon the grip force and excitation frequency.

The influence of grip force on the mean values of Y_h - component of the driving point impedance measured under sinusoidal acceleration (1.0 g peak) is illustrated in Figure 2.10. The magnitude of Y_h- component of impedance increases with increase in the grip force. The corresponding change in the impedance phase, however, is relatively insignificant. A comparison of Figures 2.7 and 2.10 reveals that a variation in grip force affects the Y_h - component of impedance more significantly than the corresponding X_h - component. The influence of grip force on the driving point impedance measured under random excitations (0.2 m/s^2 rms acceleration) is similar to that illustrated for sinusoidal excitation, as shown in Figure 2.11. The influence of grip force on the impedance is more significant at frequencies below 500 Hz. The influence of grip force on the Y_h- component of driving point impedance was further investigated for the range of variables considered in this study. An analysis of the results, presented in Tables A7 to A12 (Appendix - I), revealed similar trends.

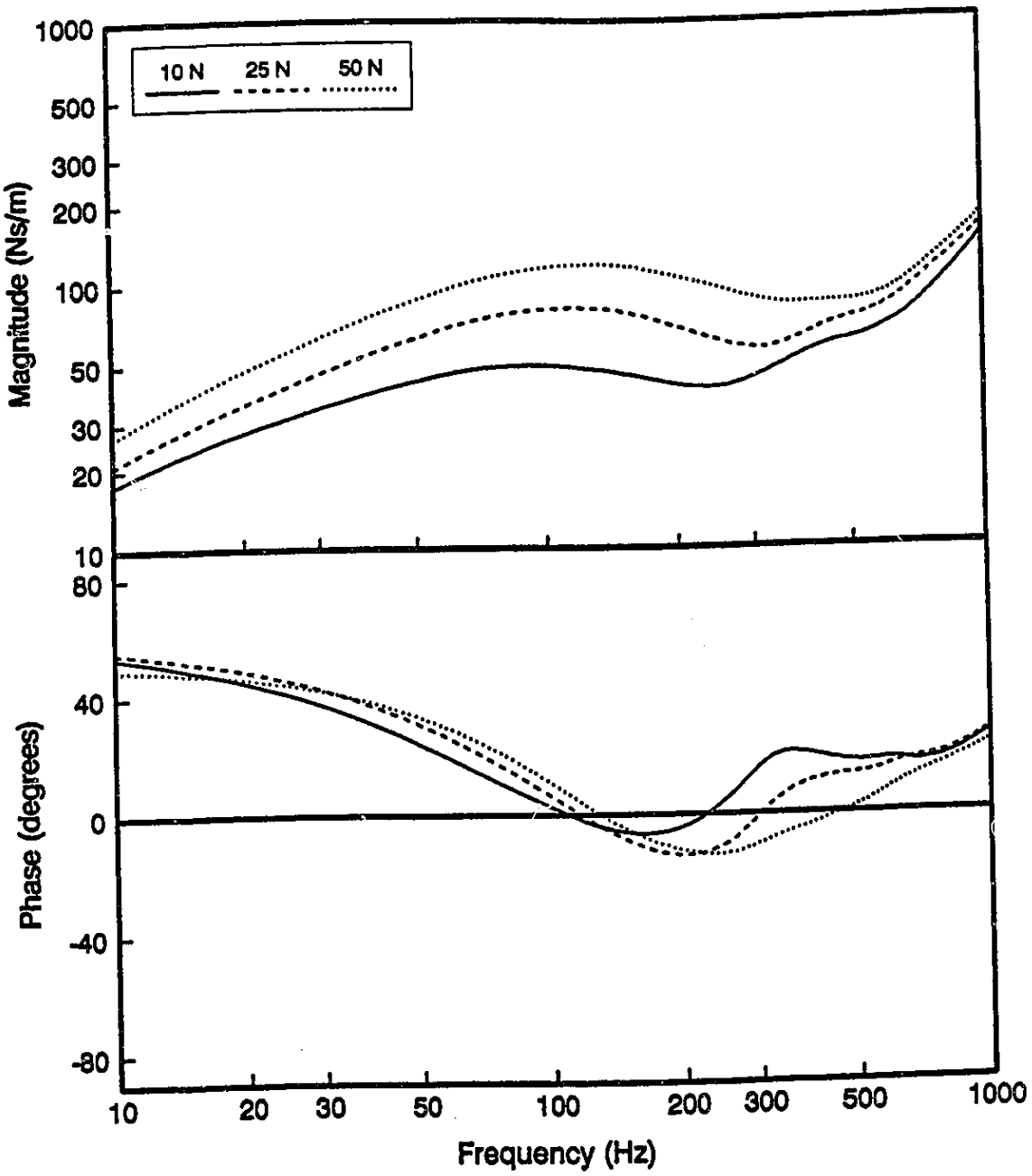

Figure 2.10: Mean values of mechanical impedance under sinusoidal excitations using three different magnitudes of grip force (Y_h- direction; 1.0 g peak acceleration).

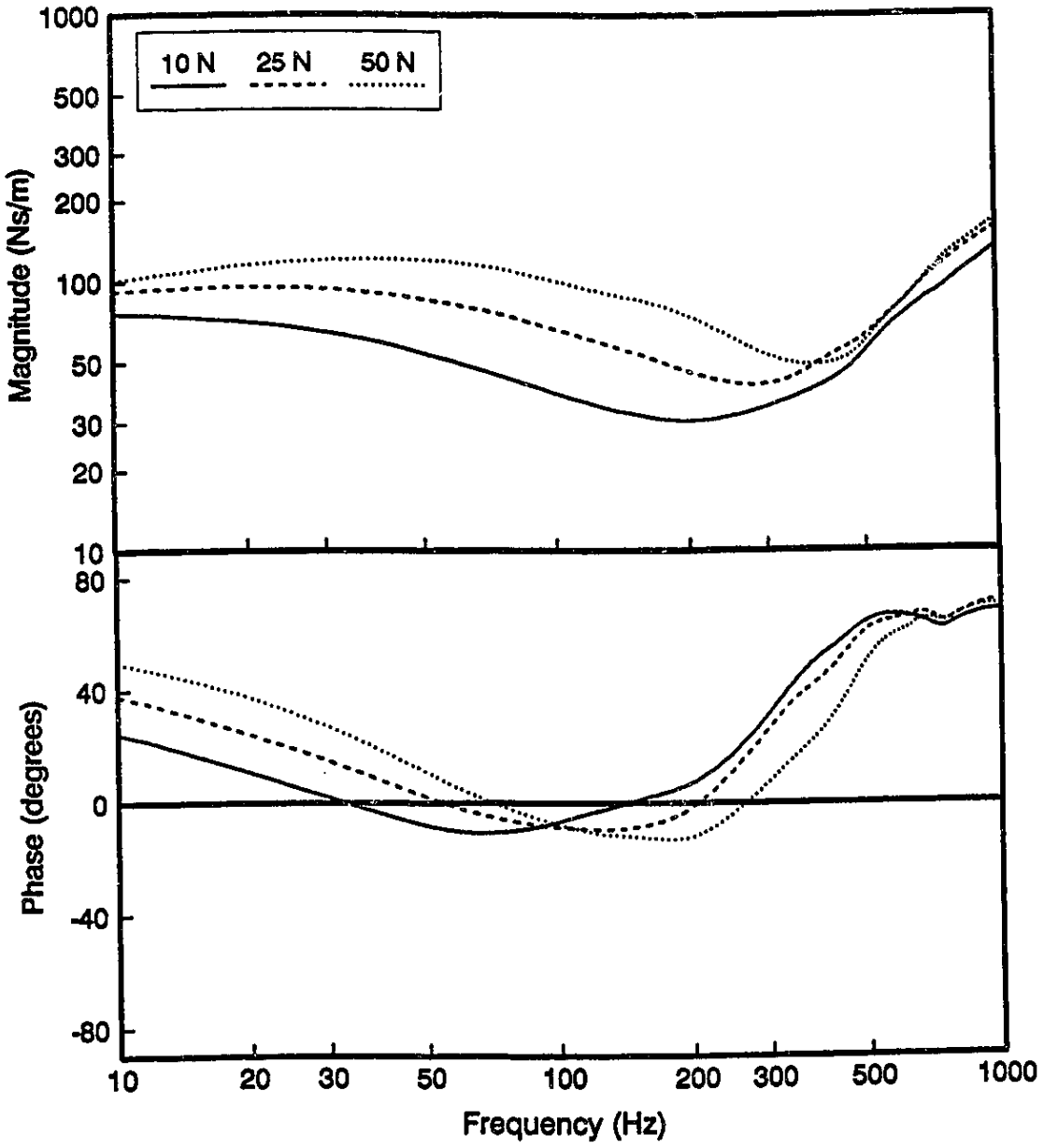

Figure 2.11: Mean values of mechanical impedance under random excitations using three different magnitudes of grip force (Y_h- direction; 0.2 m/s^2 rms).

Figures 2.12 and 2.13 illustrate the influence of grip force on the magnitude and phase characteristics of the Z_h- component measured under sinusoidal (2.0 g peak acceleration) and random excitations (0.2 m/s^2 rms acceleration) excitations, respectively. The figures reveal that the Z_h- component impedance is dependent on the grip force and the frequency, in a manner similar to that observed in X_h- and Y_h- components of the impedance. In general the impedance magnitude is observed to increase with increase in grip force and frequency. However, the influence of frequency, on the phase is relatively insignificant. The phase response in general varies in the range of 40 - 70 degrees in the entire frequency range. The change in phase with change in grip force is relatively minimum. In case of sinusoidal excitation the phase angle is varied with frequency in the narrow range of 40 - 70 degrees. In case of random excitations, the phase angle lies in the range of 30 - 70 degrees and tends to increase with increase in frequency. Tables A13 to A18 (Appendix - I) present Z_h- component of impedance for different amplitudes of excitation and grip forces. Figures 2.5 to 2.13 and Tables A1 to A18 completely describes the biodynamic response of the human hand-arm system as a function of nature of excitation, amplitude and frequency of vibration, and grip force. From the measured results, it can be observed that the magnitude of impedance in Y_h- direction is iess than that of impedance measured in X_h- and Z_h- directions. Further, the impedance phase angle in the Y_h- direction, in the 50 - 500 Hz frequency range, approach negative values, contrary to the impedance phase measured in other two directions. However, it must be noted that this frequency range, where the impedance phase approach negative values, varies with the magnitude of grip forces and excitation levels. In X_h- direction the impedance magnitude is observed to increase with increase in excitation frequency. For Y_h- and Z_h- directions this pattern is not evident at all frequencies. The

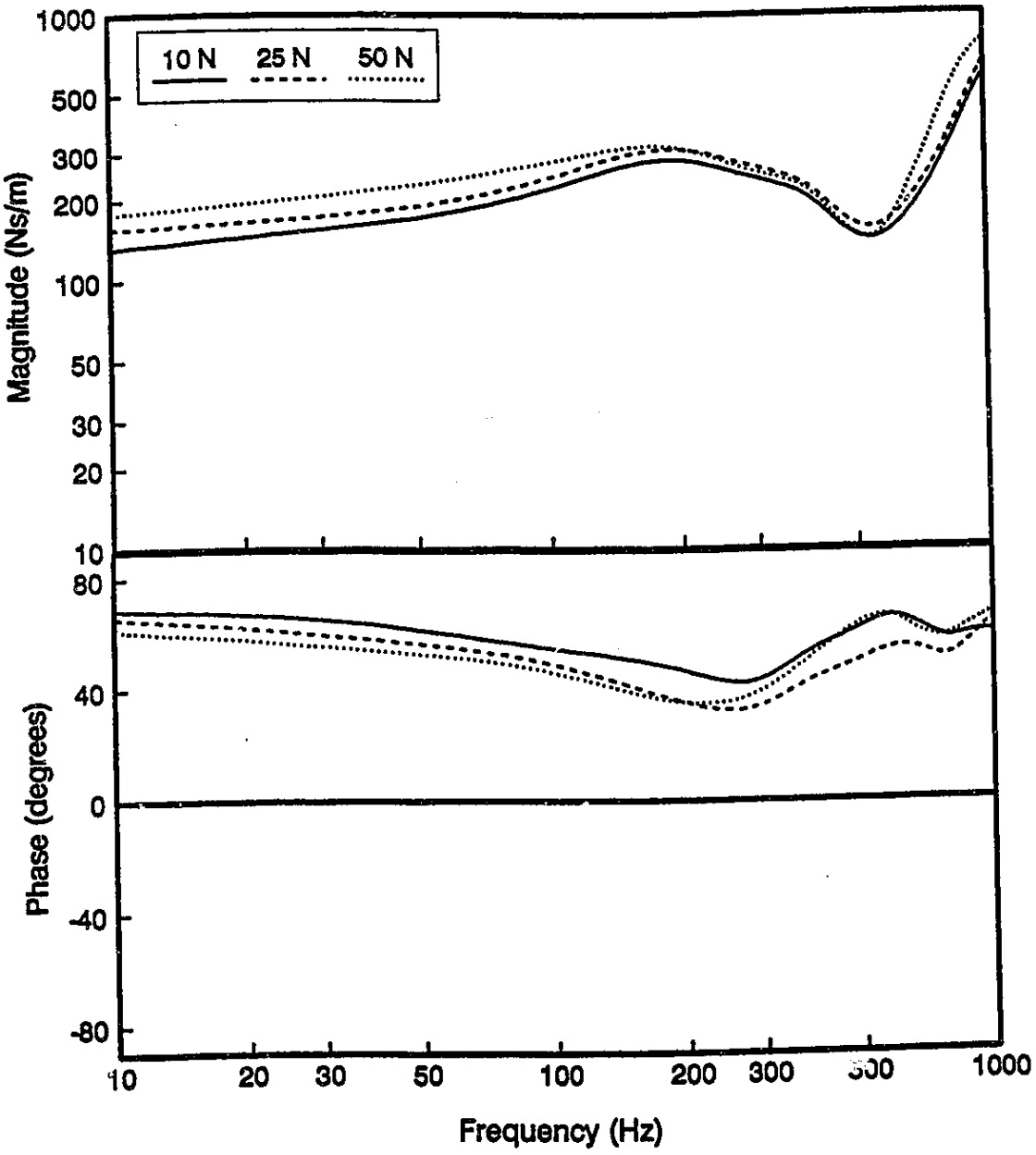

Figure 2.12: Mean values of mechanical impedance under sinusoidal excitations using three different magnitudes of grip force (Z_h- direction; 2.0 g peak acceleration).

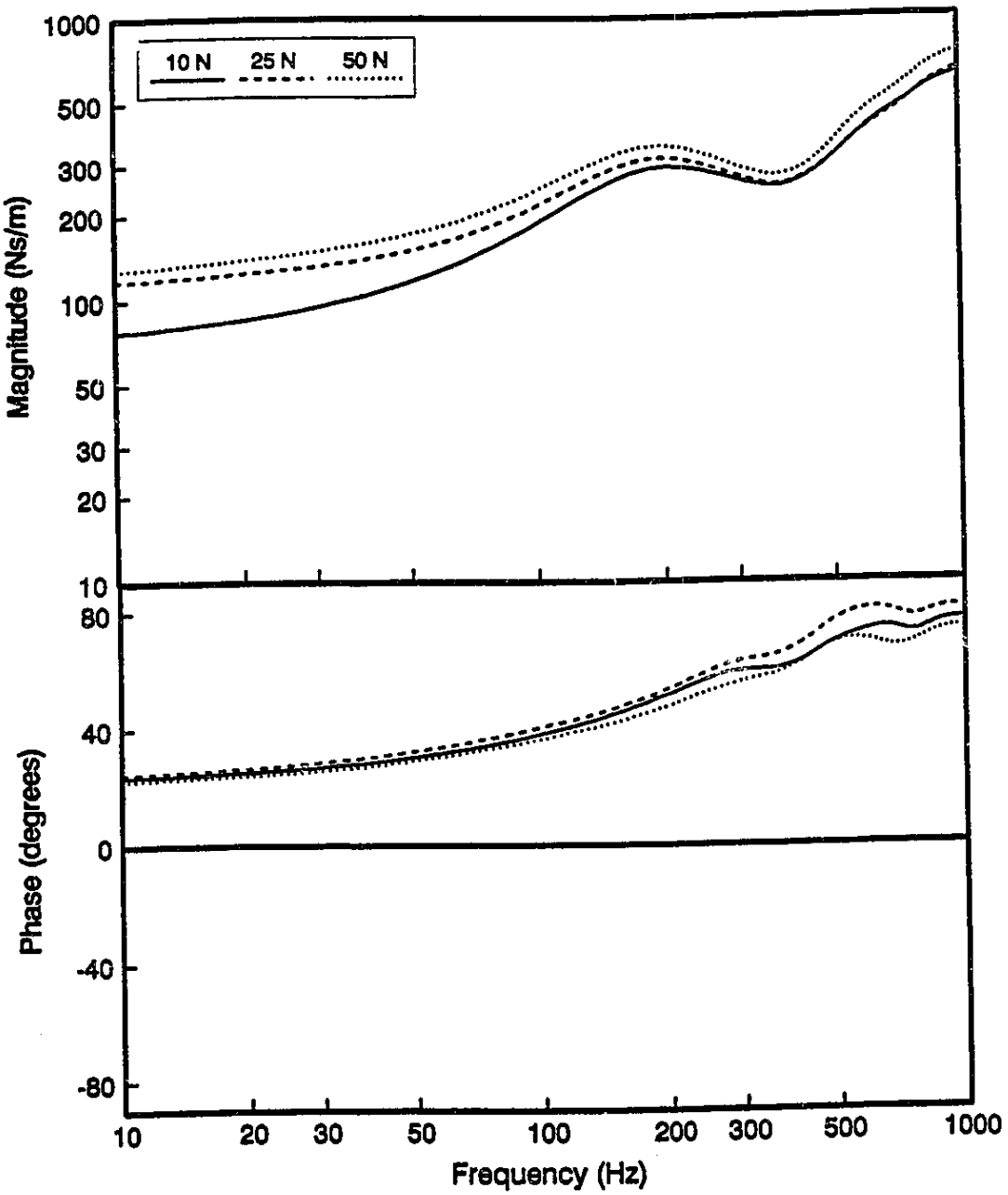

Figure 2.13: Mean values of mechanical impedance under random excitations using three different magnitudes of grip force (Z_h- direction; 0.2 m/s^2 rms).

impedance magnitude in all directions, however, tends to increase with frequencies, well above 500 Hz.

2.4.4 ESTIMATION OF DRIVING POINT IMPEDANCE USING REGRESSION ANALYSIS

A regression analysis was performed using MINITAB (*MINITAB, 1988*) statistical software to derive the functions relating impedance magnitude and phase to the hand grip force and excitation frequencies. The coefficients K_{zi} and $K_{\varphi i}$ described in equations (2.4) and (2.5) are determined from the regression analysis, while the impedance data measured under 2.0 g peak sinusoidal acceleration is used as the target values. The coefficients in equations (2.4) and (2.5) are derived for all three axis of vibration using the measured impedance characteristics in the X_h-, Y_h- and Z_h- directions. The constants, K_{zi} and $K_{\varphi i}$, obtained through regression analysis in each of the direction for magnitude and phase are given in Table 2.3. The estimated values of impedance are compared with the measured data in X_h-, Y_h- and Z_h- directions as shown in Figure 2.14 to 2.16, respectively. In all the cases the coefficient of correlation obtained between measured and predicted curves was greater than 0.9. This is also evident from the Figures which generally demonstrate a good correlation between the measured and predicted values of driving point impedance in all the directions. The magnitude of driving point impedance, however, deviates from the measured values in the narrow frequency range of 10 - 30 Hz. The error between the estimated and measured values of impedance phase is considerably small, due to low deviations, in all the three directions of vibration. In all the cases the percentage deviation between measured and computed magnitude values are high in the narrow frequency range of 10-30 Hz. Thus, the regression equations (2.4) and

TABLE 2.3
Parameters Derived from the Regression Analysis

Coefficient K_{zl} (or) $K_{\varphi l}$ (l=0, 14)	Direction of vibration					
	X_h		Y_h		Z_h	
	Magnitude (z)	Phase (φ)	Magnitude (z)	Phase (φ)	Magnitude (z)	Phase (φ)
0	4.6095E4	-6.1175E3	2.7370E4	-1.1577E4	5.9149E4	-7.9517E3
1	3.4177E0	-1.5117E-3	1.6763E0	-4.7136E-1	3.5766E0	-3.3153E-1
2	-2.9273E-1	4.6000E-2	-3.4925E-1	-5.1676E-1	2.9924E-1	4.3105E-2
3	-3.3750E-2	2.0100E-3	-9.5840E-3	3.2450E-3	-2.1278E-2	6.6800E-4
4	2.3000E-3	-6.7000E-5	6.4710E-4	2.2000E-4	-2.0268E-3	6.2820E-5
5	-3.9600E-3	1.0519E-3	-3.4648E-3	3.6264E-3	-2.2950E-3	-6.3381E-2
6	-1.0000E-8	-1.0000E-8	-1.0000E-8	7.0000E-7	3.0000E-7	-1.2000E-7
7	0.0000E0	0.0000E0	0.0000E0	0.0000E0	0.0000E0	0.0000E0
8	-1.3900E-6	2.0000E-8	-2.9000E-7	-1.4000E-7	2.0800E-6	-1.0000E-7
9	1.6600E-6	5.0000E-7	2.8900E-6	-4.3400E-6	-1.9500E-6	6.9800E-6
10	2.9790E-5	-1.6400E-5	1.7520E-5	-5.1090E-5	-1.5537E-4	1.1523E-4
11	-1.7579E6	3.8794E5	-4.2646E5	2.2280E5	-2.2054E6	2.9547E5
12	5.9360E3	-1.1632E3	3.9713E3	-1.7581E3	7.5515E3	-1.0771E3
13	-4.3678E4	1.0042E4	-2.6168E4	1.2673E5	-6.0810E4	8.6059E3
14	-8.2220E4	-2.7350E3	-5.0602E3	6.5922E2	-5.6253E3	4.6800E2

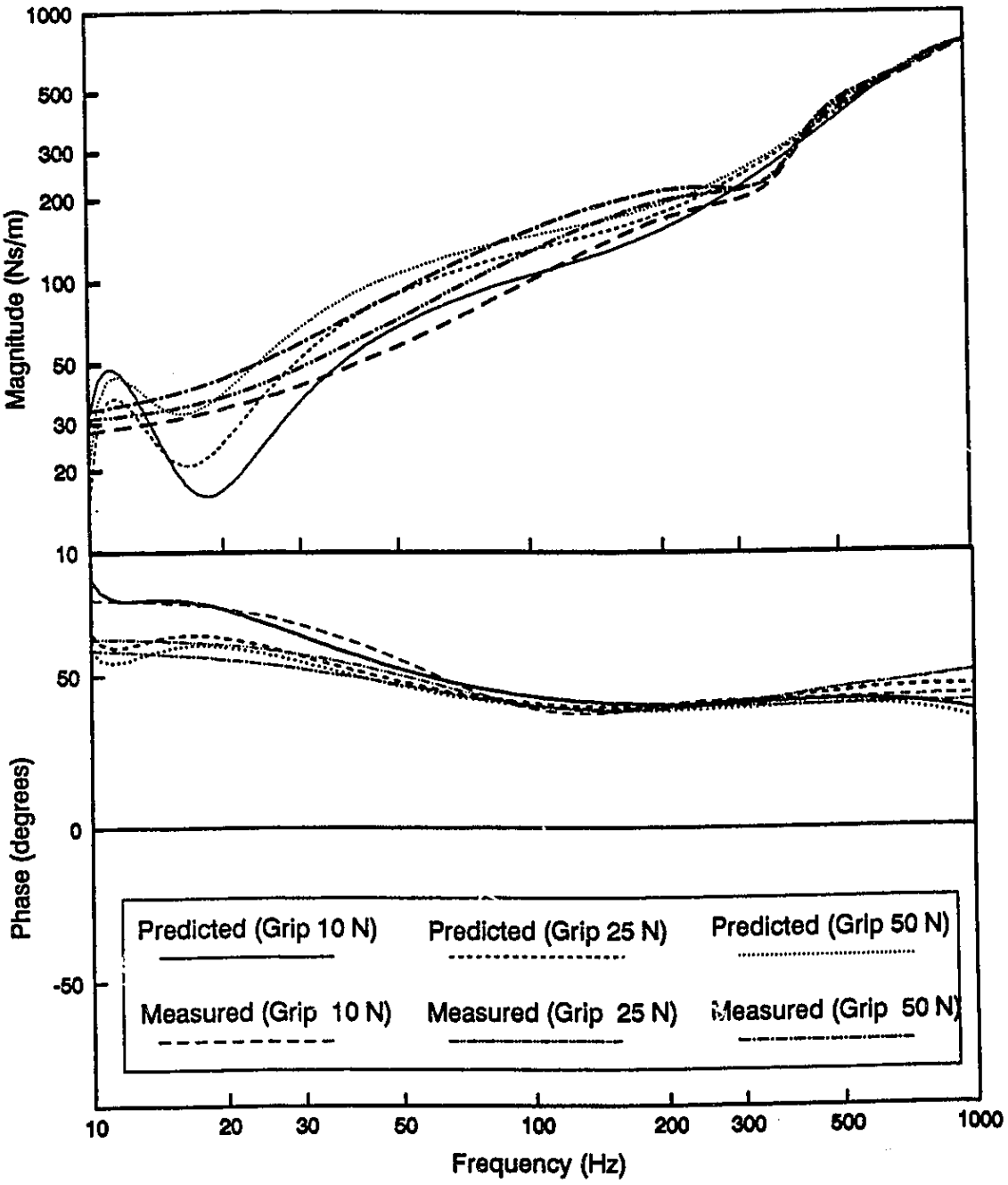

Figure 2.14: Measured and predicted values of mechanical impedance for three grip forces (X_h- direction; 2.0 g peak acceleration).

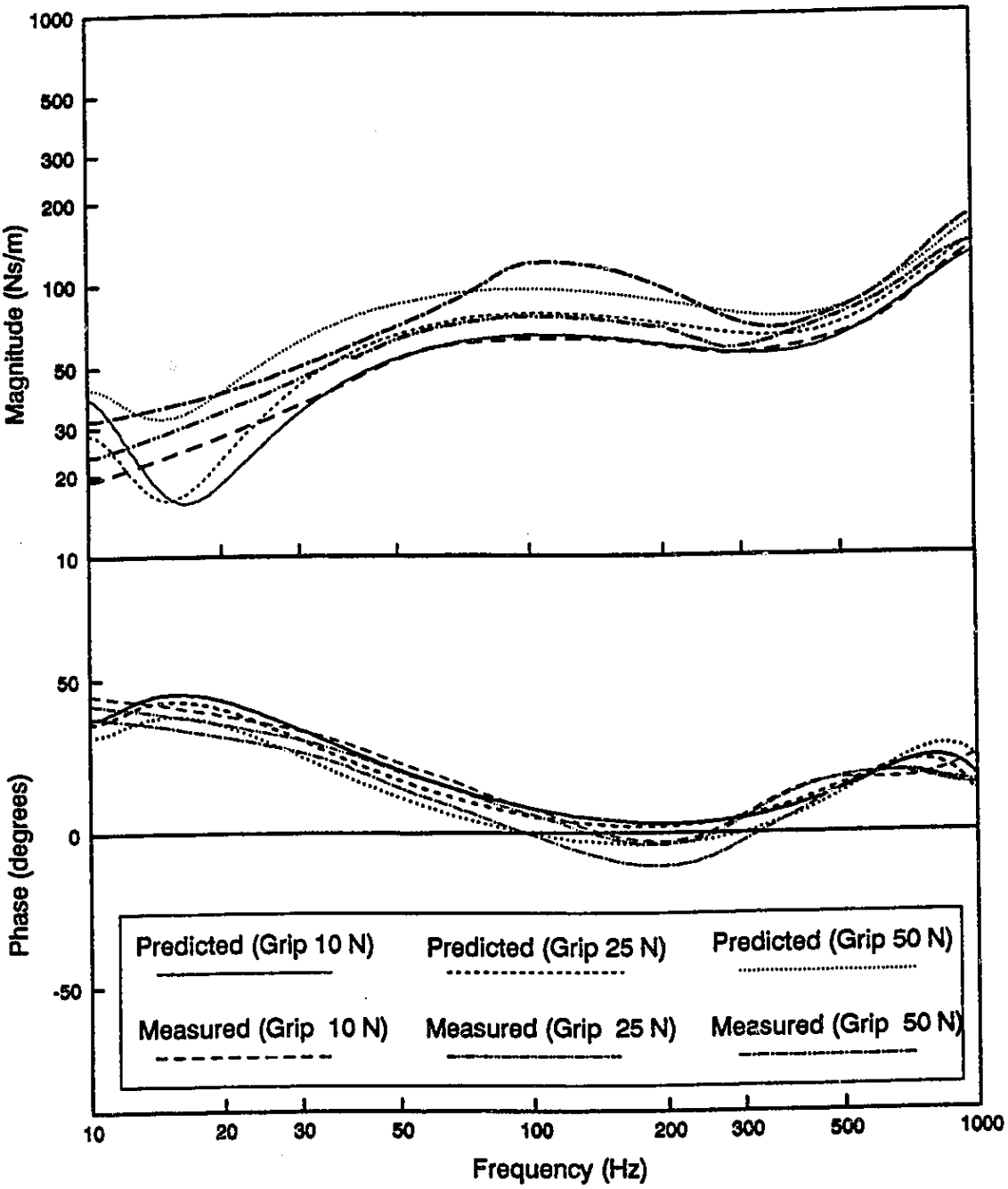

Figure 2.15: Measured and predicted values of mechanical impedance for three grip forces (Y_h- direction; 2.0 g peak acceleration).

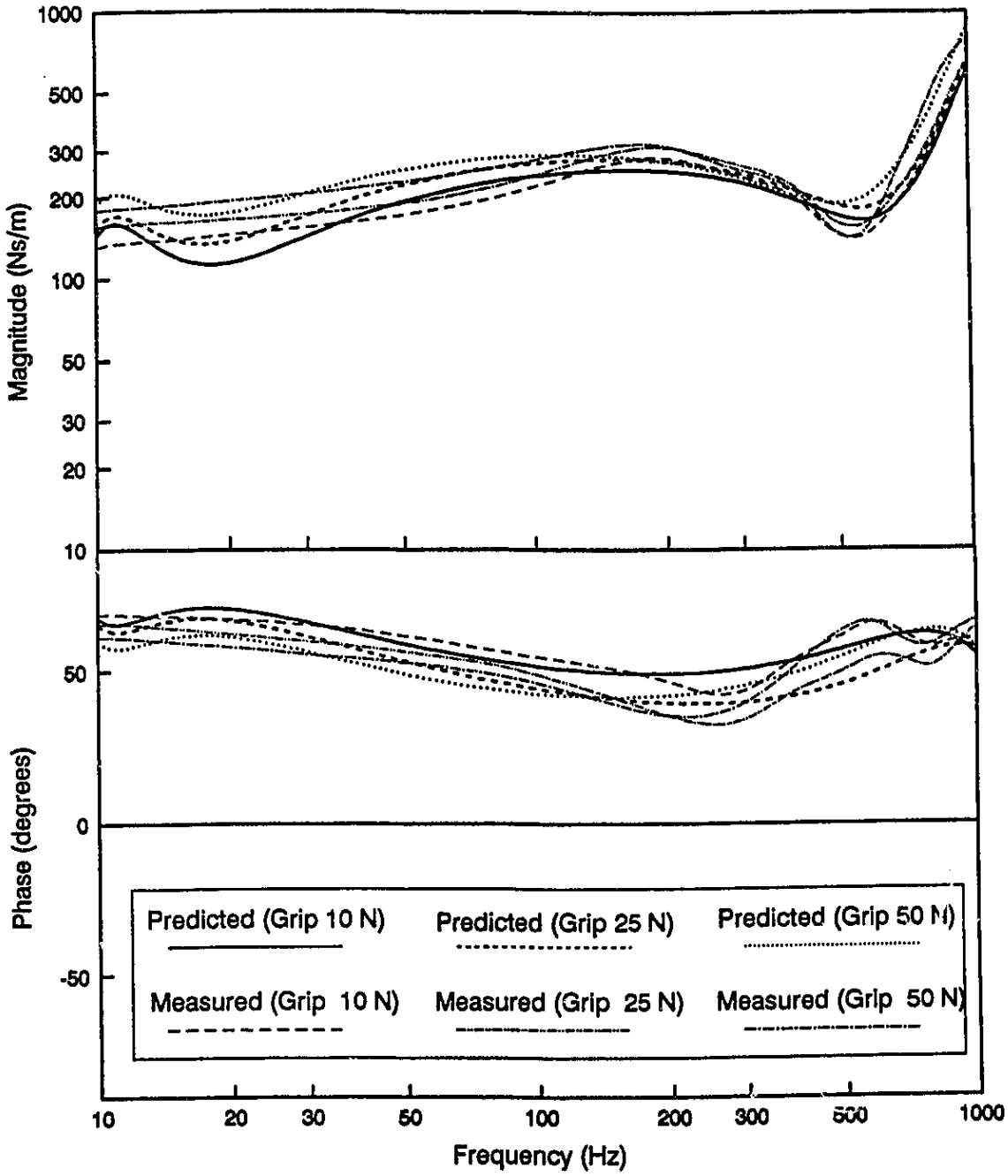

Figure 2.16: Measured and predicted values of mechanical impedance for three grip forces (Z_h- direction; 2.0 g peak acceleration).

(2.5) provide an accurate description of driving point impedance as a function of grip force and excitation frequency in the frequency range of 30 - 1000 Hz.

2.5 Summary

The biodynamic response of the human hand-arm system to sinusoidal and random vibrations is characterized in terms of driving point impedance. The driving point impedance characteristics are measured for various test conditions to determine the influence of grip force and nature of vibration on the response behavior of the hand-arm. While the intra-subject variations are observed to be less than 5 %, the results revealed high inter-subject variations. The impedance characteristics measured under different test variables revealed: (i) The effect of grip force and the excitation frequencies on the driving point impedance is significant (ii) the impedance measured under sinusoidal excitation exhibited similar patterns to that measured under random excitations. Regression analysis is performed to derive a describing function that relate impedance to the grip force and the excitation frequency. The driving point impedance characteristics obtained in this chapter are compared to the other published data in the literature in Chapter 4, and are used to develop analytical HAV models in the following chapter.

CHAPTER 3

DEVELOPMENT OF ANALYTICAL HAND-ARM VIBRATION MODELS

3.1 Introduction

The severe nature of hand-transmitted vibrations, considerable occupational exposure and the associated health hazards have all prompted many objective or subjective, experimental and analytical studies on dynamic characterization of the hand-arm system. Mechanical impedance characteristics of hand-arm system have been extensively measured to enhance an understanding of the biodynamic behavior, and to establish standards on safe vibration exposure levels. Few studies have utilized the measured data to develop linear hand-arm vibration (HAV) models (*Suggs et al., 1977*). The HAV models have been utilized to study the vibration characteristics of hand-tool system and to investigate vibration attenuation mechanisms (*Jahn et al., 1986*). Mechanical driving point impedance has been considered well suited to characterize the distributed hand-arm system with non-rigid masses. The mechanical impedance models, ranging from simple single degree-of-freedom (DOF) to many DOF with linear model parameters, have provided an insight to the effect of direction and magnitude of vibration, on the hand transmitted vibration (*Abrams, 1971; Reynolds et al., 1984).* These HAV models, invariably, are comprised of linear time invariant inertial, restoring and dissipative elements, such that convenient linear analytical tools may be implemented.

Many experimental studies have demonstrated nonlinear biodynamic response due to nonlinear visco-elastic properties of the hand-arm system (*Suggs et al., 1977*). Consequently, the linear HAV models can be considered valid in the vicinity of selected grip force, frequency range and vibration levels.

Upon recognizing the strong dependence of hand-arm system impedance on the grip force, a need to develop several linear HAV models has been identified, where each model is considered valid in the vicinity of a specific grip force in a given direction of vibration (*Reynolds et al., 1984; Mishoe et al., 1977*). Further, the derivation of a linear HAV model to fit the measured data in the broad frequency range of power tools vibration poses certain complexities. Since the HAV models are derived to achieve a compromise between the magnitude and phase errors between the measured and computed impedance data using trial and error based curve fit methods, these models fail to predict both the phase and magnitude accurately. Such trial and error methodology is extremely difficult to apply to nonlinear models. Alternatively, optimization algorithms can be effectively implemented to derive model parameters that can accurately predict the impedance characteristics in the entire frequency range.

In this chapter, a nonlinear programming based optimization technique is implemented to develop linear and nonlinear HAV models to achieve an improved compromise between the phase and magnitude errors. A local equivalent linearization technique, based upon the principle of energy similarity, is employed to analyze the nonlinear HAV models. An attempt is made to develop grip force dependent HAV models, such that a single analytical model may be used to describe the dynamic response of the hand-arm system under different levels of grip forces in a given direction of vibration excitation.

3.2 Development of Analytical Models

Research investigations conducted by *Suggs (1974)* and *Reynolds et al. (1977)* have established that the complex hand-arm system can be represented by a mass excited lumped parameter model, using either mechanical impedance

or compliance data. The validity of these models is demonstrated by their ability to predict driving point impedance magnitude as well as phase that correlate reasonably with the measured data for given operating conditions. In view of the wide frequency range of power tools vibration and complex visco-elastic properties of the hand-arm system, the accuracy of these models is directly related to the number of degrees-of-freedom (DOF) of the model. A baseline model, its DOF and parameters are often identified from the measured impedance data using the impedance relationships of pure mechanical elements. The model is then refined to fit the measured impedance data using trial and error based curve fit methods (*Reynolds et al., 1984; Mishoe et al., 1977*).

3.2.1 LINEAR HAV MODELS

Reynolds et al. (1984) proposed three- and four-DOF linear models of the hand-arm system, as shown in Figure 3.1. The model parameters were identified from the dynamic driving point compliance data (ratio of driving force to the displacement response measured near the driving point) in the frequency range 5-1000 Hz, using trial and error curve fitting techniques. The dynamic characteristics of linear models can be described by following coupled differential equations:

$$m_i\ddot{x}_i + F_{Ki} + F_{Di} = F_{Oi};\ \ i = 1,2,...,n \qquad (3.1)$$

where m_i are the masses, $\ddot{x}_i$ are the accelerations and n is the number of DOF. F_{Ki}, F_{Di} and F_{Oi} are restoring, dissipative and excitation forces, respectively

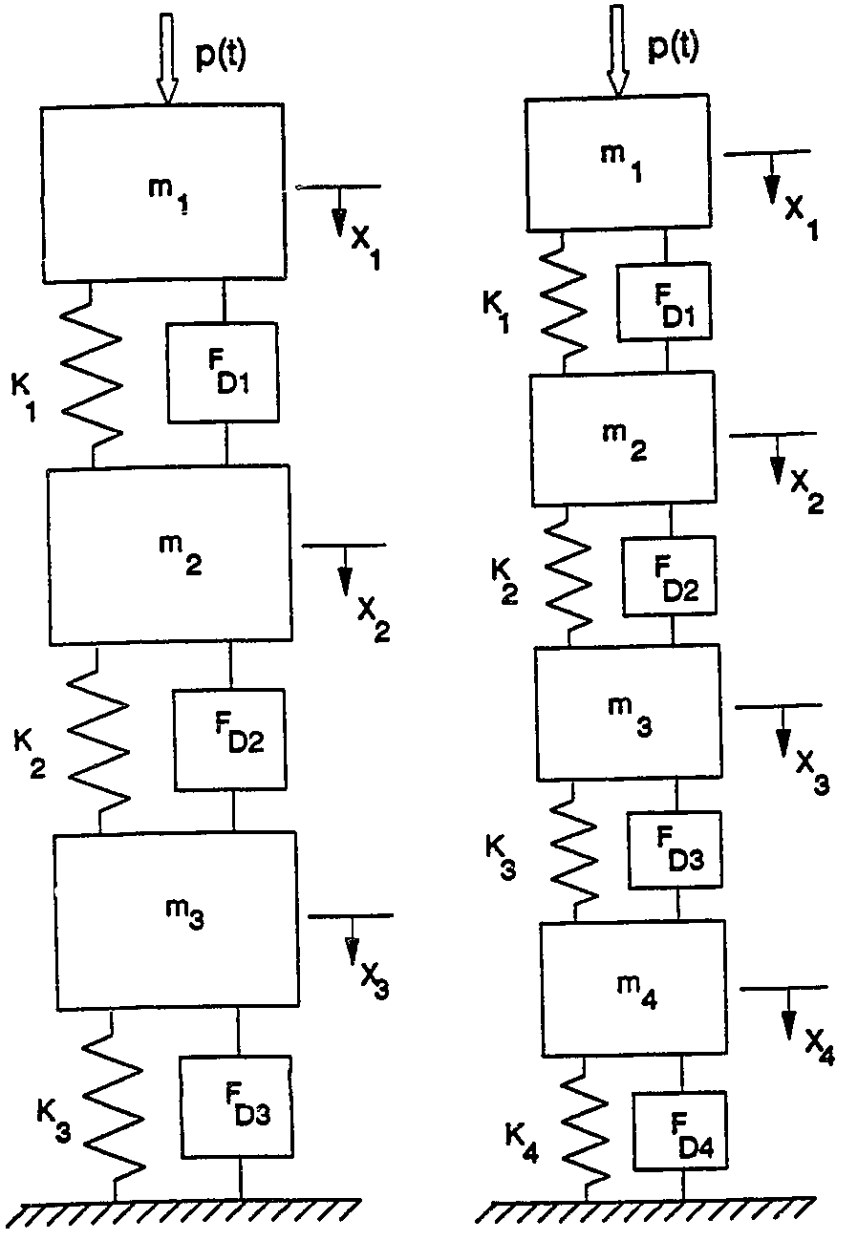

Figure 3.1: Three- and four- DOF models.

acting on mass i. Assuming linear stiffness and damping coefficients, the restoring and dissipative forces are expressed as:

$$F_{Ki} = \begin{cases} K_i(x_i - x_{i+1}); & i = 1 \\ K_{i-1}(x_i - x_{x-1}) + K_i(x_i - x_{i+1}); & i = 2,...,n-1 \\ K_{i-1}(x_i - x_{x-1}) + K_i(x_i); & i = n \end{cases} \tag{3.2}$$

$$F_{Di} = \begin{cases} C_i(\dot{x}_i - \dot{x}_{i+1}); & i = 1 \\ C_{i-1}(\dot{x}_i - \dot{x}_{x-1}) + C_i(\dot{x}_i - \dot{x}_{i+1}); & i = 2,...,n-1 \\ C_{i-1}(\dot{x}_i - \dot{x}_{x-1}) + C_i(\dot{x}_i); & i = n \end{cases} \tag{3.3}$$

$$F_{Oi} = 0; \quad i \neq 1 \qquad \text{and} \qquad F_{O1} = P(t) \tag{3.4}$$

where K_i and C_i are linear stiffness and damping coefficients identified from the measured data. Equations (3.1) to (3.4) may be expressed in the following matrix form:

$$[M]\{\ddot{q}\} + [C]\{\dot{q}\} + [K]\{q\} = \{p\} \tag{3.5}$$

where $[M]$, $[C]$ and $[K]$ are (nxn) mass, damping and stiffness matrices, respectively. $\{q\}$ is a (nx1) vector of displacement response quantities, $\{p\}$ is (nx1) excitation force vector, and '·' and '··' designate the first and second derivatives with respect to time. Fourier transform of equation (3.5) yields:

$$\{\mathbf{Q}(j\omega)\} = \left[[K] - \omega^2[M] + j\omega[C]\right]^{-1}\{\mathbf{P}(j\omega)\} \tag{3.6}$$

where $\{\mathbf{Q}\}$ and $\{\mathbf{P}\}$ are Fourier transforms of $\{q\}$ and $\{p\}$, respectively, and ω is the circular frequency. The vector $\{\mathbf{Q}(j\omega)\}$ contains the displacement response of n masses as a function of frequency, $\{\mathbf{X}_1(j\omega), \mathbf{X}_2(j\omega).....\}^T$, and $\{\mathbf{P}(j\omega)\}$ contains the excitation forces, $\{p(j\omega), 0, ...0\}^T$, where $p(j\omega)$ is the Fourier

transform of excitation force, $P(t)$. Driving point mechanical impedance is computed as the ratio of driving force to the driving point response velocity:

$$\mathbf{Z}(j\omega) = \frac{p(j\omega)}{j\omega \mathbf{X}_1(j\omega)} \tag{3.7}$$

Equations (3.6) and (3.7) clearly illustrate that driving point impedance of the hand arm vibration model, $\mathbf{Z}(j\omega)$, is a function of the model parameters (m_i, K_i, C_i), and excitation force and excitation frequency. The model parameters are selected such that the computed impedance correlates well with the measured data in both the magnitude and phase (*Suggs, 1974*).

3.2.2 Nonlinear HAV Models

Many studies have revealed that the biodynamic response of the hand-arm system is strongly related to the magnitude of the grip force and the vibration level (*Reynolds et al., 1984; Mishoe et al., 1977*). Such results imply a nonlinear biodynamic response characteristics for the hand-arm system, which may be attributed to its visco-elastic properties. Nonlinear HAV models, comprising of nonlinear inertial, restoring and dissipative mechanisms, may thus be developed to determine impedance characteristics of the hand-arm system for a broad range of operating conditions. The analysis of these nonlinear models in the frequency-domain, however, poses several complexities. In this study, attempts were made to develop three- and four- DOF HAV nonlinear models by incorporating nonlinear damping and stiffness properties. The dynamics of the nonlinear models may be described by the coupled differential equations of motion, presented in equation (3.1), where F_{Ki} and F_{Di} are nonlinear restoring and damping forces, respectively. The nonlinear damping force,, F_{Di}, acting on mass i is expressed as:

$$\begin{aligned} F_{Di} &= D_i - D_{i+1}; \quad \text{for} \quad i = 1,.....,n-1 \\ F_{Di} &= D_n; \qquad\quad \text{for} \quad i = n \end{aligned} \tag{3.8}$$

where D_i is the nonlinear damping force developed by the damper i. The nonlinear damping force is considered as a composite function of friction, viscous and quadratic damping in the following manner:

$$D_i = c_{0i} sgn(\dot{z}_i) + c_{1i}\dot{z}_i + c_{2i}\dot{z}_i^2 sgn(\dot{z}_i); \quad i = 1,.....,n \tag{3.9}$$

where $\dot{z}_i$ is the relative velocity across the damping element i, given by:

$$\begin{aligned} \dot{z}_i &= \dot{x}_i - \dot{x}_{i+1}; \quad \text{for} \quad i = 1,.....,n \\ \dot{z}_n &= \dot{x}_n; \qquad\quad \text{for} \quad i = n \end{aligned} \tag{3.10}$$

c_{0i}, c_{1i}, and c_{2i} are the nonlinear coefficients representing friction, viscous and quadratic damping mechanisms, respectively. The function sgn is used to ensure that the damping force remains in phase with the relative velocity, and is given by:

$$sgn(\bullet) = \begin{cases} 1; & \text{for } (\bullet) > 0 \\ -1; & \text{for } (\bullet) < 0 \end{cases} \tag{3.11}$$

The nonlinear restoring forces acting on mass i are represented as:

$$\begin{aligned} F_{Ki} &= \beta_i - \beta_{i+1}; \quad \text{for} \quad i = 1,.....,n-1 \\ F_{Ki} &= \beta_n; \qquad\quad \text{for} \quad i = n \end{aligned} \tag{3.12}$$

where β_i is the nonlinear spring force developed by the spring i . The nonlinear spring force is considered as a cubic function of the displacement z_i as shown below:

$$\beta_i = K_{1i} z_i + K_{2i} z_i^3; \quad i = 1,.....,n \tag{3.13}$$

where K_{1i} and K_{2i} represent the constant coefficients due to linear and cubic spring mechanisms, respectively.

Equations (3.1), (3.8) and (3.12) yield n nonlinear and coupled differential equations describing the dynamic characteristics of an n-DOF HAV model with nonlinear damping and stiffness properties. Since the linear models can be solved economically and conveniently in the frequency-domain, many equivalent linearization techniques have been proposed to derive equivalent linear models of the nonlinear models (*Roberts, 1981*). The linearization techniques are employed to express nonlinear elements by their linear equivalent, such that the response characteristics of the linearized model do not deviate significantly from that of the nonlinear one.

3.2.3 LINEARIZATION OF NONLINEAR HAV MODELS

A local equivalent linearization technique based on the principle of energy similarity is employed to derive equivalent linear HAV models (*Rakheja et al., 1985*). The validity of this technique has been demonstrated through extensive simulations of different types of nonlinear vehicle suspensions. The technique expresses nonlinear damping and spring mechanisms by arrays of locally equivalent damping and spring constants as a function of excitation frequency and amplitude, where each constant is considered valid in the vicinity of a selected excitation frequency and amplitude. The nonlinear system is thus

described by an array of local equivalent linear systems. The nonlinear response is estimated through solution of several local equivalent linear systems, such that the response can be accurately predicted in the entire frequency range.

DETERMINATION OF LOCAL EQUIVALENT DAMPING CONSTANTS

The nonlinear damping forces are expressed in terms of the local equivalent damping coefficients, $C_i^e(\omega_k)$, such that the equivalent linear force describes the nonlinear force in the vicinity of the local frequency ω_k:

$$D_i \approx C_i^e(\omega_k)\dot{z}_i; \quad i = 1,.....n \tag{3.14}$$

where ω_k (for $k = 1,....l$) is the local excitation frequency, and l is the number of discrete frequencies considered in the study. Upon substituting C_i^e as C_i in equation (3.3), the nonlinear dissipative force in equation (3.8) can be expressed by the linear equivalent damping force as a function of the local excitation frequency. The local equivalent damping coefficients are derived by balancing the energy dissipated by the nonlinear damper during a vibration cycle to that of a viscous damper for selected local excitation frequency and magnitude. Energy dissipated by the nonlinear damper during a cycle, described in equation (3.10), is expressed as (*Thomson, 1965*):

$$\Delta E_i(\omega_k) = \oint D_i dz; \quad i = 1,.....,n \quad \text{and} \quad k = 1,.....,l \tag{3.15}$$

where $\Delta E_i(\omega_k)$ is the energy dissipated by damper i corresponding to excitation frequency ω_k . The solution of integral yields the following expression for energy dissipated by damper D_i *(Rakheja et al., 1986)*:

$$\Delta E_i(\omega_k) = 4c_{0i}Z_i + \Pi c_{1i}\omega_k Z_i^2 + \frac{8}{3}c_{2i}\omega_k^2 Z_i^3 \tag{3.16}$$

where Z_i is the magnitude of relative displacement response across the nonlinear damper i . The local equivalent damping coefficient is computed by balancing ΔE_i to the energy dissipated by a linear damper, $\Pi C_i^e(\omega_k)Z_i^2$:

$$C_i^e(\omega_k) = \frac{4c_{0i}}{\Pi\omega_k Z_i} + c_{1i} + \frac{8}{3\Pi}c_{2i}\omega_k Z_i; \quad i = 1,.....,n \quad \text{and} \quad k = 1,.....,l \tag{3.17}$$

Equation (3.17) reveals that the local equivalent damping coefficients are related to the local excitation frequency, ω_k and the corresponding relative displacement response, Z_i .

DETERMINATION OF LOCAL EQUIVALENT STIFFNESS CONSTANTS

Nonlinear restoring forces are characterized by an array of local equivalent stiffness coefficients, where each coefficient is considered valid in the vicinity of a selected excitation frequency and amplitude. The nonlinear spring forces are expressed in terms of the local equivalent spring coefficients, $K_i^e(\omega_k)$, in the following manner:

$$\beta_i \approx K_i^e(\omega_k)Z_i; \quad i = 1,.....,n \tag{3.18}$$

The local equivalent spring coefficients are derived by balancing the energy processed by the nonlinear spring during a vibration cycle to that of a linear spring for a selected local excitation frequency and magnitude. Energy processed by the nonlinear spring during a cycle, is defined as the sum of absolute values of energy stored and released by the spring during a cycle:

$$\delta E_i(\omega_k) = 4\int_0^Z \beta_i dZ; \quad i = 1,. \ldots,n \tag{3.19}$$

where $\delta E_i(\omega_k)$ is the energy processed by spring i corresponding to excitation frequency ω_k. Upon substituting for the nonlinear restoring force from (3.13) and solution of integral yields the following expression for energy processed during a cycle:

$$\delta E_i(\omega_k) = 2K_{1i}Z_i^2 + K_{2i}Z_i^4; \quad i = 1,\ldots\ldots,n \tag{3.20}$$

The local equivalent spring coefficients are then computed by balancing δE_i to the energy processed by a linear spring, $2K_i^e(\omega_k)Z_i^2$.

$$K_i^e(\omega_k) = K_{1i} + \frac{1}{2}K_{2i}Z_i^2; \quad i = 1,\ldots\ldots,n \tag{3.21}$$

Equations (3.18) and (3.21) reveal that determination of the local equivalent constants necessitates a prior knowledge of relative displacement response, Z at every local excitation frequency. An iterative algorithm is thus employed to determine the local equivalent coefficients (*Rakheja et al., 1986*). The algorithm initially assumes values of local equivalent coefficients, $C_i^e(\omega_k)$ and $K_i^e(\omega_k)$, at

a selected excitation frequency, to formulate the linear system of equations. The linear equations are then solved in the frequency domain to determine the relative displacement response Z_i. The equivalent stiffness and damping coefficients are then computed using Equations (3.21) and (3.17) respectively. The errors between the assumed and computed values are determined. The assumed values are updated and the iterative procedure is repeated until convergence is achieved. The algorithm is repeated for each discrete frequency of excitation to derive the nonlinear system's response in the entire frequency range.

3.3 Development of Grip Force Dependent HAV Models

The driving point impedance characteristics of the human hand-arm characteristics, measured in Chapter 2, revealed a strong dependence of the impedance on the grip force and excitation frequency. While the linear, piece-wise linear and nonlinear HAV models can be used to describe the frequency dependence of the impedance, those models do not characterize the grip force dependence of the impedance. The linear and nonlinear models can thus yield the biodynamic response for a selected grip force only. Different models are often derived to characterize the biodynamic response of the hand-arm for different magnitudes of grip force (*Mishoe et al., 1977*). Alternatively, a grip force dependent analytical model may be derived to determine the biodynamic response characteristics of the hand-arm for a particular range of grip forces. A grip force dependent model is derived upon expressing the restoring and dissipative properties of the hand-arm as functions of the grip force, excitation frequency and amplitude of excitation.

The strong influence of the grip force on the biodynamic response of the hand-arm may be characterized by incorporating grip force dependent components of the restoring and dissipative forces. The change in blood flow and muscle tensions may be related to the variations in visco-elastic properties. The grip force dependent components of the restoring and damping forces are assumed by the following function of the grip force:

$$\begin{aligned} \beta(F_g) &= K_G F_g Z \\ D(F_g) &= C_G F_g \dot{Z} \end{aligned} \tag{3.22}$$

Where $\beta(F_g)$ and $D(F_g)$ are grip force dependent components of the restoring and dissipative forces. K_G and C_G are constants, and may be referred to as stiffness coefficient per unit grip force and viscus damping coefficient per unit grip force respectively. The term F_g represents the amount of grip force applied. The grip force dependent components, described in equation (3.22) are investigated to both the linear and nonlinear HAV models, presented in sections 3.2.1 and 3.2.2.

3.3.1 LINEAR HAV MODEL WITH GRIP FORCE DEPENDENT RESTORING AND DISSIPATIVE FORCES.

The restoring and dissipative forces acting on mass m_i of the linear HAV model are obtained by integrating equation (3.22) in equation (3.2) and equation (3.3) such that:

$$\begin{aligned} \beta_i &= (K_i + K_{Gi} F_g) Z_i \\ D_i &= (C_i + C_{Gi} F_g) \dot{Z}_i; \quad i = 1,.....,n \end{aligned} \tag{3.23}$$

where β_i and D_i are the total restoring and dissipative forces acting on mass i, respectively. K_i and C_i are the linear stiffness and damping coefficients. The equations of motion of the linear HAV model comprising grip force dependent visco-elastic forces are then obtained from equations (3.1) and (3.23).

3.3.2 NONLINEAR HAV MODEL WITH GRIP FORCE DEPENDENT RESTORING AND DISSIPATIVE FORCES.

The total restoring and dissipative forces acting on mass m_i of the nonlinear model are obtained upon combining equation (3.22) with equations (3.9) and (3.13) as shown below:

$$\beta_i = (K_{1i}z_i + K_{2i}z_i^3) + K_{Gi}F_g Z_i$$
$$D_i = \{c_{0i}sgn(\dot{z}_i) + c_{1i}\dot{z}_i + c_{2i}\dot{z}_i^2 sgn(\dot{z}_i)\} + C_{Gi}F_g\dot{Z}_i;\ \ i = 1,.....,n \qquad (3.24)$$

The nonlinear differential equation of the HAV model comprising grip force dependent components of restoring and dissipative forces can be derived upon combining equations (3.1), (3.8), (3.12) and (3.24). The nonlinear damping and restoring forces, described in (3.24), are expressed by their linear equivalent forces using the method discussed in section 3.2.3 to obtain the local equivalent

$$\beta_i(\omega_k) \approx \mathbf{K}_i^e(\omega_k)Z_i$$
$$D_i(\omega_k) \approx \mathbf{C}_i^e(\omega_k)\dot{z}_i;\ \ i = 1,.....,n \ \text{ and } \ \ k = 1,.....,l$$

where $\mathbf{K}_i^e(\omega_k)$ and $\mathbf{C}_i^e(\omega_k)$ are the local equivalent stiffness and damping coefficients due to nonlinear forces expressed as:

$$\mathbf{K}_i^e(\omega_k) = K_i^e(\omega_k) + K_{Gi}F_g$$

$$\mathbf{C}_i^e(\omega_k) = C_i^e(\omega_k) + C_{Gi}\,\mathrm{F_g}\ ; \quad i = 1,.....,n \quad \text{and} \quad k = 1,....l \tag{3.25}$$

Equation (3.24) and (3.25), together with (3.1) to (3.3), yield a system of local equivalent linear differential equation, which may be solved using the convenient frequency-domain technique.

3.4 Determination of Linear and Nonlinear Model Parameters

The model parameters of the analytical models of the hand-arm are often derived using trial and error based curve fitting techniques, such that the error between the computed and measured impedance characteristics in both the magnitude and phase is minimum (*Reynolds et al., 1984*). Such methods lead to a poor fit when broad frequency range is considered. Further the application of trial and error methods for determination of nonlinear model parameters may pose complexities. Alternatively, nonlinear programming based optimization techniques may be effectively employed to determine the parameters of linear and nonlinear models. The linear and nonlinear HAV model parameters are determined using a constrained optimization algorithm in conjunction with the mean values of human hand-arm impedance. A constrained objective function, based on the magnitude error in the entire frequency range, is formulated in the following manner:

$$U(\overline{\chi}) = Minimize\left[\sum_{k=1}^{l}\left\{|Z(\omega_k)| - |Z_m(\omega_k)|\right\}^2\right]; \quad \text{for} \quad \omega_\ell \le \omega_k \le \omega_u \tag{3.26}$$

where $U(\overline{\chi})$ is the objective function to be minimized, and $|Z(\omega_k)|$ and $|Z_m(\omega_k)|$ are magnitudes of the computed and measured impedances corresponding to

excitation frequency ω_k, respectively. ω_l and ω_u are the lower and upper limits of the frequency range considered, and $\overline{\chi}$ is a vector of model parameters, given by:

Linear HAV Model:

$$\overline{\chi} = \{m_i, K_i, C_i\}^T \quad \text{for} \quad i = 1,.....,n$$

Linear HAV Model with Grip Force Dependent Parameters:

$$\overline{\chi} = \{m_i, K_i, K_{Gi}, C_i, C_{Gi}\}^T \quad \text{for} \quad i = 1,.....,n$$

Nonlinear HAV Models:

$$\overline{\chi} = \{m_i, K_{1i}, K_{2i}, C_{0i}, C_{1i}, C_{2i}\}^T \quad \text{for} \quad i = 1,.....,n$$

Nonlinear HAV Model with Grip Force Dependent Parameters:

$$\overline{\chi} = \{m_i, K_{1i}, K_{2i}, K_{Gi}, C_{0i}, C_{1i}, C_{2i}, C_{Gi}\}^T \quad \text{for} \quad i = 1,.....,n$$

where 'T' designates the transpose. The objective function described in equation (3.26) is subject to the following constraints:

$$\begin{aligned} & m_i > 0 \\ & K_i, K_{1i}, K_{2i}, K_{Gi} > 0 \\ & C_{0i}, C_i, C_{1i}, C_{2i}, C_{Gi} > 0 \\ & 3.5 < \sum_i^n m_i < 6.0 \end{aligned} \tag{3.27}$$

The total mass of the model is constrained to be within the range of mean values of the human hand-arm system (*Chaffin et al., 1984*). The optimization is performed to minimize the magnitude error function at several discrete frequencies in 10 - 1000 Hz range. An optimization software, NCONF, based upon the sequential search (*IMSL, 1988; Schittkowski, 1986*) is employed to determine the model parameters of three- and four-DOF linear and non-linear hand-arm models, shown in Figure 3.1. The equation of motion for the linear HAV models are solved and the driving point impedance is computed using equation (3.7), at each discrete frequency. The equation of motion of the nonlinear HAV models are solved using the local equivalent algorithm described in section 3.2.3 to yield the driving point impedance at each discrete frequency. The optimization function is then formulated by summing the squares of error between the computed and measured impedance at each frequency. The sum of squared phase errors in the entire frequency range is examined at each sequence of search, and the procedure is re-initiated when computed phase error exceeds the value corresponding to previous search:

$$\{E_\varphi\}_\eta > \{E_\varphi\}_{\eta-1} \tag{3.28}$$

where, η and $\eta-1$ correspond to current and previous search, E_φ is sum of squared phase errors in the entire frequency range, given by:

$$E_\varphi = \sum_{k=1}^{l} [\varphi(\omega_k) - \varphi_m(\omega_k)]^2 \tag{3.29}$$

where $\varphi(\omega_k)$ and $\varphi_m(\omega_k)$ are computed and measured phase angles corresponding to excitation frequency ω_k . The search is terminated when both magnitude and phase errors approach the minimum values. In all the cases, optimization is performed many times using different starting values, and majority of the attempts converged to a unique set of model parameters.

3.5 Results and Discussion

The parameters of linear and nonlinear HAV models in three uncoupled orthogonal directions are derived using the measured impedance data, presented in Chapter 2. The mean impedance characteristics corresponding to 25 N grip force and swept sine vibrations of 1.0, 2.0 g and 3.0 g (presented in Table A19, Appendix - I) are considered as target values. The measured impedance characteristics reveal that the biodynamic response of the hand-arm system is similar to that of pure mechanical elements in three frequency zones, independent of the direction of vibration. For a majority of the test variables considered in the study, the response behavior at frequencies below 150 Hz is close to that of a pure mass, and the response is similar to spring in the 250 - 350 Hz frequency range. The biodynamic response at frequencies above is again similar to that of a mass, at frequencies above 500 Hz. Three DOF hand-arm models in all the three directions, assuming negligible coupling, are thus derived to characterize the HAV system response. Four DOF linear models and nonlinear models are, subsequently, attempted to achieve a better correlation with the measured data. The driving point impedance of all the models is computed from the equations (3.6) and (3.7), in conjunction with the optimization algorithm. The objective function is computed at 32 discrete frequencies in the 10 - 1000 Hz range. The impedance response characteristics of nonlinear HAV models are evaluated for constant amplitude force excitation. The magnitude of

the excitation force is selected as 25 N, which represents the approximate mean value observed from the measured data.

3.5.1 RESPONSE OF LINEAR AND NONLINEAR MODELS

The driving point impedance characteristics of the three- and four- DOF linear and nonlinear hand-arm models are compared to those established from the measurements (Table A19, Appendix - I) in X_h-, Y_h- and Z_h- directions as shown in Figures 3.2 to 3.4, respectively. The results in general, show a reasonable agreement between the computed and measured values. The optimal parameters, derived through solution of the constrained optimization problem, for X_h-, Y_h- and Z_h- directions are presented in Table 3.1 - 3.3, respectively. A comparison of the model response with the measured response in three directions of vibration reveals magnitude errors of frequencies below 100 Hz. The error between the magnitudes of the models and measured response is considerably low at high frequencies. The impedance phase response characteristics of the linear and nonlinear models correlated with the measured response in all the directions. The error between the model response and the measured values, along the Z_h- direction is relatively large as shown in Figure 3.4. Peak values of errors between the computed and measured impedance magnitude and phase data are summarized in Table 3.4. In X_h- direction the three-DOF linear model yields the peak magnitude and phase errors of 77 Ns/m and 16 degrees, respectively. The magnitude and phase errors of four-DOF model reduce to 76 Ns/m and 14 degrees, respectively. Both the nonlinear models yield identical values of peak magnitude and phase errors of 76 Ns/m and 13 degrees, respectively. The peak percent error in impedance magnitude is observed at an excitation frequency of 30 Hz.

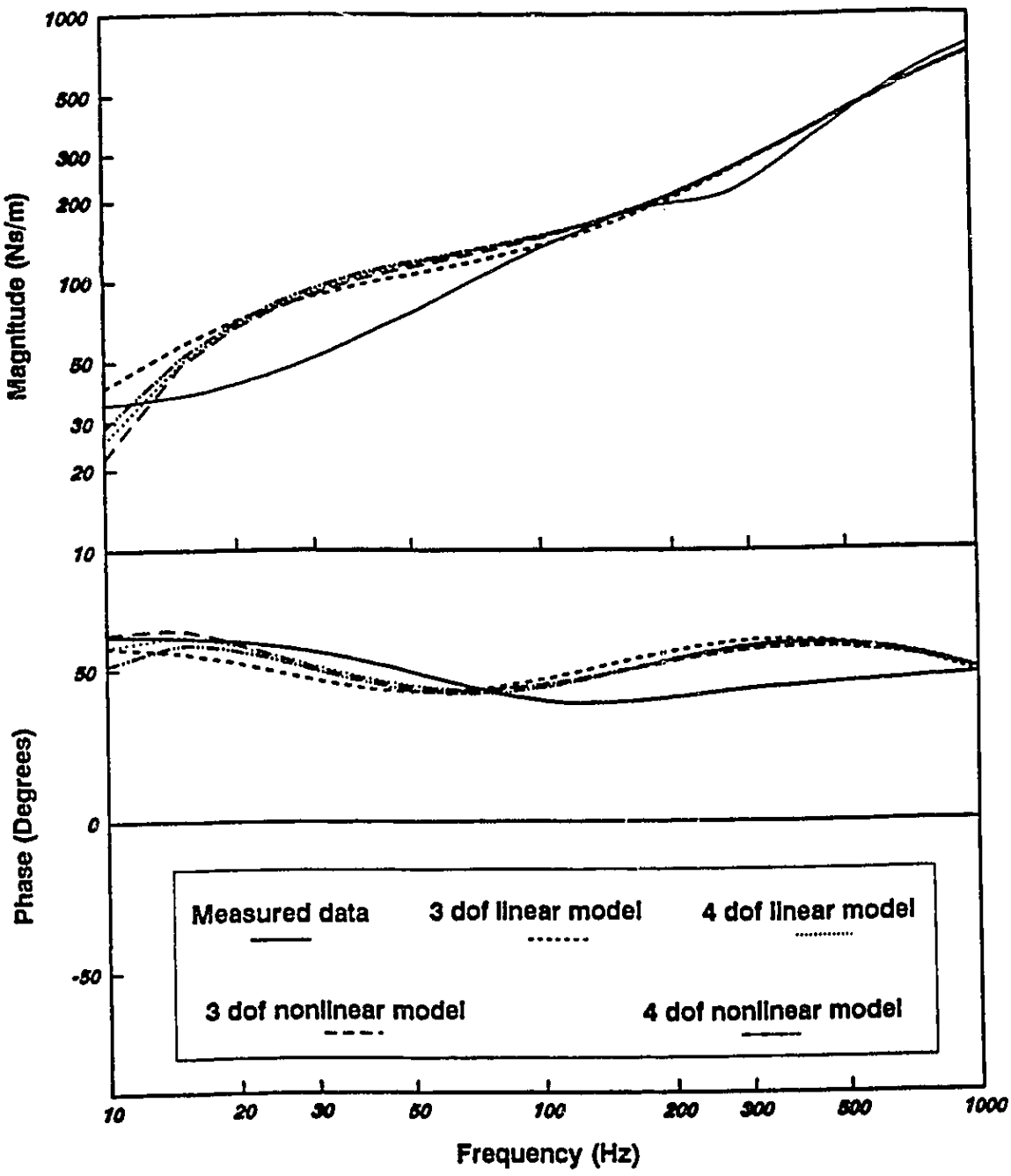

Figure 3.2: Measured and model responses compared (X_h- direction).

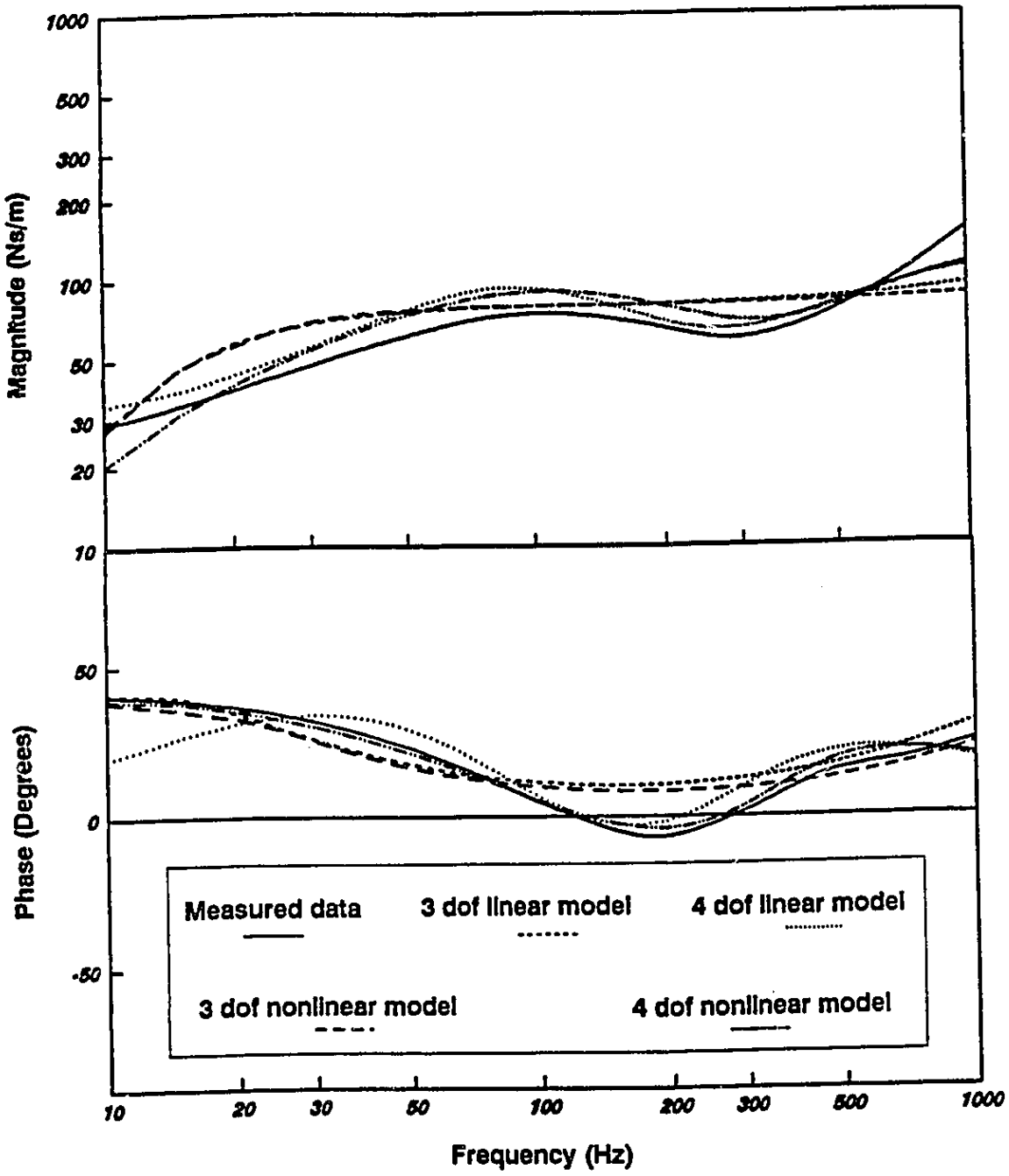

Figure 3.3: Measured and model responses compared (Y_h- direction).

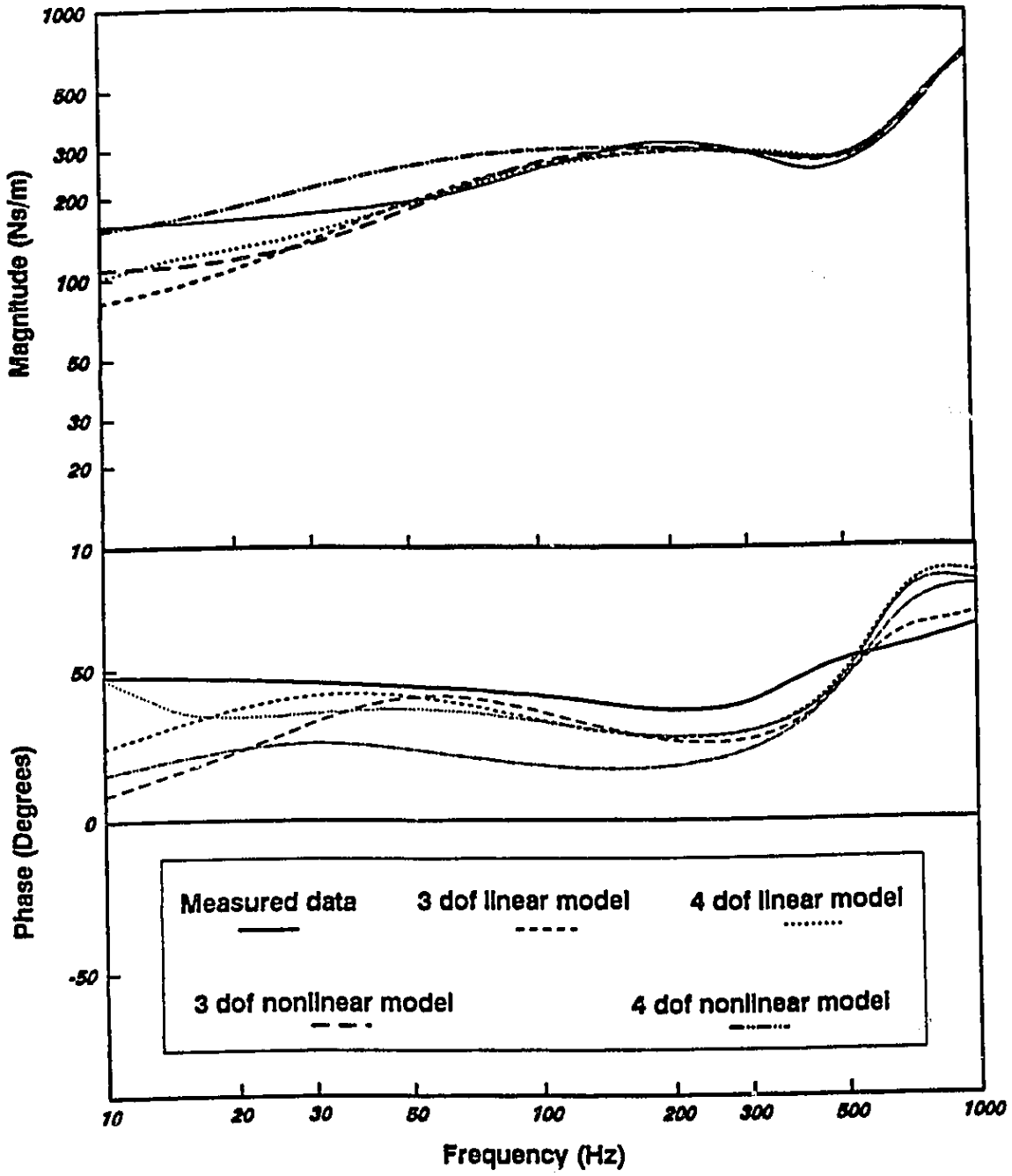

Figure 3.4: Measured and model responses compared (Z_h- direction).

TABLE 3.1
Linear and Nonlinear Model Parameters (X_h - Direction)

Model	Linear		Nonlinear	
Parameters	3 - D.O.F.	4 - D.O.F	3 - D.O.F.	4 - D.O.F.
m_1 (kg)	1.00E-05	1.00E-05	1.00-05	1.00E-05
m_2	1.69E-01	1.48E-01	1.63E-01	1.43E-01
m_3	4.10E 00	5.49E-01	3.51E 00	6.19E-01
m_4	———	3.00E 00	——	2.80E 00
K_1 or $\begin{Bmatrix} k_{11} \\ k_{21} \end{Bmatrix}^*$ (N/m)	1.00E+02	1.05E+05	1.00E+01 5.98E+04	4.87E+05 9.11E+04
K_2 or $\begin{Bmatrix} k_{12} \\ k_{22} \end{Bmatrix}^*$	1.00E+02	9.20E+02	1.00E+02 5.94E+04	1.00E+03 9.22E+01
K_3 or $\begin{Bmatrix} k_{13} \\ k_{23} \end{Bmatrix}^*$	8.79E+05	1.36E+03	1.00E+04 5.90E+04	1.26E+03 5.22E+02
K_4 or $\begin{Bmatrix} k_{14} \\ k_{24} \end{Bmatrix}^*$	--------	1.13E+06	------	1.39E+06 5.00E+03
C_1 or $\begin{Bmatrix} c_{01} \\ c_{11} \\ c_{21} \end{Bmatrix}^*$ (Ns/m)	9.30E+02	1.29E+03	1.00E-05 1.04E+03 3.91E+03	1.13E-01 1.29E+05 8.30E+02
C_2 or $\begin{Bmatrix} c_{02} \\ c_{12} \\ c_{22} \end{Bmatrix}^*$	3.70E+01	1.15E+02	2.20E-03 6.70E+01 1.00E-05	8.30E-02 1.03E+03 1.73E+01
C_3 or $\begin{Bmatrix} c_{03} \\ c_{13} \\ c_{23} \end{Bmatrix}^*$	1.00E+01	1.21E+01	4.13E-03 3.70E 00 1.00E-03	4.30E-01 1.10E+01 1.00E+01
C_4 or $\begin{Bmatrix} c_{04} \\ c_{14} \\ c_{24} \end{Bmatrix}^*$	------	2.72E+03	----------	2.70E-02 2.72E+03 5.63E+02

* NONLINEAR PARAMETERS

TABLE 3.2
Linear and Nonlinear Model Parameters (Y_h - Direction)

Model	Linear		Nonlinear	
Parameters	3 - D.O.F.	4 - D.O.F	3 - D.O.F.	4 - D.O.F.
m_1 (kg)	7.30E-03	1.00E-05	5.20E-03	5.20E-04
m_2	8.71E-01	5.06E-02	8.65E-01	5.09E-02
m_3	2.78E 00	3.04E-01	2.87E 00	3.54E-01
m_4	--------	4.00E 00	--------	3.20E 00
K_1 or $\begin{Bmatrix} k_{11} \\ k_{21} \end{Bmatrix}^*$ (N/m)	2.18E+02	1.00E+02	4.00E+01 1.64E+06	1.38E+03 7.98E+04
K_2 or $\begin{Bmatrix} k_{12} \\ k_{22} \end{Bmatrix}^*$	1.65E+03	1.23E+05	2.01E+03 5.68E+05	1.83E+05 1.00E+01
K_3 or $\begin{Bmatrix} k_{13} \\ k_{23} \end{Bmatrix}^*$	2.38E+03	1.00E+02	1.19E+04 2.82E+05	1.00E+02 7.62E+04
K_4 or $\begin{Bmatrix} k_{14} \\ k_{24} \end{Bmatrix}^*$	----------	1.07E+06	---------	1.95E+05 8.65E+04
C_1 or $\begin{Bmatrix} c_{01} \\ c_{11} \\ c_{21} \end{Bmatrix}^*$ (Ns/m)	8.00E+01	1.27E+02	3.80E-01 7.30E+01 1.30E+01	1.82E 00 1.10E+02 1.30E+01
C_2 or $\begin{Bmatrix} c_{02} \\ c_{12} \\ c_{22} \end{Bmatrix}^*$	1.90E+01	9.90E+01	2.15E-01 1.70E+01 3.50E-01	2.49E-01 1.10E+02 3.70E 00
C_3 or $\begin{Bmatrix} c_{03} \\ c_{13} \\ c_{23} \end{Bmatrix}^*$	8.16E+03	3.90E+01	1.75E-02 1.40E+02 2.31E 00	4.90E-01 1.40E+01 1.00E-03
C_4 or $\begin{Bmatrix} c_{04} \\ c_{14} \\ c_{24} \end{Bmatrix}^*$	--------	1.47E+03	----------	3.50E-01 3.64E+03 4.80E-01

* NONLINEAR PARAMETERS

TABLE 3.3
Linear and Nonlinear Model Parameters (Z_h - Direction)

Model	Linear		Nonlinear	
Parameters	3 - D.O.F.	4 - D.O.F	3 - D.O.F.	4 - D.O.F.
m_1 (kg)	9.60E-02	9.30E-02	8.80E-02	9.50E-02
m_2	1.15E-01	8.26E-02	1.45E-01	6.64E-02
m_3	3.51E 00	7.04E-01	3.50E 00	1.00E 00
m_4	——	3.23E 00	———	3.47E 00
K_1 or $\begin{Bmatrix} k_{11} \\ k_{21} \end{Bmatrix}^*$ (N/m)	1.00E+02	1.87E+03	1.00E+03 1.59E+04	4.32E+04 2.26E+03
K_2 or $\begin{Bmatrix} k_{12} \\ k_{22} \end{Bmatrix}^*$	2.83E+06	1.67E+06	3.54E+06 1.07E+05	1.67E+06 3.08E+04
K_3 or $\begin{Bmatrix} k_{13} \\ k_{23} \end{Bmatrix}^*$	5.08E+03	1.31E+02	4.15E+03 3.66E-01	1.00E+02 3.04E+04
K_4 or $\begin{Bmatrix} k_{14} \\ k_{24} \end{Bmatrix}^*$	———	6.44E+03	———	1.40E+06 9.09E+04
C_1 or $\begin{Bmatrix} c_{01} \\ c_{11} \\ c_{21} \end{Bmatrix}^*$ (Ns/m)	2.34E+02	2.81E+02	1.00E-05 1.04E+03 3.91E+03	1.06E 00 2.83E+02 2.90E+01
C_2 or $\begin{Bmatrix} c_{02} \\ c_{12} \\ c_{22} \end{Bmatrix}^*$	7.40E+01	1.06E+02	2.20E-03 6.70E+01 1.00E-05	1.04E 00 1.11E+02 1.23E+02
C_3 or $\begin{Bmatrix} c_{03} \\ c_{13} \\ c_{23} \end{Bmatrix}^*$	7.90E+01	1.31E+02	4.13E-03 3.70E 00 1.00E-03	6.90E-01 1.34E+02 8.44E 00
C_4 or $\begin{Bmatrix} c_{04} \\ c_{14} \\ c_{24} \end{Bmatrix}^*$	———	1.30E+01	———	3.70E 00 3.74E.03 9.00E+01

* NONLINEAR PARAMETERS

TABLE 3.4
Peak Values of Errors Between the Model Response and the Measured Data

Direction	Type of Model		Peak Magnitude Error (Ns/m)	Frequency (Hz)	Peak Phase Error (Degrees)	Frequency (Hz)
X_h	Linear	3 - DOF	77	1000	16	315
		4 - DOF	76	315	14	315
	Non-linear	3 - DOF	76	315	13	315
		4 - DOF	76	315	13	315
Y_h	Linear	3 - DOF	62	1000	20	200
		4 - DOF	47	1000	21	10
	Non-linear	3 - DOF	69	1000	17	200
		4 - DOF	44	1000	05	200
Z_h	Linear	3 - DOF	75	10	24	10
		4 - DOF	71	1000	21	800
	Non-linear	3 - DOF	61	500	39	10
		4 - DOF	75	1000	32	10

In Y_h- direction, all models yield maximum error in impedance magnitude at 1000 Hz excitation frequency. Excessive deviations between the measured and model phase response are observed near 200 Hz frequency. The peak impedance (magnitude, phase) errors of three-and four- DOF linear models are 62 Ns/m, 20 degrees and 47 Ns/m, 21 degrees, respectively. The four- DOF nonlinear model yield smallest peak errors in magnitude (44 Ns/m) and phase (5 degrees). The peak percentage error in magnitude is observed to be highest in the neighborhood of 20 Hz, while the maximum percent error in phase occurs near 125 Hz. In the Z_h- direction the peak magnitude errors occur either at low excitation frequencies (below 20 Hz) at very high excitation frequencies (above 500 Hz). The peak percentage error is high at low frequencies (below 20 Hz). The proposed models in Z_h - direction have peak errors of (75 Ns/m, 24

degrees) and (71 Ns/m,21 degrees), corresponding to 3 -DOF and 4 -DOF linear models. The nonlinear three - and four- DOF models have yielded errors of (61 Ns/m , 39 degrees) and (75 Ns/m, 32 degrees).

An examination of Figures 3.2 to 3.4, and Table 3.4 reveals that nonlinear HAV models yield only slightly superior fit with the measured data, in X_h- and Y_h- directions. The impedance error of the nonlinear models in Z_h- direction is slightly larger than that of the linear models. The impedance response of the nonlinear models, in general, is similar to that of the linear models. The nonlinear HAV models formulated to characterize the biodynamic response of the hand-arm *for a given* magnitude of grip force do not provide superior fit with the measured data. The linear HAV models may thus be considered to attain reasonable correlation with the measured impedance characteristics.

The total mass of the four models ($\sum_{i}^{n} m_i$) is observed to vary in the range of 3.66 kg - 4.27 kg in X_h- direction, 3.66 kg - 4.35 kg in Y_h- direction, and 3.73 kg - 4.62 kg in the Z_h- direction. Although it is not desirable to attribute these masses to actual biological system, the range of the total model mass is within the mean values of the human hand-arm system (*Chaffin et al., 1984*).

3.5.2 IMPEDANCE RESPONSE OF THE GRIP FORCE DEPENDENT LINEAR AND NONLINEAR MODELS

The measured data presented in Appendix - I for all the three directions of vibartion (Tables A2, A8, A14) at different grip force levels for an excitation level of 2.0 g peak acceleration are further utilized to propose methods of deriving grip force dependent linear and nonlinear models. The analytical model

formulation and a parameter evolution technique is discussed in sections 3.3.1, 3.3.2 and 3.3.4. The parameters of grip force dependent, three- and four- DOF, linear and nonlinear HAV models in X_h-, Y_h- and Z_h- directions are presented in Tables 3.5 to 3.7, respectively. The total mass of the three- and four- DOF models is observed to vary in the range of 3.53 kg to 5.09 kg in X_h- direction, 3.76 kg - 4.94 kg in Y_h- direction, and 3.90 kg - 4.08 kg in the Z_h- direction. Figures 3.5 to 3.8 depict the driving point impedance response characteristics of the three- and four- DOF linear and nonlinear models in the X_h- direction. The impedance response characteristics vary with the grip force, since the model parameters are dependent on the grip force. The model response corresponding to different grip force levels are compared with the measured data acquired using a constant acceleration excitation of 2.0 g peak.

The driving point characteristics of the linear three- DOF HAV model for 10, 25 and 50 N grip force are compared with the corresponding measured response in Figure 3.5. Although the magnitude response of the model deviates quantitatively from the measured data, specifically at lower excitation frequencies, the overall pattern of the model response correlates reasonably well with the measured data. The impedance magnitude response of the model increases with an increase in the grip force. This trend is also observed in the measured data. The impedance phase response of the model differs considerably from that of the measured data. The measured phase response is higher than the model phase response at low frequencies (below 100 Hz) and lower at higher frequencies (above 300 Hz). The peak phase error is observed to be nearly 40 degrees at low frequencies (below 30 Hz), and nearly (20 degrees) in 100 - 300 Hz frequency range. The error between impedance of the

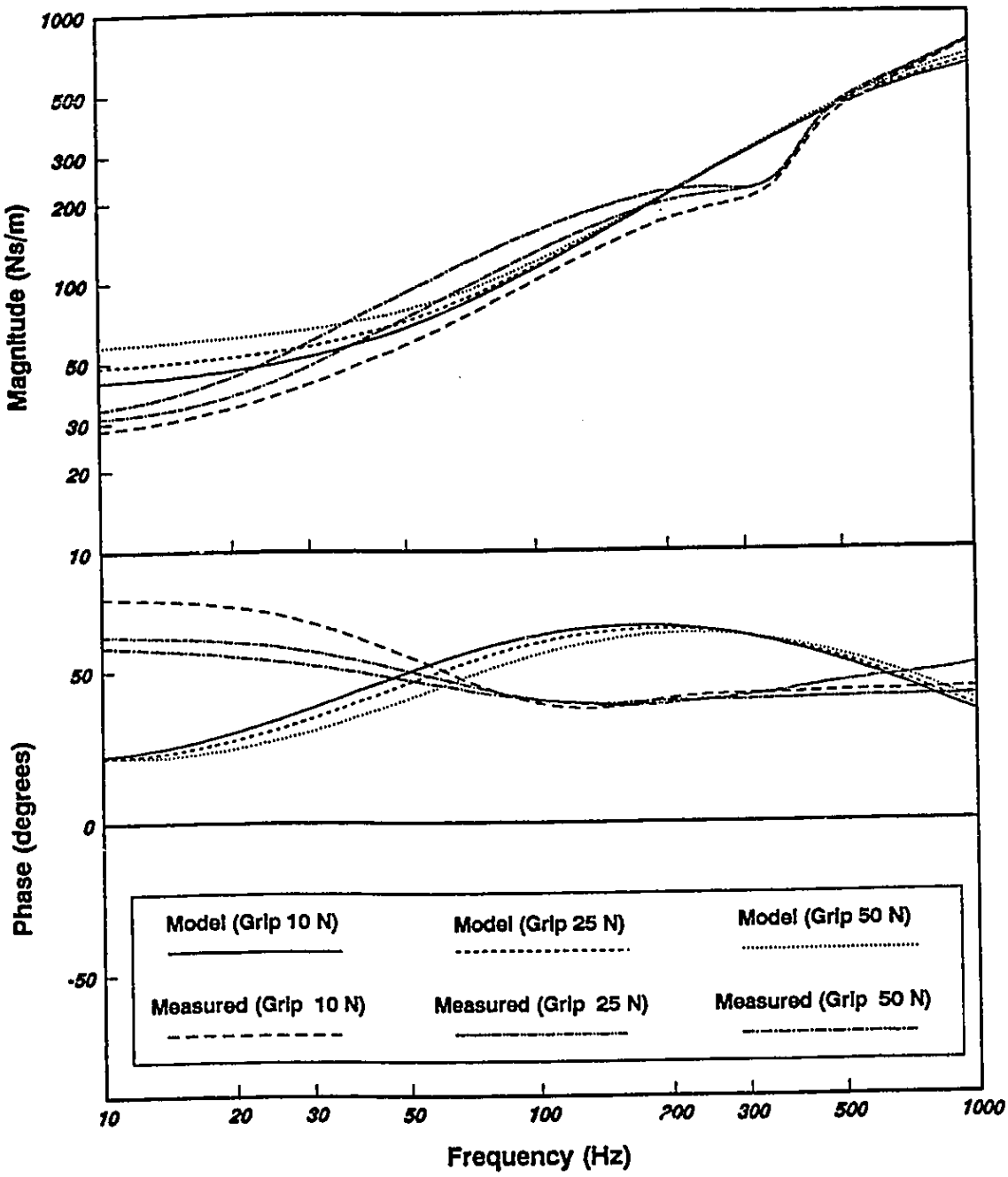

Figure 3.5: Linear three- DOF model response compared with measured data at different grip forces (X_h- direction).

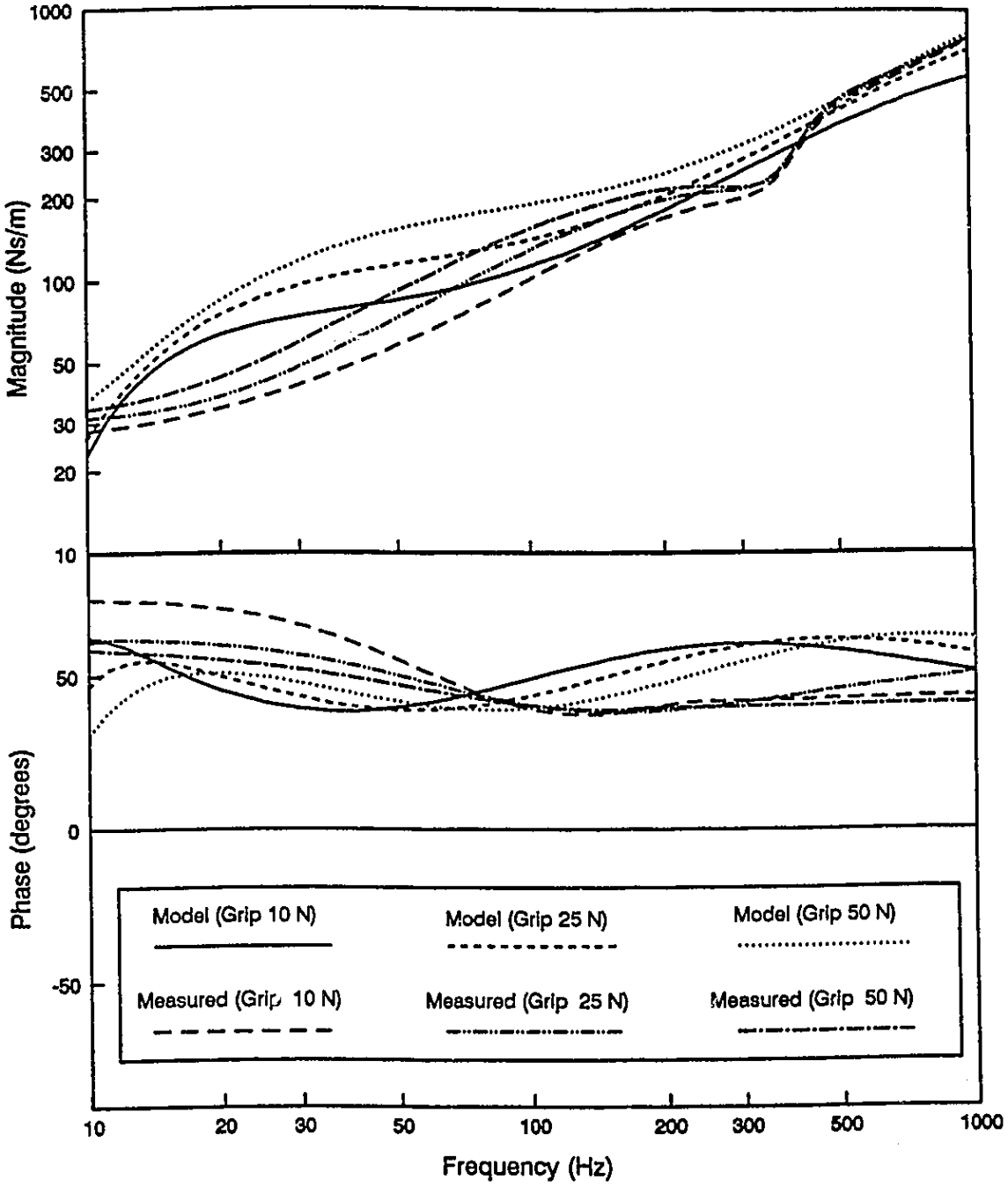

Figure 3.6: Linear four-DOF model response compared with measured data at different grip forces (X_h- direction).

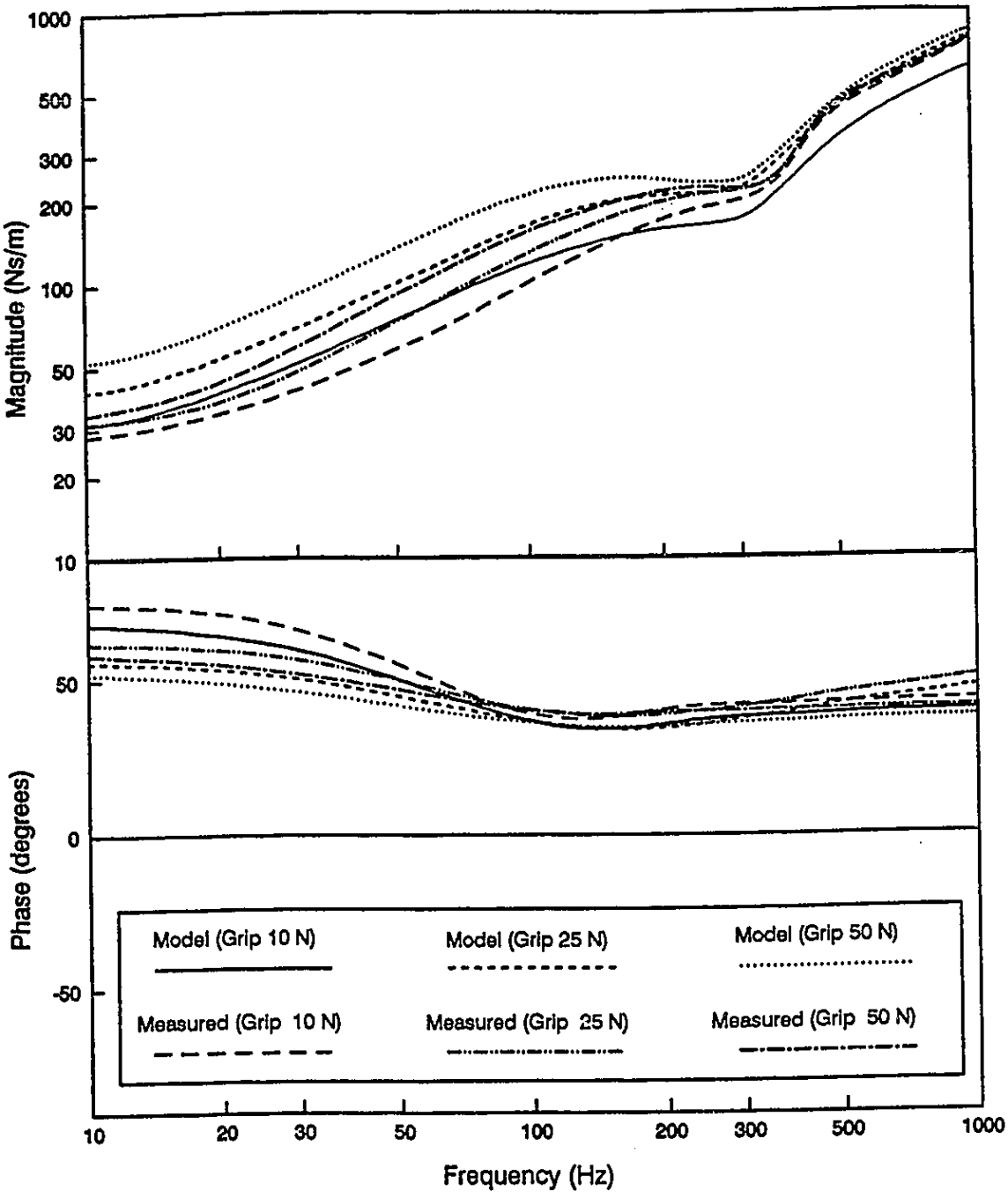

Figure 3.7: Nonlinear three- DOF model response compared with measured data at different grip forces (X_h- direction).

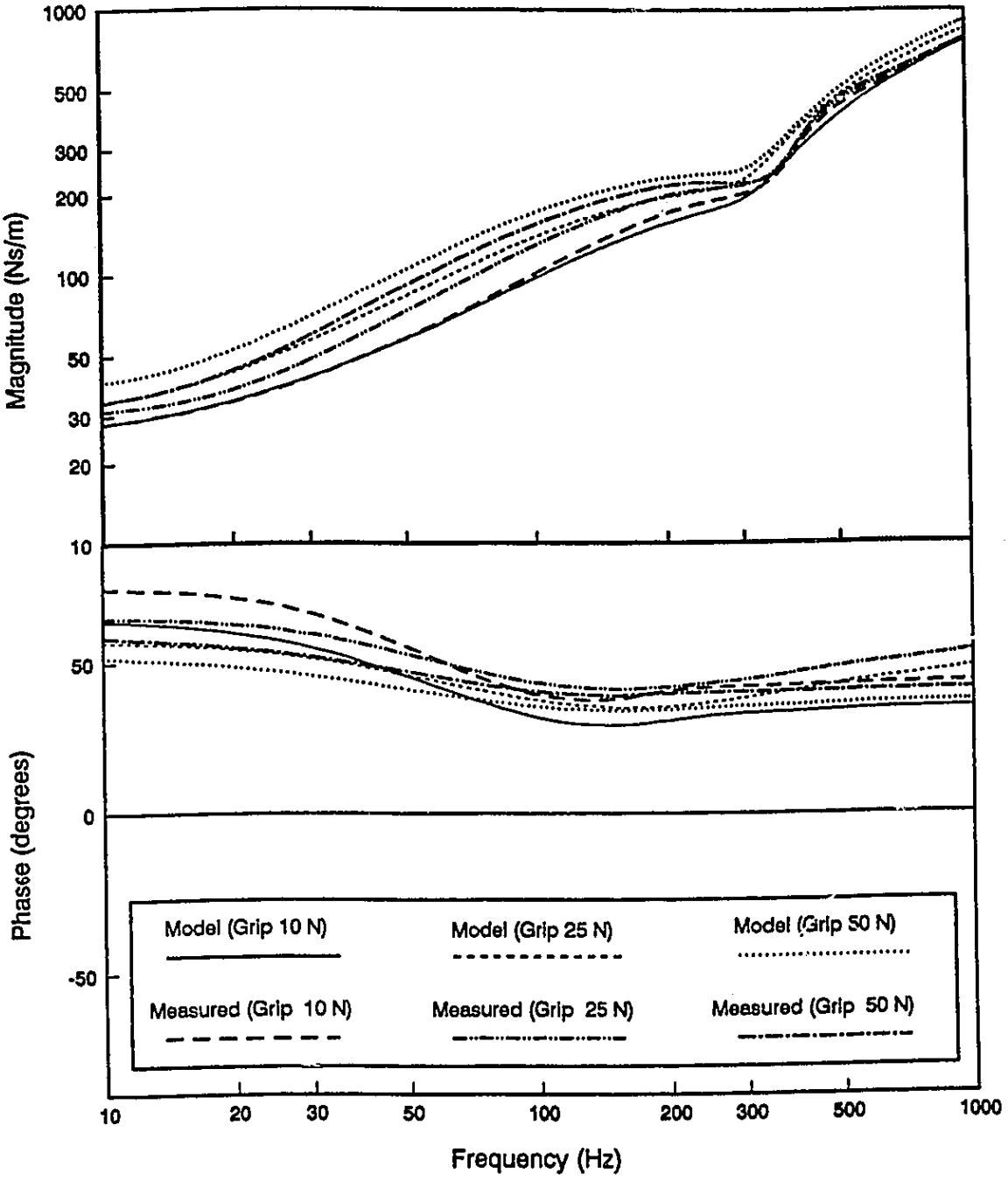

Figure 3.8: Nonlinear four- DOF model response compared with measured data at different grip forces (X_h- direction).

TABLE 3.5
Grip Force Dependent Model Parameters (X_h - Direction)

Model	Linear		Nonlinear	
Parameters	3 - D.O.F.	4 - D.O.F	3 - D.O.F.	4 - D.O.F.
m_1 (kg)	1.20E-03	3.25E-02	1.00E-05	1.22E-01
m_2	1.75E-01	1.20E-01	1.66E-01	3.87E-02
m_3	4.10E 00	8.65E-01	3.36E 00	9.48E-01
m_4	-------	3.80E 00	-------	4.00E 00
K_1 or $\begin{Bmatrix} k_{11} \\ k_{21} \end{Bmatrix}^*$ (N/m)	1.00E+02	3.10E+03	1.00E+03 1.79E+05	1.00E+03 1.07E+04
K_2 or $\begin{Bmatrix} k_{12} \\ k_{22} \end{Bmatrix}^*$	1.00E+02	2.00E+02	1.00E+03 3.43E+05	1.00E+03 1.87E+05
K_3 or $\begin{Bmatrix} k_{13} \\ k_{23} \end{Bmatrix}^*$	1.32E+04	2.50E+03	1.00E+01 3.86E+04	1.00E+01 1.52E+04
K_4 or $\begin{Bmatrix} k_{14} \\ k_{24} \end{Bmatrix}^*$	---------	2.68E+06	---------	1.00E+01 2.04E+04
K_{G1} K_{G2} K_{G3} K_{G4}	1.00E-01 1.00E-01 4.00E 00 ------	1.46E+02 2.00E-01 2.00E-01 3.75E+03	1.00E+03 1.00E+02 9.99E+02 --------	1.00E+02 1.00E+02 1.00E+02 1.00E+02
C_1 or $\begin{Bmatrix} c_{01} \\ c_{11} \\ c_{21} \end{Bmatrix}^*$ (Ns/m)	7.61E+02	2.96E+02	3.00E-04 4.75E+02 1.02E+03	2.00E-03 4.41E+01 1.00E-01
C_2 or $\begin{Bmatrix} c_{02} \\ c_{12} \\ c_{22} \end{Bmatrix}^*$	3.78E+01	5.05E+01	2.00E-04 9.86E+01 4.77E 00	1.00E-05 1.00E-01 1.00E-01
C_3 or $\begin{Bmatrix} c_{03} \\ c_{13} \\ c_{23} \end{Bmatrix}^*$	8.00E-01	2.90E 00	1.00E-05 1.00E-01 1.00E-01	1.00E-04 1.00E-01 1.00E-01
C_4 or $\begin{Bmatrix} c_{04} \\ c_{14} \\ c_{24} \end{Bmatrix}^*$	---------	7.50E+03	---------	1.00E-03 0.10E+01 2.68E+03
C_{G1} C_{G2} C_{G3} C_{G4}	3.11E 00 4.50E-01 4.10E-01 -----	2.52E+01 2.45E 00 6.90E-01 3.65E+02	4.28E+03 1.00E+01 1.00E+03 -------	1.00E-01 6.95E+02 1.00E 00 2.66E+03

* NONLINEAR PARAMETERS

TABLE 3.6
Grip Force Dependent Model Parameters (Y_h-Direction)

Model	Linear		Nonlinear	
Parameters	3 - D.O.F.	4 - D.O.F	3 - D.O.F.	4 - D.O.F.
m_1 (kg)	0.65E-02	5.90E-03	1.00E-02	7.58E-03
m_2	2.74E-01	7.02E-02	4.27E-01	6.57E-02
m_3	3.82E 00	2.10E-01	4.50E 00	6.92E-01
m_4	------	3.50E 00	------	3.00E 00
K_1 or $\begin{Bmatrix} k_{11} \\ k_{21} \end{Bmatrix}^*$ (N/m)	8.20E+03	1.66E+04	1.00E+03 1.15E+05	2.85E+04 5.05E+03
K_2 or $\begin{Bmatrix} k_{12} \\ k_{22} \end{Bmatrix}^*$	1.00E+02	1.28E+06	1.00E+03 9.27E+04	1.95E+03 1.25E+05
K_3 or $\begin{Bmatrix} k_{13} \\ k_{23} \end{Bmatrix}^*$	5.56E+05	2.00E+02	1.00E+04 8.76E+04	1.00E+03 1.60E+05
K_4 or $\begin{Bmatrix} k_{14} \\ k_{24} \end{Bmatrix}^*$	--------	1.50E+06	-------	6.68E+03 4.97E+03
K_{G1} K_{G2} K_{G3} K_{G4}	6.93E+02 2.00E-01 1.42E+03 -------	2.12E+02 1.52E+03 1.00E+01 0.75E+03	1.00E+03 1.00E+02 1.00E+03 -------	7.05E+03 1.86E+02 1.86E+02 1.19E+03
C_1 or $\begin{Bmatrix} c_{01} \\ c_{11} \\ c_{21} \end{Bmatrix}^*$ (Ns/m)	7.76E+01	6.78E+01	1.00E-03 8.36E+01 1.00E-01	1.00E-04 1.67E+02 1.07E+02
C_2 or $\begin{Bmatrix} c_{02} \\ c_{12} \\ c_{22} \end{Bmatrix}^*$	2.10E+01	1.00E 00	6.71E-04 6.75E+01 1.18E+02	1.00E-02 5.21E+01 2.14E+01
C_3 or $\begin{Bmatrix} c_{03} \\ c_{13} \\ c_{23} \end{Bmatrix}^*$	6.02E+01	1.91E+01	8.21E-04 3.42E+02 2.23E+03	1.44E-01 2.74E+01 2.73E+01
C_4 or $\begin{Bmatrix} c_{04} \\ c_{14} \\ c_{24} \end{Bmatrix}^*$	-------	5.66E+02	-------	3.80E-02 5.25E+02 8.23E+02
C_{G1} C_{G2} C_{G3} C_{G4}	1.40E-01 5.60E-01 3.40E+02 ------	3.60E-01 2.45E+02 3.60E-01 1.07E+01	1.00E+03 2.10E+02 2.10E+03 -------	1.28E+02 9.12E+01 2.81E+01 5.06E+02

* NONLINEAR PARAMETERS

TABLE 3.7
Grip Force Dependent Model Parameters (Z_h - Direction)

Model	Linear		Nonlinear	
Parameters	3 - D.O.F.	4 - D.O.F	3 - D.O.F.	4 - D.O.F.
m_1 (kg)	9.63E-02	8.27E-02	6.58E-02	7.64E-02
m_2	3.00E-01	1.38E-01	3.65E-01	1.50E 00
m_3	3.50E 00	7.58E-01	3.76E 00	1.50E 00
m_4	-----	3.15E 00	-------	2.01E 00
K_1 or $\begin{Bmatrix} k_{11} \\ k_{21} \end{Bmatrix}^*$ (N/m)	1.00E+02	1.70E+03	1.48E+04 9.53E+03	1.00E+03 1.00E+03
K_2 or $\begin{Bmatrix} k_{12} \\ k_{22} \end{Bmatrix}^*$	2.00E+06	1.72E+06	1.00E+02 1.22E+04	1.00E+03 1.00E+03
K_3 or $\begin{Bmatrix} k_{13} \\ k_{23} \end{Bmatrix}^*$	5.00E+02	1.00E+02	3.10E+03 6.80E+03	1.00E+01 1.00E+02
K_4 or $\begin{Bmatrix} k_{14} \\ k_{24} \end{Bmatrix}^*$	-------	5.60E+03	--------	1.00E+01 1.00E+03
K_{G1} K_{G2} K_{G3} K_{G4}	1.00E+01 9.50E+04 1.00E+01 ------	8.00E 00 1.42E+04 8.00E 00 8.10E+01	1.44E+03 1.00E+01 3.53E+02 -------	1.00E+02 1.00E+02 1.35E+02 1.00E+02
C_1 or $\begin{Bmatrix} c_{01} \\ c_{11} \\ c_{21} \end{Bmatrix}^*$ (Ns/m)	2.34E+02	2.42E+02	5.50E-04 7.13E 00 1.59E+03	1.00E-04 1.00E-01 1.25E+03
C_2 or $\begin{Bmatrix} c_{02} \\ c_{12} \\ c_{22} \end{Bmatrix}^*$	6.40E+01	9.55E+01	4.80E-04 1.82E 00 9.34E 00	3.16E-01 1.00E-01 1.00E-01
C_3 or $\begin{Bmatrix} c_{03} \\ c_{13} \\ c_{23} \end{Bmatrix}^*$	5.00E-01	1.06E+02	6.80E-04 4.72E 00 2.64E+03	1.00E-04 1.00E-01 1.00E-01
C_4 or $\begin{Bmatrix} c_{04} \\ c_{14} \\ c_{24} \end{Bmatrix}^*$	-------	1.05E+02	--------	6.01E-01 6.32E 00 1.00E 00
C_{G1} C_{G2} C_{G3} C_{G4}	1.00E-01 1.00E 00 1.00E+01 ------	1.52E 00 2.68E 00 6.00E-01 3.24E+01	2.08E+02 2.80E+01 4.00E+02 ------	1.00E-01 2.17E+03 1.00E+00 1.00E+00

* NONLINEAR PARAMETERS

model and measured data is observed to be in the 200 - 400 Hz frequency range.

The impedance magnitude and phase response characteristics of the four DOF linear model with grip force dependent parameters are compared to those established from laboratory measurements for different magnitudes of grip force Figure 3.6. The model response follows the general pattern of measured data, ie the impedance magnitude increased with increase in grip force. The phase response pattern also similar to the measured data, i.e. low phase angle at low frequencies and high phase angle at high frequencies as the grip force is increased. However, the deviations between the measured and model responses at two frequency ranges (15 - 60 Hz and 250 -375 Hz) are high. In view of large deviations noticed between measured and model responses, further attempts were made to investigate the response behavior of grip force dependent nonlinear models. Figure 3.8 shows the response of three- DOF nonlinear model in X_h- direction. Similar to the linear grip force dependent model parameters, the nonlinear model parameters also change with change in grip force, as these parameters are formulated as a functions of grip force. Figure 5.8 clearly illustrates the model response follows the general pattern of measured data, i.e. the impedance magnitude increased with increase in grip force. The phase response pattern also similar to the measured data, i.e. low phase angle at low frequencies and high phase angle at high frequencies as the grip force is increased. The peak error, between the measured and the model response, corresponding to 50 N grip, is high (38 Ns/m) at 100 Hz frequency range Overall, the nonlinear three- DOF model provides a better quality fit compared to the linear models. Figure 3.9 shows the nonlinear four- DOF model which provided a superior fit compared to other models in the entire frequency

range. The model parameters of all linear and nonlinear models in X_h - direction are given in Table 3.5.

Figures 3.9 - 3.12 depict the driving point impedance response characteristics of the three and four DOF linear and nonlinear models in Y_h - direction. Figure 3.9 illustrates the response of the three DOF linear model compared with the data measured using three grip forces (10 N, 25 N, 50 N; Table A8, Appendix - I) and 2.0 g peak constant acceleration. It may be observed from the figure that the model response is matching well with the measured response in the sense that the impedance increased with increase in grip force level. However, the model deviated with the measured data at frequencies above 750 Hz. The phase response also correlated reasonably well with the measured data. Figure 3.10 shows the response of four DOF linear model compared with the measured response. Similar to the case of three DOF model, the overall pattern of model response is similar to the measured response. However, the model deviated at frequencies in above 750 Hz. Owing to the large deviations noticed between the measured and model responses, complex nonlinear three and four DOF models were subsequently attempted. Figures 3.11 and 3.12 illustrate the response of nonlinear three- and four DOF models, respectively. The figures show that the model response follows the general pattern of measured data, i.e. the impedance magnitude increased with increase in grip force. The phase response pattern also similar to the measured data, i.e. high phase angle at low (below 20 Hz) and high frequencies (above 750 Hz), and the phase angle approaching zero values in the 100 - 300 Hz frequency band. As in the case of the X_h- direction (Figures 3.5- 3.8), It may be observed from Figures 3.9 - 3.12 for Y_h- direction, that with an increase in complexity of the analytical model configuration a better fit was achieved

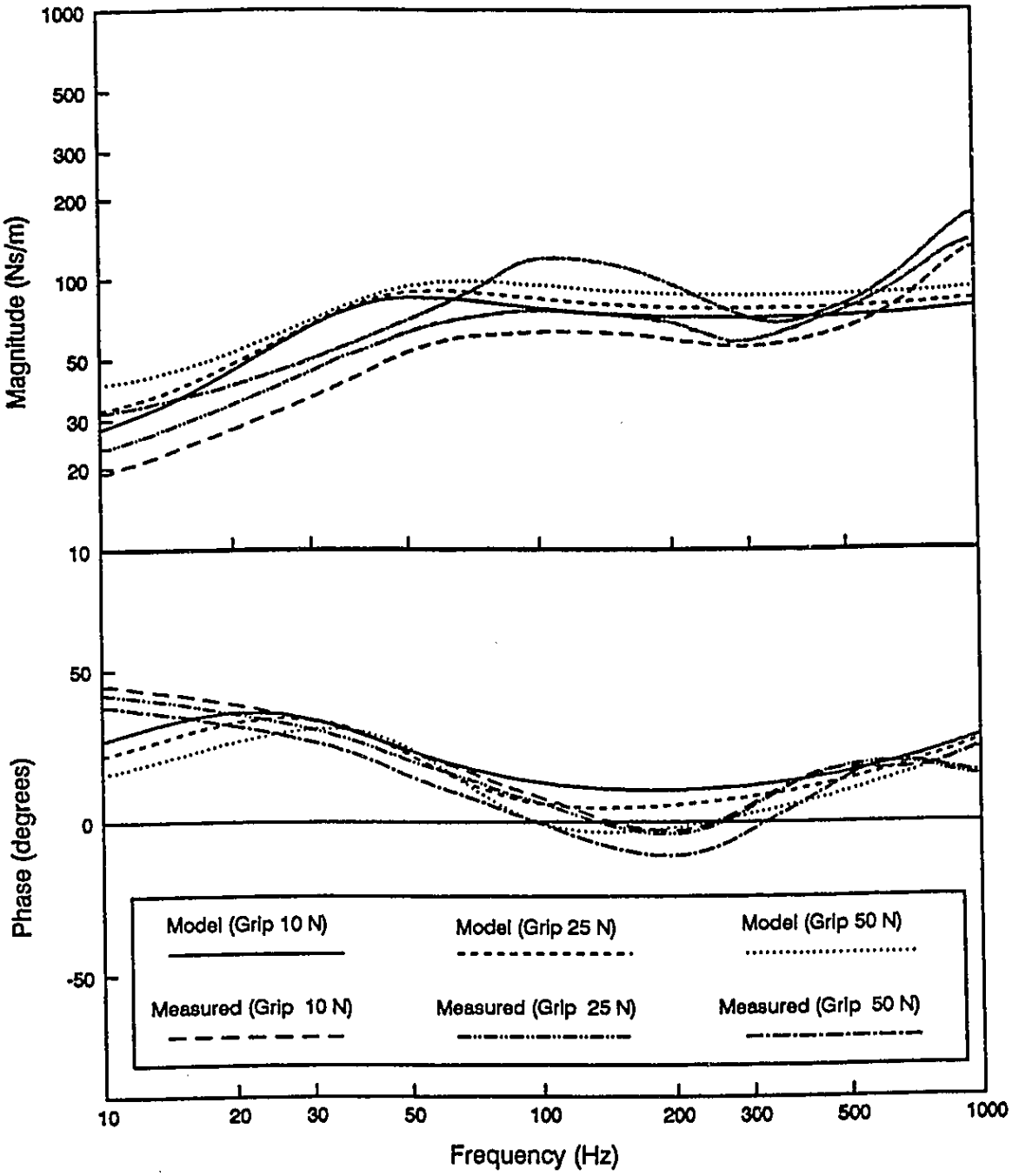

Figure 3.9: Linear three- DOF model response compared with measured data at different grip forces (Y_h- direction).

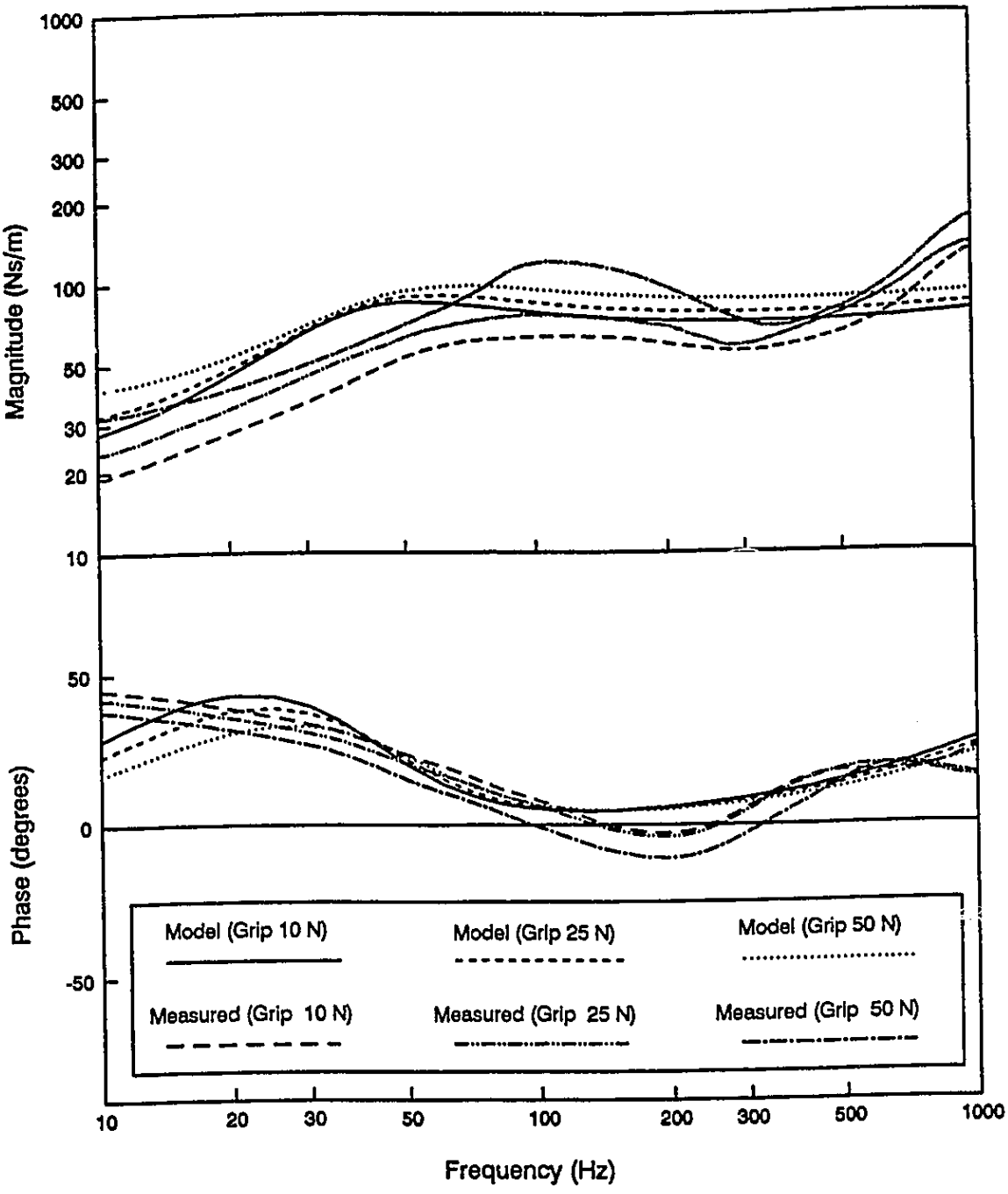

Figure 3.10: Linear four-DOF model response compared with measured data at different grip forces (Y_h- direction).

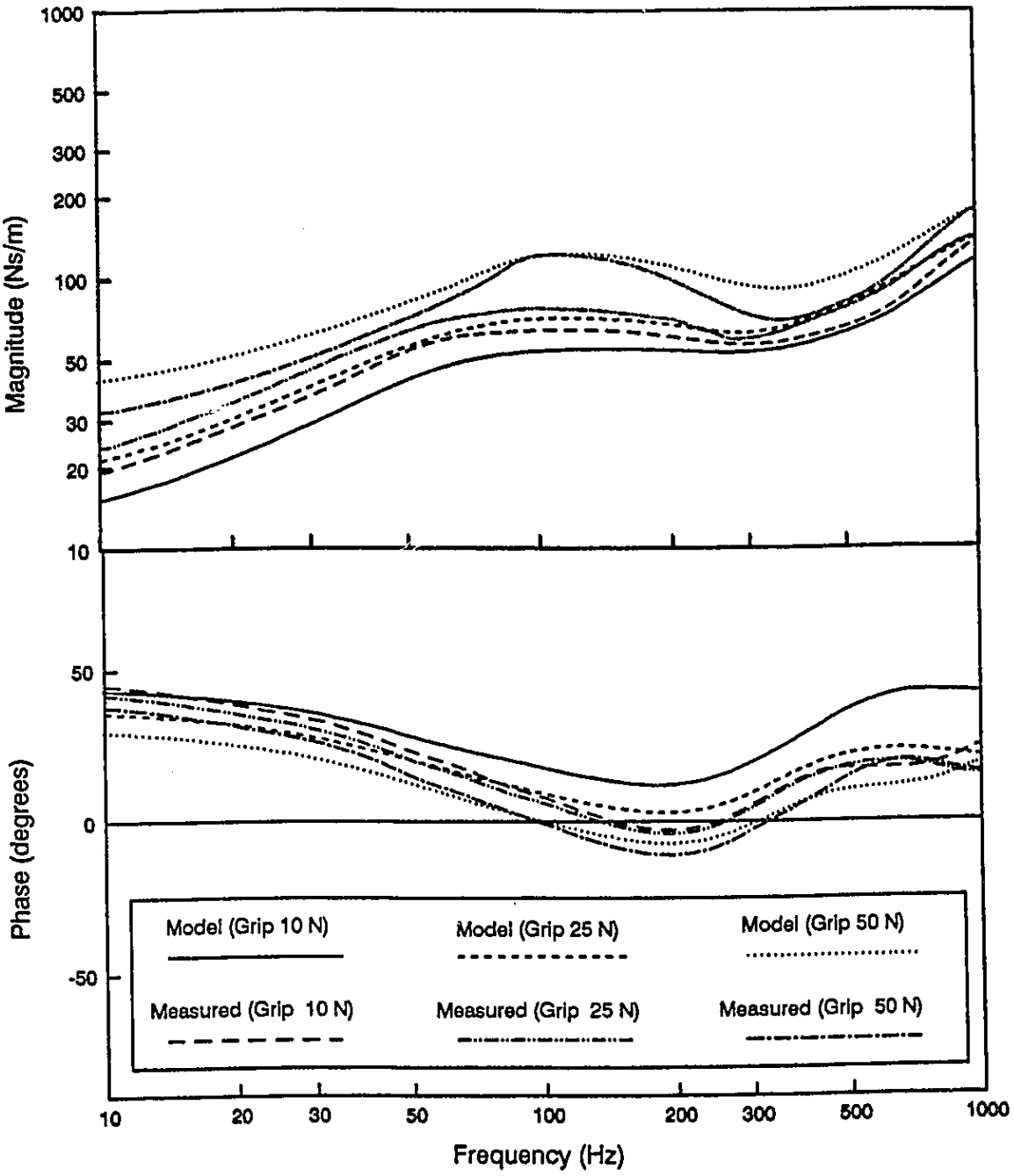

Figure 3.11: Nonlinear three- DOF model response compared with measured data at different grip forces (Y_h- direction).

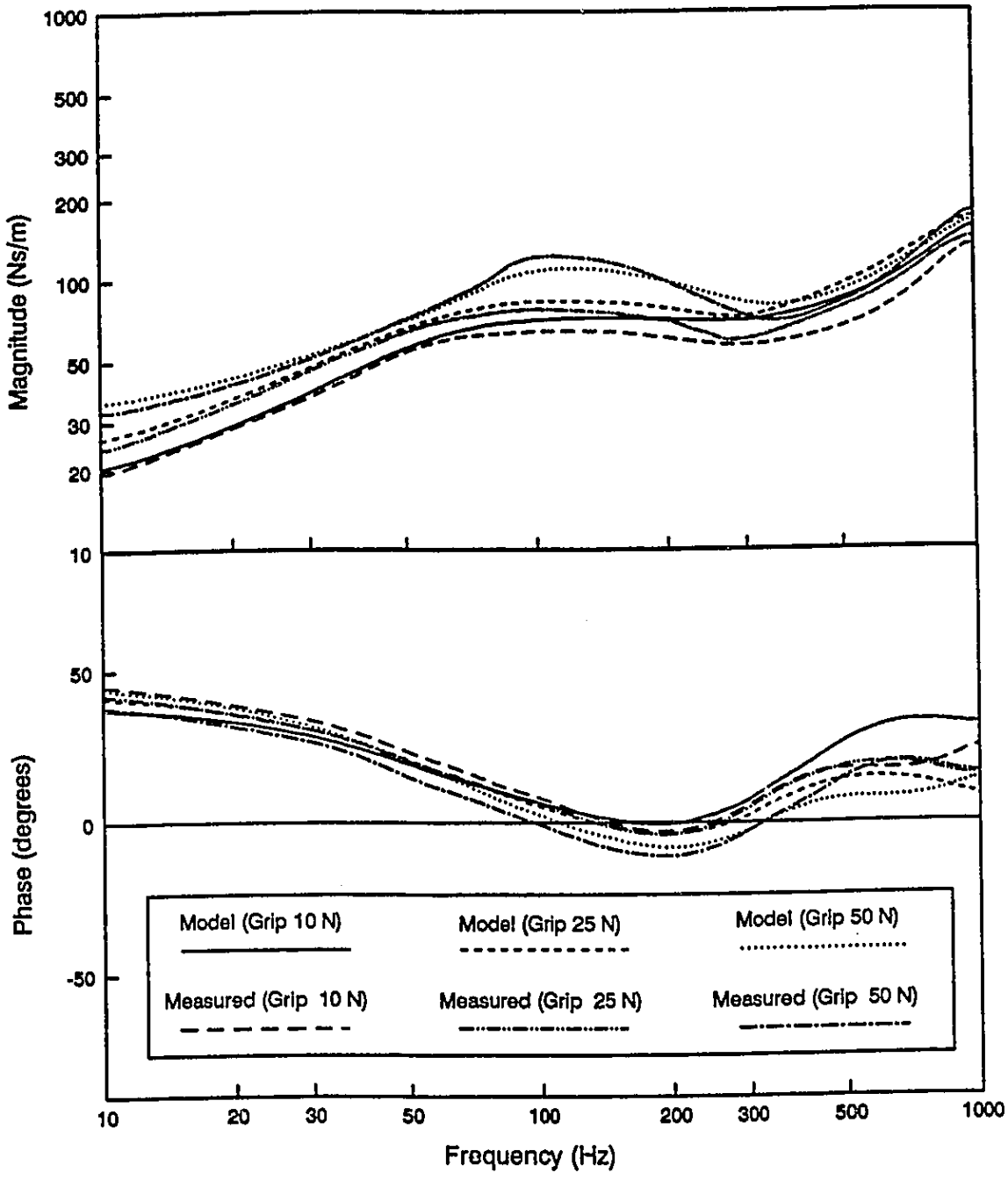

Figure 3.12: Nonlinear four- DOF model response compared with measured data at different grip forces (Y_h- direction).

between measured and model responses. The grip force dependent three and four DOF model parameters considered in Y_h- are presented in Table 3.6.

Figures 3.13 - 3.16 depict the driving point impedance response characteristics of the three and four DOF linear and nonlinear models in Z_h-direction. Figure 3.13 illustrate the response of the three DOF linear model compared with the measured data acquired using 2.0 g peak constant acceleration and three grip forces of 10 N, 25 N and 50 N (Table A14, Appendix - I). The figure illustrates that the overall pattern of model response is matching well with the measured response in the sense that the impedance magnitude increased with increase in grip force. However, the model impedance magnitude is very high (peak error 200 Ns/m) as compared to the measured data at high frequencies (above 500). Similarly, the phase response is also deviated with measured data. At low frequencies the model phase is very low (peak error 50 degrees) and at high frequencies the model phase is slightly higher as compared to the measured data. Figure 3.14 shows the response of four DOF linear model compared with the measured response. Like in the case of three DOF model, the overall pattern of model response is similar to the measured response. The additional DOF introduced into the model has reduced the model deviations considerably by reducing the error between measured and model responses in the entire frequency range. The peak errors for impedance are considerably reduced as compared to the three DOF model. The peak magnitude error is observed in the order of 100 Ns/m at frequencies above 500 Hz and the peak phase error is observed close to 40 degrees. The model yields large impedance magnitude errors at frequencies in the range of 10 - 50 Hz and 400 - 600 Hz. In view of the large deviations observed, between the model response and the measured response, complex nonlinear three and four DOF

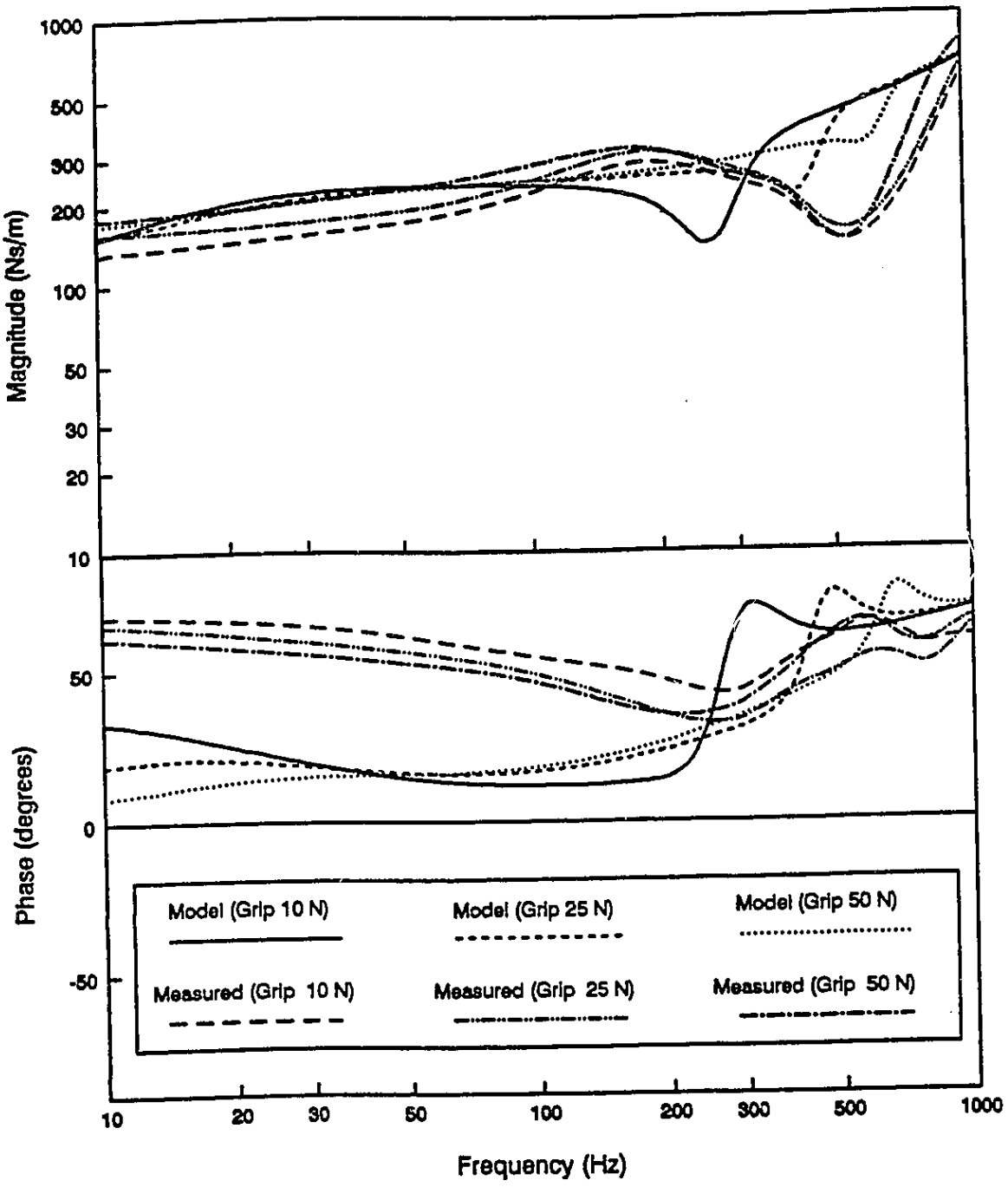

Figure 3.13: Linear three- DOF model response compared with measured data at different grip forces (Z_h- direction).

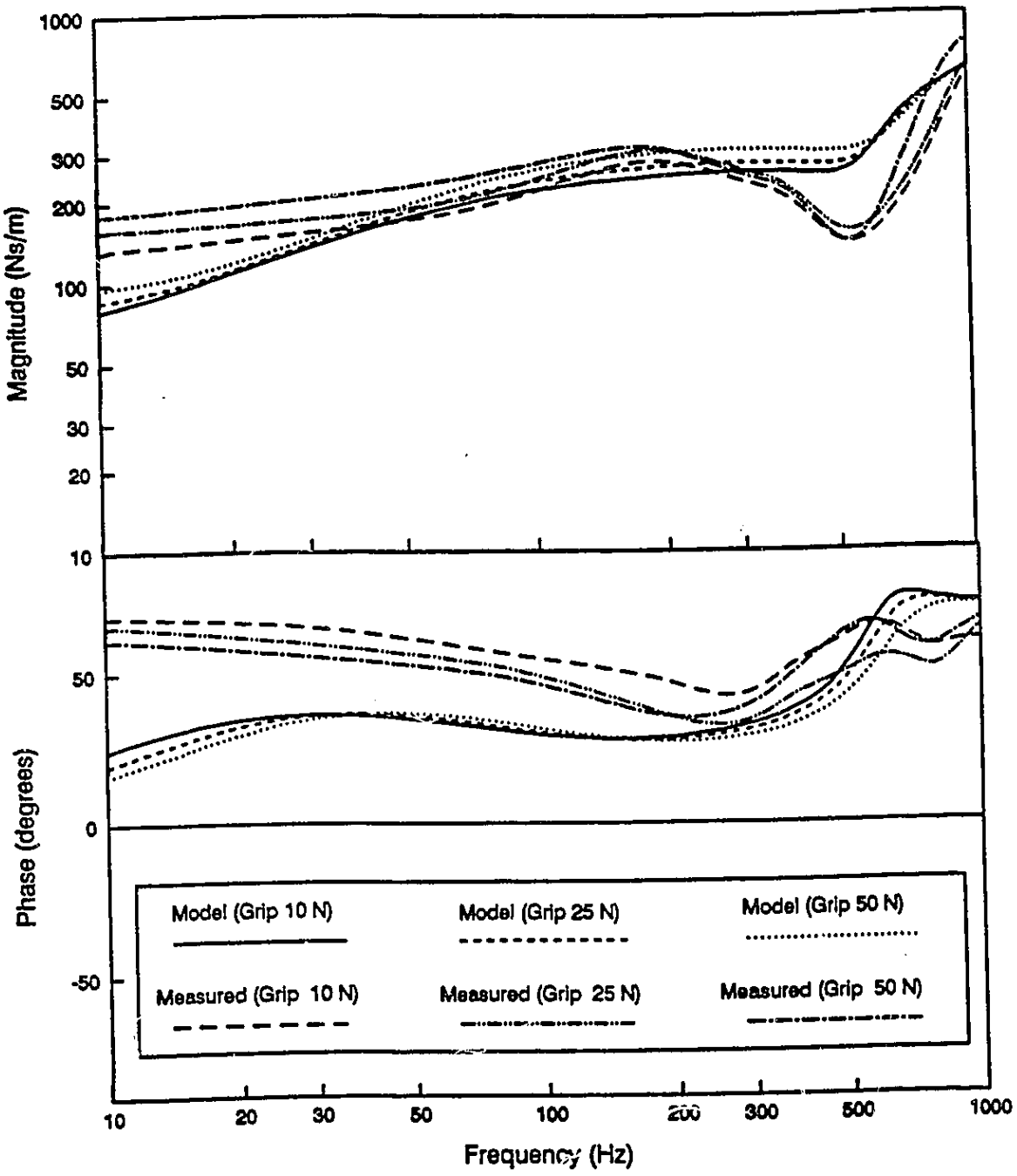

Figure 3.14: Linear four-DOF model response compared with measured data at different grip forces (Z_h- direction).

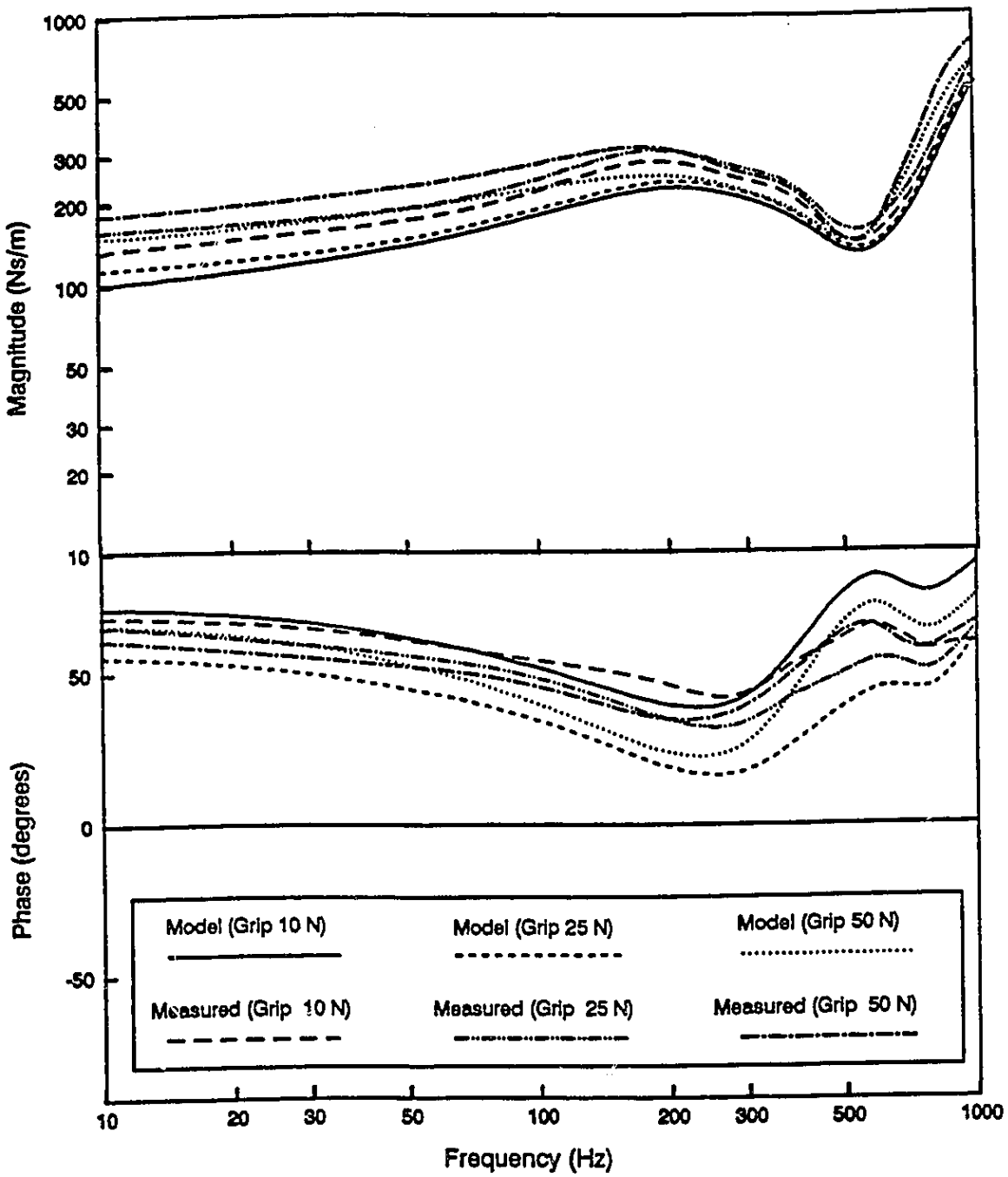

Figure 3.15: Nonlinear three- DOF model response compared with measured data at different grip forces (Z_h- direction).

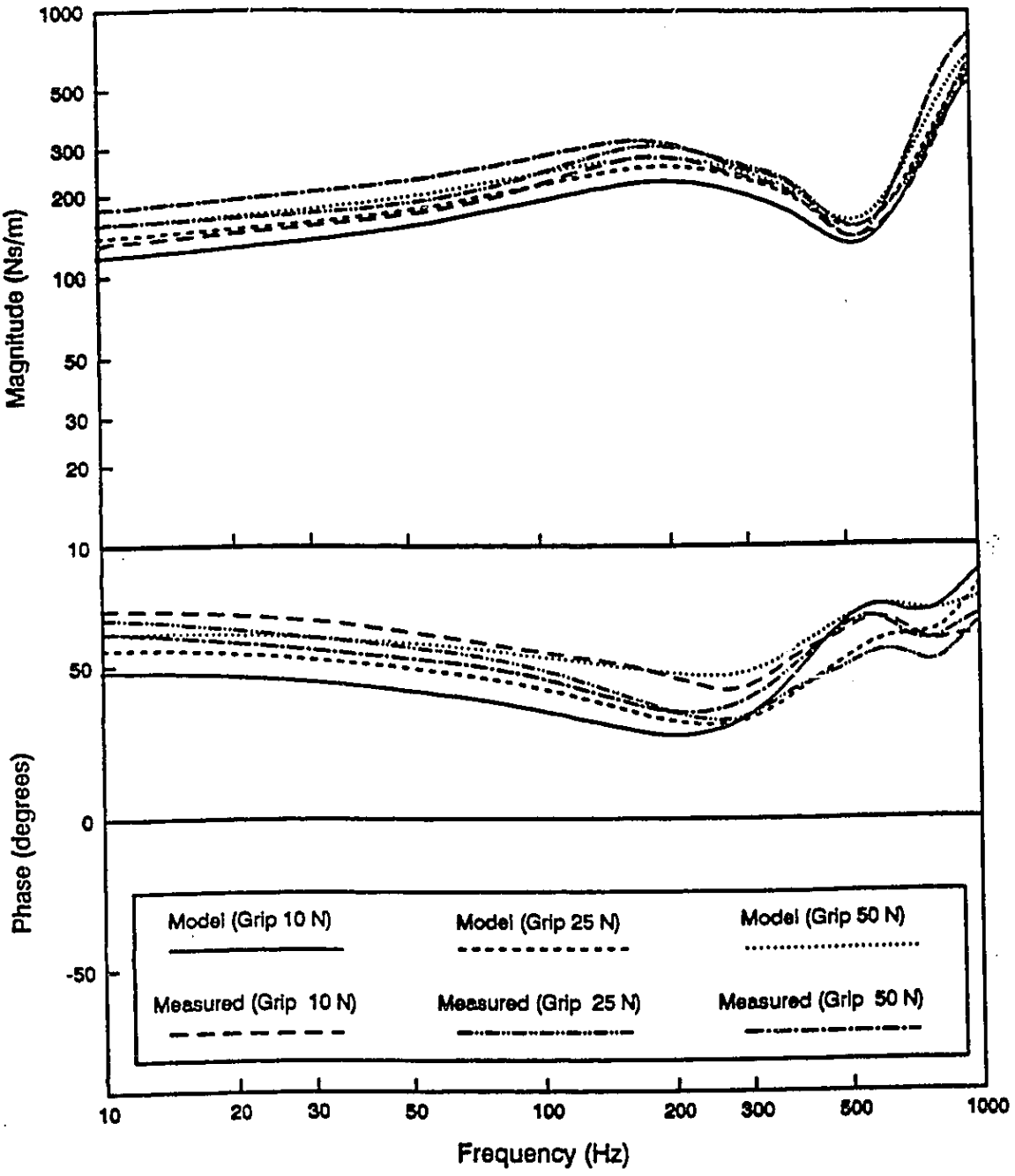

Figure 3.16: Nonlinear four- DOF model response compared with measured data at different grip forces (Z_h- direction).

models are attempted. From figures 3.15 and 3.16 it may be observed that the with increase in complexity of the model configuration a better model fit was achieved. The three- DOF models yields impedance magnitude errors ranging from 50 Ns/m at low frequencies (below 100 Hz) to 100 Ns/m at high frequencies in the range of 1000 Hz. The peak phase deviation was approximately 22 degrees in the 750 Hz frequency range. The four- DOF nonlinear model provided a further improved fit with reduced magnitude and phase errors in the entire frequency range. The model parameters in Z_h- direction are given Table 3.7.

In all the three directions of vibration, the four- DOF nonlinear model provided a superior fit when compared to other models. The superior response characteristics of these models may be attributed to the flexibility to vary a number of parameters associated with the model. However, the inclusion of a large number of parameters increases the complexity of model configuration. The nonlinear model response may further be improved by incorporating the nonlinear mass characteristics into the model.

3.6 Summary

This chapter describes a methodology to identify the parameters of hand-arm vibration (HAV) models, whether linear or nonlinear, using mechanical impedance data and nonlinear programming based optimization technique. Three- and four-degrees-of-freedom (DOF) linear and nonlinear HAV models are formulated and analyzed to yield impedance characteristics in the 10-1000 Hz frequency range. The analytical model parameters are derived to fit the measured data for all three orthogonal directions of vibrations. The results of the study show that, for a selected grip force, linear three and four DOF models

can be constructed to correlate with the measured response in the entire frequency range. This study also proposes new methods to develop grip force dependent HAV models whose response vary with change in the applied grip force. The linear three and four DOF models developed for this purpose have correlated well in meeting the overall pattern of the measured data at different grip forces. The grip force dependent nonlinear three and four DOF models provided better fit to the measured data in all the three orthogonal directions. The model response may be further improved by incorporating nonlinear inertial properties to the model. The model development techniques proposed in this chapter, will be applied in the next chapter to derive HAV model parameters from the synthesized mechanical impedance data.

□

CHAPTER 4

DRIVING-POINT MECHANICAL IMPEDANCE OF THE HUMAN HAND-ARM SYSTEM: SYNTHESIS AND MODEL DEVELOPMENT

4.1 Introduction

The driving-point mechanical impedance characteristics of the hand-arm system have been extensively investigated to enhance an understanding of the biodynamic response of the hand-arm to vibration excitations in three orthogonal axes (*Reynolds et al., 1977)* and to permit development of effective vibration isolators (*Miwa et al., 1979; Jahn et al., 1999; Dobry et al. 1992*). Although the impedance characteristics have, invariably, been measured on human subjects under carefully controlled test conditions, considerable differences are known to exist among the impedance data reported by different investigators. These differences may be attributable, in part, to the different methods and test conditions employed by individual investigators, and to the potential dependence of the mechanical impedance on: (*a*) the forces exerted by the hand on the object grasped (usually described in terms of the grip, and thrust or feed forces); (*b*) the posture adopted by the hand, arm and the torso; (*c*) anthropometric parameters of the hand and arm; and (*d*) the inherent non-linear dynamic properties of biological materials. The differences among the various reported data have raised many concerns on the validity of the reported results and the measurement techniques (*Brammer, 1993*). In view of this, a need to identify generally acceptable values for the impedance magnitude and phase of the human hand-arm that characterize its biodynamic response has been recognized.

The driving-point mechanical impedance of the hand-arm system has been characterized by mass-excited, lumped-parameter biodynamic models, where the model parameters are derived from the measured impedance data (*Dieckman, 1959; Suggs, 1974; Mishoe et al., 1977; Reynolds et al., 1977*). Lumped-parameter models, ranging from simple single DOF to many DOF, have been proposed. Although the proposed models provide little insight on the pathological changes caused by hand-transmitted vibration, they serve as useful tools to study vibration amplitudes and power flow in the coupled hand, power tool and work-piece system (*Burström et al., 1990*). In view of the wide frequency range of power-tool vibration and the non-linear viscoelastic properties of human biological materials, the accuracy of the model is related to its number of degrees of freedom. A baseline model, its DOF and parameters are often identified from the measured impedance data using the impedance relationships of pure mechanical elements. The model is then refined to fit the measured impedance data, using trial and error curve-fitting methods. Alternatively, optimization algorithms may be employed to derive the model parameters.

In this chapter, the test procedures and the experimental data reported in published studies on the driving-point mechanical impedance of the human male hand-arm system are examined in the light of known sources of variability. The results presented in Chapter 2 are further compared to the data of previous studies to highlight differences and deduce meaningful conclusions with regard to the validity and applicability of measured impedance data. Data judged suitable for further analyses are utilized to synthesize envelopes of mean values of impedance magnitude and phase, as a function of excitation frequency. The magnitude and phase envelopes are constructed for each of the three

orthogonal directions of vibration, X_h, Y_h and Z_h, specified by the International standard *ISO 5349 (1986)*. Mean values, derived from the synthesis, are considered to characterize the idealized driving-point impedance of the human male hand-arm system. A four-DOF lumped parameter model is finally derived for each direction of vibration, using the mean values of the hand-arm impedance in conjunction with a nonlinear programming based optimization algorithm.

4.2 Selection of Impedance Data for Synthesis

Driving-point mechanical impedance (Z), widely used to describe the dynamic properties of the complex hand-arm system, is defined as the ratio of the driving force (F) to the velocity ($\dot{X}$) measured at the driving-point. Mechanical compliance (ratio of driving-point displacement to the driving force, X/F) and accelerance (ratio of driving-point acceleration to the driving force, $\ddot{X}/F$) have also been employed to describe the dynamics of the hand-arm (*Meltzer, 1979; Reynolds et al., 1984*). The mechanical impedance, compliance or accelerance properties of the hand-arm have been measured by many researchers using different experimental methods, number of male human subjects, and test conditions. Table 4.1 summarizes the various test conditions employed in different investigations, specifically, the characteristics of vibration excitation, grip force, measured response variable, handle size and elbow angle. The impedance characteristics reported in these studies vary due to considerable variations in the test objectives and conditions employed by the individual researchers, as evident in Table 4.1. While a majority of the measurements were performed using a simulated circular cross-section handle (diameter ranging from 19 mm to 45 mm) mounted on a vibration exciter,

TABLE 4.1: Summary of Test Conditions and Parameters Employed by Different Investigators.

Investigators	Measured Response	Excitation Type	Excitation Magnitude	Grip Force (N)	Frequency Range (Hz)	Direction & Type of Grip	Elbow Angle (degrees)	Subjects Handle Diameter
Burström (1990)	Impedance	Sine sweep	8 - 45 mm/s	25.0 50.0 100.0	2 - 1000	X_h, Y_h, Z_h palm	60 - 180	5 Elliptic 31x42
Lundström (1989)	Impedance	Sine sweep	27 - 53 mm/s	25.0 50.0 75.0	20 - 1500	X_h, Z_h palm	90 - 180	8 Elliptic 31x42
Jandak (1989)	Impedance	Impulse	NR[1]	20.0 - 200.0	5 - 500	Z_h palm	90	25 NR
Reynolds (1984)	Compliance	Sine sweep	NR[1]	25.4	5 - 1000	X_h, Y_h, Z_h palm	NR	75 19.1 and 38.1 mm
Mishoe (1977)	Impedance	Sine sweep	6.9, 20.6 and 34.3 m/s² rms [2,4]	13.5 27.0 40.5	20 - 2000	X_h, Y_h, Z_h palm	NR	8 25.0 mm
Hesse (1989)	Impedance	Pseudo random	9.8 m/s² weighted	10.0 - 90.0	5 - 1000	X_h, Y_h, Z_h palm	60 - 180	5 45.0 mm
Meltzer (1979)	Accelerance	Stepped sine	10. N force	NR	3 - 300	Z_h palm	50 and 120	1 32.0 mm
Gurrem (1993)	Impedance	Sine sweep; random	9.8, 19.6, 29.4 m/s²[3] ; 0.2, 0.5, 0.7 m/s² rms	10.0 25.0 50.0	10 - 1000	X_h, Y_h, Z_h palm	90	4 38.1 mm
Griffin (1982)	Dynamic mass	Stepped sine	2.5 - 6.0 m/s². rms	0. - 186.	10 - 1000	X_h, Z_h palm	90 - 180	6 NR
Bernard (1990)	Dynamic mass	random	6.0, 12.0 m/s² rms	30.0 50.0 70.0	10 - 200	Z_h palm	Near 180	5 NR
Hempstock (1989,92)	Impedance	random	0.5 m/s² rms	25.0	16 - 500	X_h, Y_h, Z_h palm	120	10 NR
Daikoku (1989)	Impedance	Stepped sine	6.9 m/s² rms	33.0	8 - 200	X_h, Y_h, Z_h palm	NR	10 30

1 - Not Reported; 2 - Measured in X_h direction only; 3 - Peak acceleration ; 4 - root mean square

handles with elliptical cross section (minor axis 31 mm, and major axis 42 mm) have also been employed (*Lundström, 1989*).

Most of the measurements were performed for different magnitudes of constant grip force in order to describe the frequency dependence of the mechanical impedance. The magnitude of the hand grip force varied from 10 to 200 N, with the influence of grip force on hand-arm impedance being a parametric variation explored in some studies (*Mishoe et al., 1977; Hesse, 1989; Burström, 1990*) and the effect of thrust or feed force in others (*Griffin et al., 1982; Hesse, 1990; Bernard, 1990*). An examination of Table 1 reveals that the primary parametric variation studied was the effect of vibration frequency on impedance magnitude and phase, which was most commonly determined by exciting the system with swept or stepped pure-tone sinusoidal vibration. Pseudo-random and white-noise random excitations have also been used in a few studies (*Hesse, 1989*). The range of test conditions, employed in these studies, are summarized below:

- The frequency range of various tests were 2 to 20 Hz as the lower limit, while the upper limit varied from 200 Hz to 2000 Hz.
- The magnitude of sinusoidal excitation varied from 8 - 53 mm/s velocity to 34.33 m/s^2 *rms* (root mean square) acceleration, while the largest magnitude of weighted pseudo-random excitations was limited to 9.8 m/s^2.
- The experiments involved 1 to 75 male adult subjects with palm grip.
- Subjects maintained constant grip force levels ranged from 10 - 200 N
- The elbow angles, when reported, varied from 60 to 180 degrees.
- Circular and elliptic shaped handles with diameters of 19 mm to 45 mm.

In view of the expected discrepancies among the results reported by different studies, the mechanical impedance characteristics reported for comparable test conditions were selected for further analysis and synthesis. A selection criterion comprising the range of experimental variables and test conditions was formulated based upon the most common range of variables used in different studies. The selection criterion, listed in Table 4.2, reveals that studies were included in this analysis when:

(a). Both the magnitude and phase of the dynamic parameter measured were reported in the 20 to 500 Hz frequency range

(b). The reported values were measured in either the X_h, Y_h and/or Z_h directions of the coordinate system

(c). The hand grip force was in the range 25 to 50 N.

(d). The elbow angle, when reported data was close to an angle of 90 degrees.

Data that do not provide a quantitative measure of grip force or the impedance phase were excluded from the synthesis. Using the criterion listed in Table 4.2, the data reported by *Burström (1990), Hempstock et al. (1989), Hesse (1989), Jandak (1989), Lundström et al. (1989), Mishoe et al. (1977)* and *Reynolds et al. (1984)*, were selected. Two data sets, reported in Chapter 2 of this thesis research, for sinusoidal (19.6 m/s^2 peak constant acceleration) and random (0.7 m/s^2 *rms* acceleration) excitation were also included in the synthesis for obtaining the dynamic impedance that characterize the human male hand-arm system.

To assist the comparison of data, the measurements of dynamic compliance and accelerance were converted to their equivalent impedance values in the following manner:

$$Z(j\omega) = \frac{1}{j\omega S(j\omega)} \tag{4.1}$$

$$Z(j\omega) = \frac{A(j\omega)}{j\omega} \tag{4.2}$$

where, $Z(j\omega)$, $S(j\omega)$ and $A(j\omega)$ are complex impedance, compliance and accelerance, respectively. ω is the circular frequency in rad/s.

TABLE 4.2
Criterion Adopted for Selection of Impedance Data

Response Variables	Magnitude and Phase of Impedance, Compliance, Accelerance or Dynamic Mass
Excitation Frequency Range	20 - 500 Hz (at least)
Direction of Vibration	X_h, Y_h, and/or Z_h
Grip Force	25 - 50 N*
Grip Type	Palm
Elbow Angle	Closest to 90 Degrees, when reported
Handle Type	Circular or Elliptical
Handle Size	19 - 45 mm Diameter (minor/major Diameter)

* X_h - direction, 25 N only

4.3 Synthesis of Measured Human Hand-Arm Impedance Data

Mechanical driving-point impedance of the human hand-arm, reported in the selected studies, are synthesized to derive the range of most probable values of impedance magnitude and phase. The measured magnitude and phase characteristics reported in the selected studies, for similar test conditions, are compared to identify various similarities and differences among the data. An attempt is also made to identify the primary sources of variability.

4.3.1 COMPARISON OF HAND-ARM IMPEDANCE CHARACTERISTICS

While the test data reported in some of the selected studies were obtained directly from the researchers, the data for the other studies were derived from the published curves using a two-dimensional digitizer. The magnitude and phase characteristics of the mean driving-point impedance are presented as a function of excitation frequency in Figures 4.1 to 4.6, for studies complying with the selection rules listed in Table 4.2. The two sets of data, reported by Reynolds et al. (1984), for the studies conducted with the small (19 mm diameter) and large (38 mm diameter) handles are shown separately. The two data sets, derived from the studies reported in Chapter 2 for sine sweep and random vibration excitations, are also included. The results also include two data sets, reported by Mishoe *et al.* (1977) for the X_h direction, which correspond to two different levels of acceleration excitations: 6.9 m/s² and 34.3 m/s² rms.

It should be noted that the grip force varied from 25 - 27 N for the data reported for X_h direction (Figures 4.1 and 4.2). The grip force, however, varied from 25 - 50 N for the data reported for the Y_h and Z_h components of

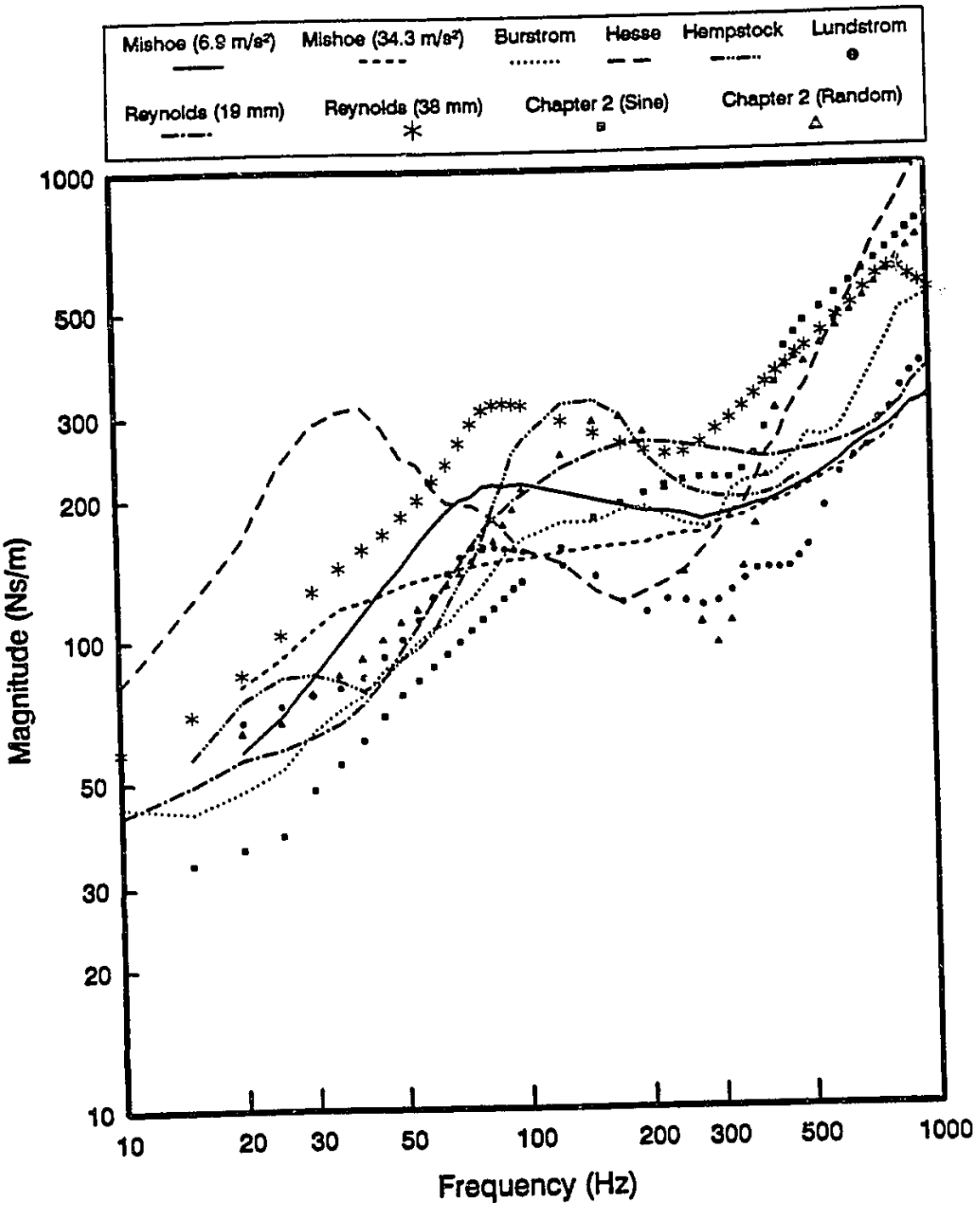

Figure 4.1: Comparison of magnitudes of driving point impedance measured in the X_h - direction.

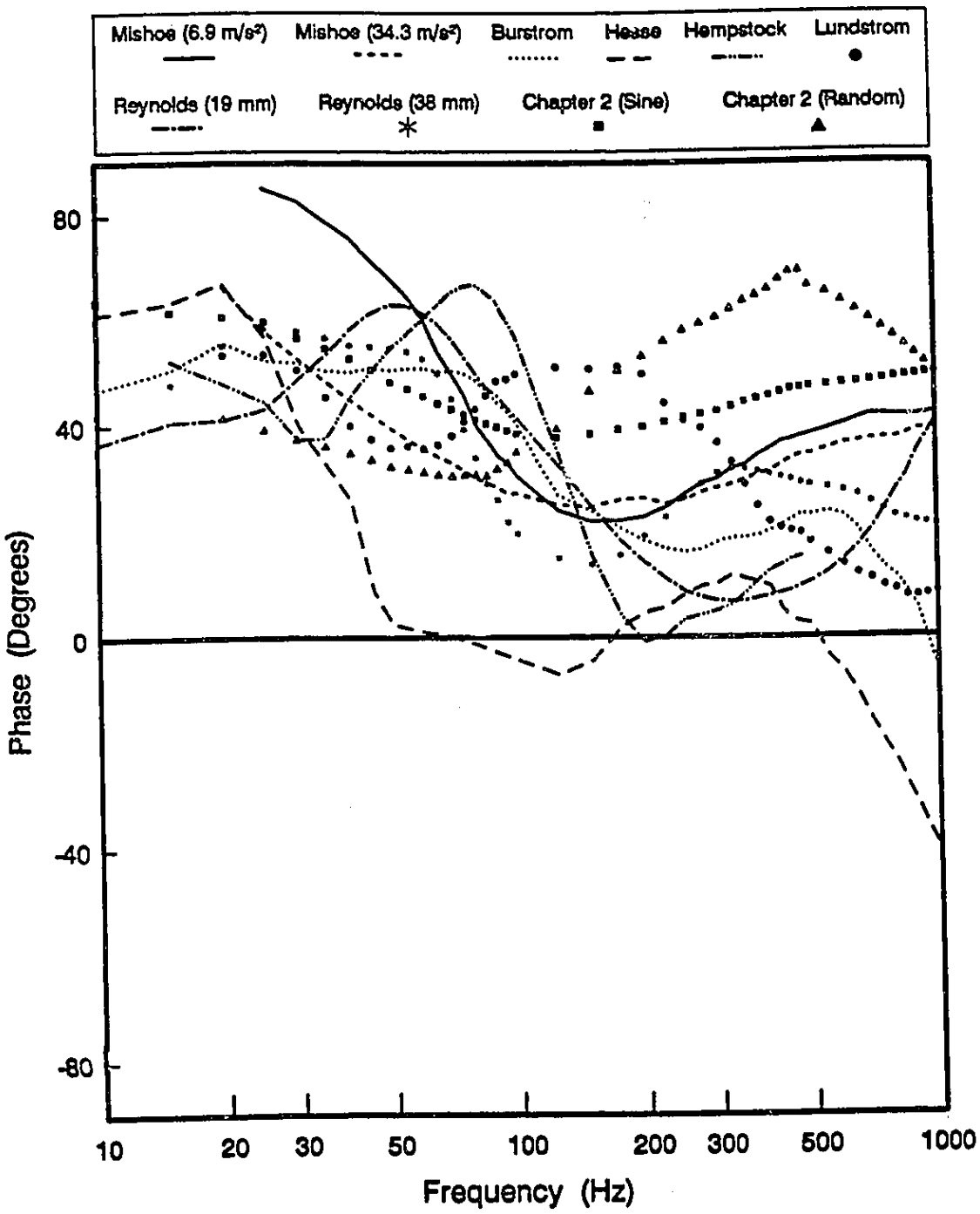

Figure 4.2: Comparison of driving point impedance phase angle measured in the X_h - direction.

impedance. The range of grip force for the Y_h and Z_h directions was broadened in order to include reasonable number of data sets in the analysis.

The magnitude of mean values of impedance characteristics in X_h direction, are compared in Figure 4.1. Inspection of this figure reveals the similarities and differences among the mean values reported for the X_h direction. While the absolute magnitudes observed in various studies clearly differ, a majority of curves reveal a peak in the 100 to 200 Hz frequency range, and tend to increase in magnitude with excitation frequencies above 300 Hz. At higher excitation frequencies, the hand-arm impedance is primarily that of a constant mass, and is subject to significant measurement errors, if the raw data are not adequately corrected for the large coupled mass of the handle. The magnitude of impedance measured under random excitations in the X_h direction is also comparable to those measured under sinusoidal excitations, except at 300 Hz excitation frequency. With the exception of the data reported by Hesse (1989) at frequencies below 50 Hz, it is evident that the X_h components of reported hand-arm impedance magnitudes may be represented by an upper and lower envelopes of mean values that possess similar trends, and together define a band of most probable values. The definition of the most probable values of human hand-arm impedance from a synthesis of measured values is discussed in a separate section in the ensuing pages.

The corresponding differences and similarities among the mean values of the impedance phase measured in the X_h direction, are illustrated in Figure 4.2. Although no general agreement can be observed among the data, a majority of the results possess a positive phase angle between the driving force and the velocity measured at the driving-point, with the exception of the data reported by

Hesse (1989), which display negative phase angle in the 60 - 140 Hz frequency range and above 500 Hz. The data reported by *Hesse (1989)* also form outliers in the 50 to 150 Hz frequency range, as shown in Figure 4.2 The impedance phase data reported in this thesis research, for random vibration excitations, also form outliers at frequencies above 300 Hz, which may be attributed to the low level of accelerations associated with the random excitation. The magnitude and phase data reported by *Hesse (1989)* and phase data reported for random excitation in Chapter 2 of this thesis have thus been excluded from the synthesis of the mean values of impedance in the X_h direction. While there are considerable variations in mean phase among the remaining data sets, there is no clear evidence to remove other data sets from the analysis. Accordingly, upper and lower contours of mean phase may be constructed to encompass the mean values of the remaining data sets. These curves serve as the basis for the definition of the most probable values for the phase of the human male hand-arm impedance in the X_h direction, in the 10 to 1000 Hz frequency range.

A comparison of mean values of driving-point impedance magnitude measured in the Y_h direction, presented in Figure 4.3, reveals that most data sets display a peak in the 20 to 50 Hz frequency range. The magnitude of this impedance component tends to increase with excitation frequency, at frequencies above 300 Hz. An examination of Figure 4.3 further reveals that impedance magnitude measured under random excitations is comparable to those measured under sinusoidal excitations at all frequencies above 80 Hz. The data reported by *Hesse (1989)*, again form outliers at frequencies above 300 Hz. The mean values of corresponding impedance phase, presented in Figure 4.4, show that the scatter among the reported phase data for the Y_h component of impedance is somewhat less than that observed for the X_h

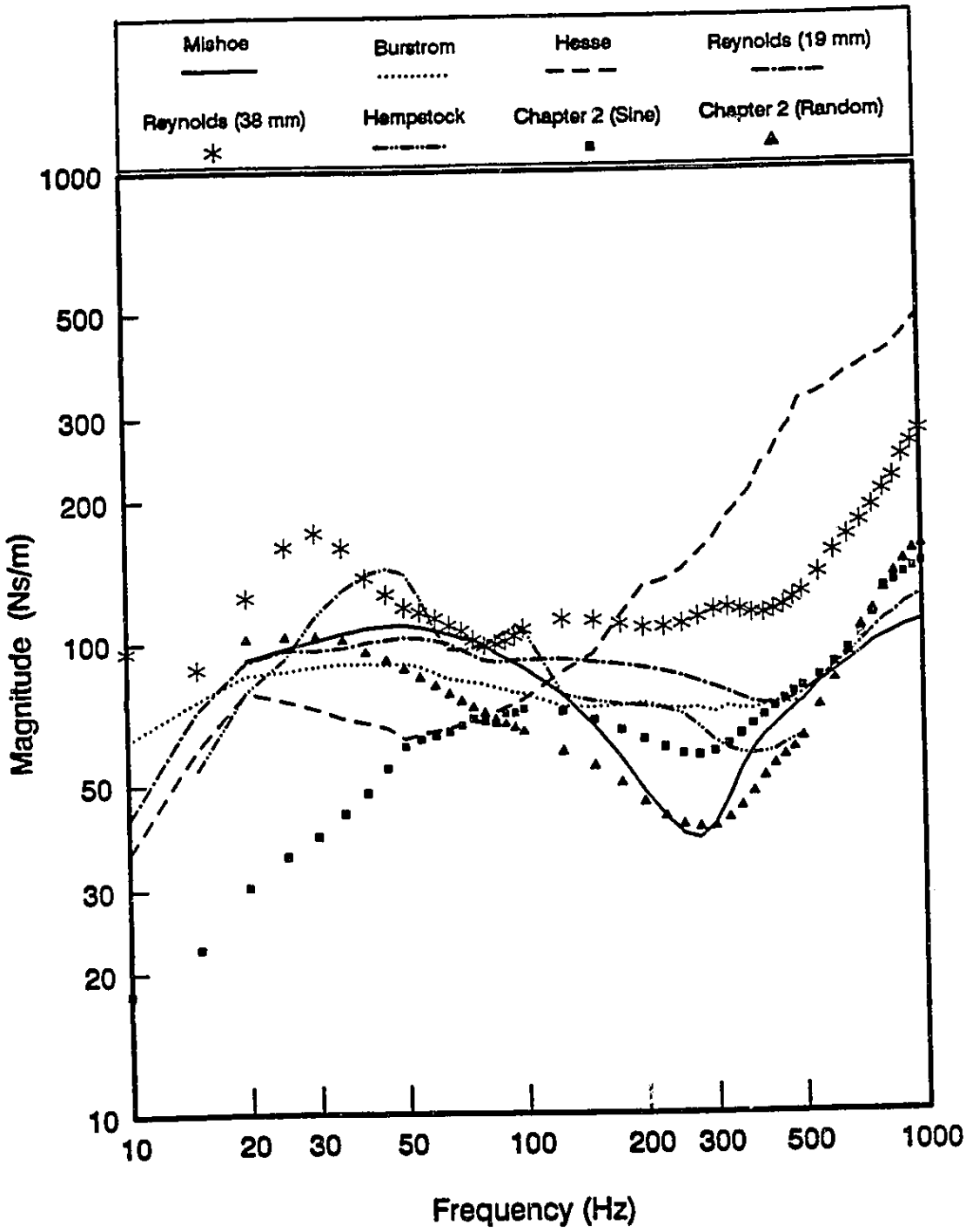

Figure 4.3: Comparison of magnitudes of driving point impedance measured in the Y_h - direction.

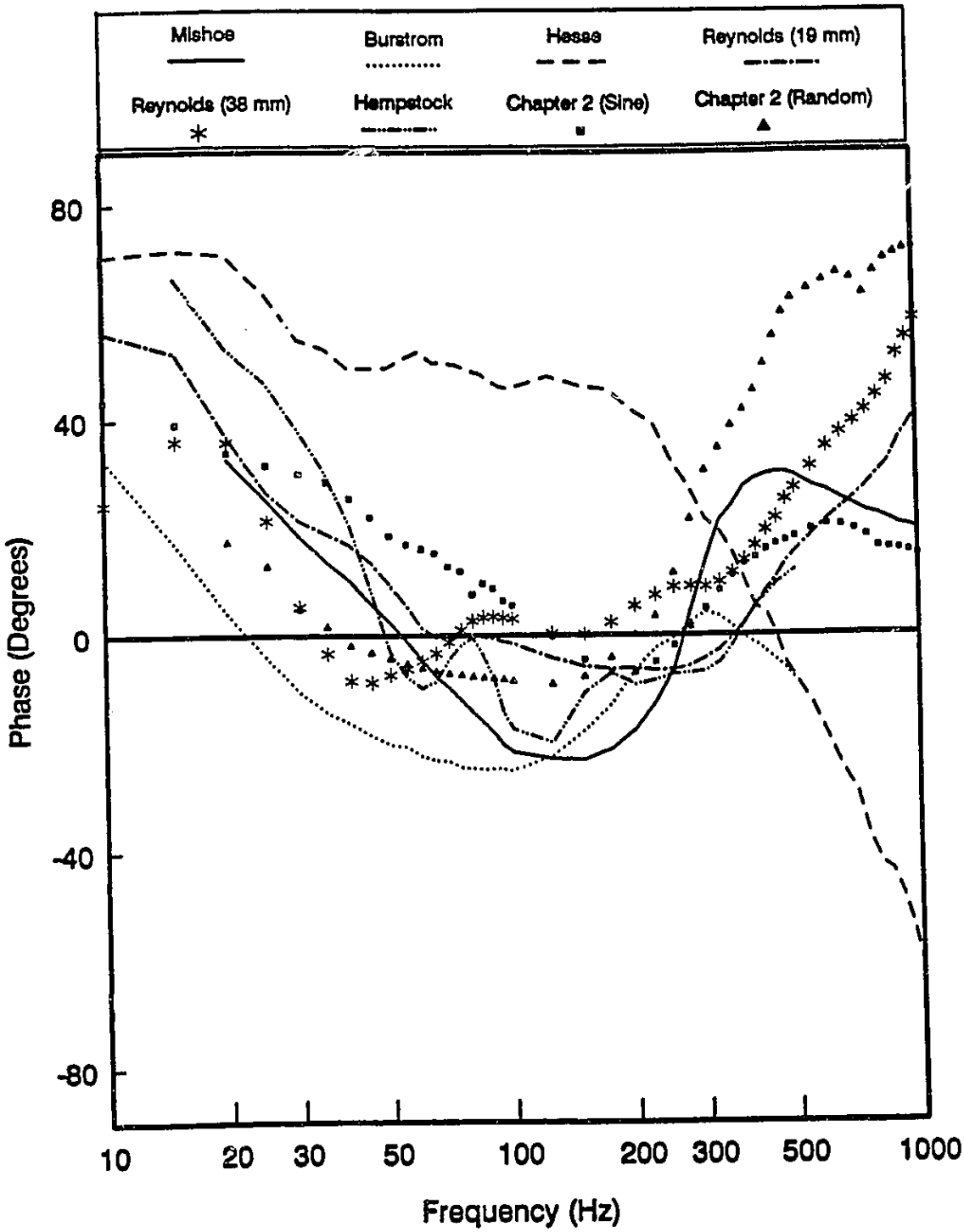

Figure 4.4: Comparison of driving point impedance phase angle measured in the Y_h - direction.

component (Figure 4.2), when the outlying data set is excluded. Figure 4.4 clearly shows that the data reported by *Hesse (1989)* form outliers at almost all frequencies, and deviate considerably from the results of other investigators. The general trend of phase response, measured under random excitations, is also similar to those reported for the sinusoidal excitations. The magnitude and phase data sets, presented in Figures 4.3 and 4.4, with the exception of data set reported by *Hesse (1989)*, are thus used to construct envelope contours that define the upper and lower bounds of the mean values. The envelope contours, thus formulated, are used to define the range of most probable values for the magnitude and phase of the human male hand-arm impedance in the Y_h direction.

The mean values of driving-point impedance magnitude and phase measured in the Z_h direction are compared, as shown in Figures 4.5 and 4.6, respectively. Although most data sets exhibit a peak in impedance magnitude in the 20 to 50 Hz frequency band (Figure 4.5), the magnitude data reported by *Mishoe et al. (1977)*, deviate considerably from the general pattern. The magnitude values reported by *Jandak (1989)* exceed the entire ensemble in the frequency range of 20 to 50 Hz, and the impedance magnitude reported by *Hesse (1989)* exceeds the entire ensemble above 500 Hz. It would therefore appear appropriate to exclude these data sets from the envelope contours of the impedance magnitude. While the impedance phase data, presented in Figure 4.6, do not indicate a clear trend, the data reported by *Lundström et al. (1989),* and *Hesse (1989)*, definitely form the outliers. Similarly, the data derived from this thesis research (Chapter 2) for random excitations evidently form the outliers. Envelope contours have thus been constructed, excluding these data

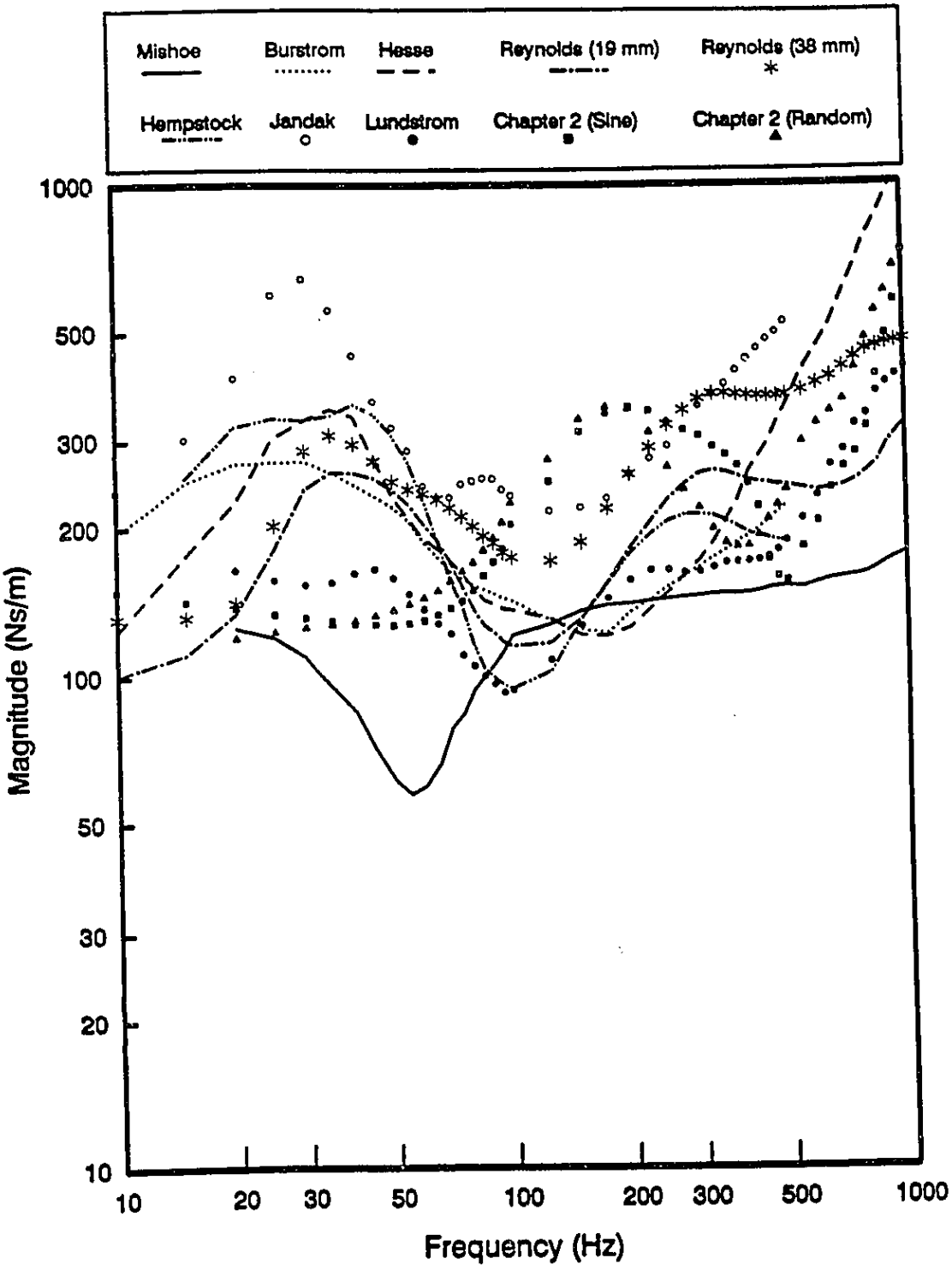

Figure 4.5: Comparison of magnitudes of driving point impedance measured in the Z_h - direction.

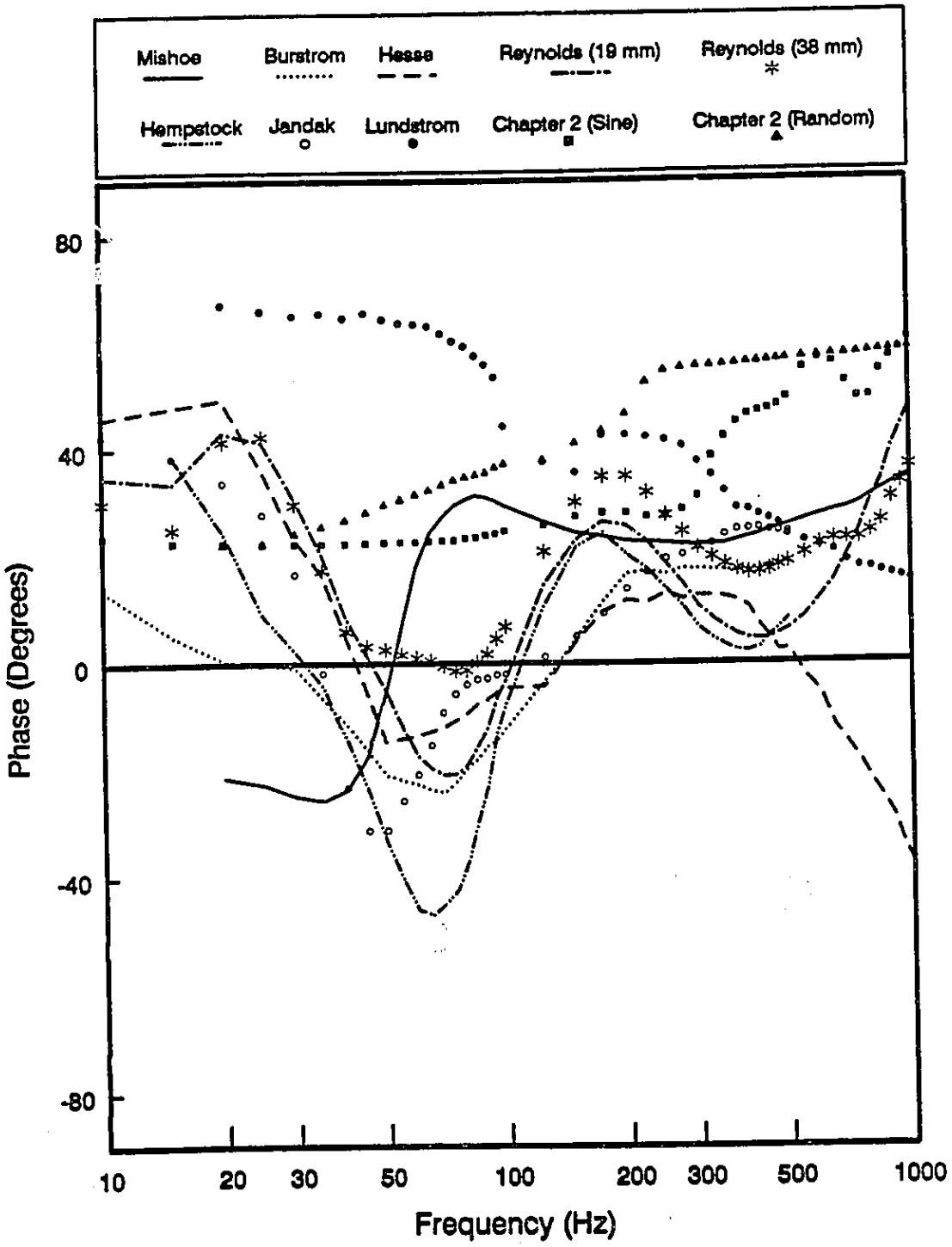

Figure 4.6: Comparison of driving point impedance phase angle measured in the Z_h - direction.

sets, for use in the definition of the most probable values for the magnitude and phase of the human male hand-arm impedance in the Z_h direction.

4.3.2 SOURCES OF VARIABILITY

From the data reported in Chapter 2 of this thesis research, and by many other investigators, many factors contribute to the variations in the impedance data. The grip force and frequency have significant influence on the measured response. The type and levels of excitation have relatively little influence on the measured data. Other factors such as elbow angle, handle size and subject related parameters also contribute to variations.

From Figures 4.1 to 4.6, it is evident that large variations exist among the mean values of both impedance magnitude and phase, reported by different investigators. While these large variations are quite disturbing and lead to questions concerning the measurement procedures, it is extremely difficult to precisely establish the sources of variability. All the studies included in this analysis employed a similar range of vibration frequencies, identical directions of excitation, four or more male human subjects, closely controlled hand grip forces, and similar elbow angles, though the effects of posture cannot be completely discounted (*Hesse,1989*). The effects of variations in the forces exerted by the hand on the handle have been quantified in several investigations, and for this reason are discussed separately in a separate section.

In these circumstances, it is instructive to explore the variations in hand-arm impedance due to changes in a single parameter that resulted in a single investigation. A comparison of impedance characteristics measured using swept

sinusoidal or random vibration stimulation, and otherwise the same subjects and apparatus, may be obtained from the results of this thesis research discussed in Chapter 2. The experiments involving different vibration excitations were conducted under equivalent conditions, and are believed to possess similar random and systematic errors except at low frequencies, where the statistical fluctuations of the random excitations lead to increased error.

An inspection of Figures 4.1 and 4.5 reveals that the X_h and Z_h components of impedance magnitude measured using stochastic excitations are generally similar to those recorded under sinusoidal excitations. It should be noted, however, that the two methods of excitation do appear to produce different impedance magnitudes in the X_h direction near 150 and 300 Hz excitation frequencies. While the impedance magnitude measured in the Y_h direction using random excitations (Figure 4.3) compares well with majority of the data sets, reported by other investigators, it is comparable to the impedance magnitude acquired in the same study under sinusoidal excitations only at frequencies above 80 Hz. The impedance magnitude measured under sinusoidal excitations becomes progressively smaller than the mean values reported in other studies as the excitation frequency decreases. These differences may be attributable to the significantly different amplitudes of sinusoidal and random accelerations employed, as illustrated in Table 4.1.

The comparison of mean phase values measured under sinusoidal and random excitations (Figures 4.2, 4.4 and 4.6) shows that the phase response under stochastic excitation tends to be somewhat greater than that measured with sinusoidal vibration at frequencies above 200 Hz. The mean values of impedance phase in the X_h and Z_h directions at these frequencies are greater

than those reported by other investigators. The difference between the impedance magnitudes in the Y_h direction at low frequencies (Figure 4.3) does not appear in the phase measurements (Figure 4.4), and both mean values are within the envelope of mean values formed by the other studies. The phase response of this component measured using random and sinusoidal excitation at frequencies above 200 Hz, however, differ. At these frequencies, the phase observed with random excitation substantially exceeds that observed with sinusoidal excitation, and also exceeds the envelope of mean values from other studies.

Some dependence of the measured impedance magnitude on the magnitude of acceleration excitation can also be observed in the results of *Mishoe et al. (1977)* presented in Figure 4.1. While the X_h component of impedance magnitude is relatively insensitive to magnitude of sinusoidal excitation at frequencies above 250 Hz, the impedance magnitude at lower frequencies varies with variations in excitation level. The impedance magnitude corresponding to high amplitude vibration, however, tends to be lower than that corresponding to low amplitude vibration excitation in the 40 - 250 Hz frequency range. A comparison of the mean values of impedance phase measured under different levels of excitations (Figure 4.2) reveals that at excitation frequencies below 100 Hz the mean phase measured under larger acceleration excitation (34.3 m/s^2 rms) is smaller than that under lower excitation level (6.9 m/s^2 rms).

The influence of handle diameter on the measured impedance characteristics can be deduced from the study conducted by *Reynolds et al. (1984)*. The impedance magnitude and phase, reported for two handle sizes, exhibit similar trends for all the three directions, as illustrated in Figures 4.1 to

4.6. The magnitude of impedance measured with large diameter handle, however, tends to be greater than that measured using the small diameter handle, in all the three directions. The impedance phase measured using the two handles differ only slightly.

It is evident from this discussion that, while some trends in the data have been identified, no overall pattern of variations or errors can be deduced.

4.3.3 MOST PROBABLE VALUES OF HUMAN HAND-ARM IMPEDANCE

The unexplained differences in mean values of impedance characteristics emerging from a single study or from the studies conducted by different investigators, serve to justify the exclusion of outliers from the synthesis of most probable values of human hand-arm impedance. The data thus excluded have been identified in the earlier discussion. The impedance magnitude as well as phase reported in a study for a specific direction are excluded from the synthesis when both are considered outliers. The exclusion of either the magnitude or the phase data of a study does not imply the exclusion of the other (magnitude or phase) from the synthesis. This treatment of the data is considered justified by the patterns of agreements and disagreements between the results of studies conducted by *Mishoe et al. (1977),* and others discussed in the previous section.

Most probable values of impedance may be defined as the range of values that represent the mechanical impedance of a normal human male hand-arm system subjected to sinusoidal or random excitations, under the influence of usual known sources of variability such as grip force, feed force and posture. The most probable values are derived from the envelope of the mean values reported in selected studies, upon removal of the outliers. The envelope curves

thus formed have been smoothened using closely approximated cubic spline functions (*Pokorny et al., 1989*) in the selected frequency range of 10 -1000 Hz.

The smoothed envelopes representing the range of most probable values of impedance magnitude and phase of the human male hand-arm in the 10 to 1000 Hz frequency range are shown in Figures 4.7 to 4.9, for X_h, Y_h and Z_h directions, respectively. The envelopes, presented in Figures 4.7 to 4.9, define the range of mean values of all the data sets selected for the synthesis, in the entire frequency range. The contours of magnitude and phase may be considered to characterize the range of *idealized* values of the human male hand-arm impedance in all three directions. The impedance are referred to as *idealized* in the sense that the contours encompass the impedance characteristics reported in all the investigations judged suitable for synthesis. The impedance data that fall within the range of *idealized* values, defined by the envelope curves, may be considered acceptable representations of human hand-arm impedance.

The values of upper and lower bounds of the *idealized* values of impedance envelopes are computed at 1/3 octave centre frequencies in the 10 - 1000 Hz range. Table 4.3 to 4.5 present the upper and lower bounds of the *idealized* values of impedance magnitude and phase for X_h, Y_h and Z_h directions, respectively. Mean values of impedance magnitude and phase of the data sets at the 1/3 octave centre frequencies are computed in the following manner:

$$\overline{Z}(\omega) = \frac{1}{N}\sum_{i=1}^{N}|Z_i(\omega)| \qquad (4.3)$$

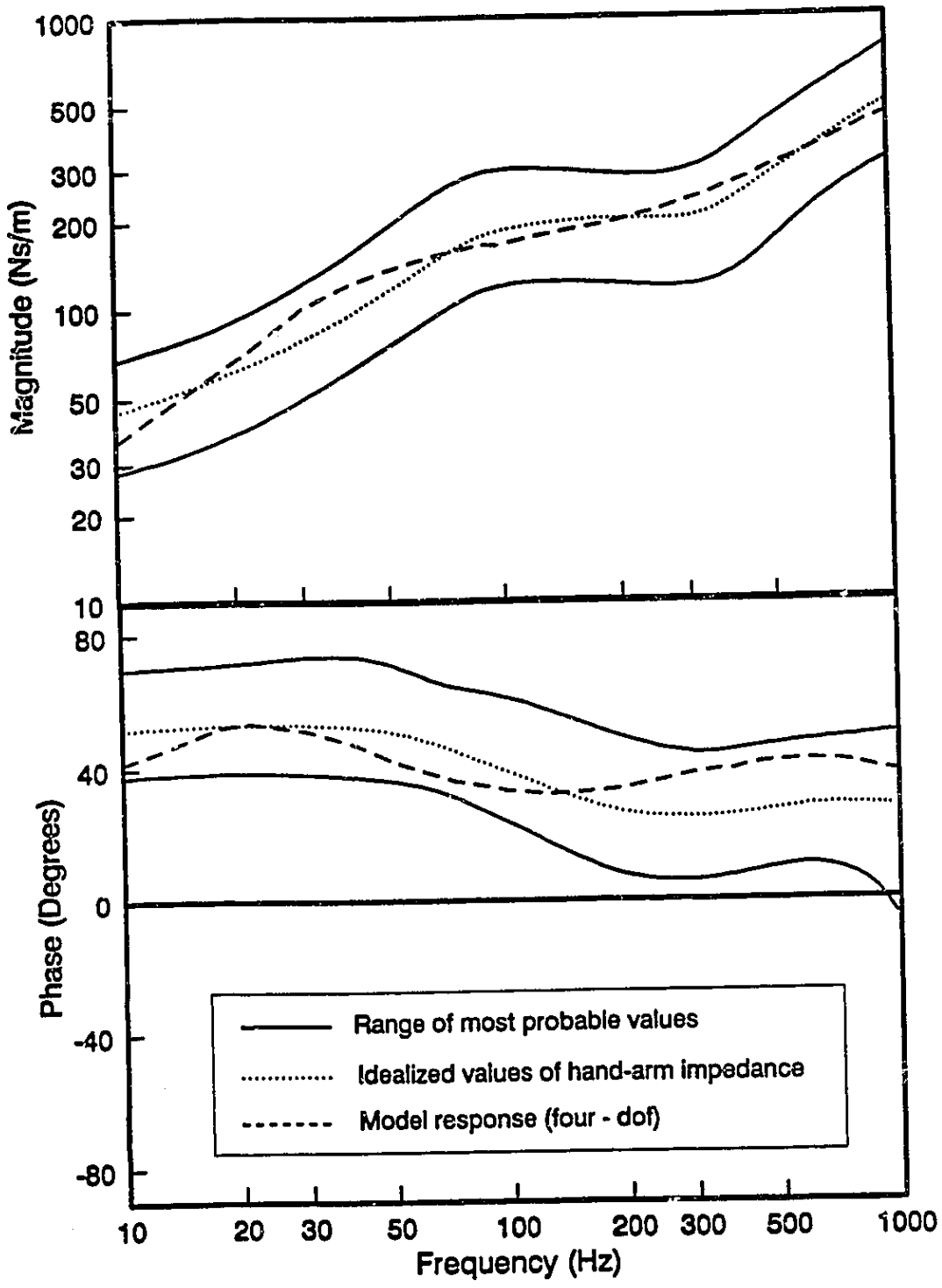

Figure 4.7: Idealized impedance data envelopes in X_h - direction.

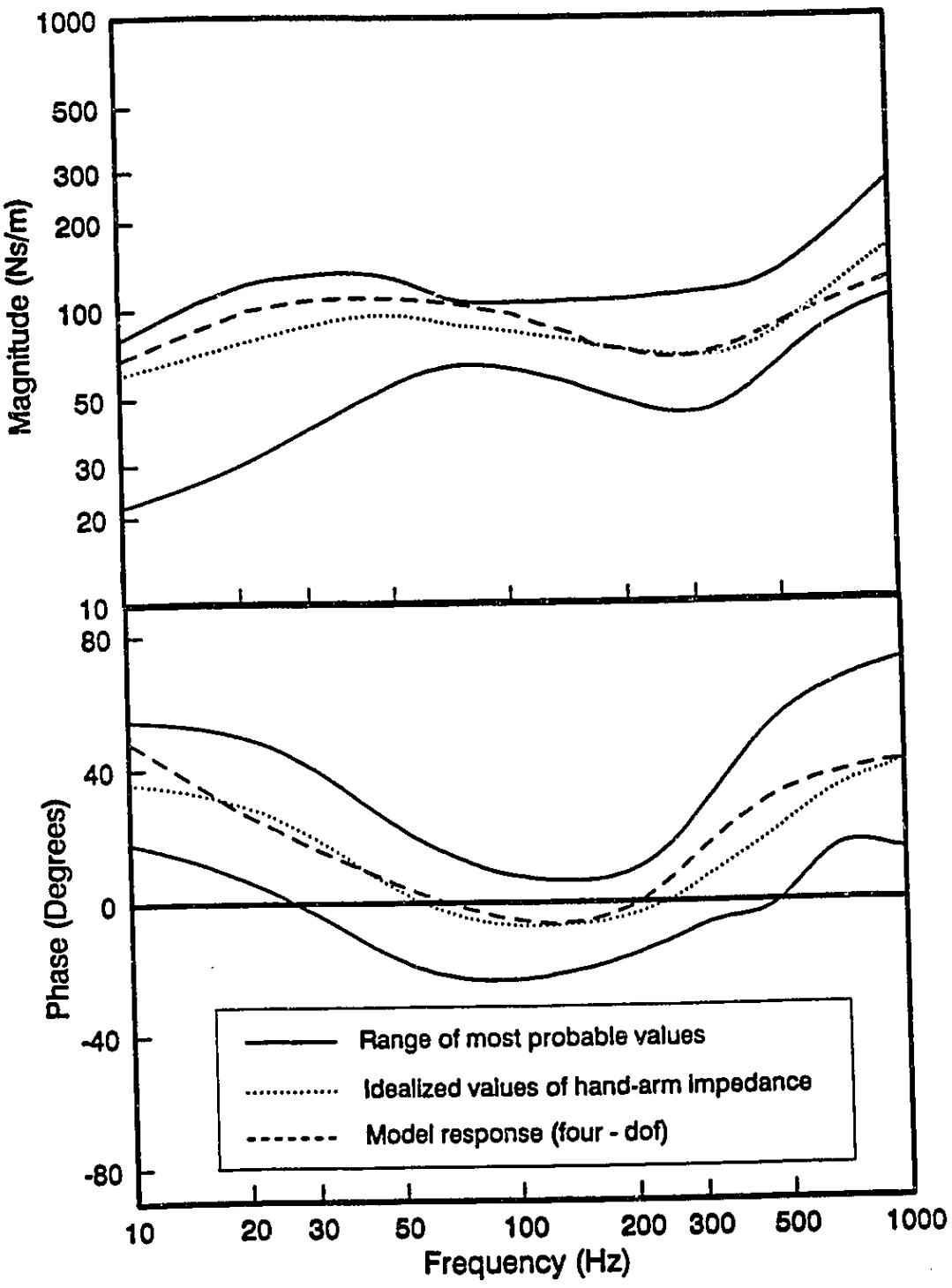

Figure 4.8: Idealized impedance data envelopes in Y_h - direction.

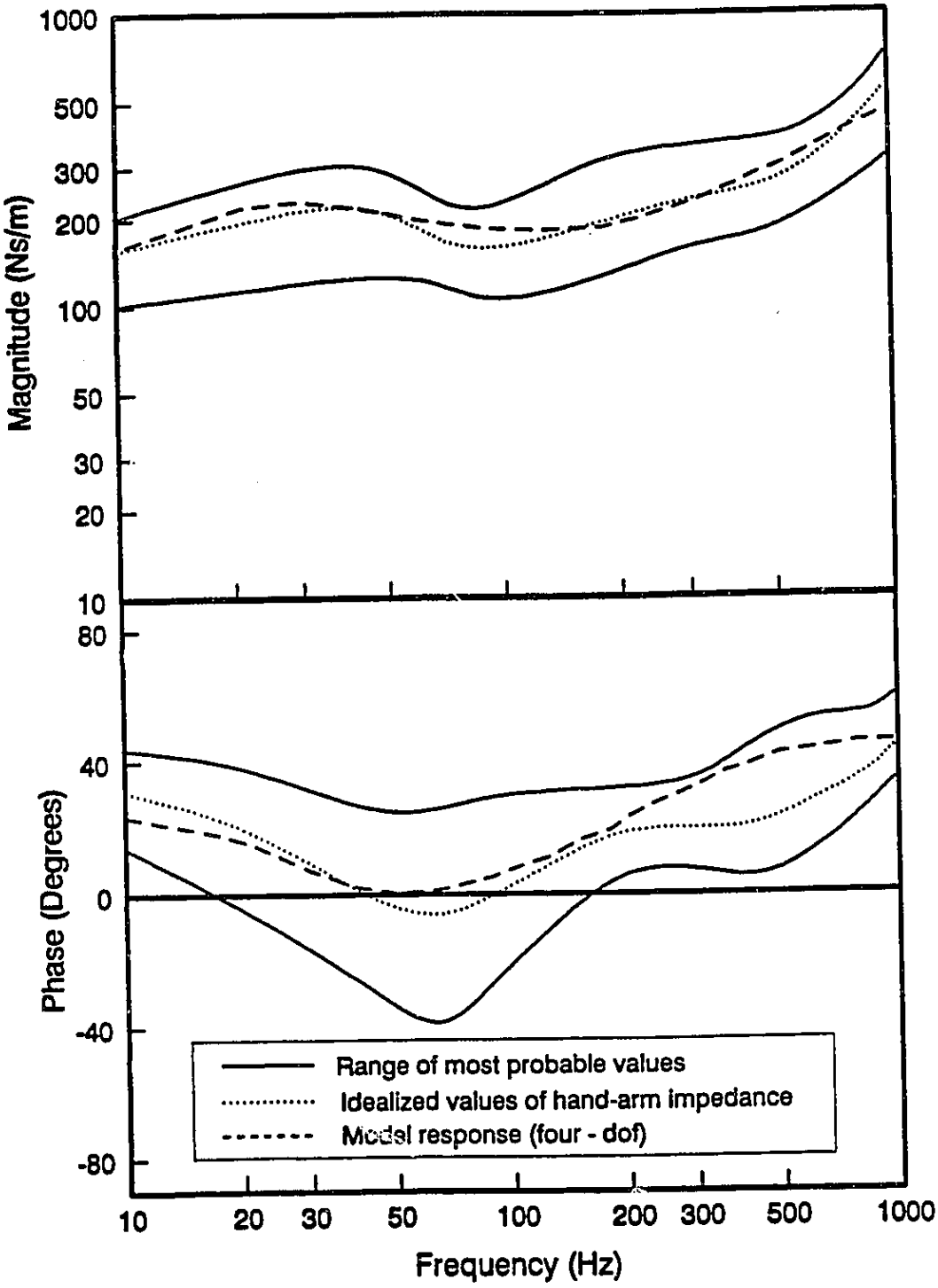

Figure 4.9: Idealized impedance data envelopes in Z_h - direction.

TABLE 4. 3
Idealized Impedance Values (X_h - Direction)

	Magnitude (Ns/m)				Phase (degrees)			
Frequency (Hz)	Upper limit	Lower limit	Standard error	Mean value	Upper limit	Lower limit	Standard error	Mean value
10	60	27	13	38	68	36	14	53
12.5	71	30	13	49	69	38	10	53
16	80	33	14	54	70	38	8	53
20	84	36	14	64	71	38	8	54
25	104	43	19	72	72	38	12	57
31.5	125	51	21	80	73	38	12	55
40	154	62	28	95	73	37	10	53
50	189	74	31	112	70	36	10	51
63	233	90	38	140	66	33	10	47
80	280	109	54	172	63	29	11	43
100	300	120	56	199	60	23	11	37
125	302	124	58	211	57	18	10	31
160	294	123	55	210	52	11	11	29
200	287	120	50	208	48	7	14	23
250	287	119	44	189	45	6	13	24
315	302	120	52	207	44	6	13	25
400	360	134	55	224	45	9	12	26
500	442	168	111	292	47	10	12	29
630	540	219	120	336	47	10	12	29
800	655	270	153	428	49	6	14	28
1000	775	320	168	498	50	-5	19	28

TABLE 4.4
Idealized Impedance Values (Y_h - Direction)

	Magnitude (Ns/m)				Phase (degrees)			
Frequency (Hz)	Upper limit	Lower limit	Standard error	Mean value	Upper limit	Lower limit	Standard error	Mean value
10	80	21	28	55	55	18	12	36
12.5	90	23	24	62	54	15	13	35
16	106	26	23	70	52	11	16	32
20	119	30	27	77	49	6	15	30
25	128	35	34	83	44	1	15	23
31.5	132	40	28	88	39	-6	15	18
40	135	48	29	95	30	-12	15	10
50	130	55	23	96	22	-18	12	3
63	117	61	14	93	16	-22	11	-2
80	106	64	12	88	10	-23	10	-5
100	106	63	15	86	7	-23	11	-7
125	106	60	16	80	6	-22	10	-7
160	107	54	17	77	7	-19	7	-6
200	108	49	20	71	9	-16	7	-6
250	110	45	23	67	17	-11	7	0
315	113	45	22	69	30	-7	14	8
400	118	51	19	71	45	-4	15	16
500	134	66	20	79	56	1	20	22
630	163	82	25	104	63	14	17	31
800	210	97	37	134	68	17	18	36
1000	270	108	59	161	71	15	22	41

TABLE 4.5
Idealized Impedance Values (Z_h - Direction)

	Magnitude (Ns/m)				Phase (degrees)			
Frequency Hz	Upper limit	Lower limit	Standard error	Mean value	Upper limit	Lower limit	Standard error	Mean value
10	200	100	34	153	44	15	10	30
12.5	220	104	45	165	42	10	12	28
16	241	108	60	180	40	2	15	24
20	260	112	70	190	38	-4	22	19
25	275	116	70	200	34	-11	22	15
31.5	297	121	75	215	30	-18	18	8
40	305	125	80	220	27	-26	16	1
50	288	126	61	207	25	-33	18	-4
63	247	122	40	181	25	-38	23	-6
80	219	109	30	160	28	-31	22	-3
100	227	105	47	160	30	-21	15	2
125	257	110	65	175	31	-10	11	8
160	298	120	85	185	31	0	10	14
200	325	130	84	200	32	6	7	18
250	345	146	65	216	33	8	5	19
315	355	160	65	231	36	7	12	19
400	365	169	63	246	43	5	14	20
500	377	183	64	265	49	7	13	23
630	420	214	69	315	53	14	15	28
800	520	260	85	400	54	24	10	35
1000	720	320	167	550	60	35	10	47

$$\overline{\varphi}(\omega) = \frac{1}{N}\sum_{i=1}^{N}\varphi_i(\omega) \qquad (4.4)$$

where $\overline{Z}(\omega)$ and $\overline{\varphi}(\omega)$ are mean values of impedance magnitude and phase at center frequency ω. $|Z_i(\omega)|$ and $\varphi_i(\omega)$ are the impedance magnitude and phase, respectively of the data set i, and N is the number of data sets available at the center frequency ω. The mean values of impedance magnitude and phase are illustrated as the central dotted curves in Figures 4.7 to 4.9. These mean values are considered to represent the *idealized* or target impedance magnitude and phase values for biodynamic modeling. Tables 4.3 to 4.5 also illustrate the mean or target values together with the standard errors, and range of idealized impedance magnitude and phase at 1/3 octave frequencies. The range of idealized impedance values provide the lower and upper limits of the envelopes constructed for all three directions. Mean values of each component of impedance magnitude possess at least one maximum and minimum, which are suggestive of the mechanical resonances of the human hand-arm system.

The mean or idealized values of X_h component of impedance magnitude, presented in Table 4.3, generally increase with increase in frequency, with a peak occurring in the 125 Hz band. The corresponding mean impedance phase values tend to decrease with increase in frequency. The frequency dependence of the Y_h component of impedance, as shown in Figure 4.8 and Table 4.4, is comparatively small in the entire frequency range, while slight peaks can be observed in 40 - 50 Hz bands, . The corresponding mean values of phase tend to decrease with increase in frequency, approaching the minimum value in 100 -

minimum value in 100 - 125 Hz bands. The mean phase value then increases gradually with frequency in the 125 - 1000 Hz frequency range. The mean values of Z_h component of impedance magnitude also tends to increase with increase in excitation frequency, with a small peak occurring in the 40 - 50 Hz band. The corresponding mean impedance phase tend to decrease with increase in frequency, and approaches a minimum value near the 63 Hz band. The mean phase increases with increase in the frequency, as illustrated in Figure 4.9 and Table 4.5.

The standard error of impedance magnitude and phase, in general, is high for each component of impedance, and varies with excitation frequency to reflect the variability of the human data. The error in impedance magnitude tends to increase with frequency, and approaches 30% to 37% at 1000 Hz, for each impedance component. The absolute error in the phase of the X_h and Y_h components of impedance also tends to increase with frequency, while that of the Z_h component peaks in the 63 Hz frequency band.

4.3.4 EFFECTS OF FORCES EXERTED BY THE HAND

It has been established that the driving-point impedance of the hand-arm system is influenced by the magnitude of the forces exerted by the hand. The impedance data sets included in this analysis may be further examined to study the variations in magnitude and phase of driving-point impedance with variations in the hand grip force. Although insufficient data are available to study the influence of grip force variations on the Y_h and Z_h components of impedance, a number of studies have reported the X_h impedance for different magnitudes of grip force (*Mishoe et al., 1977; Lundström, 1989, Burström et al. 1990*) as illustrated in Table 4.1. A reference grip force (F_g^*) of 25 N ± 2.5 N was thus

selected to examine the relative variations in the magnitude and phase characteristics of the driving-point impedance. The variations in magnitude and phase are computed as:

$$\Delta Z = Z(F_g, \omega) - Z(F_g^*, \omega)$$
$$\Delta\phi(\omega) = \phi(F_g, \omega) - \phi(F_g^*, \omega) \quad (4.5)$$

where ΔZ and $\Delta\phi$ characterize the variations in magnitude and phase, respectively, with variation in the grip force F_g relative to the reference grip force. $|Z(F_g, \omega)|$ and $\varphi(F_g, \omega)$ are the magnitude and phase values, respectively, corresponding to the selected grip force F_g. $|Z(F_g^*, \omega)|$ and $\varphi(F_g^*, \omega)$ are the magnitude and phase values, respectively, corresponding to the reference grip force F_g^*. The X_h component of driving-point impedance data, reported in this thesis (Chapter 2), and by *Burström (1990), Lundström (1989) and Mishoe et al. (1977)* for different values of constant grip force, were available to study the dependence of impedance on grip force. These studies have reported the X_h component of driving-point impedance for nearly constant magnitude of grip force ranging from 25 to 27 N.

Burström et al. (1990) and Lundström (1989) reported the human hand-arm impedance characteristics for three constant magnitudes of grip forces: 25 N, 50 N, and 75 N. The thesis research (Chapter 2) has conducted the impedance measurements for grip forces of 10 N, 25 N and 50 N. *Mishoe et al. (1977)* reported the impedance data for three magnitudes of contact grip forces; 13 N, 27 N and 40 N. The data reported by these studies are thus analyzed to quantify the dependence of impedance on the magnitude of the grip force. The

reference grip force was selected as 25 N, except for the data reported by *Mishoe et al. (1977)*, where the grip force was selected as 27 N.

Figures 4.10 and 4.11 illustrate the variations in impedance magnitude and phase values, respectively, for the available magnitudes of grip forces. It should, however, be noted that the magnitude of vibration excitation varied considerably in these studies, as indicated in the Figures. Figure 4.10 shows an increase in the magnitude of the driving-point impedance with increased grip force, in all the studies, at frequencies of 50 Hz and above. Pooling the data suggests that an increase in impedance magnitude of approximately 25 Ns/m will result above 50 Hz, when the grip force is increased from 25 to 50 N. The impedance magnitude increases by approximately 50 Ns/m with an increase in grip force from 25 to 75 N, in the 50 to 500 Hz frequency interval. At these frequencies, a reduction in grip force from 25 to 10 N is accompanied by a decrease in impedance magnitude of approximately 25 Ns/m. An adjustment by these amounts to the idealized X_h component of impedance magnitude, listed in Table 4.3, would therefore appear warranted for such changes in the grip force.

The variations in impedance phase due to change in the hand grip force, presented in Figure 4.11, show only small variations in the phase in the entire frequency range. The variations in the phase, observed in all the four studies, are generally less than ±15 degrees. However, there is little agreement among these studies as to the degree of change in impedance phase with hand grip. A pooling of the results reveals that a change in the grip force from 10 to 75 N would result in a change in impedance phase of less than ±15 degrees. This variation is considered small compared to the magnitude of standard error of the idealized phase values listed in Table 4.3. Accordingly, no adjustment to the

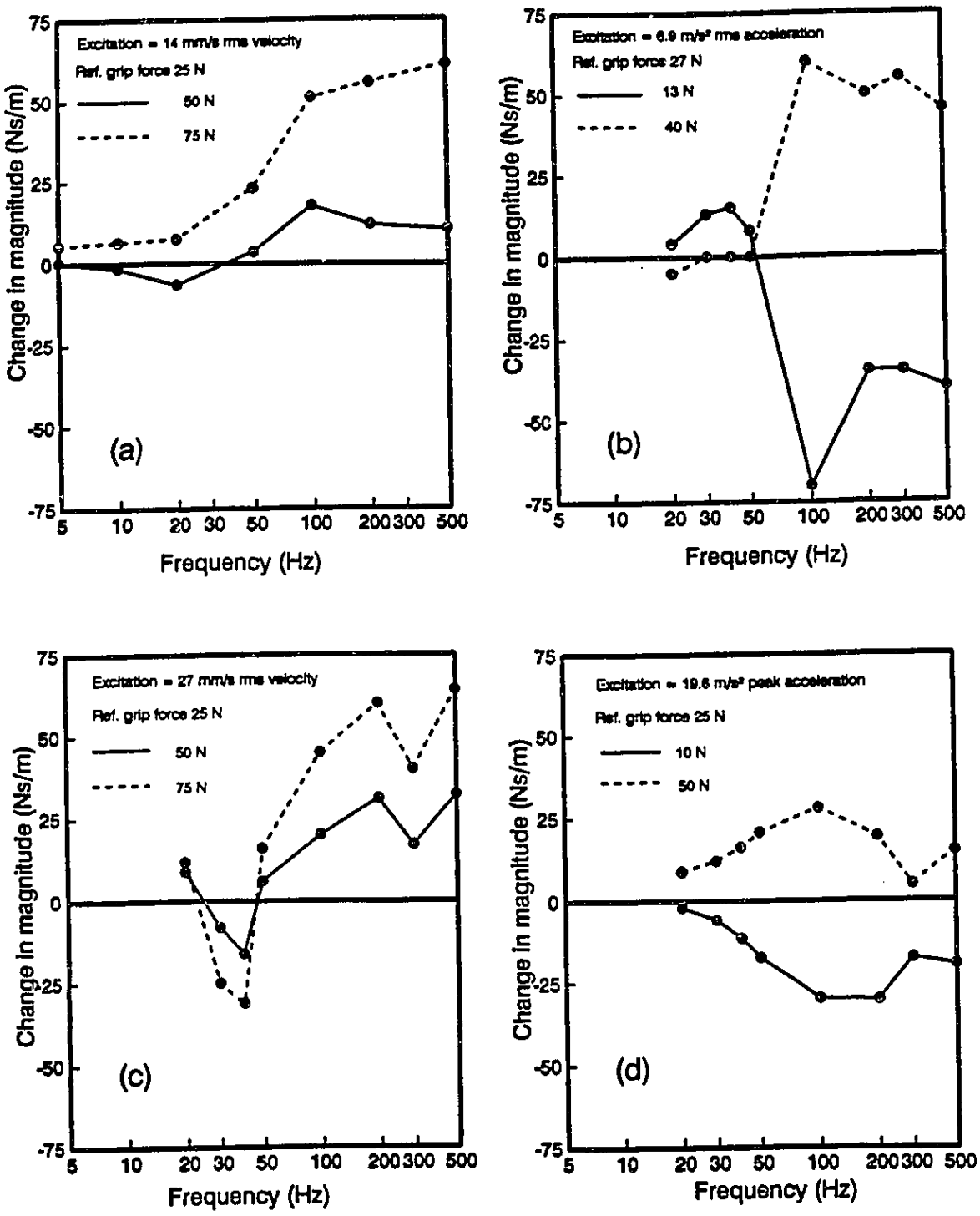

Figure 4.10: Variation in impedance magnitude with variation in grip force: (a) Burström (1990); (b) Mishoe (1977); (c) Lundström (1989); (d) derived from data presented in Chapter 2.

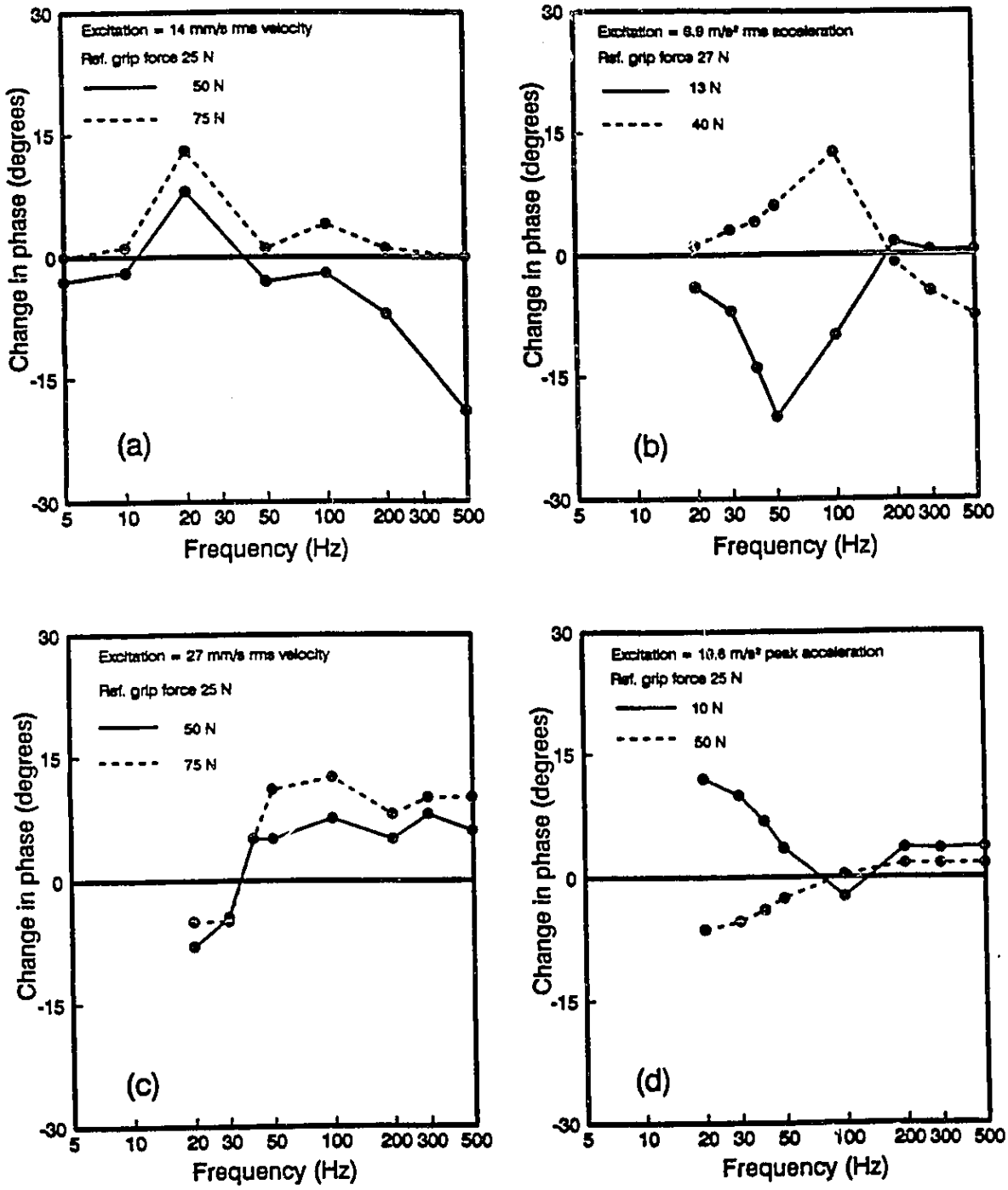

Figure 4.11: Variation in impedance phase with variation in grip force: (a) Burström (1990); (b) Mishoe (1977); (c) Lundström (1989); (d) derived from data presented in Chapter 2.

idealized values of impedance phase would appear to be warranted for changes in the grip force.

The influence of feed forces on the driving-point impedance has been investigated by *Bernard (1990), Griffin et al. (1982) and Hesse (1989).* These studies show that the magnitude of thrust force yields insignificant influence on the driving-point impedance, specifically at frequencies above 100 Hz. Small changes (<10%) in both magnitude and phase, were recorded at frequencies between 20 and 70 Hz. This parametric variation is substantially smaller and thus no adjustment to the idealized values of hand-arm impedance would appear to be justified for changes in thrust force.

4.4 Development of the Human Hand-Arm Model to Characterize the Idealized Impedance values

A four-DOF lumped-parameter model of the hand-arm system is formulated as shown in Figure 4.12. The lumped-parameter model is conceptually equivalent to each impedance component. Assuming linear restoring and dissipative elements, the equations of motion of the model may be expressed in the following matrix form:

$$[M]\{\ddot{x}\}+[C]\{\dot{x}\}+[K]\{x\}=\{p\} \tag{4.6}$$

where [M], [C] and [K] are (4x4) mass, damping and stiffness matrices, respectively. {x} is the displacement response vector and $\{p\}$ is the forcing vector. The model parameters, such as masses, damping coefficients and stiffness coefficients, are derived from the measured values of impedance using a constrained optimization algorithm as described in Chapter 3. An optimization

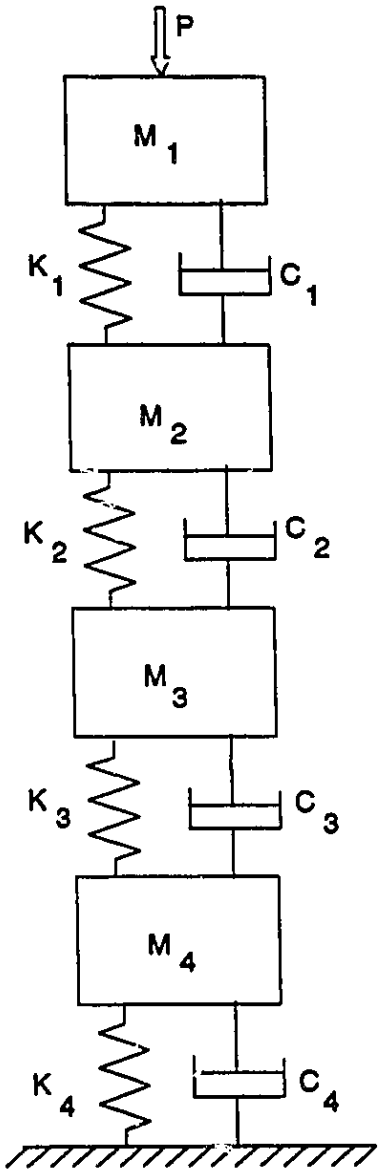

Figure 4.12: Four - DOF lumped parameter model of the human hand-arm system.

function is formulated to minimize the sum of squares of the errors between the magnitudes of measured and model driving-point impedance characteristics as a function of the excitation frequency. For the frequency range of interest (10 to 1000 Hz):

$$U(\bar{q}) = \text{Minimize}\left[\sum_{k=1}^{n}\left\{|Z(\omega_k)| - |Z_m(\omega_k)|\right\}^2\right]; \text{for} 10 \le \Omega_k \le 1000.\text{Hz} \qquad (4.7)$$

where $|Z_m(\omega_k)|$ is the magnitude of driving-point impedance derived from the lumped-parameter model at an excitation frequency ω_k, $|Z(\omega_k)|$ is the corresponding magnitude of driving-point impedance derived from the synthesis of measured values. Ω_k is the excitation frequency in Hz, and n is the number of discrete frequencies selected in the frequency range of interest. $U(\bar{q})$ is the optimization function , and $\bar{q}$ is a vector of model parameters, given by:

$$\bar{q} = \{m_i, c_i, k_i\}^T; i = 1,..4 \qquad (4.8)$$

where T designates the transpose, and m_i, c_i, k_i are the masses, damping constants and stiffness coefficients of the lumped-parameter model, respectively. The optimization function is subject to following parametric constraints:

$$\begin{aligned} &m_i > 0.; c_i > 0.; k_i > 0. \\ &3.50 \le \sum_{1}^{4} m_i \le 6.00\text{kg} \end{aligned} \qquad (4.9)$$

The total model mass is constrained within a range of average values for the human male hand-arm system *(Chaffin et al., 1984).* The model parameters

have been determined using the target values of impedance magnitude and phase through solution of the constrained optimization problem described by Equations (4.5) to (4.7). The optimization algorithm attempts to minimize the sums of the squares of the errors in both impedance magnitude and phase, computed at 30 discrete frequencies in the 10 to 1000 Hz frequency range. The target impedance values are the mean values of component impedance magnitude and phase listed in Tables 4.3 to 4.5, and shown by the dotted curves in Figures 4.7 to 4.9.

TABLE 4.6
Parameters of the Lumped-Parameter Models
Derived From the Synthesized Data

Parameters	Direction of Vibration		
	X_h	Y_h	Z_h
m_1 (*kg*)	4.30E-03	9.10E-03	1.90E-02
m_2	1.05E-01	5.44E-02	9.47E-02
m_3	5.66E-01	1.42	6.55E-01
m_4	4.304	3.62	4.29
k_1 (*N/m*)	8.88E04	6.50E02	3.00E05
k_2	1.50E03	1.93E05	6.80E04
k_3	1.00E02	6.50E02	1.99E02
k_4	3.99E03	1.00E03	2.04E03
c_1 (*Ns/m*)	6.78E02	1.15E02	5.91E02
c_2	1.85E02	1.47E02	2.03E02
c_3	2.39E01	8.00E00	1.99E02
c_4	3.49E01	1.00E03	2.3902

The parameters of the four-DOF model that best fit the idealized impedance values, both in magnitude and phase, are listed in Table 4.6. The

impedance magnitude and phase response characteristics of the model, for each component, are shown by the dashed curves in Figures 4.7 to 4.9. A comparison of the model response and idealized impedance characteristics reveals that the proposed lumped-parameter models, presented in Figure 4.12, can predict the mean idealized impedance in the entire frequency range for all the three directions. Further, the predicted values remain within the upper and lower bounds of idealized impedance, as defined by the continuous curves in Figures 4.7 to 4.9, in the entire frequency range. though the Y_h component of impedance magnitude approaches close to the upper bound of idealized values near an excitation frequency of 60 Hz.

In the optimization based curve-fit algorithm, the total hand-arm mass was constrained within the 3.50 - 6.00 kg range, which is approximately 5% of the total body mass. The model parameters, presented in Table 4.6, reveal that the total model mass is 4.98, 5.10 and 5.06 kg in the X_h, Y_h and Z_h directions, respectively. While the different model masses cannot be related to physiological structures in the hand-arm system, it is evident the model mass is concentrated near the fixed base of the hand-arm (m_4, *i.e.* near the torso). The mass m_3, closest to the fixed base, is observed to be the second largest in all three directions of excitation. The hand-arm model mass, directly in contact with the handle (m_1) and subjected to the excitation, is the smallest in magnitude, irrespective of the impedance component or direction of excitation. Dynamic masses in direct contact with the handle, ranging from 4.3 to 19 grams, may be expected to represent a superficial component of the flesh or skin (*e.g.* palm and the fingers) coupled to the motion. For the X_h and Z_h axes impedance models, the spring constant k_1 and damping coefficient c_1 are large in comparison with the remaining visco-elastic elements of the model, suggesting a strong coupling

between masses m_1 and m_2. This observation, together with the magnitudes of m_2 (between 54 and 105 grams) suggest that these masses may represent a subcutaneous component of the flesh within the hand coupled to the motion. In the Y_h axis model, however, the relatively large values of k_2, k_4 and c_4 suggest couplings between m_2, m_3, m_4 and the fixed base.

4.5 Summary

The driving-point mechanical impedance data of the human hand-arm system, reported in the literature, differ considerably in magnitude as well as phase angle response. While an attempt has been made to enhance an understanding of these differences with variations in test parameters and conditions employed by different investigators, these discrepancies generally remained unexplained though certain patterns of impedance dependence are established. Although considerable differences exist among the various impedance data, the impedance data acquired under similar test conditions can be grouped within reasonable envelopes of magnitude and phase angle. A synthesis of the measured values of human male hand-arm impedance characteristics reported in the literature has been performed. The driving-point mechanical impedance data of the human hand-arm grasping a vibrating handle have been compared to highlight the various similarities and differences among the data. The unexplained differences among the results of various studies, conducted independently under nominally equivalent measurement conditions, are taken to justify the exclusion of outliers from the analysis. The most probable values of impedance phase and magnitude are defined by lower and upper envelopes of the mean values of the accepted data sets. The weighted mean of the data sets, together with the smoothened envelopes, are used to define the target and range of idealized values of X_h, Y_h and Z_h components of

impedance in the 10 to 1000 Hz frequency range. A four-degree-of-freedom, lumped-parameter model is derived to fit the target impedance magnitude and phase values using a constrained optimization algorithm. The predicted values correlate well with the target values in the selected frequency range. In view of considerable differences noticed among studies, the need to examine more closely the various parameters influencing the dynamic response of hand-arm system is recognized. Among various factors considered, grip force is the most important factor to have significant influence on hand-arm response characteristics. Although, several authors have attempted to measure the hand response under controlled total grip force levels, the local pattern and distribution of grip forces have not been studied. In the ensuing chapter, a new method of studying hand grip pressure distribution is proposed. The hand grip pressure distribution data is further analyzed in relation to hand response to vibration and the occurrence of VWF syndrome.

CHAPTER 5

HAND GRIP PRESSURE DISTRIBUTION UNDER STATIC AND DYNAMIC LOADING

5. 1 Introduction

Numerous clinical investigations have identified the symptoms of VWF related to hand-transmitted vibration, and the stomach and spinal disorders caused by the whole-body vibration (*Wasserman, 1987; Griffin,1990*). Objective measures of hand and whole-body vibration have been thoroughly investigated to identify a definite relationship between the vibration exposure and the operator fatigue, loss of productivity, and the various symptoms related to VWF, spinal disorders and stomach diseases (*Griffin,1990*). The studies involving measurement of transmitted vibration, together with clinical studies, and the epidemiological studies have succeeded in identifying a definite relationship between the vibration exposure and the occurrence of VWF symptoms among the operators. These studies, however, do not provide an insight to the mechanism leading to the symptoms related to VWF.

While the response characteristics of the human-arm system have been extensively investigated for different values of overall hand-grip forces (*Reynolds et al., 1984*), only few attempts have been made to study the distribution of dynamic forces transmitted to the operator's hand (*Krause et al., 1979*). The hypothesis proposed by several studies indicating that VWF may be related to impaired blood flow in the hands of the power tool operators (*Pelmear et al., 1992*), however, has not been critically examined considering the dynamics involved at the hand-tool interface.

A study of distribution of forces at the human-machine interface under static and dynamic loads can provide considerable insight to the transmission of forces and stresses experienced by operators. The local grip pressure distribution may be more closely related to the finger blood flow, fatigue and loss of productivity. In the case of hand-held power tools, the hand grip pressure distribution (GPD) under dynamic conditions can be used to investigate hand injury and fatigue mechanisms, and to carry out ergonomic design and evaluation of handle grips. Particularly, the GPD data may provide additional input to the VWF phenomena as the disease is known to be associated with reduced blood supply to the fingers.

In this phase of thesis research, flexible pressure sensors are investigated to acquire the pressure distribution at hand-handle interface under static and dynamic conditions. The vibration response characteristics of the human hand-arm system are investigated through analysis of the measured distribution of the grip pressure at the hand-handle interface. The magnitude and location of the peak pressures are identified as a function of the handle vibration and grip force. The location of peak pressure is finally related to the possible impairment of blood flow to the fingers

5. 2 Measurement of Grip Pressure Distribution

The VWF disease among the operators of hand-held power tools has been related to the nature of vibration exposure and the grip force. A Number of studies have also concluded that the tips of index, middle and ring finger are the first parts of the hand that are affected by the VWF disease (*Brubaker et al., 1983; Hellstrom et al., 1972*). These conclusions are further supported by a study of the hand of stone-cutters affected by VWF, which characterizes the

severity of the symptoms in different parts of the hands as shown in Figure 5.1. The figure clearly illustrates that the tips of the index, middle and ring fingers are mostly affected by the VWF disease. Further, the loss of sensation in the right hand is relatively severe in the entire region from base of thumb to tip of index finger. Closer lines in Figure 5.1 indicates the intensity of the disease. *Nerem (1977)* indicated that occurrence of high pressure and frictional forces influence the hemodynamic forces in the arterial walls and produce alteration to blood flow. The finger skin friction caused by prolonged action of vibration has been related to formation of subcutaneous callosities, and the callosed finger pads lead to capillary occlusion which decreases the blood volume in capillaries *(Stewart et al., 1970)*.

A knowledge of the distribution of contact forces of the hand is thus extremely vital to identify location of concentration of high forces that may cause reduced blood flow to the finger tips, and thus the VWF disease. Measurement of distribution of forces at the hand-handle interface, however, is complex due to the requirements of a large number of thin and flexible sensors, and a signal analysis system with capabilities to acquire and analyze many channels of data.

5.2.1 INTERFACE PRESSURE SENSORS

Measurement of pressure distribution at a human-machine interface requires a comprehensive grid of thin and flexible sensors, such that the visco elastic properties of the interface remain unaltered during static and dynamic measurements. In the recent past, a number of interface pressure measuring systems have been developed. Sensors such as rubber butterfly valves, manometers, sprung flat boards, strain gages, silicon diaphragms and foil

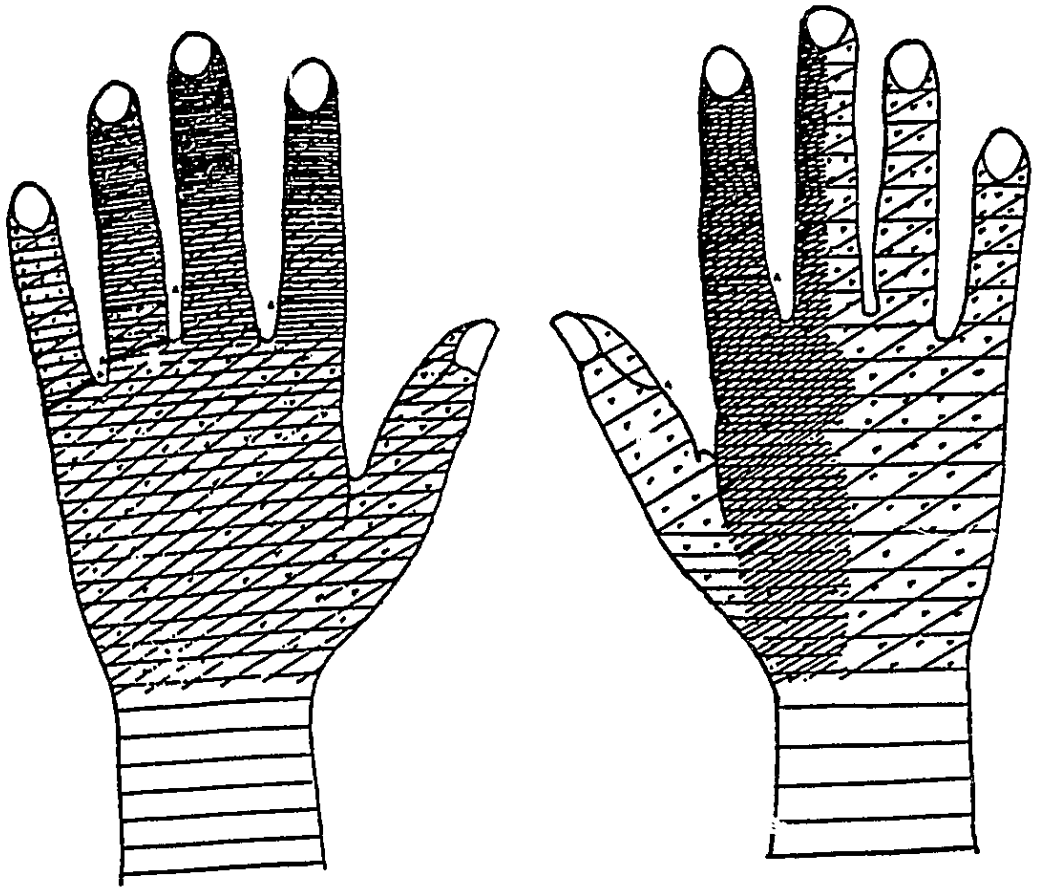

Horizontal lines indicate decrease in sense of touch.

Diagonal lines indicate decrease in sense of pain.

v - shaped marks indicate decrease in sense of heat and cold.

Thick lines (A) indicate margin of anemic area after immersion in cold water.

Figure 5.1: Hands of a stonecutter showing VWF symptoms (US *department of labor report, 1918; and cited by Brammer, 1984; Yodaiken et al., 1985*).

capacitors have been used in conjunction with multi channel data acquisition systems to acquire the distribution of pressure at the human-seat interface (*Linden et al 1965, Holley 1979*). All these sensors pose severe limitations in view of the flexibility of the interface. These sensors either are applicable to hard surfaces or alter the elastic properties of the interface surface. Attempts have also made to acquire hand grip pressure distribution at the hand-tool interface, under static loading conditions, using a pressure resistive paint (*Abrams, 1971*), conductive thioplastic sensors (*Krause et al., 1979*), and force sensing resistors (*Fellows et al., 1991*). But, these attempts were met with moderate success due to nonlinear behavior of the transducers. In this study, flexible resistive and capacitive sensors, which offer the potential to acquire static as well as dynamic pressures, were investigated to acquire the GPD at the hand-handle interface.

Force Sensing Resistive Sensors

Piché et al. (1988) have used force sensing resistors to study the pressure distribution pattern at a human-seat interface under static conditions. The basic sensing element was an ultra thin and flexible force sensing resistor, and a film of foil conductors. The force sensing resistor consisted of a polymer sheet with a layer of flexible sensing film. The foil conductor film was a mylar sheet with a pattern of open ended conductors. The infinite resistance of open ended conductors was shunted by placing the force sensitive resistor against the foil film. The change in resistance of the assembly was related to the force applied to the surface. The sensors used in the study formed a 9.75 mm diameter sensing assembly, comprising of two polymer sheets, and was 0.25 mm thick.

A resistive pressure sensing grid of 10 sensors was first fabricated to conduct the feasibility study. Each sensor was supplied with a 0.24 mA constant current at 1.5 V. A conditioning circuit was integrated and the sensors were calibrated to determine the force-resistance relationship, and the precision and repeatability using a pneumatic actuator. The static calibration curve, shown in the Figure 5.2, exhibited nonlinear characteristics with large hysteresis. Although the sensors showed good repeatability over a short period, the repeatability and dynamic range deteriorated rapidly due to oxidation of the foil conductors. These sensors were thus considered infeasible for the present study.

Variable Capacitive Pressure Sensors

Alternatively, a pressure measurement system comprising flexible variable capacitance sensors, a conditioning circuit and data-acquisition software, referred to as the EMED system, was employed to acquire the GPD (*NOVEL gmbh, 1989*). EMED is an electronic measurement system for recording and evaluating pressure distributions on flat and curved surfaces (*Seitz, 1990*). The EMED sensor consisted of a pressure sensing element sandwiched by an elastic synthetic mat. Figure 5.3 illustrates the schematic of a variable capacitance pressure sensing element and its equivalent electrical circuit. The measurement system provided digital voltage (AD) values proportional to the variations in sensor capacitance with the applied load. The sensors, designed for a maximum pressure of 400 kPa, were excited with 20 V peak-to-peak voltage at 200 kHz. Each sensor was calibrated by applying known pressures using a pneumatic actuator. The schematic of the sensor calibrating

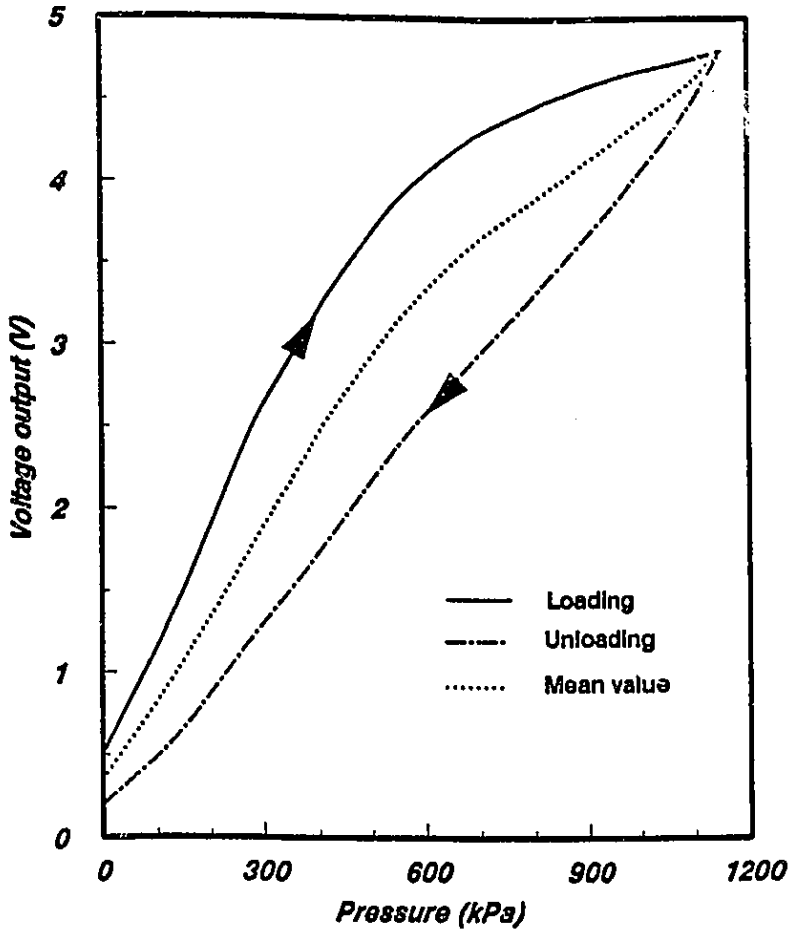

Figure 5.2: Calibration curve of a resistive pressure sensor.

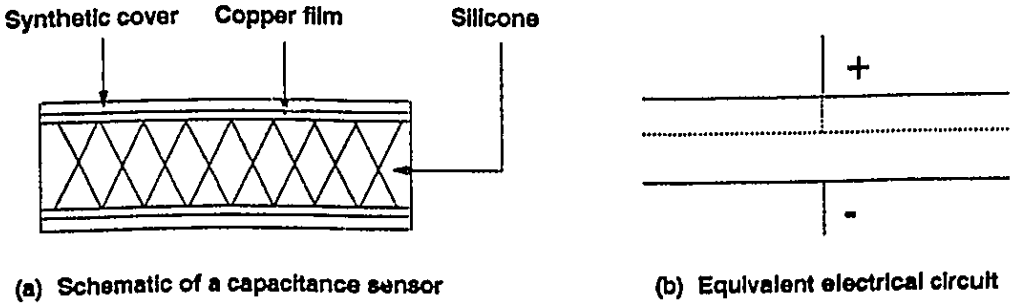

Figure 5.3: Schematic of a EMED capacitive sensor and its equivalent electrical circuit.

on a fixture is shown in Figure 5.4. The sensor signals were then digitized to obtain the corresponding AD values. Figure 5.5 illustrates the typical nonlinear calibration curve of the capacitive sensor in the pressure range of 0 - 400 kPa. The calibration curve, approximated by a third order polynomial, reveals nonlinear characteristics and poor resolution for pressures in excess of 250 kPa.

A grid of 20 sensors was fabricated to acquire the local pressure distribution at the hand-handle interface. The instantaneous AD values, the time and the coordinates of each sensor were recorded using the EMED data acquisition software. The data acquisition and EMED system allowed both static and dynamic measurements with a maximum speed of 150,000 samples/s.

5.2.2 METHOD OF MEASUREMENT

The experimental setup with a handle diameter of 38 mm was designed to enable it to excite in any of the three orthogonal directions of vibration (ISO 5349). The hand-handle orientation in different directions is as shown in Figure 2.1. The handle was instrumented with strain gages to measure total grip force and a matrix of 20 flexible variable capacitance EMED pressure sensors to measure the corresponding hand GPD under various static and dynamic loading conditions. The instrumented handle was mounted on an electro-dynamic vibration exciter such that either harmonic or random vibrations may be applied. In view of the symmetric nature of the grip force on either side of the split handle only two strain gages were mounted in a half-bridge configuration. One gage was mounted in the axial direction to measure the bending strain caused by the grip force, while the second gage was

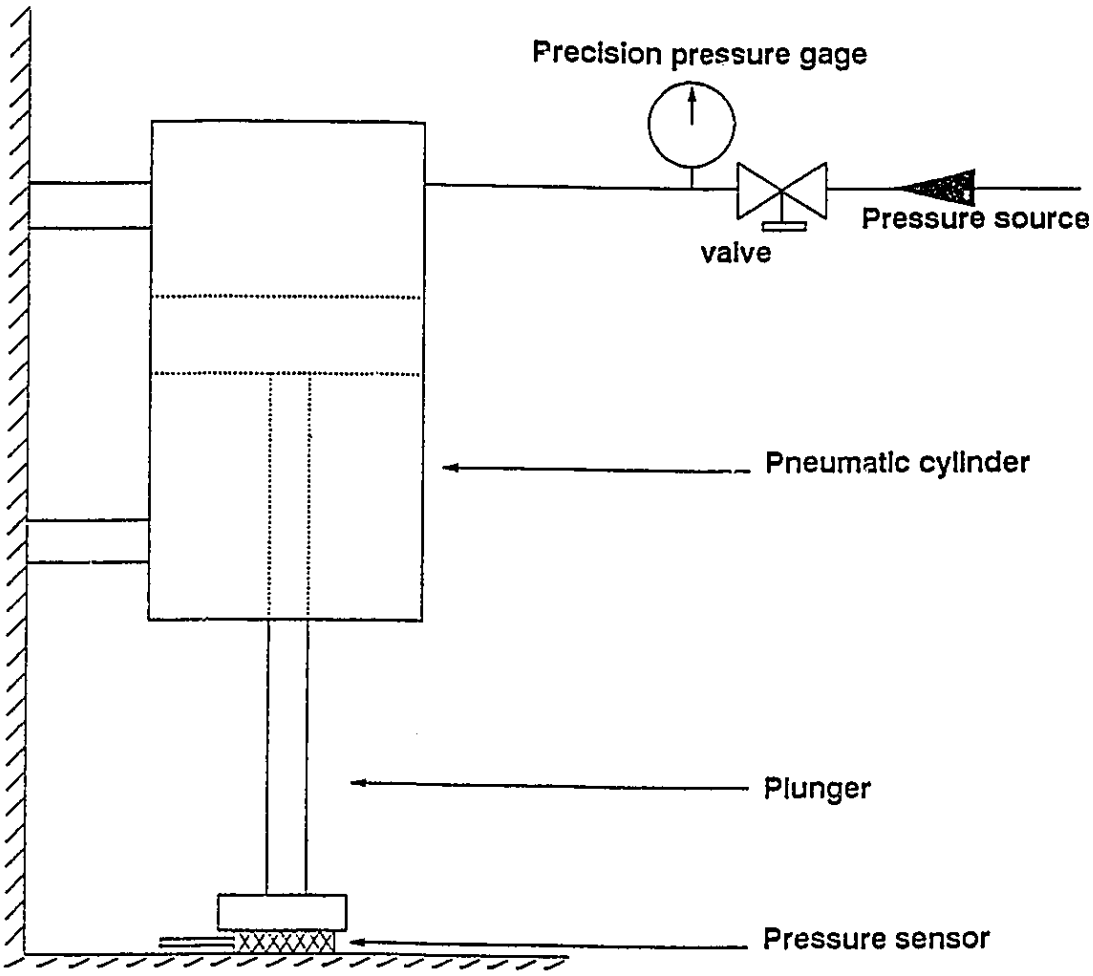

Figure 5.4: Schematic of the sensor calibration setup.

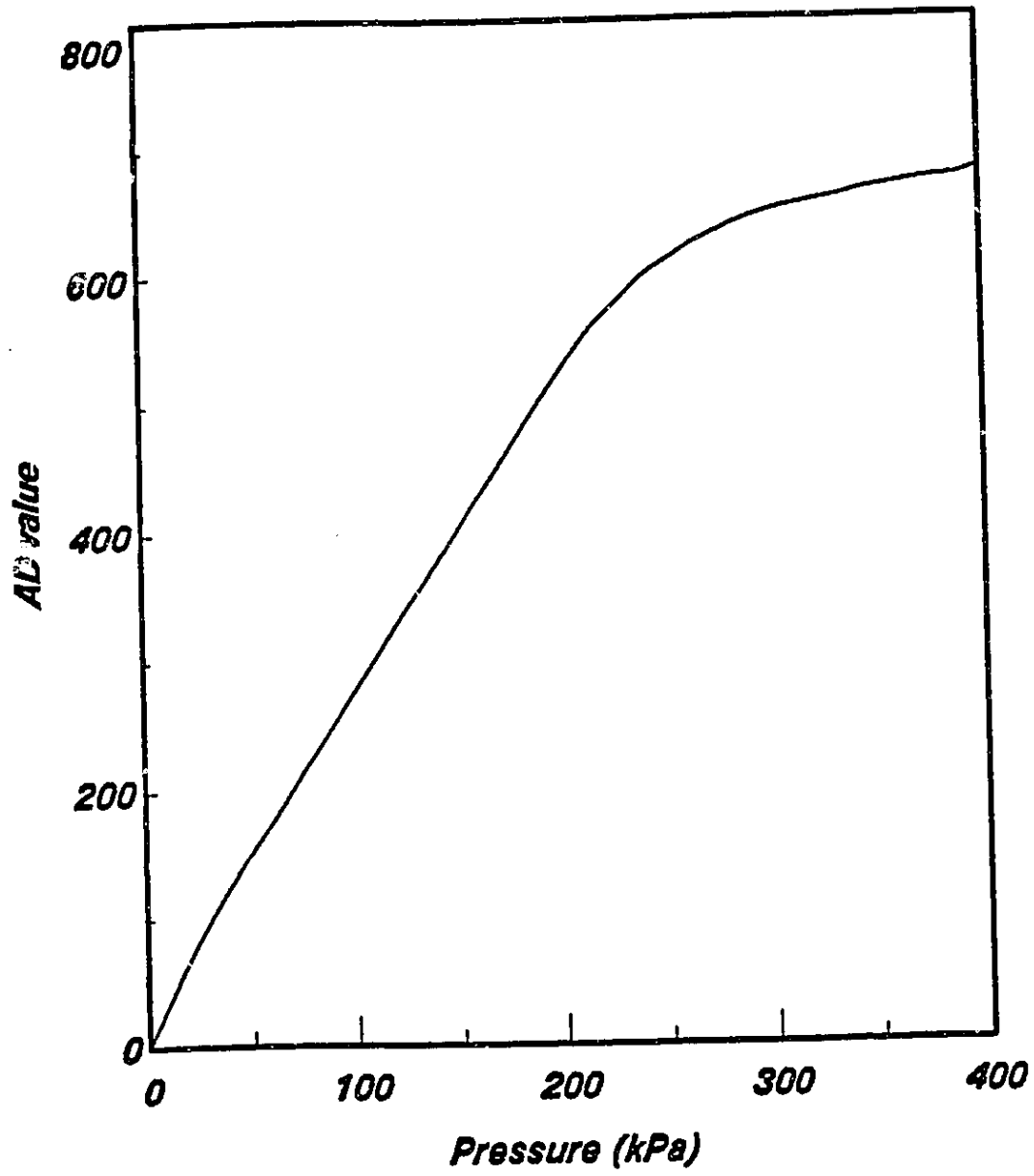

Figure 5.5: Calibration curve of a EMED capacitive pressure sensor.

oriented perpendicular to the first gage for temperature compensation. The strain gages were calibrated using *Vishay Electronics* strain conditioner, by applying known loads at a preselected location along the axial axis of the handle. The total grip force was derived from the conditioned and amplified strain gage signal. The subjects were advised to grip the handle around the preselected location. The total grip force measured by the strain gages was displayed to the subjects through a digital voltmeter to enable the subjects to maintain nearly constant grip force. Figure 5.6 illustrates the schematic of the measurement system.

Hand GPD of four subjects were acquired under static and dynamic loading conditions. The attributes of subjects are listed in Table 2.2. The subjects were trained under simulated experimental conditions several times. Each subject was advised to maintain an identical body posture during all the experiments and to grip the handle with the dominant right hand while keeping the forearm horizontal with an elbow angle of 90. The subjects were advised to maintain nearly constant grip force by monitoring the strain gage signal displayed on the digital voltmeter. The gripping hand of each subject was positioned on the handle in a specific manner to attain a pre-determined sensor pattern as shown in Figure 5.7.

The hand GPDs under static and dynamic conditions were acquired for grip forces of 25 N, 50 N, and 100 N. The GPDs under dynamic conditions were obtained using harmonic excitations of constant peak accelerations of 1.0 g, 2.0 g and 3.0 g at discrete frequencies of 20 Hz, 50 Hz, 100 Hz, 200 Hz, 500 Hz and 1000 Hz. The GPD measurements under static conditions were performed four times with a 50 N grip force and the data were examined for

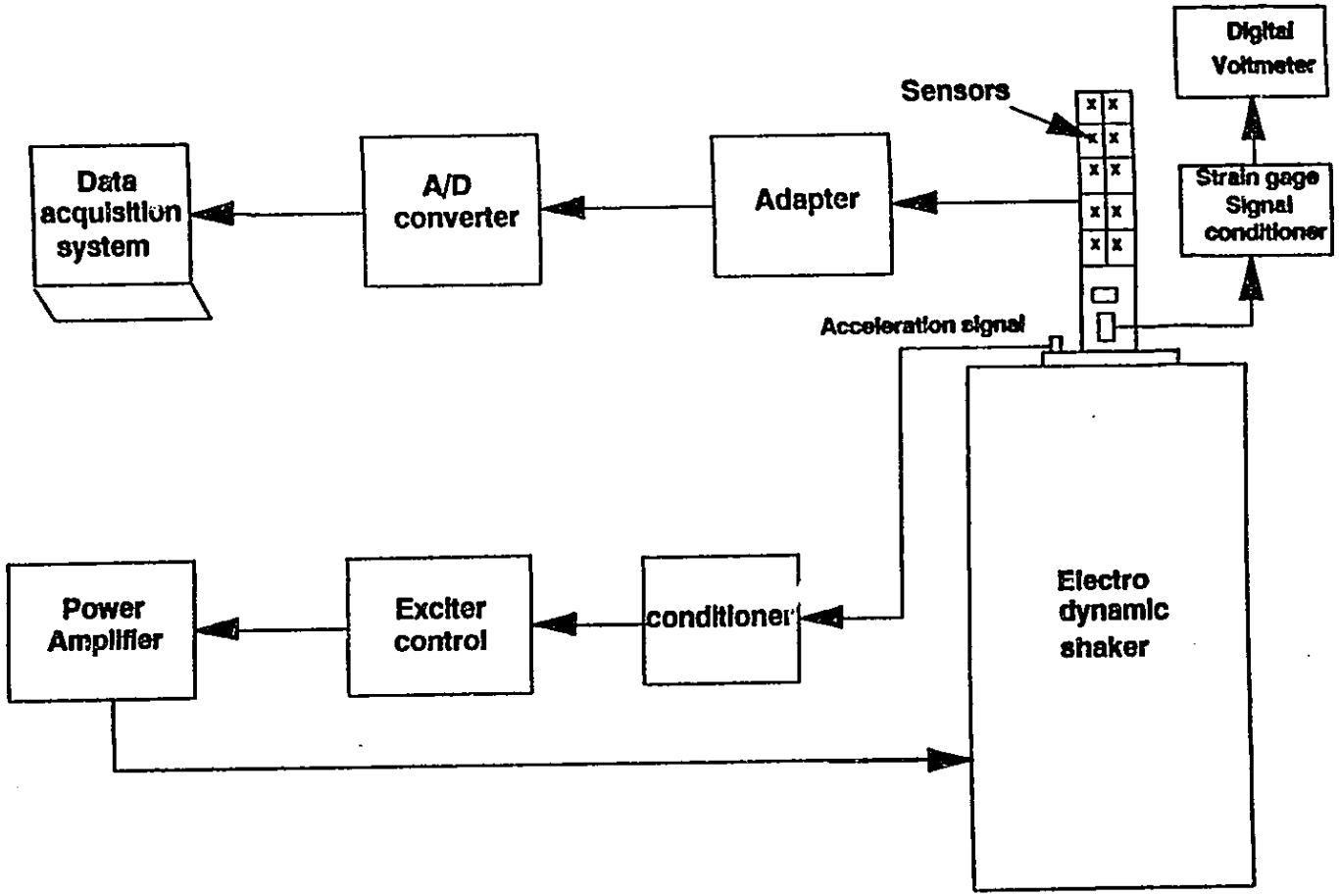

Figure 5.6 Schematic of the grip pressure measurement system.

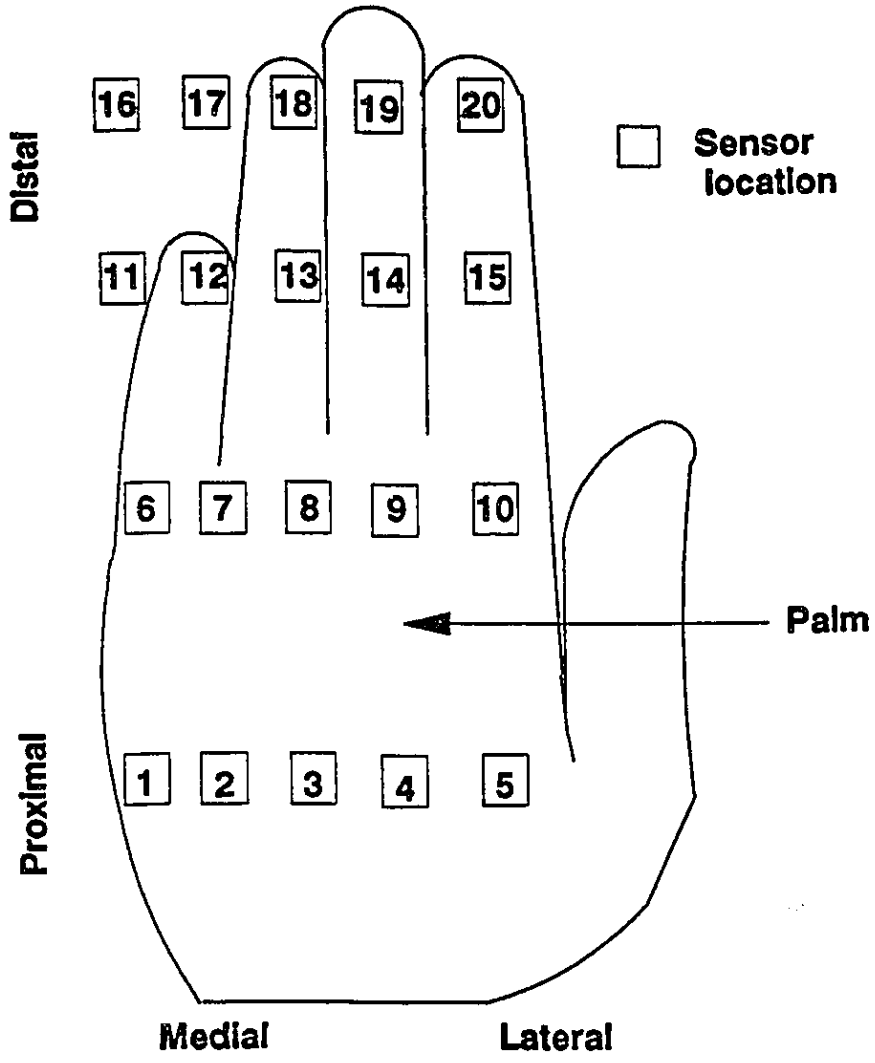

Figure 5.7: Location of pressure sensors on a stretched hand.

repeatability. Similarly, the repeatability of GPD under dynamic conditions was examined by measuring GPD for 50 N grip force and 2.0 g peak acceleration at 100 Hz. The experiments showed good repeatability.

5.3. Results and Discussion

The measured data were averaged and analyzed for different static and dynamic test conditions to highlight the influence of grip force, and characteristics of handle vibration on the local concentration of forces at the hand-handle interface. The measurements performed on the selected subjects revealed a high degree of consistency in terms of the **location of the peak pressures**. In order to demonstrate the effectiveness of the method of measuring hand-tool interface pressure and to fulfill the stated objective of this phase of research, representative sets of data acquired at different experimental conditions are discussed. The unreported results, however, revealed similar patterns of GPD under varying dynamic conditions. The GPD data are analyzed to determine the **location of high pressure peaks** at the hand-handle interface. The location of peak pressure is then examined to derive a correlation with the onset of VWF disease caused by impaired blood flow to the index, middle and ring fingers. The GPD results are thus discussed to highlight the **location of peak pressures** under static and dynamic loading conditions, while the magnitudes of pressure peaks are given secondary consideration

Figure 5.8 - 5.10 presents the hand grip pressure distribution measured on a single subject (subject # 1) for a total grip force of 25 N, 50 N and 100 N in X_h - direction under static loading condition. The magnitudes of pressures measured by 20 sensors in the grid are presented, as a function of the

longitudinal and lateral coordinates of the hand. The sensor location and corresponding magnitude of pressure on the hand is described in terms of its coordinates with reference to the approximate mid-point of the base of the hand. The location of sensors is described as distal and proximal along the longitudinal axis, and as lateral and medial along the lateral axis. From Figure 5.9, it should be noted that sensors numbered 18, 19 and 20 are located at the tips of ring, middle and index fingers, respectively. Sensors numbered 13, 14 and 15 are located at middle of the fingers, while the sensors numbered 4,5 and 6 are located near the base of the thumb.

Figures 5.8 - 5.10 reveal a high concentration of pressure at the index finger tip (sensor # 20) under static loads irrespective of the magnitude of the total grip force. At low grip force (25 N), the pressure distribution over the entire hand is nearly uniform, and the magnitude of local pressures is small except for the high peak observed at the tip of the index finger, as shown in 5.8. The magnitude of interface pressures at the tip to the middle finger (sensor # 19) and middle of the index finger (sensor # 15) increase, when the grip force is increased to 50 N. The magnitude of pressure measured at the tip of the index finger, however, remains considerably high, as shown in Figure 5.9. A further increase in the grip force to 100 N yields high interface pressure at the base of the thumb (sensor # 5), as shown in Figure 5.10. The highest magnitudes of interface pressures, however, are observed at the finger tips. A comparison of the interface pressure distributions, presented in Figures 5.8 - 5.10, reveals that while the magnitude of peak pressure varied significantly with the grip force the peak pressure occurs at the tip of index finger (sensor # 20), irrespective of the magnitude of grip force.

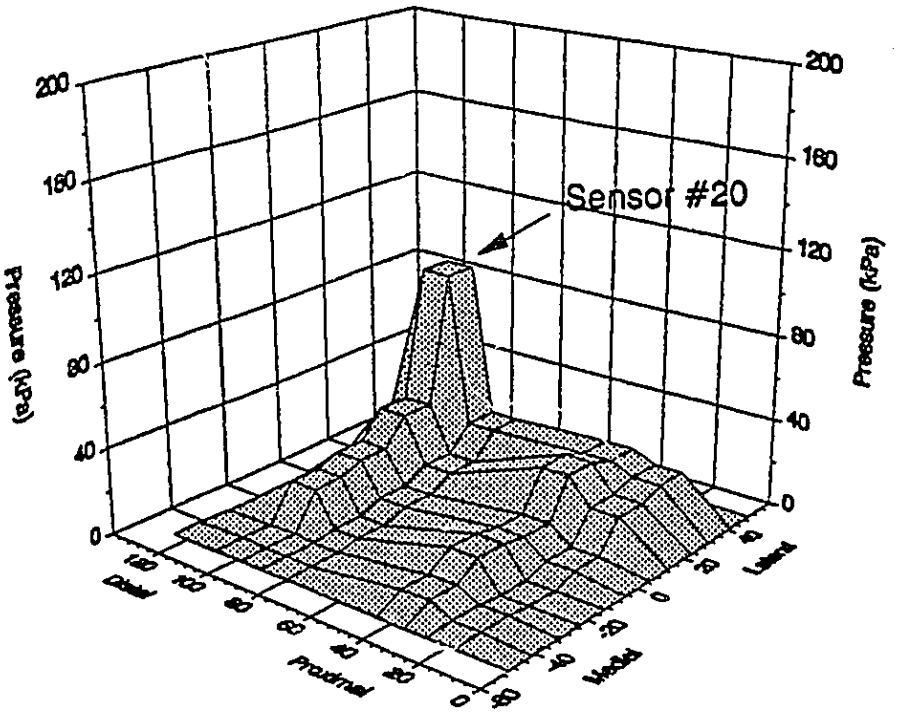

Figure 5.6: Hand grip pressure distribution of subject # 1; 25 N grip force; Static loading; X_h- direction.

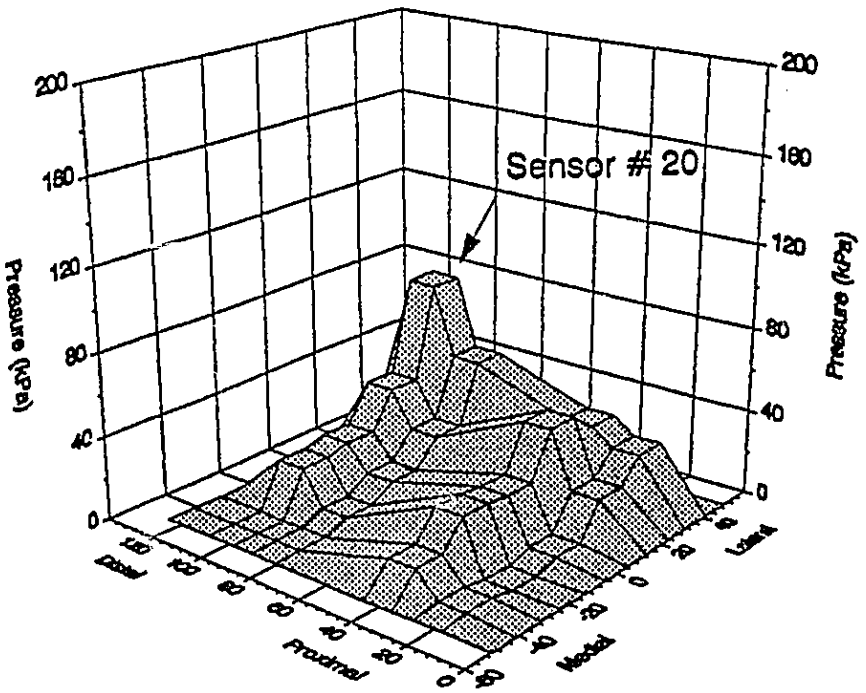

Figure 5.9: Hand grip pressure distribution of subject # 1; 50 N grip force; Static loading; X_h- direction.

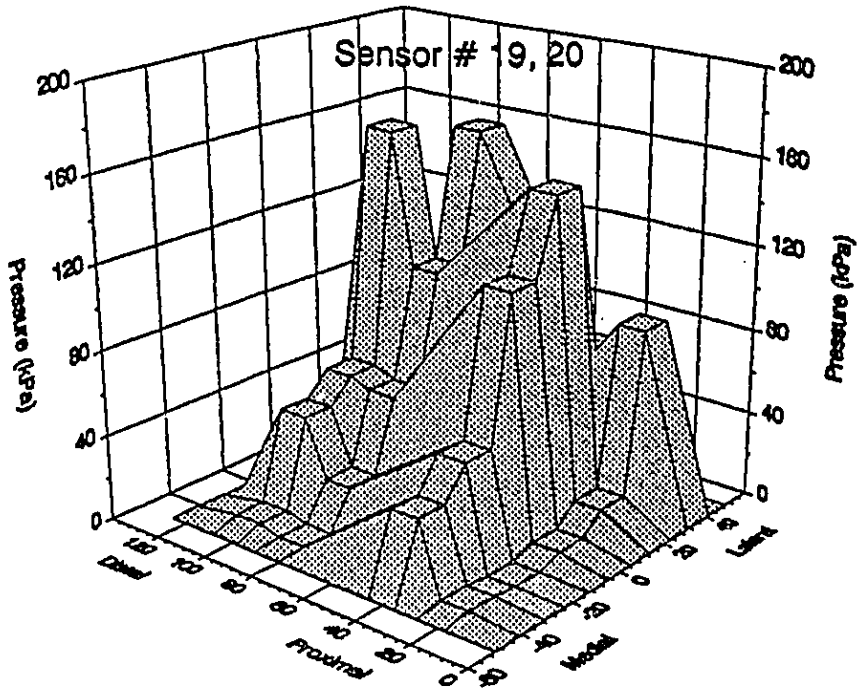

Figure 5.10: Hand grip pressure distribution of subject # 1; 100 N grip force; Static loading; X_h- direction.

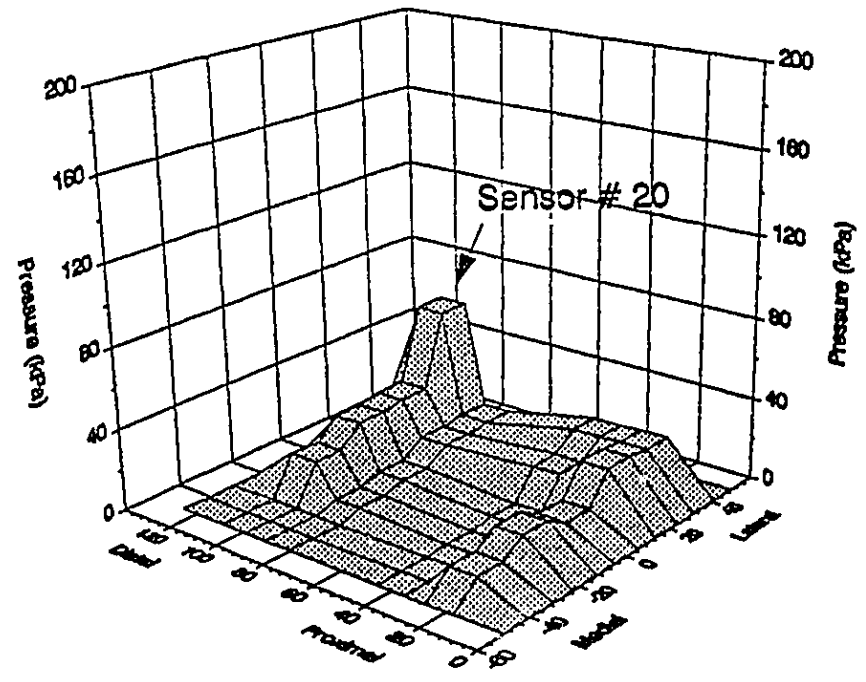

Figure 5.11: Grip pressure distribution of subject # 1; 25 N grip force; Static loading; Y_h- and Z_h- directions.

Figures 5.11 - 5.13 illustrate the interface pressure distribution of the same subject in the Y_h and Z_h- directions for static grip forces of 25 N, 50 N and 100 N, respectively. Under static loading the hand-handle orientation in Y_h- and Z_h- directions is identical (see Figure 2.1). The results presented in these figures are similar to the data illustrated in Figures 5. 8 - 5.10. In all the cases it may be observed that the pressure peak was located at the tip of the index finger (sensor #20). While the magnitude of peak pressure increased considerably with an increase in the grip force, the *location* of the peak pressure remained unchanged. Data obtained on other subjects showed similar results with high degree of consistency in terms of the *location* of the peak pressures. Figures 5.14 - 5.16 show representative hand GPDs of subject # 2, 3 and 4 under static loading in Y_h- and Z_h directions using 25 N total grip force. Once again, the data clearly illustrate the consistency of *location* of peak pressure at the tip of the index finger (sensor # 20). However, it may be observed the magnitude of peak pressure recorded at the tip of the index finger differed among subjects tested. Table 5.1 summarizes the magnitudes of pressure peaks measured on the four subjects.

The interface pressure is also measured under dynamic conditions using different magnitudes of grip and peak acceleration levels at various discrete excitation frequencies. Figures 5.17 - 5.19 illustrate the GPD measured on the hand of the subject # 1 for 1.0 g, 2.0 g and 3.0 g peak acceleration levels, respectively, at an excitation frequency of 100 Hz. The interface pressure distribution corresponding to the different magnitudes of acceleration reveal many peaks of considerable magnitude. The magnitudes of interface pressure measured at tip, middle and base of the fingers (sensor # 14, 15, 19, 20, 9) are observed to be larger than those measured at other locations. The magnitude

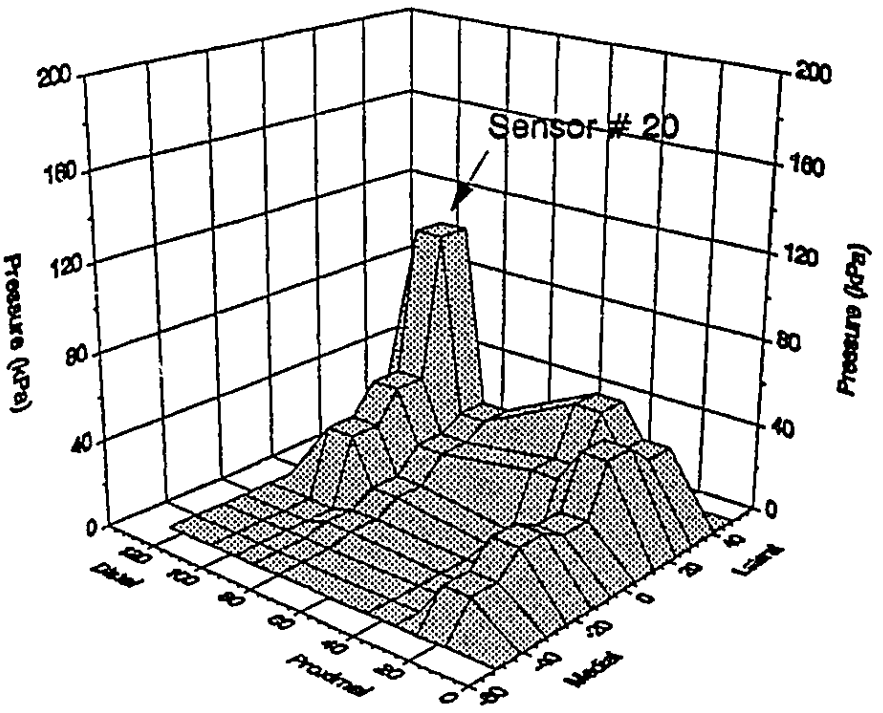

Figure 5.12: Grip pressure distribution of subject # 1; 50 N grip force: Static loading; Y_h- and Z_h - directions.

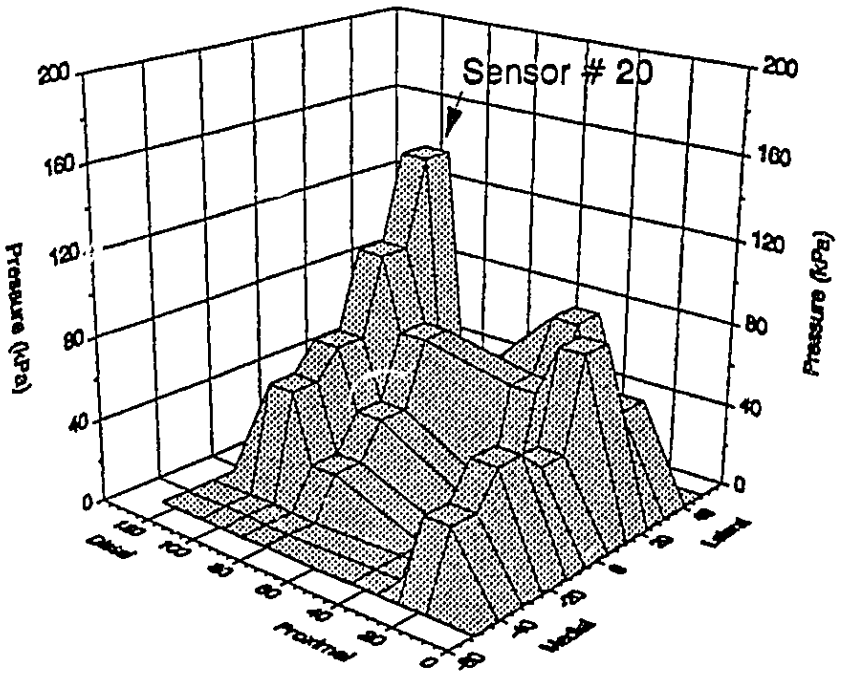

Figure 5.13: Grip pressure distribution of subject # 1; 100 N grip force; Static loading; Y_h- and Z_h - directions.

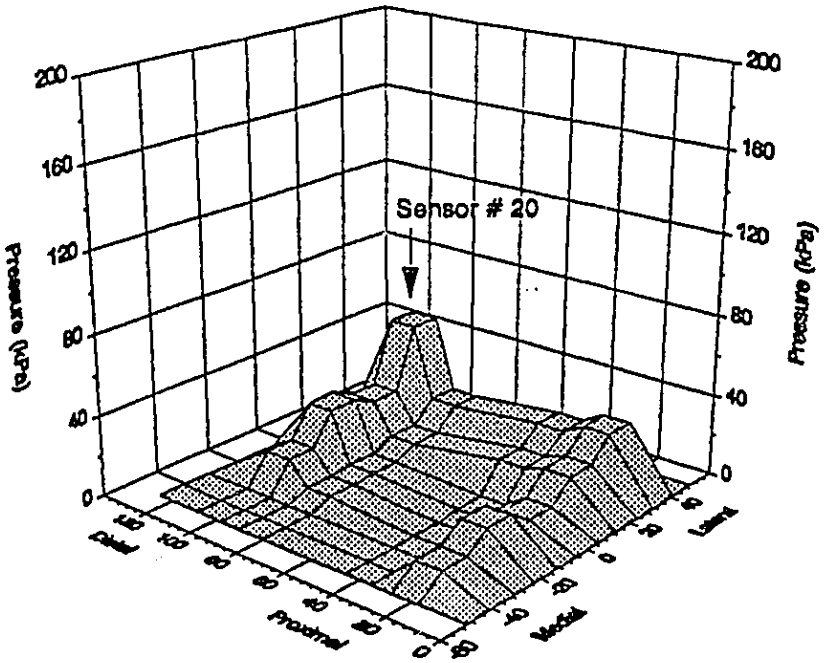

Figure 5.14: Grip pressure distribution of subject # 2; 25 N grip force; Static loading; Y_h- and Z_h- directions.

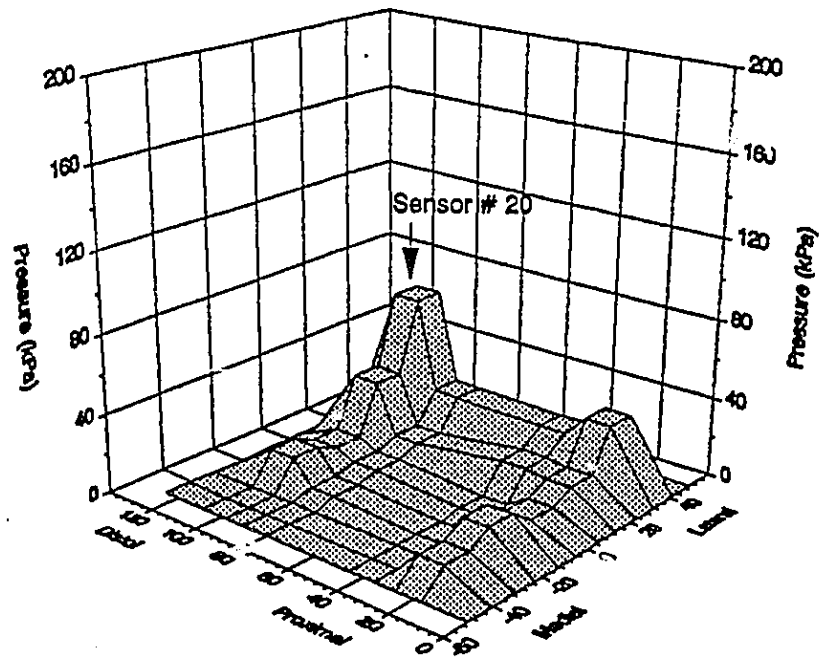

Figure 5.15: Grip pressure distribution of subject # 3; 25 N grip force; Static loading; Y_h- and Z_h- directions.

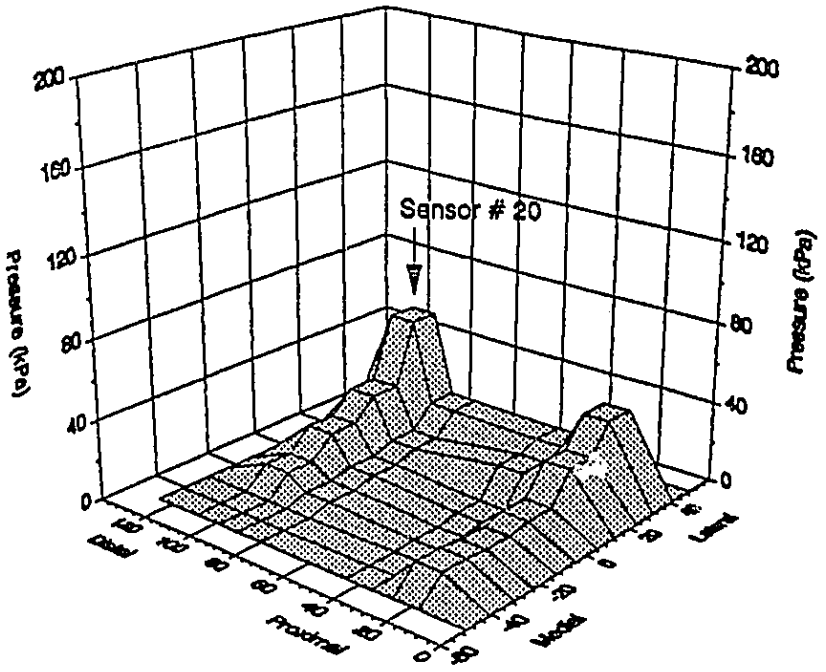

Figure 5.16: Grip pressure distribution of subject # 4; 25 N grip force; Static loading; Y_h- and Z_h- directions.

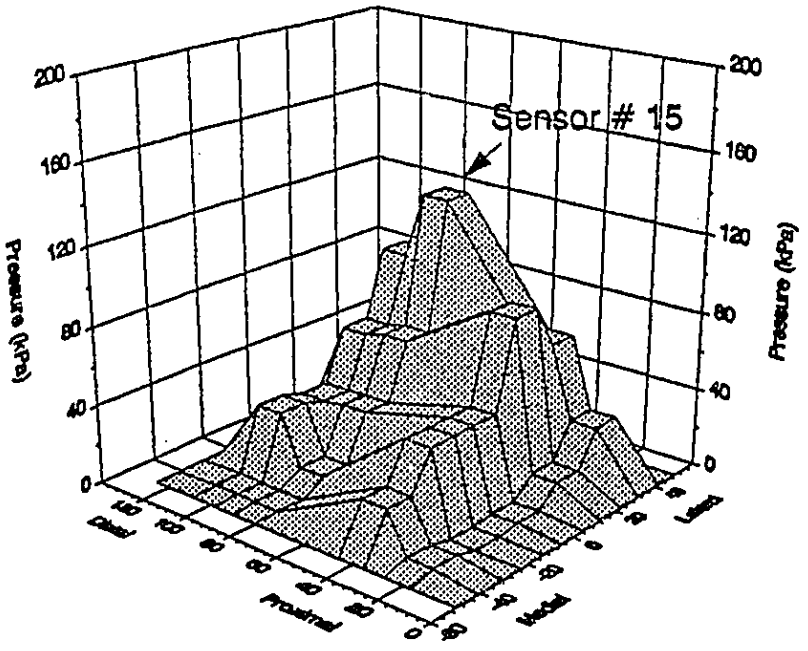

Figure 5.17: Grip pressure distribution under a 100 N grip force: Subject # 1; 100 Hz; 1.0 g peak acceleration; X_h- direction.

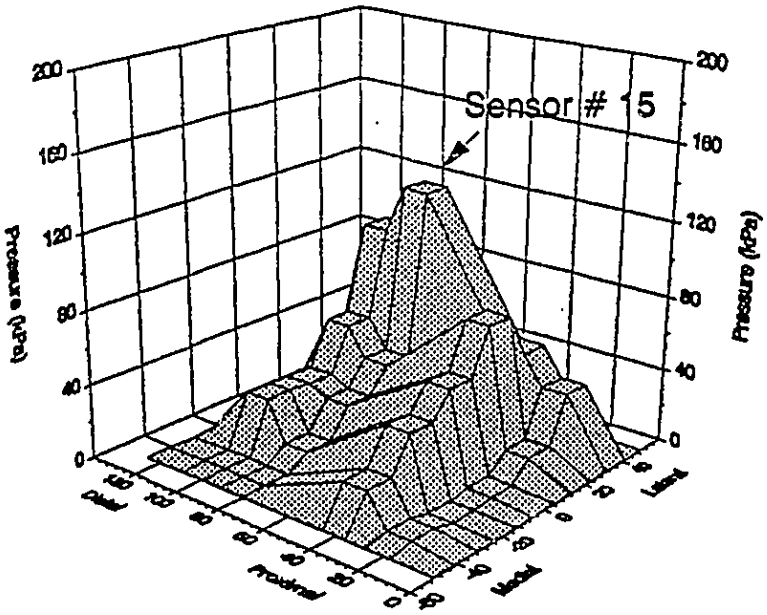

Figure 5.18: Grip pressure distribution under a 100 N grip force: Subject # 1; 100 Hz; 2.0 g peak acceleration; X_h- direction.

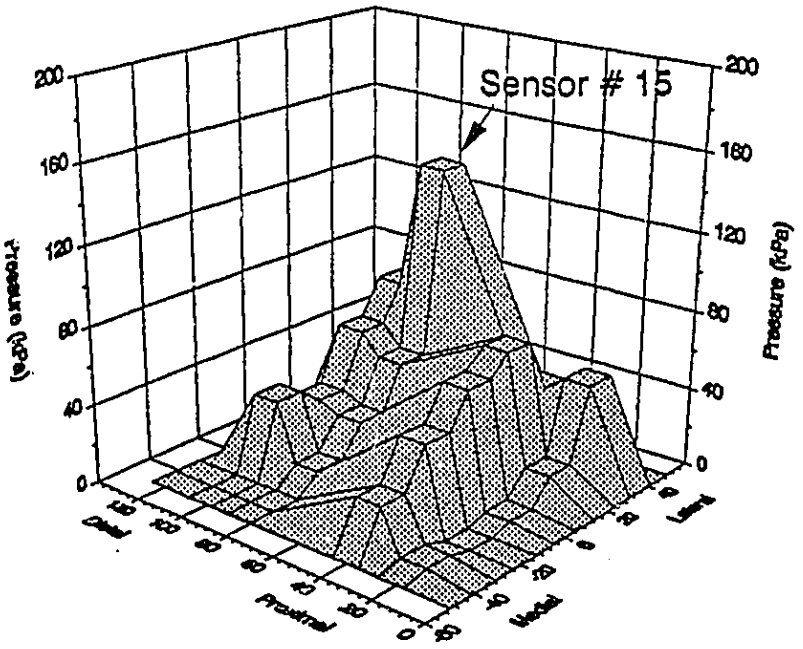

Figure 5.19: Grip pressure distribution under a 100 N grip force: Subject # 1; 100 Hz; 3.0 g peak acceleration; X_h- direction.

TABLE 5.1
Magnitude of Interface Pressures at the Index Finger Tip Under Static Loading

Direction	Grip Force (N)	Magnitude of Interface Pressure (kPa)			
		Subject # 1	Subject # 2	Subject # 3	Subject # 4
X_h	25	65	40	54	43
	50	60	57	66	60
	100	154	140	137	133
Y_h	25	40	45	43	50
	50	92	85	90	86
Z_h	100	130	150	142	162

of the interface pressure, however, highest at the middle of the index finger (sensor # 15), irrespective of the acceleration levels. Figure 5.20 and 5.25 present hand GPD data under similar dynamic testing conditions (100 N grip force, 100 Hz frequency, 1 - 3 g peak acceleration) in Y_h and Z_h directions, respectively. A comparison of interface pressures in X_h , Y_h and Z_h directions (Figures 5.17 to 5. 25) reveals that the magnitudes of peak interface pressures measured in Y_h direction are considerably higher than magnitudes of those measured in the X_h and Z_h directions. The interface pressure distribution, measured in Y_h direction reveals excessive pressures at the middle of fingers (sensor # 13,14,15), irrespective of the amplitude of vibration. The magnitudes of interface pressures measured at the base of the middle and index fingers (sensor # 9, 10) are also high. The interface pressure distribution measured under Z_h direction (Figures 5.23 - 5.25) reveals high pressure peaks at the index finger tip (sensor # 20), and at base and middle of the middle finger (sensor # 9, 14). Figures 5.17 to 5.25 reveal that the peak pressure locations

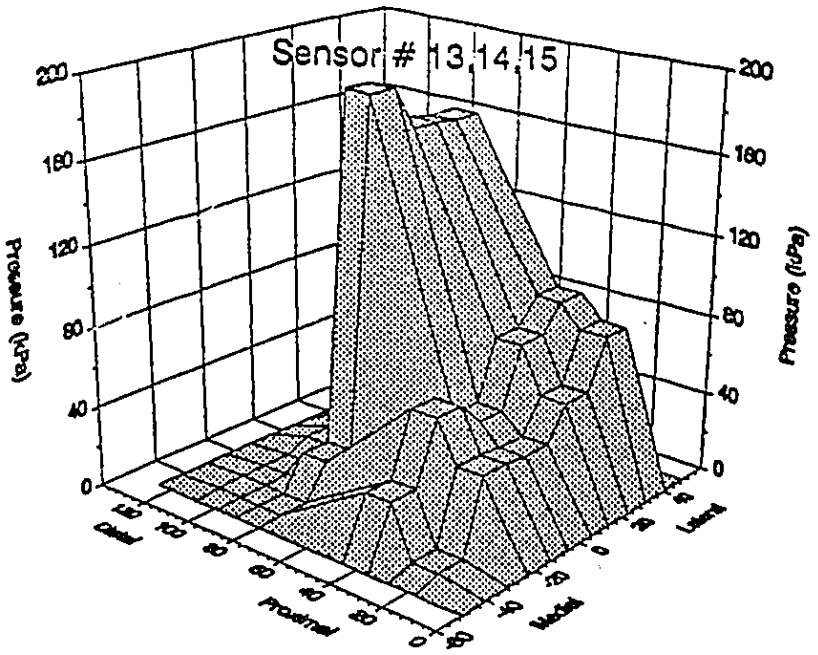

Figure 5.20: Grip pressure distribution under a 100 N grip force: Subject # 1; 100 Hz; 1.0 g peak acceleration; Y_h- direction.

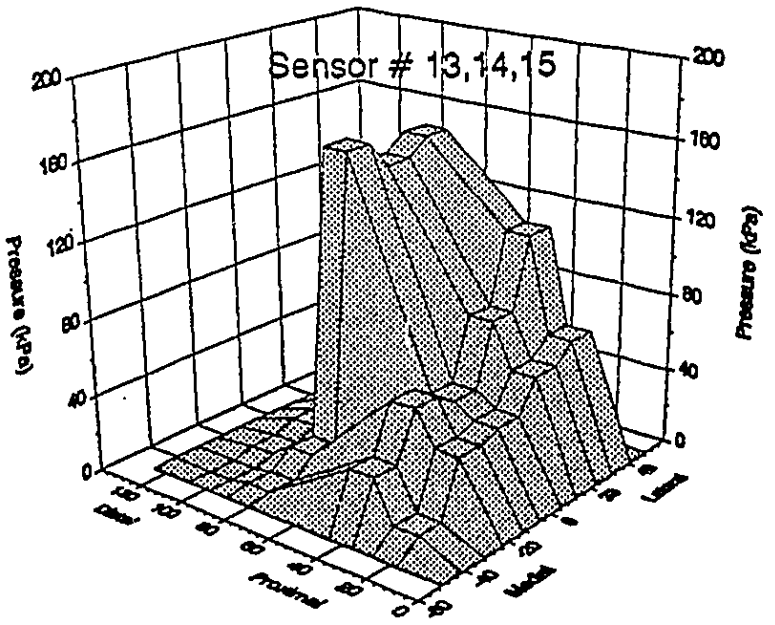

Figure 5.21: Grip pressure distribution under a 100 N grip force: Subject # 1; 100 Hz; 2.0 g peak acceleration; Y_h- direction.

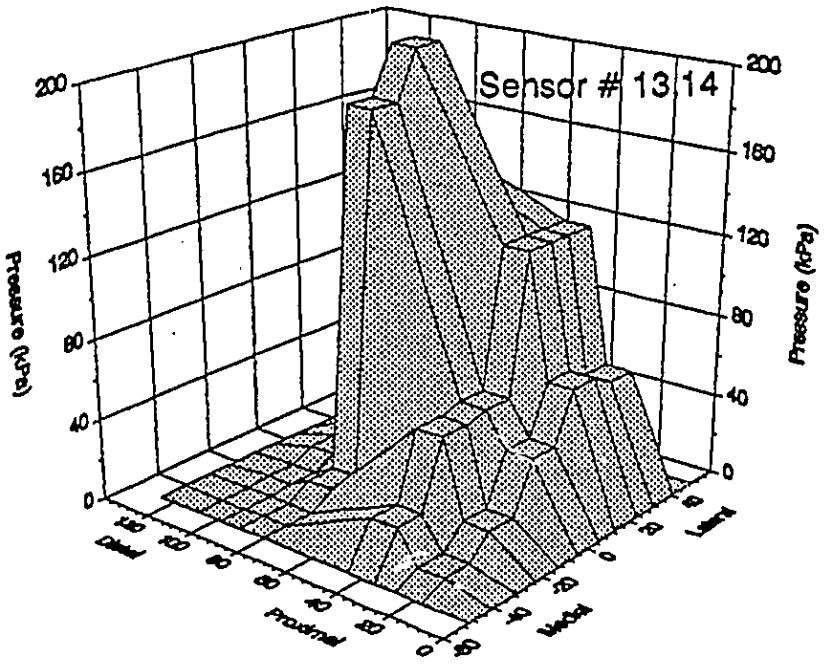

Figure 5.22: Grip pressure distribution under a 100 N grip force: Subject # 1; 100 Hz; 3.0 g peak acceleration; Y_h- direction.

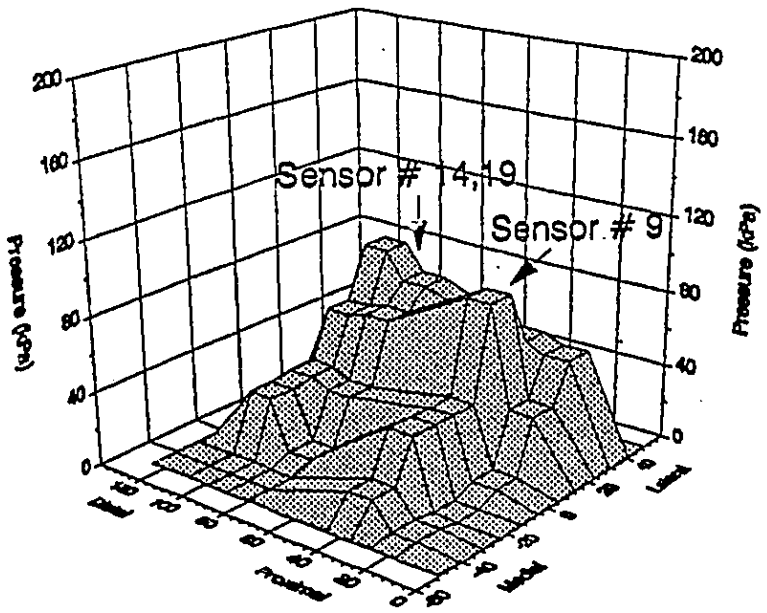

Figure 5.23: Grip pressure distribution under a 100 N grip force: Subject # 1; 100 Hz; 1.0 g peak acceleration; Z_h- direction.

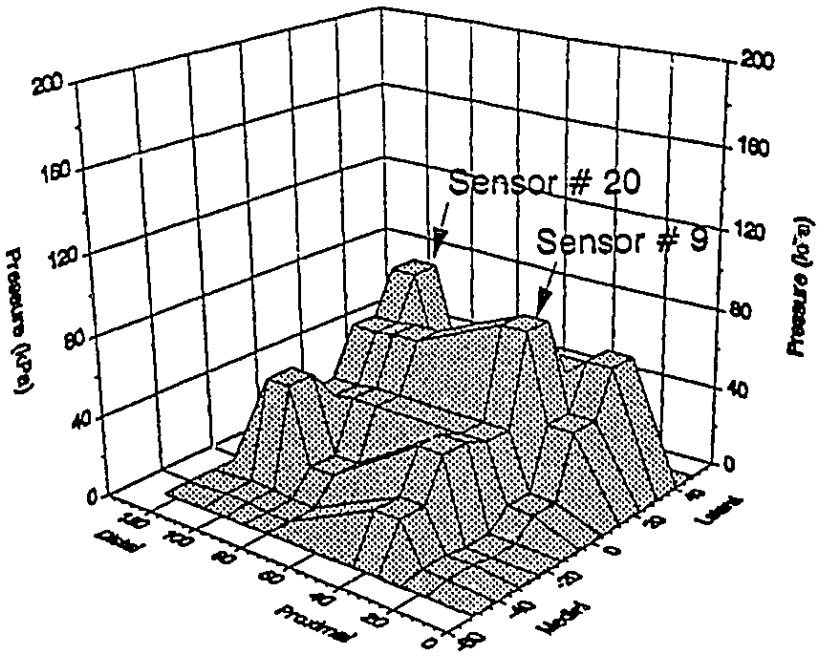

Figure 5.24: Grip pressure distribution under a 100 N grip force: Subject # 1; 100 Hz; 2.0 g peak acceleration; Z_h- direction.

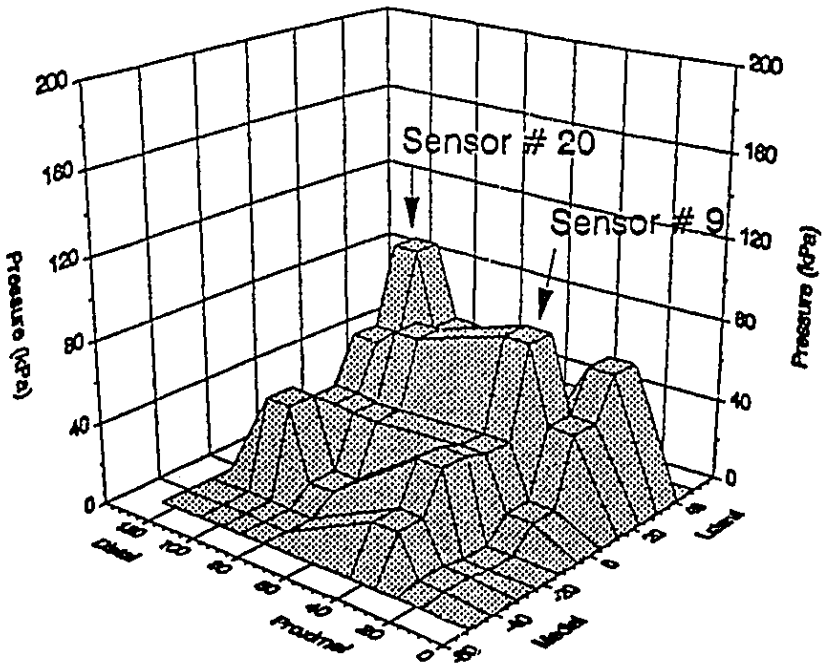

Figure 5.25: Grip pressure distribution under a 100 N grip force: Subject # 1; 100 Hz; 3.0 g peak acceleration; Z_h- direction.

are insensitive to amplitude of vibration. The influence of amplitude of vibration on the magnitudes of peak pressures is not considerable.

Figures 5.26 - 5.34 illustrate the hand GPD acquired for a total grip force of 25 N on subject # 2, 3 and 4 in the X_h -, Y_h - and Z_h - directions, respectively. The measurements were obtained using 2.0 g peak constant acceleration at a frequency of 20 Hz. The interface pressure presented in these figures is similar to that presented in Figure 5.17 - 5.25, for 100 N grip force. Further, the distributions of interface pressure measured on the hands of different subjects are similar in location as well as magnitudes of the significant peaks. The results show a concentration of high pressures near the middle of the index finger (sensor # 15), when subject to vibration along the X_h - and Y_h - directions. The high pressures peaks, however, occur near base of the index finger (sensor # 10) when vibration excitation is applied in the Z_h - direction.

The interface pressure distributions measured on the hands of all four subjects under 50 N grip force and 1 g peak acceleration at 500 Hz along Y_h - direction are illustrated in Figure 5.35. The figure reveals that the GPD measure of all the four subjects is reasonably consistent in magnitude and location of the high pressure peaks. The concentration of high pressure peaks is observed near the middle of fingers (sensor # 13,14,15) and base of the thumb (sensor # 5). The magnitudes of pressure peaks measured on the hands of all the subjects are observed to lie in the range of 60 - 70 kPa at sensors # 5, 13 and 15. The interface pressure distribution at the hand-handle interface was measured at different excitation frequencies and acceleration levels. The magnitudes and locations of peak pressures observed with two subjects in the Y_h - direction for various test conditions are summarized in

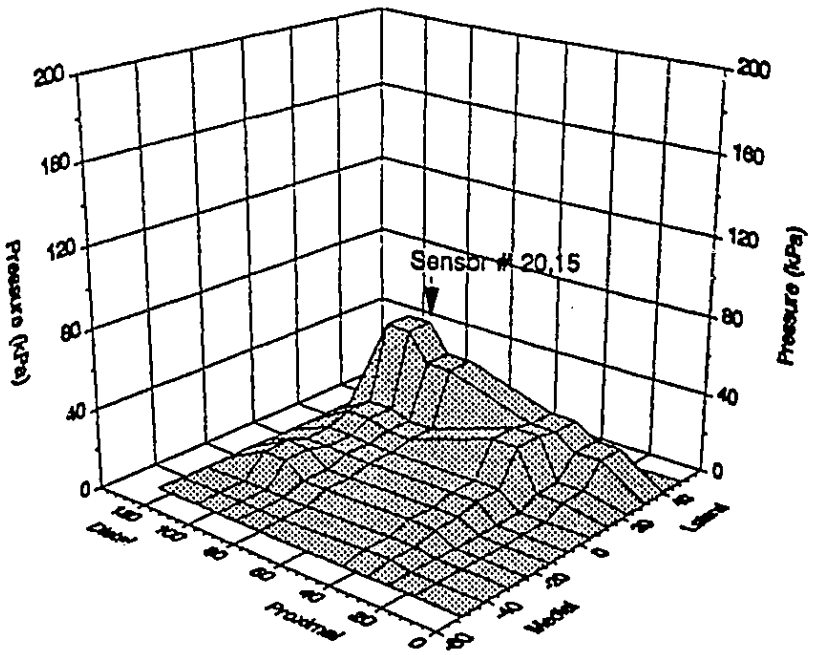

Figure 5.26: Grip pressure distribution under a 25 N grip force: Subject # 2; 20 Hz; 2.0 g peak acceleration; X_h- direction.

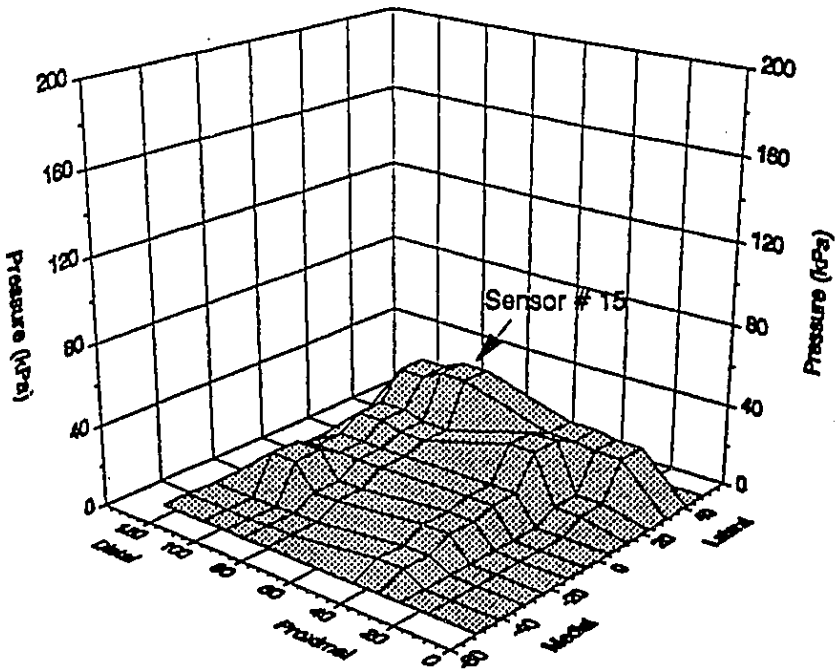

Figure 5.27: Grip pressure distribution under a 25 N grip force: Subject # 3; 20 Hz; 2.0 g peak acceleration; X_h- direction.

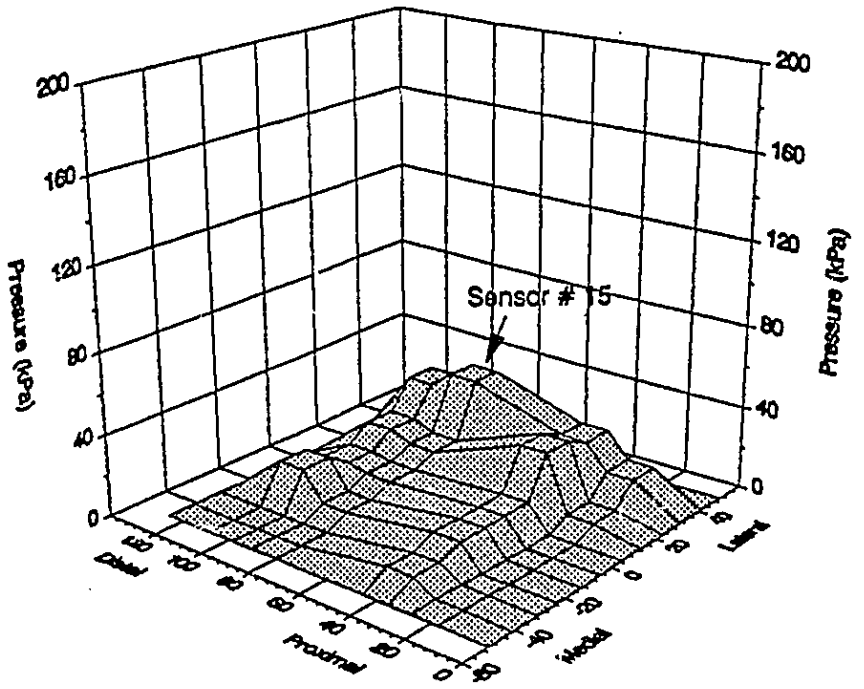

Figure 5.28: Grip pressure distribution under a 25 N grip force: Subject # 4; 20 Hz; 2.0 g peak acceleration; X_h- direction.

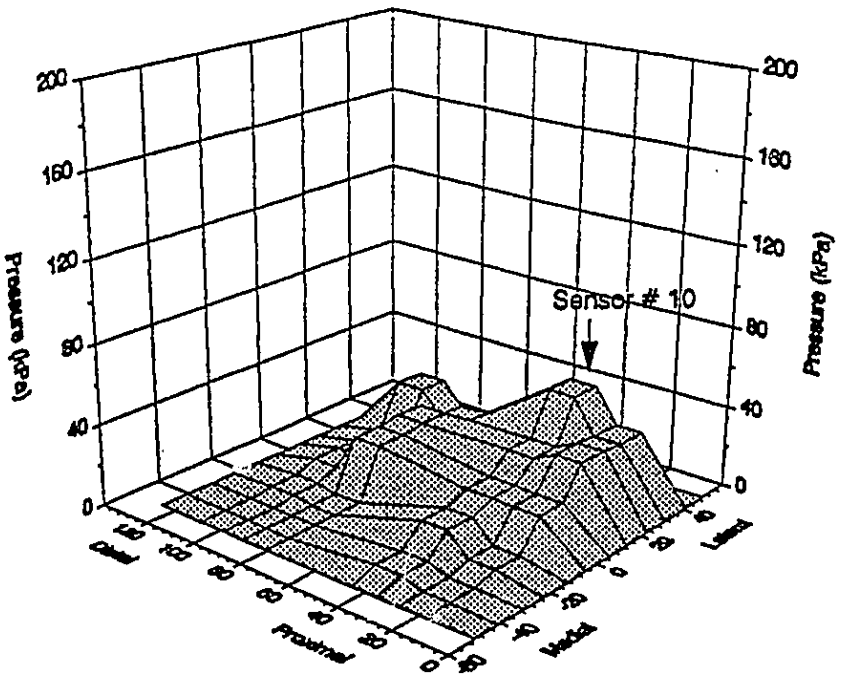

Figure 5.29: Grip pressure distribution under a 25 N grip force: Subject # 2; 20 Hz; 2.0 g peak acceleration; Y_h- direction.

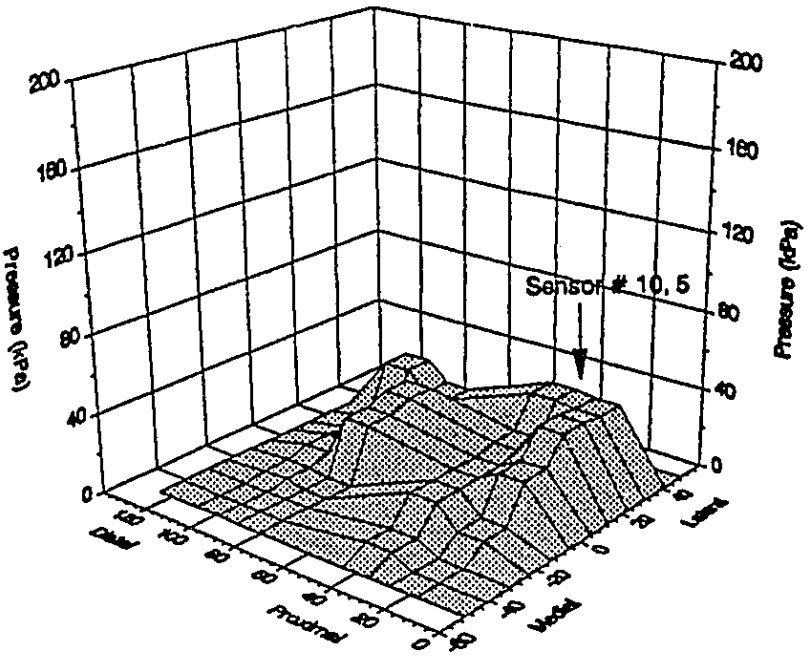

Figure 5.30: Grip pressure distribution under a 25 N grip force: Subject # 3; 20 Hz; 2.0 g peak acceleration; Y_h- direction.

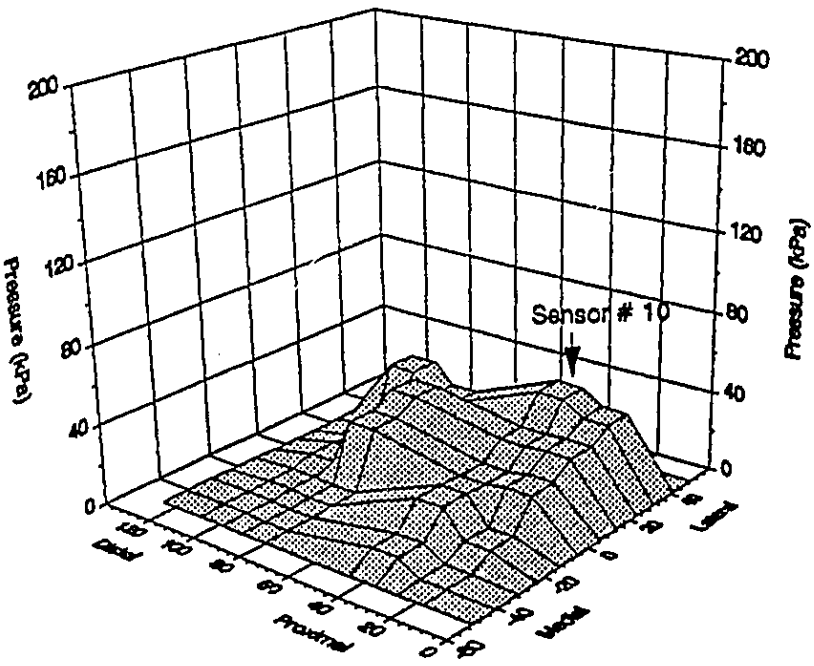

Figure 5.31: Grip pressure distribution under a 25 N grip force: Subject # 4; 20 Hz; 2.0 g peak acceleration; Y_h- direction.

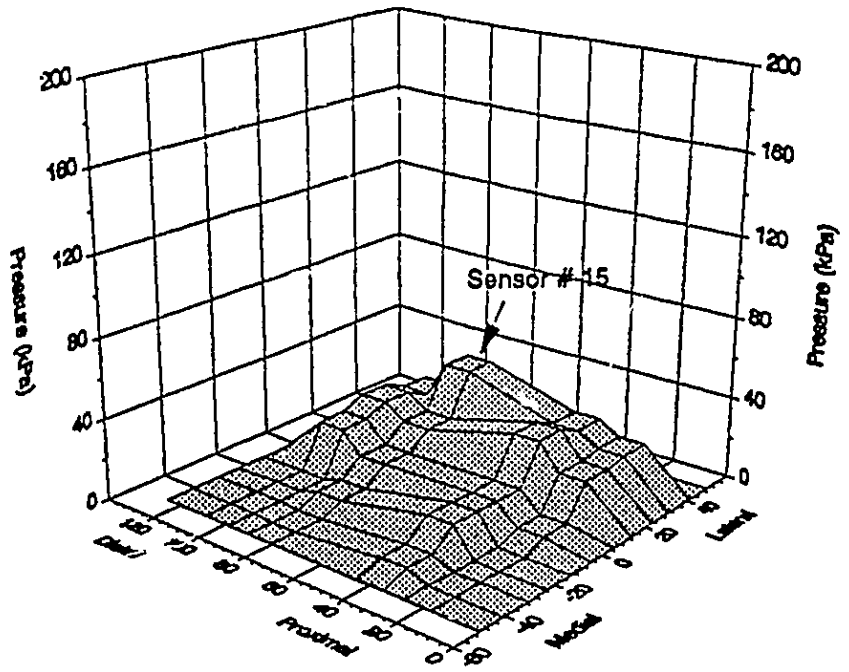

Figure 5.32: Grip pressure distribution under a 25 N grip force: Subject # 2; 20 Hz; 2.0 g peak acceleration; Z_h- direction.

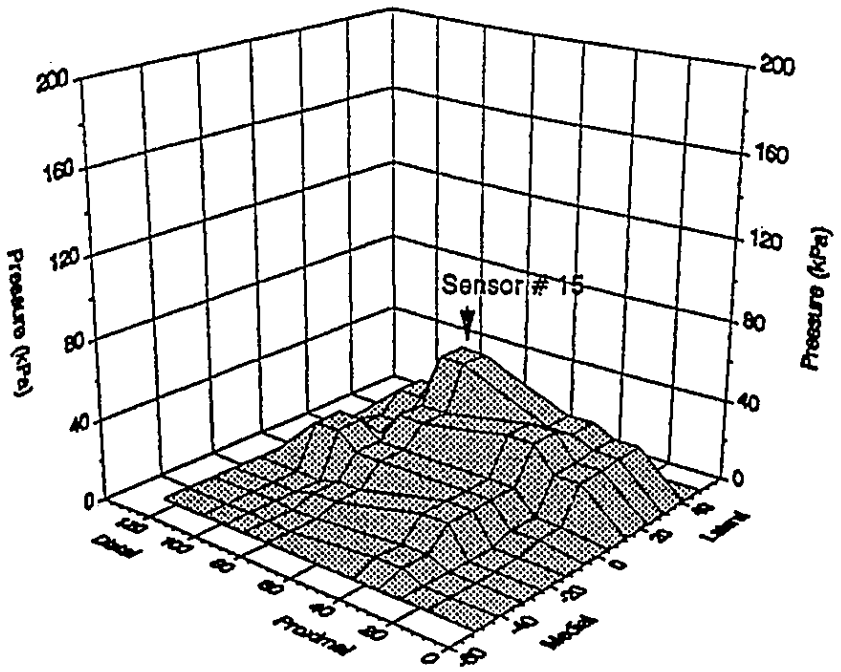

Figure 5.33: Grip pressure distribution under a 25 N grip force: Subject # 3; 20 Hz; 2.0 g peak acceleration; Z_h- direction.

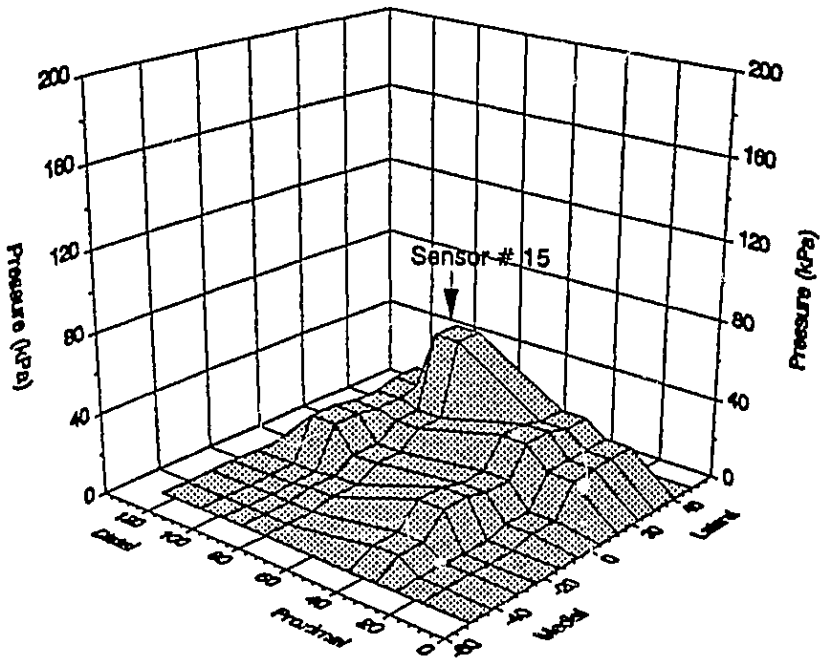

Figure 5.34: Grip pressure distribution under a 25 N grip force: Subject # 4; 20 Hz; 2.0 g peak acceleration; Z_h- direction.

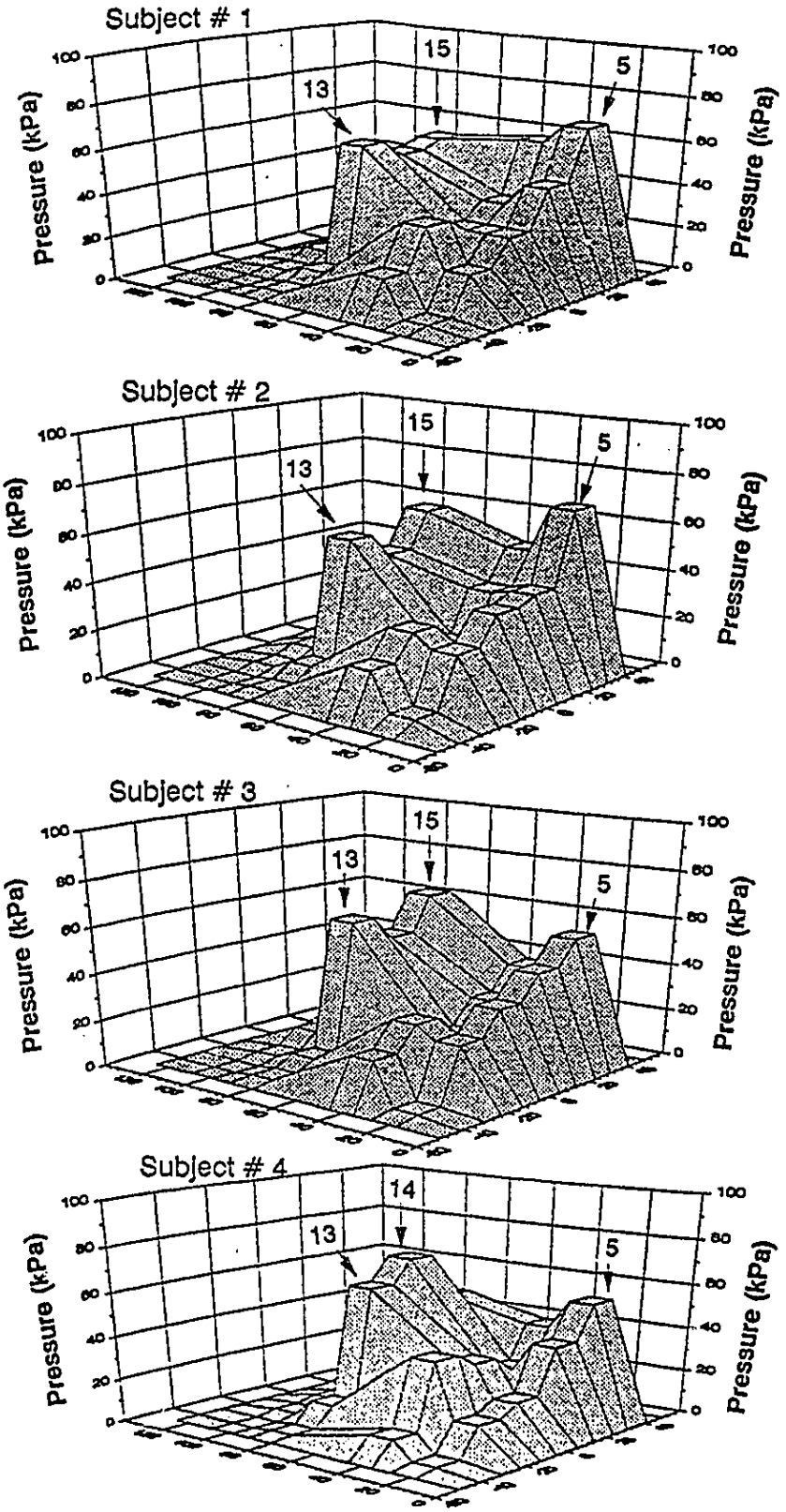

Figure 5.35: Grip pressure distribution under a 50 N grip force: All subjects; 500 Hz; 1.0 g peak acceleration; Y_h- direction.

Table 5.2. The dependence of the magnitude and location of highest pressure on the magnitude of grip force, acceleration levels and excitation frequencies is summarized below:

(a) For a given magnitude of total grip force and acceleration, the magnitude of peak pressure is somewhat insensitive to excitation frequency.

(b) For a given magnitude of total grip force and excitation frequency, the magnitude of peak pressure is somewhat insensitive to excitation level.

(c) The magnitude of peak pressure is strongly dependent upon total grip force.

(d) For a majority of experimental conditions examined, the location of peak pressures are observed at the middle of fingers. The pressures recorded at the base of the thumb is also observed to be high.

A comparison of the GPD obtained under static and dynamic loads reveals that the pressure peaks at the tips of index and middle fingers under static load (sensors # 20,19) tend to shift towards the middle of fingers under dynamic load (sensors # 13,14,15). The magnitude of the pressure peak at the index finger tip, measured under static load decreased considerably under dynamic load, while the magnitude of the local pressure at middle of the fingers increased. Further, the high pressure peaks are, invariably, concentrated in the lateral section of the hand, while the medial section was exposed to considerably lower levels of local pressures. Studies of hand held power tool operators affected by the VWF disease have established that lateral section of the hand is most severely affected by the VWF symptoms (see Figure 5.1). The figure clearly illustrates that the index, middle and ring fingers are mostly affected by the VWF symptoms and the loss of sensation in right hand is relatively severe in the entire region from base of thumb to the tip of index finger. The asymmetric nature of distribution of VWF symptoms (concentrated

TABLE 5.2

Summary of Peak Pressures and Their Location Under Different Test Conditions for Two Subjects (Y_h - Direction).

	Peak Acceler-ation (g)	Grip Force (N)	Peak Pressure (kPa) and [Sensor Number] Frequency (Hz)					
			20	50	100	200	500	1000
SUBJECT # 1	0.5	25	48 [10]	35 [10]	39 [10]	52 [10]	37 [20]	44 [20]
		50	78 [10]	81 [10]	73 [10]	73 [10]	79 [10]	68 [10]
		100	135 [14]	162 [14]	161 [14]	153 [14]	133 [14]	148 [14]
	1.0	25	36 [20]	44 [14]	35 [10]	32 [14]	39 [05]	34 [05]
		50	71 [14]	75 [14]	79 [14]	73 [05]	69 [05]	87 [05]
		100	189 [13]	175 [13]	189 [13]	153 [13]	162 [13]	169 [13]
	2.0	25	47 [10]	37 [10]	40 [10]	67 [10]	39 [20]	38 [20]
		50	90 [10]	91 [10]	82 [10]	105 [05]	62 [10]	89 [05]
		100	167 [13]	164 [13]	159 [13]	170 [13]	130 [13]	166 [13]
	3.0	25	37 [10]	38 [10]	37 [05]	37 [14]	41 [10]	37 [05]
		50	88 [10]	87 [10]	87 [10]	79 [14]	84 [10]	98 [05]
		100	225 [14]	184 [14]	205 [14]	185 [13]	170 [13]	185 [13]
SUBJECT # 2	0.5	25	34 [10]	43 [10]	52 [10]	39 [10]	33 [20]	44 [20]
		50	82 [10]	89 [10]	65 [10]	59 [10]	89 [10]	79 [10]
		100	212 [13]	149 [13]	185 [14]	145 [14]	191 [14]	180 [14]
	1.0	25	36 [20]	44 [14]	35 [10]	32 [14]	39 [13]	31 [13]
		50	72 [14]	73 [14]	77 [14]	64 [13]	69 [05]	89 [05]
		100	185 [14]	170 [13]	195 [13]	155 [13]	169 [13]	149 [13]
	2.0	25	45 [14]	30 [14]	31 [14]	38 [10]	41 [14]	46 [14]
		50	72 [10]	101 [14]	68 [13]	91 [13]	78 [10]	71 [05]
		100	175 [14]	145 [13]	158 [13]	181 [13]	173 [13]	198 [13]
	3.0	25	32 [10]	39 [10]	41 [05]	40 [14]	32 [10]	36 [13]
		50	91 [10]	88 [10]	81 [10]	82 [14]	89 [10]	75 [10]
		100	204 [14]	201 [14]	187 [14]	194 [13]	190 [13]	210 [13]

on lateral side of hand, see Figure 5.7) in the hands of stonecutter was correctly pointed out earlier (*Brammer, 1984*). The results presented in this section clearly demonstrates high concentration of peak pressures on the lateral side of hand than the medial side, and this may be related to the asymmetrical distribution of VWF symptoms on the hands of power tool operators.

Several authors have advanced the theory of reduced blood flow as the reason for occurrence VWF. Gemne (1983) advanced the concept of growth of muscle layer in the vessel wall caused by repeated contraction, thereby flow of blood in vessels is reduced, often under the external influence of cold. *Nerem (1977)* indicated that occurrence of high pressure and frictional forces influence the hemodynamic forces in the arterial walls and produce alteration to blood flow. Furthermore, the tips of the index, middle and ring fingers are the first parts of the hand affected by the VWF disease (*Brubaker et al 1983, Hellström 1972, Wasserman, 1987*). The occurrence of excessive pressure at the middle of these fingers can greatly reduce the blood supply to their tips. This factor, together with several other factors, such as prolonged exposure to vibration, may be related to causation of VWF among hand-held power tool operators.

5.4 Summary

The hand GPD at the hand-handle interface was measured under static and dynamic loading to study the influence of the magnitude of grip force, and the vibration characteristics on the local pressures at the interface. Variable capacitance pressure sensors were used to obtain the hand GPD at various loading conditions. The dynamic tests were performed for 25 N, 50 N, and 100 N grip forces at 1.0 g, 2.0 g and 3.0 g peak acceleration levels in the frequency

range of 20 - 1000 Hz. The results of the study revealed a high concentration of pressure at the tips of the index and middle fingers, and the base of the thumb under static grip forces. These pressure peaks shifted towards the middle of the fingers under application of dynamic loads, irrespective of magnitude of the grip force, vibration frequency and acceleration level. A high concentration of pressure at middle of the fingers can cause reduced blood flow to the finger tips. This impairment of blood flow may contribute to the causation of vibration white finger upon prolonged exposure to vibration. In the following section, the vibration response of the human hand-arm is further investigated through EMG of the finger-flexor muscle to gain an insight to the muscle fatigue caused by vibration exposure.

CHAPTER 6

RESPONSE OF FINGER FLEXOR MUSCLES TO HAND TRANSMITTED VIBRATION

6.1 Introduction

Exposure to hand-transmitted vibration has been related to muscle fatigue leading to occupational health injuries and loss of productivity of the operators of the power tools. An insight to the muscle fatigue associated with exposure to hand-transmitted vibration can be gained through a study of electrical activity of muscles subject to vibration. While the grip pressure distribution, presented in Chapter 5, was related to possible phenomenon leading to white finger disease caused by impaired blood flow, the study of the vibration response of muscles that are primarily responsible for exerting grip force can provide further insight to impact of transmitted vibration.

The effects of vibration on human muscles were studied as early as 1860 (*Rood, 1860*). It was observed that vibrations and resulting involuntary contractions in the hand and arm affect the ability to release the grip. Subsequently, several researchers have attempted to study various hand-arm muscle activities under different static and dynamic loading using electromyography (EMG, the graphing of the electrical activity of muscle). EMG measurements have been extensively used to estimate the hand forces, grip strength and optimum handle size (*Armstrong et al., 1979; Janda et al., 1987; Ayoub et al., 1971*). Measurements performed on biceps brachii muscles, in the frequency range of 6.3 -100 Hz, showed a decrease in muscle activity with an increase in frequency at low levels of grip force (*Iwata et al., 1970*). The muscle activity corresponding to high grip forces, however, increased considerably at 10

and 50 Hz, due to resonances of the hand-arm system. The electrical activities of flexor carpi ulnaris, biceps and triceps have been studied under 2.0 g peak constant acceleration along the forearm axis at many discrete frequencies in the 8 - 500 Hz range. The electrical activity of these muscles were measured, for five different elbow angles, and a grip force equal to 40% of maximum voluntary contraction (MVC) (*Dupuis et al., 1979*). The study concluded that activity of flexor carpi ulnaris muscle was least influenced by vibration frequency and elbow angle, while the activity of the triceps and biceps were influenced by the frequency. The response characteristics of hand flexor and extensor muscle have been investigated through EMG measurements performed under 8 m/s^2 weighted acceleration at four different discrete frequencies in the 20-160 Hz range, and grip forces of 5 % to 15 % of MVC (*Radwin et al., 1987*). The study observed an increase in grip force due to operation of vibrating tools, which was attributed to the so-called tonic vibration reflex. EMG techniques have been used to study the response characteristics of the forearm flexor muscle subject to sinusoidal and trapezoidal forces (*Berthoz and Metral, 1970*). The study observed maximum forearm oscillations in the 3 - 5 Hz frequency range with EMG leading the limb displacement.

Although the EMG of biceps and triceps brachii, flexor carpi ulnaris, and flexor extensor muscles have been extensively investigated to establish a relation between muscle activity and the hand-arm vibration characteristics (*Dupuis et al., 1979; 1986*), the EMG of finger flexor muscles, a muscle group primarily responsible for exertion of grip force (*Basmajian et al., 1982*) has not been reported. In this section the electrical activities of the finger flexor muscles are investigated to enhance an understanding of the muscle response to static and dynamic loads under different levels of vibration.

6.2 EMG of Finger Flexor Muscles

EMG measurements may be influenced by a variety of factors, which may be grouped as: (i) subject related and (ii) tool operating parameters. The subject related parameters include age, sex, hand size, posture, elbow angle, while the tool related parameters include direction, magnitude and frequency of vibration, and grip and thrust force. The objective of the present study is to investigate the influence of tool operating parameters such as direction of vibration, magnitude and frequency of vibration, and grip force on the EMG of finger flexor muscles. The tool operating parameters are considered to have significant influence on hand transmitted vibration (*Reynolds et al., 1979; Griffin et al., 1982*). Among all muscle groups present in the hand-arm system, finger flexor muscles are relatively proximal to the excitation source, while grasping the vibrating tools. A study of vibration response characteristics of finger flexor muscles, the muscles primarily responsible for exerting grip force, may thus help to quantify the influence of impinged vibrations and provide an insight to the muscle fatigue and injury mechanisms.

The EMG of the finger flexor muscles is thus examined for tool related parameters. The measurements are performed for static and dynamic grip conditions, and harmonic vibration along the three directions proposed in ISO - 5349 (1986). The results are discussed to highlight the influence of tool related experimental factors on the electrical activities of the muscles. Silver-silver chloride surface electrodes, standard EMG measurement equipment in conjunction with a data acquisition system are utilized to record the electrical activity of finger flexor muscles under different static and dynamic loading conditions.

6.3 EMG Measurement Techniques

When a muscle contracts, electro-chemical charges occur in the muscle fibers. The electro-chemical activity can be quantified by electromyography. Therefore, the EMG relates directly to the stress state of a muscle and provides a useful tool to study muscle activities under different loading conditions. The stressed muscle is known to produce high electrical activities. The muscle electrical activities can be measured by using two types of electrodes: (i) Surface electrodes, where the sensors are placed on the skin overlying the muscle; and (ii) needle electrodes, where needle type sensors are placed inside the muscle. Each of these techniques offer their respective advantages and limitations. Surface electrodes, which can be applied very easily, provide a measure of the overall activity of a muscle but are limited only to superficial muscles, the muscles that lie directly beneath the skin. The electrode spacing determines the volume of muscle tissue under investigation. Muscle selectivity is ensured by placing electrodes as close as possible. Needle electrodes can be used to measure the activity within a muscle, even of individual muscle fibers. Since these electrodes are placed directly in the muscle, the activity of deep as well as superficial muscles can be effectively investigated. Needle electrodes are thus utilized for greater selectivity and accuracy. The primary limitations of these electrodes are that they are invasive and difficult to apply. Surface electrodes are thus used to acquire the electrical activities of finger-flexor muscles. Surface electrodes may be either disposable type or reusable type with a plastic housing and a double sided adhesive tape collar. The electrodes act as transducers by converting the ionic activity of contracting muscle fibers into electron flow in equipment circuitry.

The EMG electrode-assembly, used to measure the electrical activities, comprises two active electrodes and one inactive (ground) electrode. The active electrodes are usually placed in a bipolar configuration along the long axis of the muscle. The ground electrode places the subject at the same ground potential that exists in the biofeedback unit. The amount of EMG recorded by the assembly is the algebraic sum of all the potentials of the contacting muscle fibers located between the electrodes. An electrolytic gel is used between electrode and the skin so as to reduce movement artifacts, and to ensure adequate electrical contact between the sensor and skin. Skin preparation is an essential part of EMG measurements for reduced electrical noise and improved conductivity (*Basmajian et al., 1982*). The EMG value measured using surface electrodes may be influenced by: (a) size of electrodes and (b) inter-electrode distance. The electrodes must be placed closely such that the undesired myoelectric signals of underlying muscles may be minimized. Overlapping the adhesive discs provides minimal inter-electrode distance, thus reducing the chances of recording myoelectric signals from undesired muscles.

The application of EMG techniques necessitates amplification of the desired EMG signals with minimal contamination due to other physiological signals or by electrical noise. The most common sources of noise in an EMG signal are due to instrumentation and motion artifact. Motion artifact is introduced by movements of the electrodes relative to the skin, the movement of electrode leads, and flexing of connecting cables during motion. A preamplifier comprising a high pass filter with a cut off frequency of 10 Hz, is used to amplify the EMG signals, and to eliminate the noise due to motion artifacts.

Figure 6.1 illustrates the location of surface electrodes for measurement of activities of the finger flexor muscles. The electrodes are located to maximize the specificity of the muscle group, as suggested by *Basmajian et al. (1982)*. The EMG signal is amplified and rectified using an amplifier and a full-wave rectifier. The rectified signal, filtered using a low-pass filter with cut-off frequencies of 1, 3 or 6 Hz, is recorded on a data acquisition system. Figure 6.2 illustrates a block diagram representation of the EMG measurement system.

6.3.1 EXPERIMENTAL PROCEDURE

The specially designed split handle, described in Chapter 2 was mounted on an electrodynamic vibration exciter to generate sinusoidal handle vibrations of different magnitudes of constant acceleration. The hand-handle orientation for all the three recommended directions of vibration (*ISO-5349, 1986*) are shown in Figure 2.1. The handle was instrumented with strain gages to measure total grip force. The grip force was measured using the handle mounted strain gages and displayed to the subject through a digital voltmeter. The EMG measurements were performed using the procedure outlined in the previous discussion on a male subject. The attributes of the subject are described in Table 2.2 (subject # 1). The subject was instructed to maintain identical standing posture during all the experiments, and was advised to grip the instrumented handle with his dominant right hand with an elbow angle of 90 degrees and maintained forearm parallel to the ground. The subject was trained for several days under simulated experimental conditions and was advised to maintain the desired total grip force during an experiment using the digital voltmeter display. Figure 6.3 illustrates the experimental procedure employed for a selected set of experimental conditions including direction of vibration, excitation level, frequency, and grip force.

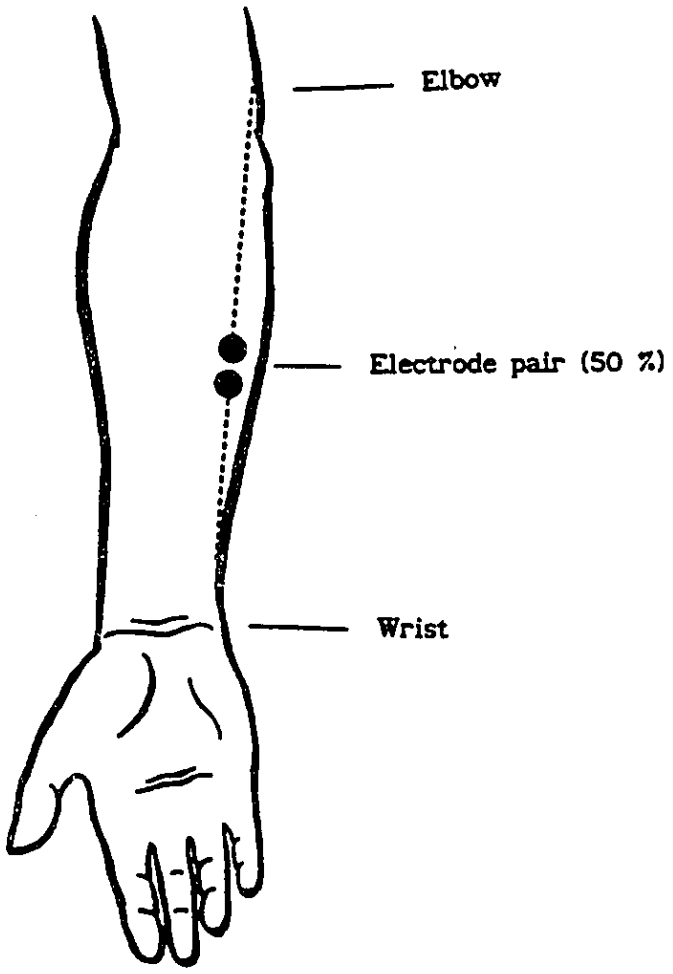

Figure 6.1: Location of EMG electrodes on the finger flexor muscles (*Basmajian et al., 1982*).

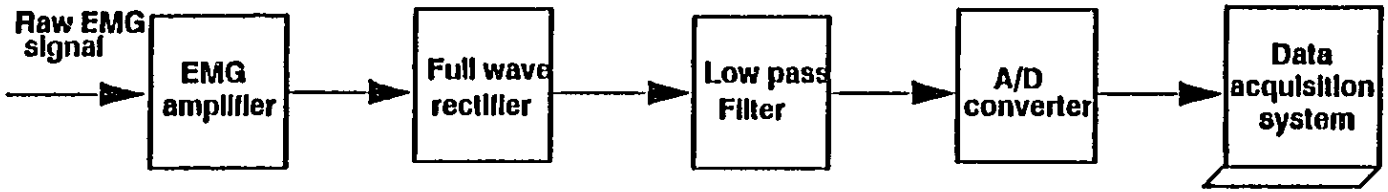

Figure 6.2: Schematic of the EMG acquisition system.

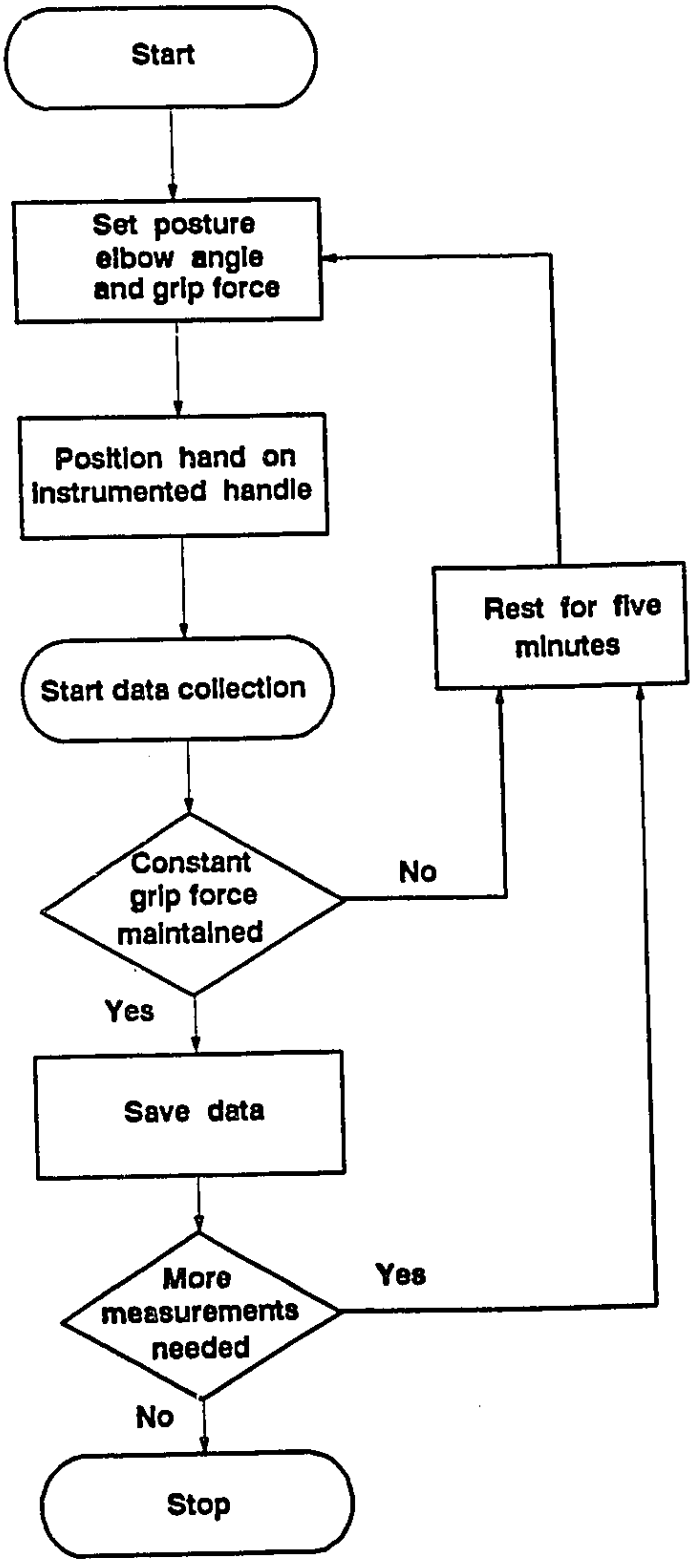

Figure 6.3: Experimental procedure employed for a selected set of tool related parameters.

EMG measurements were performed under static and dynamic conditions. The EMG measurements under static conditions were conducted at grip force levels of 25 N, 50 N, 75 N, 100 N, 125 N and 150 N. This range of grip forces corresponds to 6 - 40 % of maximum voluntary contraction (MVC). EMG measurements under dynamic conditions were conducted at grip force levels of 25 N, 50 N and 100 N (or 6 - 25 % of MVC). The dynamic measurements were performed for harmonic excitations of peak constant acceleration levels of 0.5 g, 1.0 g, 2.0 g, 3.0 g at six discrete frequencies of 20 Hz, 50 Hz, 100 Hz, 200 Hz, 500 Hz, and 1000 Hz. The duration of each experiment was approximately 20 seconds and the subject was given a five minutes rest between experiments to minimize the influence of muscle fatigue.

The muscle activities were recorded using a standard EMG data acquisition and processing system, as described in Figure 6.2. The EMG signal was amplified and rectified using an amplifier and a full wave rectifier. The rectified signal was then filtered using a low-pass filter with 1 Hz cut-off frequency. The low frequency processed EMG data was acquired for a 10 s period at a rate of 100 samples/s. Figure 6.4 illustrates a typical time trace of the EMG recorded during the 10 s interval. The data acquired in the initial 2 s ($0 < t \leq 2$) period were rejected to avoid the contributions due to transients. The EMG data acquired in the final 3 s ($7 \leq t \leq 10$) period were also rejected to minimize the possible influence of muscle fatigue, especially at high grip forces. The EMG recorded corresponding to zero grip force position was subtracted from all the measurements in order to derive the absolute values of EMG under the selected test conditions. The EMG data, recorded in the 2 - 7 s time interval, were observed to be uniform. The measured data were thus averaged in this interval.

6.4 Results and Discussion

A nonlinear regression analysis was performed on the EMG data acquired under static and dynamic test conditions. The nonlinear regression analysis based on a power curve provided an excellent fit to the data with a correlation coefficient (r) ranging from 0.94 - 0.99 for different grip forces under static loading. This type of regression analyses was thus considered for curve fitting the measured data under dynamic conditions. The measured EMG of finger-flexor muscles is analyzed to highlight the influence of grip force, vibration frequency, vibration levels and direction of vibration.

6.4.1 INFLUENCE OF GRIP FORCE ON MUSCLE ACTIVITY - STATIC LOADING

Figure 6.5 illustrates the measured EMG of the finger flexor muscles as a function of grip force in Y_h- and Z_h- directions under static conditions. The processed EMG data is characterized by a power curve of the form, $y = ax^b$ ($a = 7.9E-06$, $b = 1.84$), as shown in the Figure. The correlation coefficient (r) was 0.99. It is evident from the figure that EMG value increases with an increase in the grip force under static conditions in the 25 N - 150 N range. The increase in the EMG of finger-flexor muscles is considerably larger at high grip forces than at lower grip forces. The increase in muscle activity with increase in grip force indicates the muscle stress under high levels of grip forces.

6.4.2 RESPONSE OF FINGER FLEXOR MUSCLES TO VIBRATION

A regression analysis was also performed to curve fit the EMG data acquired under different dynamic test conditions. Table 6.1 presents the correlation coefficients obtained for EMG measurements performed under

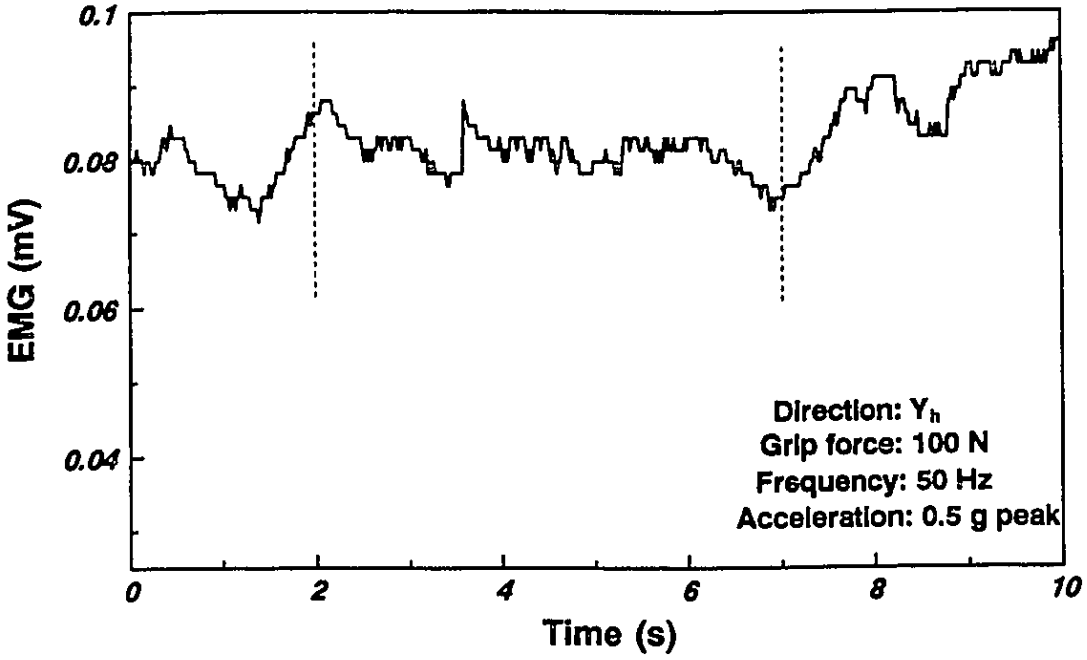

Figure 6.4: Processed EMG signal shown for a 10 s period.

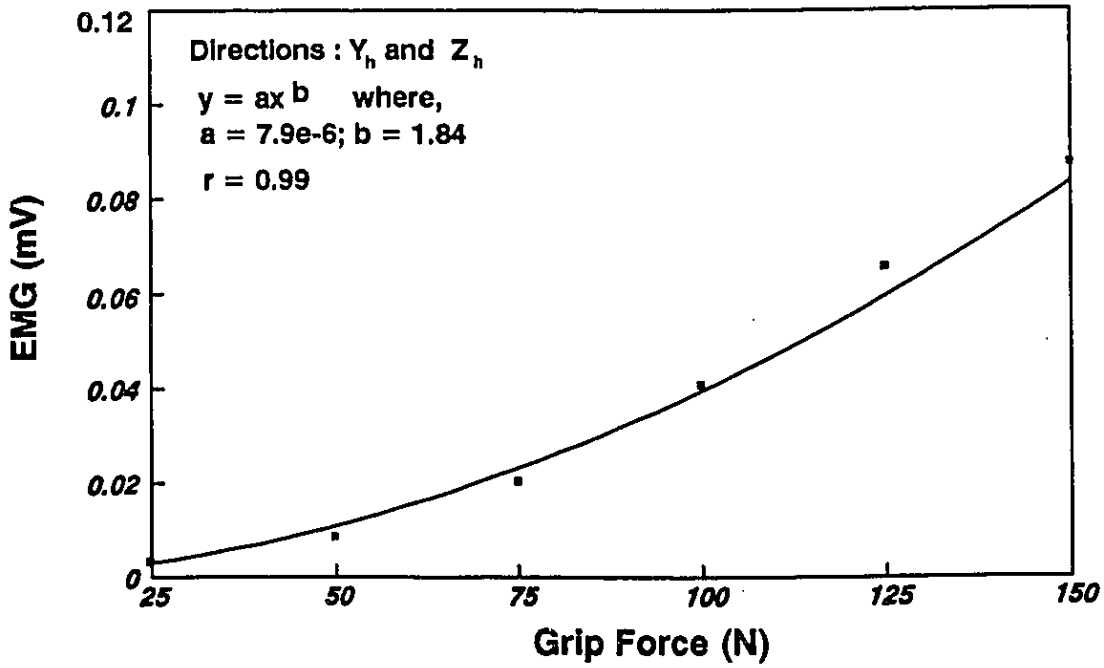

Figure 6.5: EMG of finger flexor muscles at different grip force levels; Static conditions, Y_h- and Z_h- directions.

TABLE 6.1
r Values for Different Conditions of Loading.

Vibration direction	Frequency (Hz)	Coefficient of correlation (r)				
		Acceleration level (g peak)				Static
		0.5	1.0	2.0	3.0	
X_h	20	0.981	0.847	0.993	0.975	0.935
	50	0.989	0.991	0.951	0.998	
	100	0.987	0.958	0.955	0.922	
	200	0.927	0.879	0.828	0.933	
	500	0.991	0.989	0.994	0.999	
	1000	0.966	0.999	0.987	0.997	
Y_h	20	0.996	0.999	0.999	0.997	0.986
	50	0.995	0.987	0.988	0.992	
	100	0.994	0.997	0.997	0.999	
	200	0.998	0.997	0.999	0.997	
	500	0.985	0.992	0.991	0.993	
	1000	0.992	0.985	0.993	0.994	
Z_h	20	0.998	0.979	0.946	0.863	0.986
	50	0.993	0.999	0.986	0.998	
	100	0.994	0.998	0.996	0.916	
	200	0.963	0.961	0.994	0.997	
	500	0.980	0.982	0.982	0.999	
	1000	0.944	0.986	0.976	0.850	

different directions, amplitudes and frequencies of vibration. For the range of test conditions, considered in the study, the correlation coefficients are observed to be in the 0.83 - 0.99 range.

Figure 6.6 illustrates the EMG of the finger-flexor muscles as a function of the grip force, and acceleration level in the X_h- direction at three different discrete frequencies; 20 Hz, 50 Hz and 100 Hz. The EMG values measured under different levels of vibration are also compared to those acquired under static conditions. It can be observed that the electrical activities of the muscles increase considerably with increase in the grip force and acceleration level, irrespective of the vibration frequency. At low grip forces, the EMG values increase marginally with an increase in the acceleration level, specifically at the excitation frequencies of 50 Hz and 100 Hz. At an excitation frequency of 20 Hz, however, the EMG values increase considerably with the amplitude of vibration. At an excitation frequency of 20 Hz, the increase in EMG value with the acceleration levels remains nearly constant over the entire range of grip force. At an excitation frequency of 50 Hz the change in EMG values with variations in the amplitudes of vibration becomes more significant at higher magnitudes of grip forces.

Figure 6.7 illustrates the EMG values as a function of grip force and amplitude of vibration corresponding to higher excitation frequencies: 200 Hz, 500 Hz and 1000 Hz. The EMG values increase with increase in grip force and the amplitude of excitation in a similar manner. The relative increase in the EMG value, however, is smaller than that observed at excitation frequencies of 20 Hz and 50 Hz, as shown in Figure 6.6. An examination of Figures 6.6 and 6.7 reveals that the electrical activity of the finger flexor muscle under dynamic

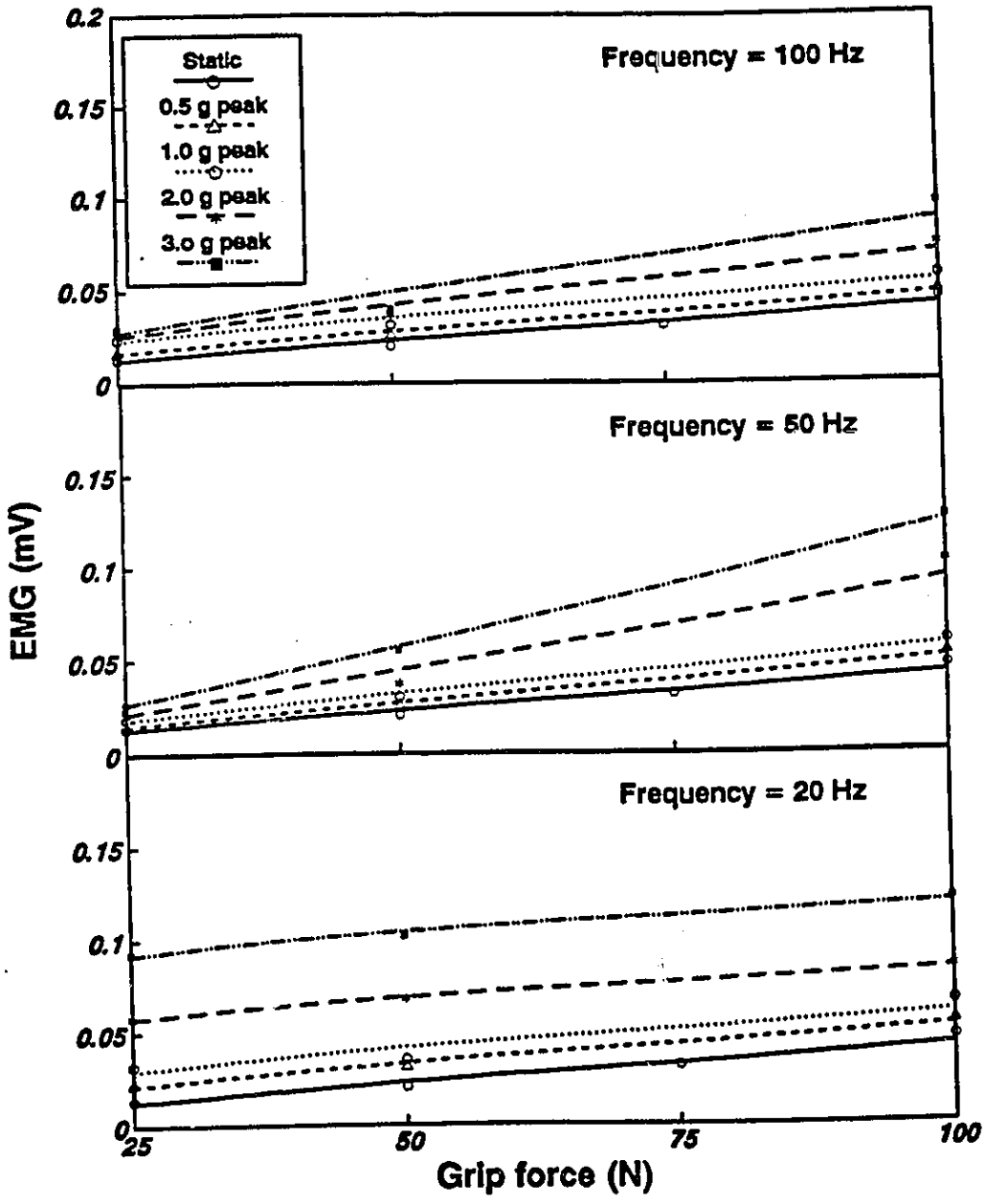

Figure 6.6: EMG of finger flexor muscles as a function of grip force, vibration frequency and peak acceleration; X_h- direction.

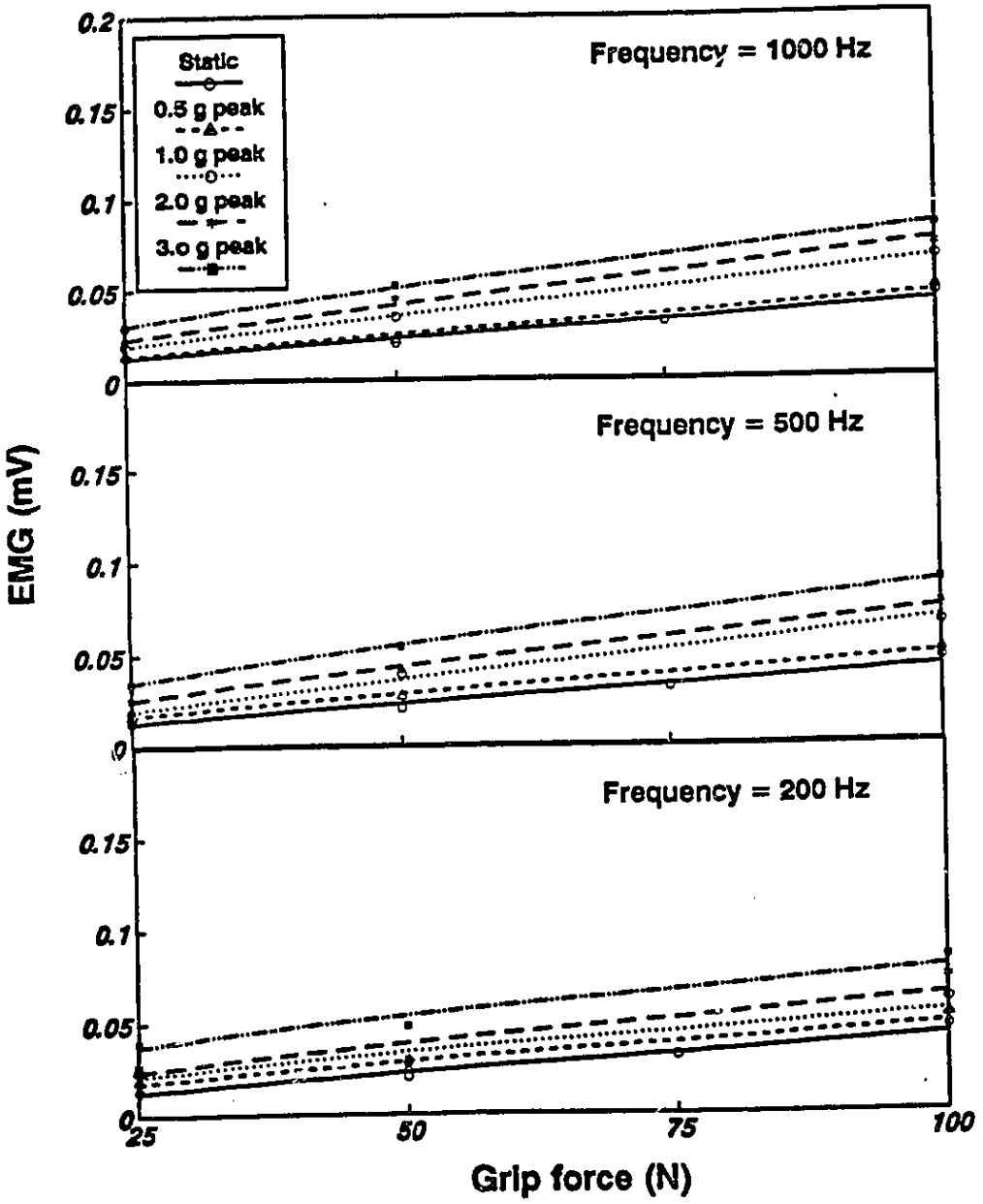

Figure 6.7: EMG of finger flexor muscles as a function of grip force, vibration frequency and peak acceleration; X_h- direction.

loads in the X_h - direction approaches a value which is six times the EMG measured under static loads. This increase in electrical activity of finger flexor muscles is an indication of high muscle stress under dynamic conditions.

Figure 6.8 illustrate the EMG of the finger-flexor muscles as a function of the grip force, and acceleration level in the Y_h- direction at three different discrete frequencies; 20 Hz, 50 Hz and 100 Hz. The EMG values measured under different levels of vibration are also compared to those acquired under static conditions. It can be observed that the electrical activities of the muscles increase considerably with increase in the grip force and acceleration level, irrespective of the vibration frequency. At low grip forces, the EMG values increase only marginally with an increase in the acceleration level. At frequencies of 50 Hz and 100 Hz the increase in EMG corresponding to grip forces of 25 N and 50 N are higher. At an excitation frequency of 50 Hz the change in EMG values with variations in the amplitudes of vibration becomes more significant. Figure 6.9 illustrates the EMG values as a function of grip force and amplitude of vibration corresponding to higher excitation frequencies (200 Hz, 500 Hz, 1000 Hz) in Y_h- direction. The EMG values increase with increase in grip force and the amplitude of excitation in a manner similar to the data presented in Figure 6.8. An examination of Figures 6.8 and 6.9 reveals that the electrical activity of the finger flexor muscle under dynamic loads in the Y_h - direction increases by a value ranging from 1 - 6 times the EMG measured under static loads.

Figure 6.10 illustrate the EMG of the finger-flexor muscles as a function of the grip force, and acceleration level in the Z_h- direction at three different discrete frequencies (20 Hz, 50 Hz and 100 Hz). The EMG values measured

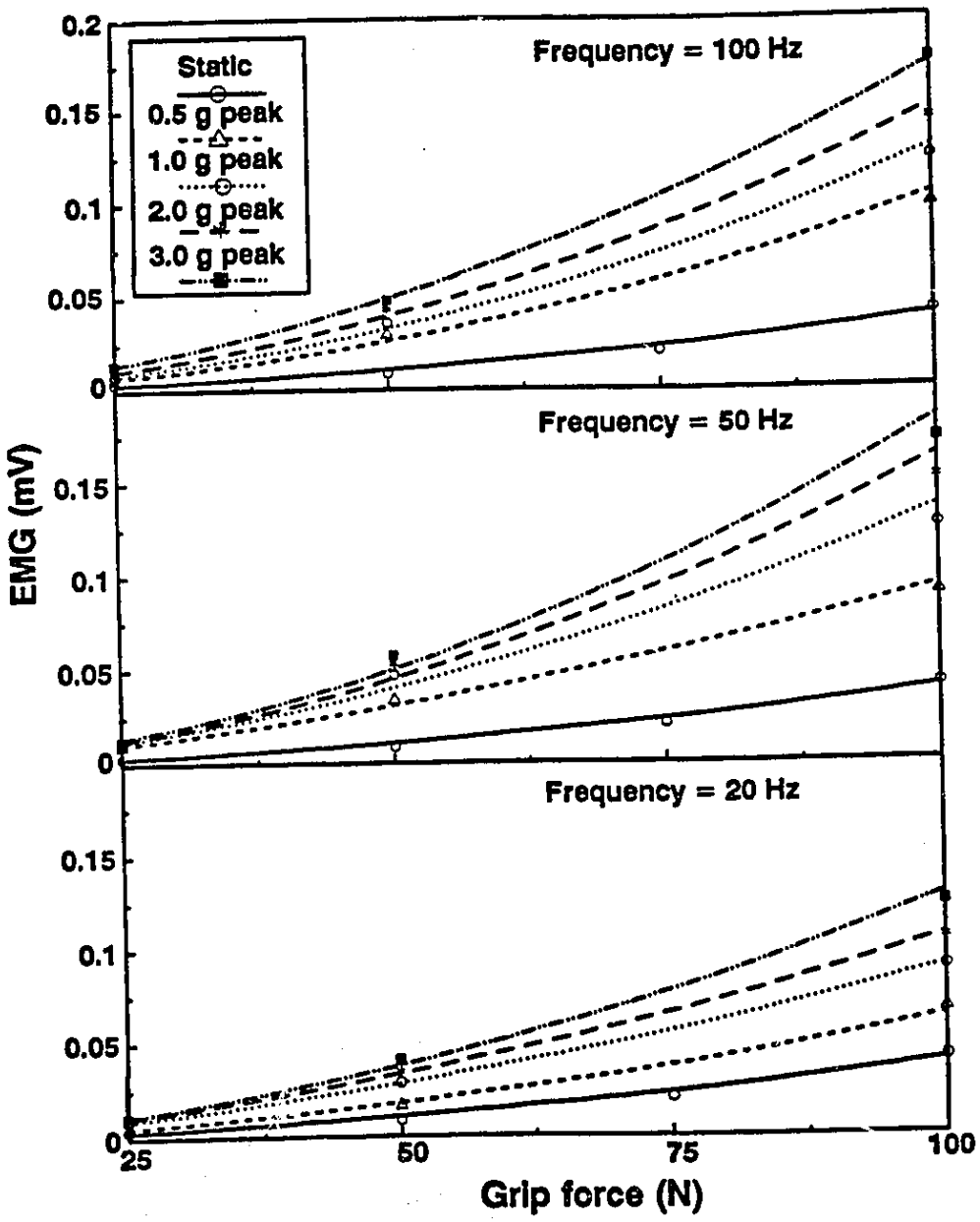

Figure 6.8: EMG of finger flexor muscles as a function of grip force, vibration frequency and peak acceleration; Y_h- direction.

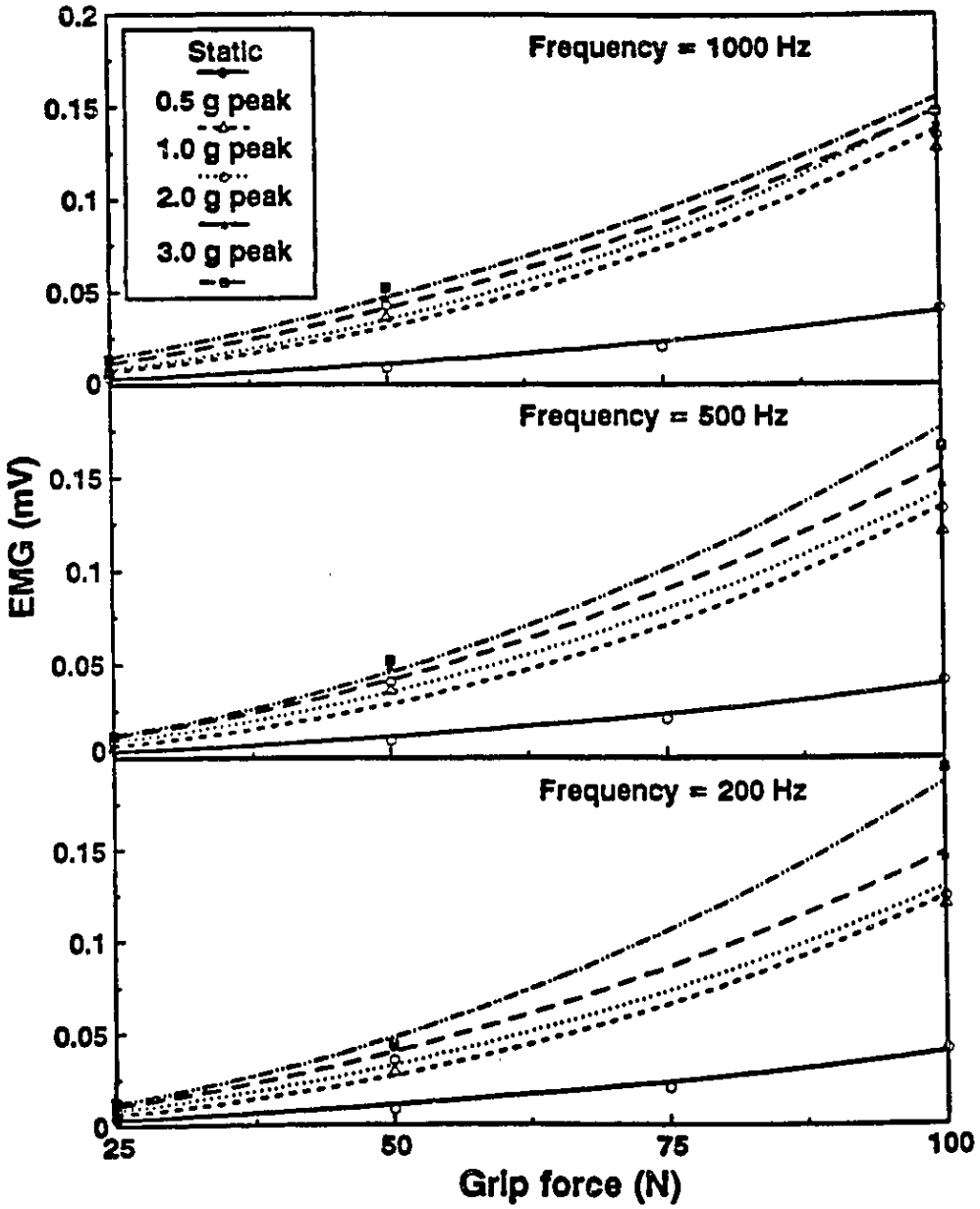

Figure 6.9: EMG of finger flexor muscles as a function of grip force, vibration frequency and peak acceleration; Y_h- direction.

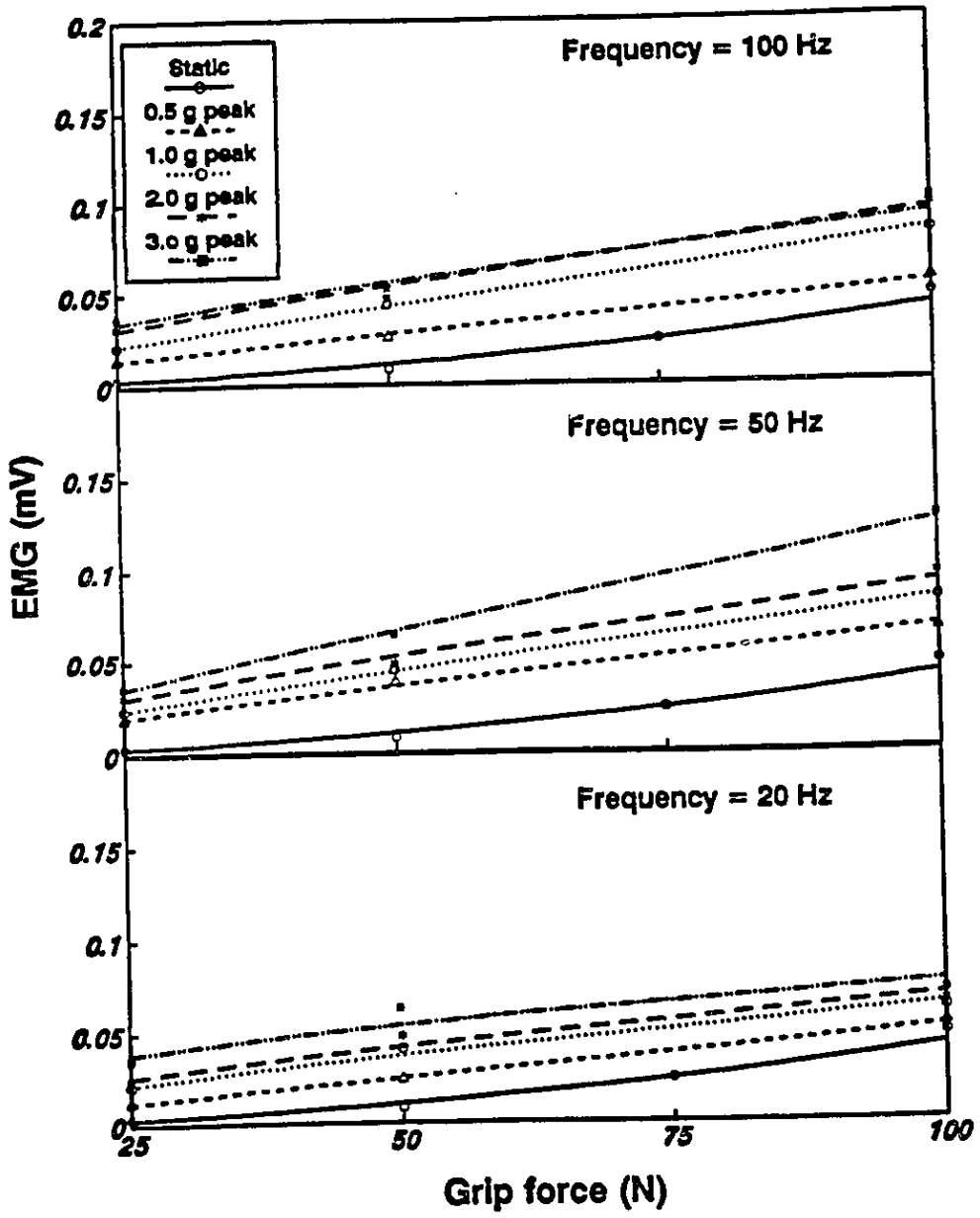

Figure 6.10: EMG of finger flexor muscles as a function of grip force, vibration frequency and peak acceleration; Z_h- direction.

under different levels of vibration are also compared to those acquired under static conditions. It can be observed that the electrical activities of the muscles increase considerably with increase in the grip force and acceleration level, irrespective of the vibration frequency. At an excitation frequency of 50 Hz the change in EMG values with variations in the amplitudes of vibration becomes more significant at all the grip forces. Similar tendencies were noticed in Y_h-direction corresponding to 50 Hz frequency (Figure 6.8), which may be attributed to the presence of resonance of the hand-arm system in the vicinity of this frequency. Figure 6.11 illustrates the EMG values as a function of grip force and amplitude of vibration corresponding to higher excitation frequencies (200 Hz, 500 Hz and 1000 Hz). The EMG values increase with increase in grip force and the amplitude of excitation in a manner very much similar to the data observed in other two directions. Similar to the data presented in X_h - direction, in all the cases depicted in Figure 6.8 - 6.11, EMG of finger flexor muscles increased with increase in grip force and acceleration. Although the influence of acceleration is clearly evident from these figures, the increase is varied by 1 - 6 times as compared to the EMG measured under static loading conditions. The increase in EMG under dynamic conditions may be attributed to various factors such as frequency and direction of vibration tested. This increase in electrical activity of finger flexor muscles observed in all the three directions of vibration under static and dynamic conditions clearly indicates that the finger flexor muscles undergo high amounts of stress at high grip force levels. The peak grip pressures recorded at the hand-handle interface and the high electrical activities of finger flexor muscles recorded in this section clearly demonstrate the effects of handle vibrations on the hand-arm system.

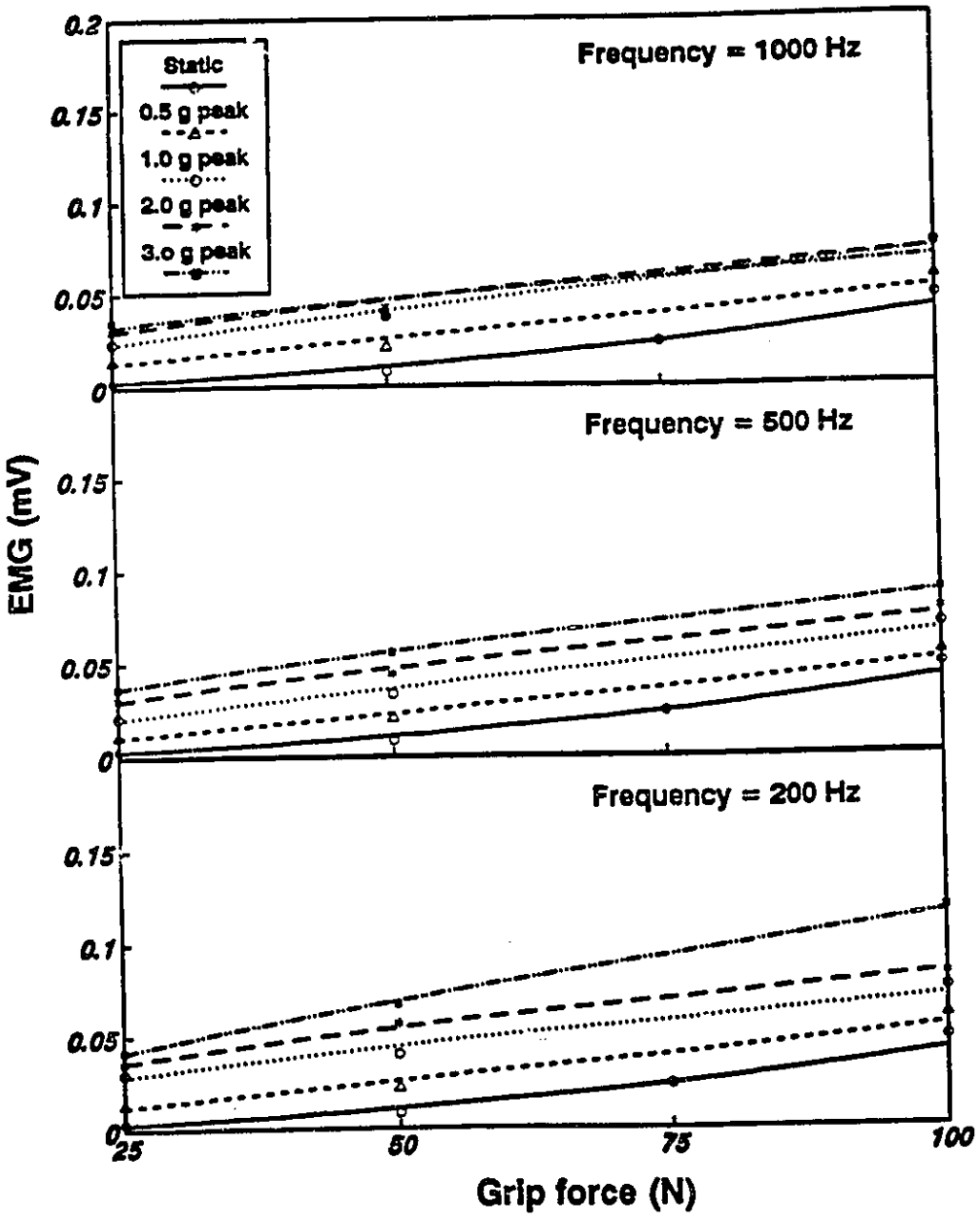

Figure 6.11: EMG of finger flexor muscles as a function of grip force, vibration frequency and peak acceleration: Z_h- direction.

Figure 6.12 illustrates grip force vs. EMG at different frequencies in Y_h-direction at constant peak acceleration levels of 0.5, 1.0 and 3.0 g. In all the cases the EMG recorded during dynamic testing was higher than the corresponding EMG level under static loading, with increases varying from 100 - 600 %. The EMG curves presented in Figure 6.12 can be grouped into one for frequencies ranging from 50 - 1000 Hz and a separate curve for 20 Hz and the influence of frequency on finger flexor EMG is not very clear. Similar patterns were observed in other two directions as well. The high excitation frequency vibrations are attenuated in the palm of the hand and very little vibration is transmitted to the wrist and beyond. The electrical activity of finger flexor muscles, therefore, did not vary significantly due to change in frequency. This aspect was further tested using statistical analysis techniques. Single factor and Multifactor analysis of variance (ANOVA) were performed to investigate the influence of various parameters tested on the measured EMG of finger flexor muscles.

6.4.3 SIGNIFICANCE ANALYSIS

Single-factor and Multifactor variance analyses were carried out to study the dependence of EMG values on various tool related parameters. Single factor analysis of variance was performed independently in all the three orthogonal directions of vibration. In this analysis, the influence of only one tool-related parameter (grip force, frequency, acceleration) is considered at a time as a source of variation. In the multi factor analysis of variance (ANOVA) the source of variation due to the influence of main effects (direction, grip force, acceleration and frequency) and interactions among the main effects are investigated. The techniques used for analysis of variance are well developed and are treated extensively in statistics literature (*Miller et al., 1985*).

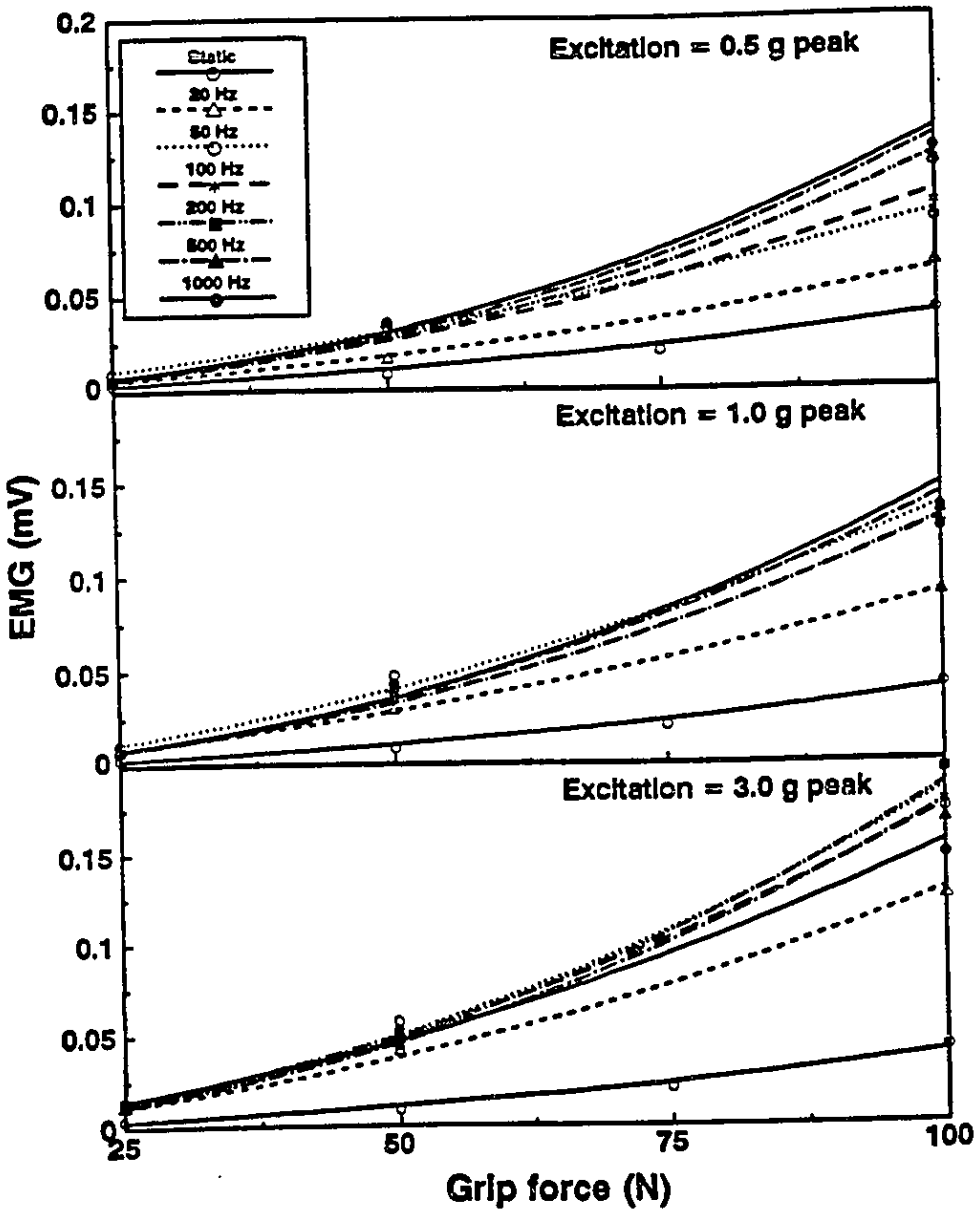

Figure 6.12: EMG of finger flexor muscles at different excitation frequencies as a function of grip force and peak acceleration; Y_h- direction.

Single Factor Analysis:

The single factor analysis of variance can be expressed by the following model (*Miller et al., 1985*)

$$Y_{ij} = \mu + \alpha_i + \varepsilon_{ij} \qquad \text{for} \quad i = 1,.....,k; \quad j = 1,.....,n \tag{6.1}$$

where, μ is the grand mean of the measured data, α represents the influence of primary factor considered and ε represents the values due to independent random variables. i corresponds to number of levels of main factors and j represents sample size of a specific level. Thus Y_{ij} corresponds to the jth EMG value corresponding to i th level of the main factor. (For example, if five observations are made under an identical set of experimental conditions all the five data points expect to have contributions from the main factor considered and from several random variables present. Therefore, the five readings are expected to vary slightly due to presence of random variables.) In the present analysis there are three main factors (grip force, acceleration and frequency) present in each of the directions of vibration. The grip forces considered are 10 N, 25 N and 50 N. Therefore, the number of levels (i =1,2,3) in this main effect are three. Similarly the number of levels corresponding to acceleration and frequency are 4 (i = 4 and i = 6), respectively. The EMG measurements made at each of the level is expected to have contributions due to random variables and the effect due to these variables are represented by (ε).

Singe factor analysis (also known as ONEWAY ANALYSIS) was carried out using the MINITAB statistical software. In this analysis, the source of variation due to one main effect only is investigated, based upon the hypothesis:

Hypothesis:

> The main factor (frequency, acceleration or grip force) influences the EMG of the finger flexor muscle in a significant manner in each of the preselected directions of vibration.

The significance level (p), mean ($\overline{X}$), group standard deviation (σ) for data acquired with one level of main factor, and pooled standard deviation ($\overline{\sigma}$) for data acquired with all levels of main factor, and confidence intervals were then computed. The significance level indicates the degree of confidence with regard to the influence of a main factor on the measured data. For p less than or equal to 0.05 the confidence level is 95 % for the main effect to influence the measured data. Similarly, the individual 95 % confidence intervals for mean values was calculated for all levels in each of the factor analyzed. The confidence intervals for the mean indicate the expected variation due to the combined influence of all the variables in a sample. The confidence intervals for the mean were calculated using the following relations:

$$\text{Upper confidence limit (UCL)} = \overline{X} + Z\left(\frac{\overline{\sigma}}{\sqrt{N}}\right) \tag{6.2}$$

$$\text{Lower confidence limit (LCL)} = \overline{X} - Z\left(\frac{\overline{\sigma}}{\sqrt{N}}\right)$$

where, $\overline{X}$ = Sample mean, $\overline{\sigma}$ = Pooled standard deviation, N = Sample size, and Z is the standardized normal mean for 95 % confidence (1.96). The UCL and

LCL limits are calculated to highlight the expected variation in the measured EMG due to influence of various tool related parameters.

Table 6.2 shows the output obtained from the MINITAB, for the data in X_h-direction when frequency is considered as the main factor. The table presents sample and pooled standard deviations, sample mean and its 95% confidence intervals, degrees of freedom (DF), sum of the squares (SS) and mean squares (MS) of the data points, and statistical measures of significance (F, p). The results presented in Table 6.2 indicate that the frequency influence is not significant at 95% confidence level ($p > 0.3$). The hypothesis can thus be rejected in this case. The mean values obtained at different frequency levels do not indicate a clear pattern. However, the mean EMGs obtained at 20 Hz and 50 Hz are higher than the mean EMGs obtained at higher frequencies. Table 6.3 shows the results obtained in X_h- direction with acceleration as the main factor. The results indicate clearly that the EMG values are influenced by the acceleration ($p < 0.001$). The mean EMG values obtained at different acceleration levels also indicate a clear pattern as the mean values increased with increase in the acceleration level. Table 6.4 shows the results obtained in X_h- direction with grip force as the main factor. The results indicate the influence of grip force on EMG is significant ($p < 0.001$). Also the mean values obtained at 25 N, 50 N and 100 N show clearly that the EMG increased with increase in grip force.

Table 6.5 shows the results obtained in Y_h- direction with frequency as the main factor. The results are more or less similar to those presented for the

TABLE 6.2
Single Factor Analysis of Variance on EMG of Finger Flexor Muscles; X_h-Direction; Source of Variation - Frequency (Hz).

SOURCE	DF	SS	MS	F	p
FREQUENCY	5	0.004113	0.000823	1.18	0.328
ERROR	66	0.045949	0.000696		
TOTAL	71	0.050062			

LEVEL	N	SAMPLE $\bar{X}$	SAMPLE σ
20 Hz	12	0.06360	0.03114
50 Hz	12	0.04747	0.03461
100 Hz	12	0.04265	0.02342
200 Hz	12	0.04230	0.02096
500 Hz	12	0.04463	0.02268
1000 Hz	12	0.04247	0.02252

$\bar{\sigma}$ = 0.02639

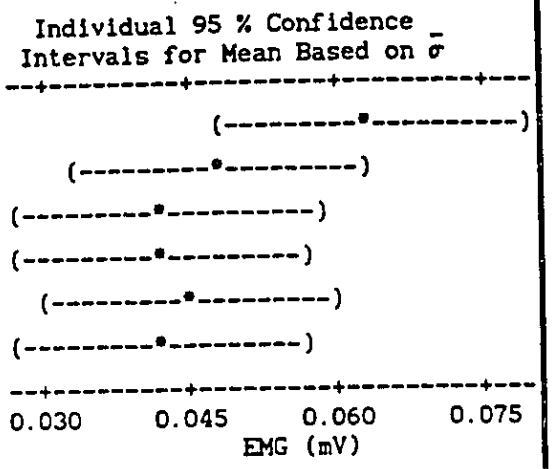

TABLE 6.3
Single Factor Analysis of Variance on EMG of Finger Flexor Muscles; X_h-Direction; Source of Variation - Acceleration (g - peak).

SOURCE	DF	SS	MS	F	p
EXCITATION	3	0.012823	0.004274	7.80	0.000
ERROR	68	0.037240	0.000548		
TOTAL	71	0.050062			

LEVEL	N	SAMPLE $\bar{X}$	SAMPLE σ
0.5 g	18	0.03145	0.01486
1.0 g	18	0.03929	0.01765
2.0 g	18	0.05116	0.02474
3.0 g	18	0.06685	0.03234

$\bar{\sigma}$ = 0.0234

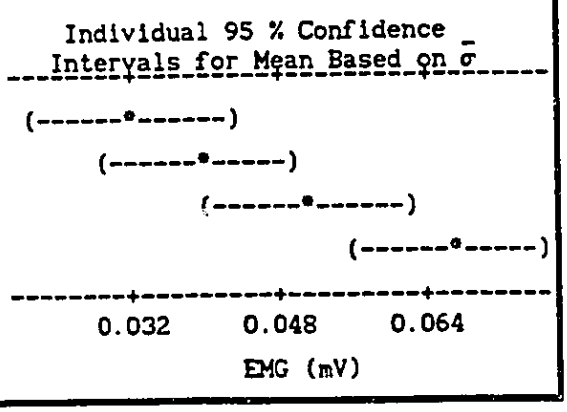

TABLE 6.4
Single Factor Analysis of Variance on EMG of Finger Flexor Muscles; X_h-Direction; Source of Variation - Grip Force (N).

SOURCE	DF	SS	MS	F	p
GRIP FORCE	2	0.025993	0.012996	37.26	0.000
ERROR	69	0.024069	0.000349		
TOTAL	71	0.050062			

LEVEL	N	SAMPLE $\bar{X}$	SAMPLE σ	Individual 95 % Confidence Intervals for Mean Based on $\bar{\sigma}$
25 N	24	0.02823	0.01667	(---•---)
50 N	24	0.04017	0.01744	(---•---)
100 N	24	0.07316	0.02155	(---•--)

$\bar{\sigma}$ = 0.01868

0.040 0.060 0.080
EMG (mV)

TABLE 6.5
Single Factor Analysis of Variance on EMG of Finger Flexor Muscles; Y_h-Direction; Source of Variation - Frequency (Hz).

SOURCE	DF	SS	MS	F	p
FREQUENCY	5	0.00357	0.00071	0.22	0.952
ERROR	66	0.21200	0.00321		
TOTAL	71	0.21558			

LEVEL	N	SAMPLE $\bar{X}$	SAMPLE σ	Individual 95 % Confidence Intervals for Mean Based on $\bar{\sigma}$
20 Hz	12	0.04496	0.04104	(----------•----------)
50 Hz	12	0.06453	0.05739	(----------•----------)
100 Hz	12	0.06141	0.05882	(----------•----------)
200 Hz	12	0.06411	0.06399	(----------•----------)
500 Hz	12	0.06453	0.05943	(----------•----------)
1000 Hz	12	0.06366	0.05664	(----------•----------)

$\bar{\sigma}$ = 0.05668

0.025 0.050 0.075
EMG (mV)

X_h- direction in Table 6.2. The frequency dependence is not clearly seen from the mean EMG values. However, the mean EMG obtained at an excitation frequency of 50 Hz is slightly higher than the mean values of EMGs obtained at other frequencies. Table 6.6 shows the results obtained in Y_h- direction with acceleration as the main factor. Although the mean values of EMG increased with increase in acceleration levels, the influence of acceleration is insignificant at 95% confidence level ($p > 0.47$). This could be observed from the overlapping of the 95% confidence intervals in all the cases. Table 6.7 presents the results obtained in the same direction with grip force as the main factor. The results clearly demonstrate that the EMG is strongly influenced by the grip force in Y_h- direction (($p < 0.001$).

Table 6.8 presents the results obtained for Z_h- direction with frequency as the main factor. Similar to the results obtained in X_h- and Y_h- directions the frequency influence on mean values of EMG is insignificant ($p > 0.97$). The mean EMGs obtained at 50 Hz and 100 Hz, however, are higher than the mean values of EMG obtained at other excitation frequencies. From the results obtained in all three directions of vibration (Tables 6.2, 6.5 and 6.8), the mean values of EMG obtained in the neighborhood of 50 Hz excitation frequency seem to be high compared to the mean values of EMG obtained at other excitation frequencies. This may be due to the presence of a natural frequency of the hand-arm system in this frequency range. Studies conducted by (*Iwata et al., 1970)* on biceps brachii muscles, in the frequency range 6.3-100 Hz, showed a decrease in muscle activity with an increase in frequency at low levels of grip force. It was further observed that the muscle activity corresponding to high grip forces, increased considerably at 10 and 50 Hz, due to resonances of the hand-arm system. Table 6.9 shows the results obtained for Z_h- direction of vibration

TABLE 6.6
Single Factor Analysis of Variance on EMG of Finger Flexor Muscles; Y_h-Direction; Source of Variation - Acceleration (g - peak).

SOURCE	DF	SS	MS	F	p
EXCITATION	3	0.00776	0.00259	0.85	0.473
ERROR	68	0.20782	0.00306		
TOTAL	71	0.21558			

LEVEL	N	SAMPLE $\bar{X}$	SAMPLE σ	Individual 95 % Confidence Intervals for Mean Based on $\bar{\sigma}$
0.5 g	18	0.04668	0.04448	(----------*---------)
1.0 g	18	0.05618	0.05015	(----------*----------)
2.0 g	18	0.06441	0.05639	(----------*---------)
3.0 g	18	0.07486	0.06746	(----------*---------)

$\bar{\sigma}$ = 0.05528

0.025 0.050 0.075 0.100
EMG (mV)

TABLE 6.7
Single Factor Analysis of Variance on EMG of Finger Flexor Muscles; Y_h-Direction; Source of Variation - Grip Force (N).

SOURCE	DF	SS	MS	F	p
GRIP FORCE	2	0.193219	0.096609	298.12	0.000
ERROR	69	0.022361	0.000324		
TOTAL	71	0.215579			

LEVEL	N	SAMPLE $\bar{X}$	SAMPLE σ	Individual 95 % Confidence Intervals for Mean Based on $\bar{\sigma}$
25 N	24	0.00953	0.00256	(*-)
50 N	24	0.04050	0.00939	(-*-)
100 N	24	0.13158	0.02962	(-*-)

$\bar{\sigma}$ = 0.0180

0.040 0.080 0.120
EMG (mV)

TABLE 6.8
Single Factor Analysis of Variance on EMG of Finger Flexor Muscles; Z_h-Direction; Source of Variation - Frequency (Hz).

SOURCE	DF	SS	MS	F	p
FREQUENCY	5	0.000432	0.000086	0.15	0.979
ERROR	66	0.037774	0.000572		
TOTAL	71	0.038207			

LEVEL	N	SAMPLE $\bar{X}$	SAMPLE σ
20 Hz	12	0.04282	0.01952
50 Hz	12	0.04680	0.02559
100 Hz	12	0.05032	0.02834
200 Hz	12	0.04427	0.02339
500 Hz	12	0.04499	0.02405
1000 Hz	12	0.04403	0.02168

$\bar{\sigma}$ = 0.02392

Individual 95 % Confidence Intervals for Mean Based on $\bar{\sigma}$

TABLE 6.9
Single Factor Analysis of Variance on EMG of Finger Flexor Muscles; Z_h-Direction; Source of Variation - Acceleration (g - peak).

SOURCE	DF	SS	MS	F	p
EXCITATION	3	0.004943	0.001648	3.37	0.023
ERROR	68	0.033263	0.000489		
TOTAL	71	0.038207			

LEVEL	N	SAMPLE $\bar{X}$	SAMPLE σ
0.5 g	18	0.03203	0.01938
1.0 g	18	0.04574	0.02223
2.0 g	18	0.05357	0.02291
3.0 g	18	0.05081	0.02370

$\bar{\sigma}$ = 0.02212

Individual 95 % Confidence Intervals for Mean Based on $\bar{\sigma}$

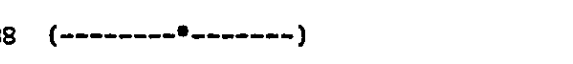

with acceleration as the main factor. The results indicate that the influence of influence is significant at 95% confidence level ($p < 0.05$). Table 6.10 clearly shows the strong influence of grip force ($p < 0.001$) on EMG when subjected to vibration in the Z_h- direction. In all the three directions of vibration it can be concluded that the grip force has significant influence ($p < 0.001$) on EMG of finger flexor muscles. From Tables 6.2, 6.5 and 6.8, it may be observed that the hypothesis was rejected in all the cases for frequency as the main effect, at 90 % confidence ($p < 0.1$). Multi factor analysis of variance was performed to further verify the results obtained in this analysis, and to test the significance of influence of main effect interactions.

Multifactor Analysis of Variance

Multi factor analysis of variance (ANOVA) was performed on the EMG data obtained under dynamic loading conditions. In this analysis, an hypothesis is formulated based on the assumption that the EMG is influenced by the main factors and the interactions among the main factors.

Hypothesis:

> Frequency, grip force, acceleration and direction of vibration influence the EMG of finger flexor muscles in a significant manner.

A multi factor model was initially formulated and the data was later analyzed by using MINITAB statistical analysis software. The analysis is performed using the following model (*Miller et al., 1985*).

TABLE 6.10
Single Factor Analysis of Variance on EMG of Finger Flexor Muscles; Z_h-Direction; Source of Variation - Grip Force (N).

SOURCE	DF	SS	MS	F	p
GRIP FORCE	2	0.021154	0.010577	42.80	0.000
ERROR	69	0.017053	0.000247		
TOTAL	71	0.038207			

LEVEL	N	SAMPLE $\bar{X}$	SAMPLE σ
25 N	24	0.02625	0.00926
50 N	24	0.04246	0.01355
100 N	24	0.06790	0.02173

$\bar{\sigma}$ = 0.01572

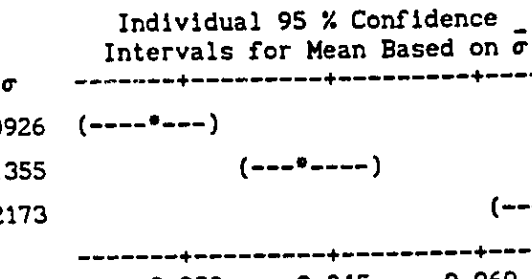

$$Y_{ijkl} = \mu + \alpha_i + \beta_j + \gamma_k + \psi_l + (\alpha\beta)_{ij} + (\alpha\gamma)_{ik} + (\alpha\psi)_{il} + (\beta\gamma)_{jk} + (\beta\psi)_{jl} + (\alpha\beta\gamma)_{ijk} + (\alpha\gamma\psi)_{ikl} + (\beta\gamma\psi)_{jkl} + (\alpha\beta\gamma\psi)_{ijkl} + \varepsilon_{ijkl}; \quad \text{for} \quad (6.3)$$
$$i = 1,2,3; \quad j = 1,2,3; \quad k = 1,2,3,4; \quad \text{and} \quad l = 1,2,3,4,5,6$$

where, i,j,k,l represent the number of levels corresponding to direction of vibration (X_h , Y_h , Z_h), grip force (10 N, 25 N, 50 N), acceleration level (0.5 g, 1.0 g, 2.0 g, 3.0 g), and excitation frequency (20, 50, 100, 200, 500, 1000 Hz), respectively. Y_{ijkl} corresponds to the EMG obtained using i th direction level, j th grip force level, k th acceleration level and l th excitation frequency level. μ is the grand mean, and α,β,γ, and ψ represent the effects of i th, j th, k th and l th level, respectively. $(\alpha\beta)_{ij},(\beta\gamma)_{jk},.....,(\alpha\beta\gamma\psi)_{ijkl}$ represent the effects of interactions among the main factors. ε_{ijkl} are the values of effects due to independent random variables. It may be noted that any of the interaction effects indicated in the model equation may be ignored. In such a case the effect due to the omitted interaction will be treated as a random variable (ε) effect.

Table 6.11 shows the results obtained by performing ANOVA on EMG data. The results indicate that the direction of vibration, amplitude of vibration and grip force have significant influence ($p < 0.001$) on the measured EMG values, while the vibration frequency is observed as an insignificant ($p > 0.94$). These results confirm the observations made in the Single factor analysis. Studies conducted on EMG of forearm flexor and extensor muscles also provided similar observations (*Radwin, 1986*). The direction of vibration and grip force were observed to have significant influence at $p < 0.05$ and $p < 0.001$,

TABLE 6.11
Multi Factor Analysis of Variance on EMG of Finger Flexor Muscles.

Sources of variation	DF	SS	MS	F	*p*
Main effects:					
Direction (A)	2	0.00974	0.00487	28.55	0.0001*
Grip force (B)	2	0.18499	0.09249	542.55	0.0001*
Acceleration (C)	3	0.02277	0.00759	44.52	0.0001*
Frequency (D)	5	0.00021	0.00004	0.25	0.940
Two-factor interactions:					
A*B	4	0.05537	0.01384	81.18	0.0001*
A*C	6	0.00275	0.00045	2.69	0.0200*
A*D	10	0.00790	0.00079	4.64	0.0001*
B*C	6	0.00212	0.00035	2.08	0.066
B*D	10	0.00313	0.00031	1.84	0.069
C*D	15	0.00195	0.00013	0.76	0.712
Three-factor interactions:					
A*B*D	20	0.00402	0.00020	1.18	0.296
A*C*D	30	0.00413	0.00014	0.81	0.738
B*C*D	30	0.00218	0.00007	0.43	0.994
Error	72	0.01227	0.00017		
Total	215	0.31358			

*($p < 0.05$)

respectively. Whereas, the influence of frequency was proven to be insignificant.

Table 6.11 also indicates that the two factor interactions {direction (A) * grip force (B), direction (A) * acceleration amplitude (C); and direction (A) * frequency (D} have significant influence on EMG of the finger flexor muscles ($p < 0.05$). The influence of two factor interactions is also highlighted in Figures 6-6 through 6 -12. Further, Table 6.11 indicates that the influence of several multi factor interactions (B*C, B*D, C*D, A*B*D, A*C*D, B*C*D) on EMG of finger flexor muscles is insignificant.

6.5 Summary

In this chapter, the influence of grip force, vibration direction, acceleration and excitation frequency on finger flexor muscle activities was investigated using surface electromyography (EMG). The electrical activity of the finger flexor muscles increased considerably with the grip force under static as well as dynamic loads. The electrical activity under dynamic loads, however, was observed to be 1.5 - 6.0 times higher than the electrical activity under the static loads. The ANOVA results indicated that the vibration direction, acceleration and grip force have a very significant influence on EMG of finger flexor muscles ($p < 0.001$), whereas the effect of vibration frequency was observed to be insignificant. This may be attributed to the attenuation of high frequency vibrations in the palm of the hand. This aspect is further investigated in the subsequent chapter. The peak grip pressures observed at the hand-handle interface corresponding to different grip forces (Chapter 5) and the high muscle activities of finger flexor muscles recorded in this section demonstrate the effects of transmitted vibrations on hand-arm system. In the next chapter, vibration

transmissibility patterns in the hand and arm is investigated. A method of evaluating the performance of vibration isolation gloves is proposed.

CHAPTER 7

VIBRATION TRANSMISSIBILITY CHARACTERISTICS OF THE HAND-ARM AND GLOVES

7.1 Introduction

The electrical activities of the muscles, magnitudes of pressure peaks at the hand-handle interface, and biodynamic response behavior of the hand-arm system are directly related to hand-transmitted vibration. A reduction in magnitude of hand-transmitted vibration is thus extremely important to minimize the health risks posed by hand-transmitted vibration. A study of vibration transmissibility characteristics of the hand-arm can provide a significant insight to the characteristics of hand-transmitted vibration, and may contribute to the development of vibration isolators. The vibration transmissibility can also be used to determine the relative motions of various parts of the hand-arm, and to assess the vibration attenuation performance of protective devices, such as anti-vibration gloves. The lack of appropriate sensors, and standardized measurement and assessment procedures, however, have severely limited studies to enhance an understanding of vibration transmissibility characteristics of hand-arm, and the protective devices.

Attempts have been made to establish the vibration transmissibility characteristics of the hand-arm system through measurement of vibration transmitted to different locations of the upper limb (*Abrams et al., 1969; Pyykkö et al., 1976; Reynolds et al., 1977; Griffin et al., 1982*). The transmitted vibration was measured using accelerometers attached to the skin. The measurement of transmitted vibration of various parts of upper limb, however, posed certain complexities associated with the attachment of the transducers to the skin.

Therefore, the transmissibility studies were essentially limited to low frequency vibrations. *Abrams et al. (1969)* have utilized cadaver arms to measure the transmitted vibration by attaching accelerometers directly to the bone. The primary reason cited for attaching accelerometers directly to the bone was to eliminate measurement errors caused by relative motions between the skin, muscle and the bone. The study concluded that at higher frequencies (above 300 Hz) the transmitted vibration tends to become localized to the hand. The measurement of transmission characteristics along the radius bone in the forearm revealed the presence of resonances at frequencies near 125 Hz and 500 Hz. Measurements performed on the cadaver arms, however, may not characterize the human hand-arm due to two primary factors: (i) the muscle tension in a detached cadaver arm differs considerably from the tension in a live muscle; and (ii) the cadaver arms can not be utilized to determine the transmissibility characteristics under different magnitudes of grip and push forces.

Pyykkö et al. (1976) have used miniature accelerometers to measure the vibration transmitted to wrist, elbow and upper arm for different vibration excitations and grip forces in the 20 - 630 Hz frequency range. The measurements were performed in a longitudinal direction of vibration corresponding to the Z_h- direction (*ISO - 5349, 1986*). The study observed vibration attenuation of 3 dB per octave in the 20 - 100 Hz frequency range, in the entire hand-arm system. At frequencies above 100 Hz, an attenuation of 6 dB per octave was observed in the wrist, and a 10 dB/octave attenuation was noticed in the elbow and upper arm. The study also observed that for a constant grip force the vibration transmission of the hand-arm system may be characterized by a linear system. The vibration transmission characteristics of

the hand-arm have been extensively studied for palm and finger types of grip under X_h, Y_h and Z_h directions (*Reynolds et al., 1977*). The measurement were performed for grip forces of 8.9 N and 35.6 N using palm- and finger- type of grips. The measurements were performed using sub miniature accelerometers mounted at eight different locations on the upper arm. The accelerometers were mounted on the fingers, directly above the metacarpal bones, wrist, elbow and shoulder. The results of this investigation, similar to the results reported by *Abrams et al. (1969)*, suggested that vibration at frequencies above 200 Hz was primarily limited to the hands and fingers. The possibility of large relative motions between adjacent tissues and across the bone joints was further highlighted by the study.

Christ (1982) conducted an experimental investigation on the performance of anti-vibration gloves by mounting a triaxial accelerometer on the back of the palm. The study reported the vibration transmissibility of the hand-arm with gloves made of PVC and knitted-texture nylon in the 8 - 1000 Hz frequency range. While the vibration attenuation of the gloves was not noticeable, the gloves resulted in amplification of vibration in some frequency bands. Further, the subjective evaluation of gloves revealed not only their ineffectiveness in attenuating vibration but also their interference with the work.

Griffin et al. (1982) performed transmissibility measurements to establish an objective method of assessing the glove like materials in the 10 - 500 Hz frequency range. The measurements were performed using miniature accelerometers mounted on the index finger nail, and the skin over third metacarpal bone. The study revealed that the glove attenuates handle vibration at frequencies above 100 Hz. At excitation frequencies below 100 Hz, however,

the glove may increase transmitted vibrations due to resonances of the coupled glove hand-arm system. The vibration transmissibility characteristics of anti-vibration and conventional gloves have been measured in some recent studies (*Goel et al., 1987; Rens et al., 1987; Starck et al., 1990*). Similar to the method proposed by *Christ* (*1982*), *Goel et* al. (1987) have used a small triad, consisting of three accelerometers, on the back of the palm to measure the vibration attenuation characteristics of gloves. The base of the triad was secured to the hand with tape and an elastic bandage. While the triad permitted the subject to wear a glove, the possible contacts between the triad head and the glove may influence the outcome of transmissibility measurements. *Rens et al.* (*1987*) have evaluated the vibration attenuation performance of general purpose gloves by measuring the hand acceleration using a special adapter held between the hand and the handle. The round metal adapter was held within the palm by means of a metal stem squeezed between the third and fourth fingers. The accelerometer was mounted on the stem at the level of the head of the third metacarpal bone. The study concluded that the general purpose gloves do not provide attenuation at all the frequencies. The dexterity loss experienced by the subjects due to use of gloves was also assessed subjectively. The vibration transmitted to the wrist and the head were measured under vibration excitations to the hand-handle with and without the gloves (*Starck et al., 1990*). The study concluded that the levels of transmitted vibration with the gloves were greater than those without the gloves in the 40 - 630 Hz frequency range.

Upon recognizing the lack of a uniform measurement procedure, the International Standards Organization (ISO) and the European Committee for Standardization (CEN) have jointly mounted efforts to develop a standardized method to assess the vibration attenuation performance of gloves (*ISO/108/4/3/*

N65 and CEN/231/3 N46, 1992). While a standard method of measurement has not yet been developed, a measurement procedure based on a transducer mounted on palm-held adapter is currently being considered. In this method, the transducer is rigidly mounted on an adapter, which is held within tne palm while gripping the vibrating handle with and without a glove. Many concerns have been expressed due to several limitations of the proposed method, which include: (i) difficulties in retaining the direction of sensitivity axis of the transducer with the direction of vibration; (ii) Variations in the dynamic characteristics of the hand-arm system due to added adapter at the hand-tool interface; (iii) the relative motions between the handle, adapter and the palm. In view of these limitations, the need for further experimental and analytical research investigation in this aspect of occupational hand-arm vibration has been recognized.

In this section, a measurement procedure to evaluate the vibration transmission characteristics of the gloves and the hand-arm system is proposed. The vibration transmission properties of the hand-arm are characterized through the measurement of vibration of fingers, knuckle and the wrist. The measured data are used to develop the analytical vibration transmission models of the hand with and without the glove.

7.2 Measurement of Vibration Transmission - General Considerations and Constraints

The hand-arm system is a complex composition of bones, muscles, tissues and the skin. Measurement of dynamic response characteristics of the hand-arm system has been very complex due to lack of measurement techniques and transducers that may be attached to various parts of the hand-

arm system. Since the physical size and weight of the transducer affects the measurements in a significant manner, it is vital that sub miniature accelerometers with minimal weight be used to measure the transmitted vibration. The measurement of hand transmitted vibration using live human subjects, however, poses many difficulties, which include: (i) difficulties in mounting the transducer rigidly with its sensitivity axis in a desired direction; (ii) poor signal to noise ratio due to presence of high noise in the human transmitted vibration; and (iii) mounted transducers often cause interference with the intended activity of the subjects. The transducers together with their mounting devices, such as rings or wrist bands further cause discomfort to the subjects and induce measurement errors by altering the interface characteristics. To avoid these problems, laser based non-contacting sensors may be selected to measure the transmitted vibration. The laser based sensors, however, are not applicable at frequencies beyond 1 kHz due to their low sensitivity. The measurement of hand-arm vibration characteristics thus necessitates appropriate considerations of many factors, such as selection of transducers, location of sensors, characteristics of vibration excitations, grip force, and push-pull forces.

7.2.1 SELECTION AND LOCATION OF TRANSDUCER

Measurement of the vibration transmissibility of gloves is mostly affected by the location and mounting of the transducer. The ideal location of the transducer is perhaps the palm of the hand (*ISO/108/4/3/ N65, CEN/231/3 N46, 1992*). The transducer mounted on the subjects palm, however, interferes with the normal gripping of a handle. Further, the subjects experience difficulties in holding the transducer at the hand-tool interface at low frequency excitations (below 100 Hz). Alternate locations of transducers include finger, carpal bones,

wrist, elbow, etc.. Earlier studies have indicated that energy directed to hand is dissipated in the cutaneous and subcutaneous tissue of the hand resulting in only low levels of vibrations (less than 10 %) transmitted to the wrist and beyond at frequency excitations above 250 Hz (*Reynolds et al., 1984; Abrams et al., 1969*). Measurement of vibration at the elbow thus may not be possible. Ideally, the transducer should be located on the hand, such that it does not alter the properties of hand-tool interface situation. In view of this, the transducer located on the head of third metacarpal bone is considered to be most appropriate due to the following:

(i) the skin at this location is relatively thin;

(ii) the measurement errors, caused by relative motions between the transducer and the bone, and between skin and the transducer can be minimized as a laser beam may be focused directly on the intended location as opposed to a mounted transducer;

(iii) the location of transducer is relatively proximal to the source of vibration;

(iv) high frequency vibrations may also be measured with a reasonable accuracy.

7.2.2 VIBRATION EXCITATIONS

While the vibration of hand-held power tools occurs in a broad frequency range, the vibration generated by most industrial tools predominate in the 10 - 500 Hz frequency range (*Griffin et al., 1982*). At high excitation frequencies the vibration is primarily confined to the cutaneous and subcutaneous tissues and the signal to noise ratio at points further from the vibrating skin surface tends to decrease. It may thus be appropriate to conduct the transmissibility studies in the frequency range of 10 - 500 Hz.

The vibration transmission characteristics of the hand-arm system are strongly related to the magnitude and dominant directions of vibration (*Reynolds et al., 1977*). The variation in transmissibility in different directions is primarily attributed to variations in hand-handle orientation. The factors such as hand size, elbow angle and shoulder abduction may also contribute to the variations in the amount of vibration transmitted. While the grip force and excitation levels considerably influence the visco elastic properties of the glove materials, the relative performance analysis of gloves may be carried out in any one of the three orthogonal directions using a chosen set of experimental parameters. The vibration transmission characteristics of the hand-arm and the gloves in this study are evaluated under vertical direction corresponding to the X_h- direction proposed in ISO - 5349 (1986).

For laboratory evaluations of gloves and study of hand-arm vibration transmissibility, three types of excitations may be considered; stochastic, sinusoidal sweep, and stepped sinusoid. Although it is most appropriate to use vibration spectra generated by power tools while in operation, it may require several evaluations since the various power tools generate different vibration spectra. Alternatively, sinusoidal excitations may be used to study the vibration characteristics of the hand-arm, and to carry out a relative performance evaluation of gloves. The muscles are known to produce tonic vibration reflexes when subjected to rapidly varying frequencies (*Radwin, 1986; Pyykkö et al., 1976*). The tonic vibration reflex produced in muscles restricts the use of random and sinusoidal sweep excitations. Swept sinusoidal vibration with very low sweep rates have been used to measure the vibration transmissibility of hand-arm system (Pyykkö et al., 1976). Stepped sinusoid excitations, are perhaps ideally suited to study the vibration transmissibility characteristics such

that sufficient time is permitted for the muscles to adjust to the changing excitation frequencies.

7.2.3 GRIP FORCE AND PUSH FORCE

Grip force and push force are known to influence the dynamic characteristics of the hand-arm system (*Griffin et al., 1982; Bernard, 1990).* While the push force is known to influence the dynamic characteristics at only low frequency excitations, the considerable influence of grip force on the biodynamic response is evident from the results presented in Chapter 2. These forces further affect the visco elastic properties of the hand-handle and glove-handle interface. The transmissibility tests are thus performed for different magnitudes of hand grip forces (10 N, 25 N and 50 N), while neglecting the corresponding variations in the push force. The selected grip forces represent the most commonly used range of grip forces in the industry (*Abrams, 1971; Reynolds et al., 1984; Färkkilä et al., 1979*)

The experimental parameters selected for obtaining the hand transmissibility characteristics with and without gloves are summarized in Table 7.1.

7.3 Experimental Procedure

A 38 mm diameter test handle fixture was mounted on an electrodynamic exciter to deliver sinusoidal vibrations in X_h- direction (see Chapter 2). The handle setup used in this experiment behaved like a pure mass with no resonant frequencies in the frequency range of interest (10 - 500 Hz). A laser sensor (B&K 3544), pre-calibrated by the manufacturer, was used to measure the

TABLE 7.1
Range of Selected Test Parameters for Vibration Transmissibility Analysis

Frequency	10 - 500 Hz
Direction	X_h
Excitation	
Type	Stepped sinusoid
Magnitude	1.0 g and 2.0 g peak
Grip force	10 N, 25 N and 50 N
Push force	0 N
Elbow angle	90 degrees
Shoulder abduction	0 degrees
Body posture	Standing upright
Subjects	4 male subjects
Handle size	38 mm diameter

velocity response. Since only one laser sensor was available, miniature accelerometers were utilized to measure vibration transmitted to the tip of the index finger and wrist. Preliminary tests were conducted by vibrating the handle setup alone to correlate the velocity and acceleration signals measured by the laser sensor and accelerometers, respectively. The schematic of calibration setup is shown in Figure 7.1. All input and output acceleration signals were converted to velocity signals using preconditioners (B&K 2635) to facilitate data comparison. The responses of the transducers were verified by exciting the experimental setup at various frequencies using constant acceleration excitation.

The accelerometer signals correlated very well with the laser signal in the entire frequency range. In this manner the responses of all transducers were verified to ensure measurement accuracy.

The vibration transmissibility tests were performed on four subjects in standing body posture. The subjects were advised to apply a desired grip force with their dominant right hand, and maintain an elbow angle of 90 degrees with zero shoulder abduction. The shaker was excited at constant acceleration levels at 18 discrete frequencies in the 10 - 500 Hz frequency range. The non-contact laser sensor was used to measure the vibration transmitted to the head of the third metacarpal bone. A reflective tape was placed on the head of the bone to deflect the laser beam. The vibration transmitted to the index finger was measured by an accelerometer glued directly to the nail of the subject. The transmitted vibrations to wrist was measured using accelerometers mounted on a specially designed bracelet shown in Figure 7.2 (*Boileau et al., 1992*). Although the bracelet is designed to accommodate three miniature accelerometers oriented in three orthogonal directions, only one accelerometer was mounted to measure transmitted vibration in the X_h- direction. A resonance test was performed to determine the resonant frequency of the bracelet for a specific tension considered tolerable by the subjects. The resonant frequency of the bracelet with the accelerometer was observed at 1.2 kHz. A leather strap was used to hold the accelerometers firmly in place on the wrist. Usually, the bracelet was attached with the maximum tolerable force by the subjects. The orientation of the transducers was such that their sensitivity axis was parallel to the direction of the vibration.

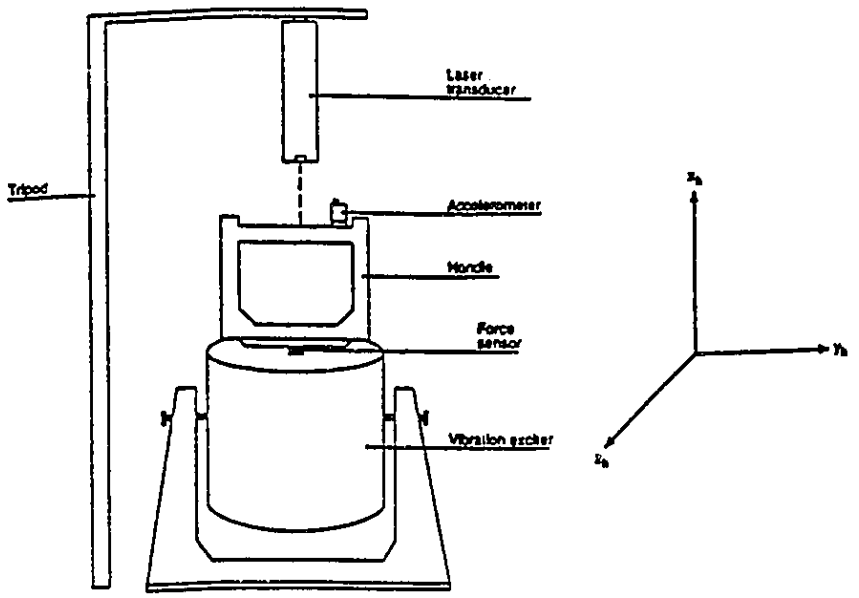

Figure 7.1: Experimental setup utilized to calibrate transducers.

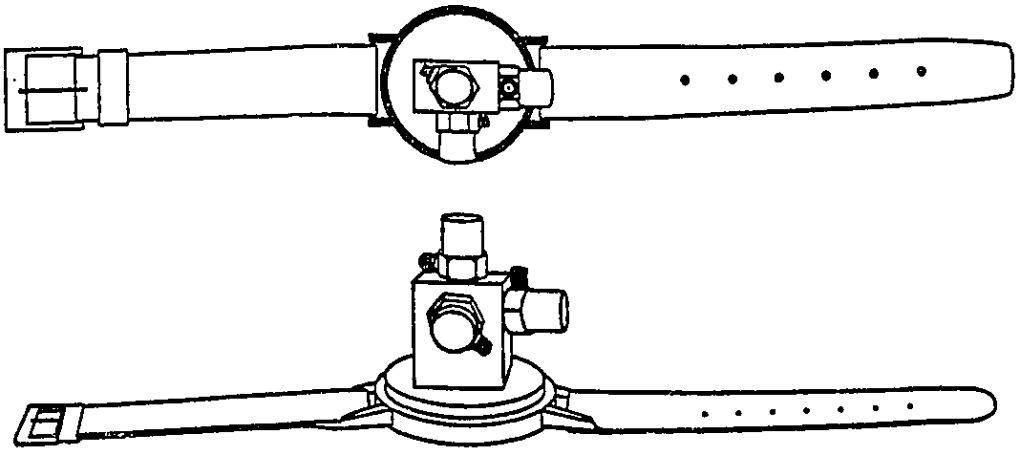

Figure 7.2: Schematic representation of bracelet with three accelerometers.

TABLE 7.2
Summary of Different Gloves Tested

No.	Type of glove	Material description	Weight (kg)	Manufacturer (or) Trademark	Country
1	AV* - FL♦	85% Nylon and 15% Lycra	0.045	ERGOTECH	Canada
2	AV - FL	NA#	0.060	VIBRASORB	Canada
3	AV - F$	Poron and Cotton	0.105	WOLVERINE	U.S.A.
4	GP£ - F	PVC; Cotton and Polyurethane	0.085	WINTER MONKEY GRIP	Canada
5	AV - F	Sorbothane	0.165	HYPASAFE	U.K.
6	AV - F	Sorbothane	0.205	HYPASAFE	U.K.
7	AV - F	Sorbothane and Ultrilure lining	0.110	ERGODYNE	Canada
8	AV - F	NA	0.075	IMPACTO	Canada
9	AV - FL	Sorbothane and Ultrilure lining	0.100	ERGODYNE	U.S.A.

* Antivibration; ♦ Fingerless; # Not available; $ Full; £ General purpose

A total of nine anti-vibration and general purpose industrial gloves were selected to study their vibration transmissibility characteristics. The anti-vibration gloves were procured directly from manufacturers in Canada, Great Britain and U.S.A.. Specifications of the selected gloves are summarized in Table 7.2. A tiny circular hole (5 mm diameter) was made in all the gloves so as to facilitate attachment of laser deflection tape on the head of the third metacarpal bone. The vibration transmitted to the head of the third metacarpal bone, index and wrist were measured using stepped sinusoidal excitation at 18 discrete frequencies. Data thus obtained on all subjects for each of the glove were averaged to obtain the mean levels of vibration transmitted.

7.4 Mathematical Modeling

While many lumped parameter models have been developed to characterize the biodynamic response of the hand-arm using mechanical impedance data, only a few attempts have been made to develop vibration transmissibility models due to lack of reliable hand transmissibility data. Analytical models of the hand-transmitted vibration may serve as an important tool to design and evaluate vibration isolation mechanisms. Vibration transmissibility characteristics of the hand and coupled glove-hand system may be represented by two - and three -degrees of freedom (DOF) lumped parameter linear models, respectively. Figure 7.3 illustrates the lumped parameter models of the hand with and without the glove, where m_1 conceptually represents the mass of the hand, m_2 represents the coupled mass of the upper arm with the hand, and mass of the glove is represented by m_g in the three - DOF hand-glove model. The dynamic characteristics of these linear models can be described by coupled linear differential equations in the matrix form:

$$[M]\{\ddot{q}\}+[C]\{\dot{q}\}+[K]\{q\}=\{\mathrm{F}\} \tag{7.1}$$

where [M], [C] and [K] are (nxn) mass, damping and stiffness matrices, respectively. {q} is a (nx1) vector of displacement response quantities, {F} is (nx1) displacement excitation vector, and '·' and '··' designate the first and second derivative with respect to time. Fourier transform of equation (7.1) yields

$$\{Q(j\omega)\}=\left[[K]-\omega^2[M]+j\omega[C]\right]^{-1}\{F(j\omega)\} \tag{7.2}$$

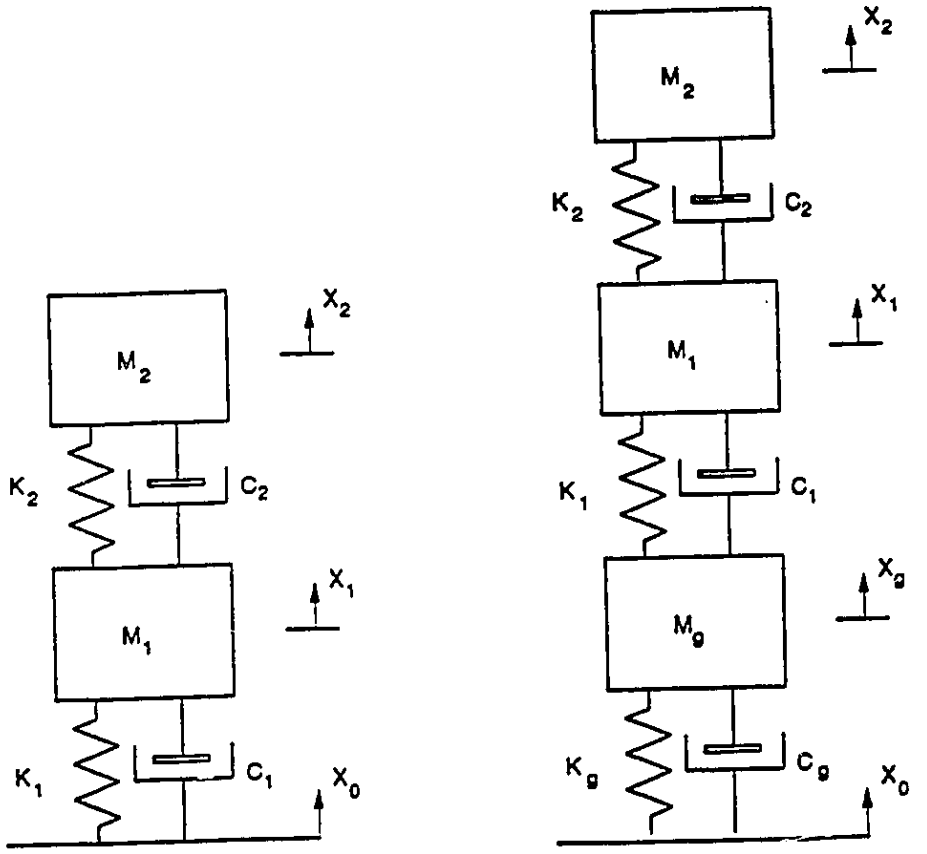

(a) Two- DOF hand model

(b) Three- DOF hand-glove model

Figure 7.3: Vibration transmissibility models of the hand and coupled hand-glove system.

where $[Q]$ and $[F]$ are Fourier transforms of {q} and {F}, respectively, and ω is the circular frequency. The vibration transmissibility ratio of different masses is obtained as a ratio of the respective displacement response to the applied displacement excitation. The transmissibility ratio is defined as follows:

$$TR_i(\omega) = \left| \frac{X_i(j\omega)}{X_0(j\omega)} \right| \quad \text{for } i = 1, \ldots\ldots, n \tag{7.3}$$

where $X_0(j\omega)$ is the displacement amplitude of excitation. The model parameters are selected such that the vibration transmissibilities, computed using equation (7.3), correlate well with the measured transmissibility characteristics.

7.4.1 ESTIMATION OF MODEL PARAMETERS

The model parameters are often derived using trial and error based curve fitting techniques, such that the computed transmissibility characteristics are matched with the measured transmissibility characteristics (*Griffin et al., 1982*). The trial and error methods may lead to a poor fit when a broad frequency range is considered. Alternatively, optimization techniques may be effectively employed to derive the model parameters by minimizing the errors between the model and the measured response characteristics. A constrained objective function, based on the transmissibility error in the entire frequency range, is thus formulated in the following manner:

$$U(\bar{\chi}) = Minimize \left[\sum_{i=1}^{n} \sum_{k=1}^{l} \left[W\{TR_i(\omega_k) - TR_m(\omega_k)\} \right]^2 \right]; \quad \text{for} \quad \omega_L < \omega_k < \omega_u \tag{7.4}$$

where $U(\overline{\chi})$ is the transmissibility error function to be minimized, and $TR_i(\omega_k)$ and $TR_m(\omega_k)$ are computed and measured transmissibilities of mass m_i, corresponding to excitation frequency ω_k . ω_L and ω_u are the lower and upper limits of the frequency range considered, W is a weighting function, and $\overline{\chi}$ is a vector of model parameters defined as

$$\overline{\chi} = \{m_i, K_i, C_i\}^T \quad \text{for} \quad i = 1,.....n \tag{7.5}$$

where 'T' designates the transpose. The objective function described in Equation (7.4) is subject to following constraints:

$$m_i > 0.; \quad K_i > 0.; \quad \text{and} \quad C_i > 0. \quad \text{for} \quad i = 1,.....,n \tag{7.6}$$

The model parameters are derived upon minimizing the transmissibility error function using the optimization software described in Chapter 3.

7.5 Results and Discussion

The vibration transmitted to the finger, knuckle and wrist are obtained at eighteen discrete excitation frequencies, which are selected as the 1/3 octave band center frequencies in the 10 - 500 Hz range. The measurements are performed to measure vibration transmissibility of the hand, with and without the glove at the third metacarpal bone (knuckle) with the selected gloves at individual frequencies for all the subjects. The vibration transmissibility of finger and wrist are obtained without glove for all the four subjects. The data thus obtained are subsequently averaged and smoothened to obtain the vibration transmissibility characteristics of the hand with and without a glove in the entire

frequency range. The results are critically analyzed and discussed to highlight the transmissibility characteristics of hand-arm system with and without gloves.

7.5.1 HAND-ARM TRANSMISSIBILITY CHARACTERISTICS

Figure 7.4 illustrates the average vibration transmissibility characteristics of the finger, knuckle and the wrist for a constant acceleration excitation level of 1.0 g peak and different magnitude of grip forces (10 N, 25 N and 50 N). The results clearly illustrate the resonances of the finger near 150 Hz and 315 Hz, irrespective of the grip force. The response measured at the knuckle also exhibits two resonant frequencies. The higher frequency resonant peak is observed near 250 Hz, irrespective of the grip force. The first resonant frequency, however, tends to increase with the grip force. The resonant frequency is observed in the 63 - 80 Hz range at 10 N, and 80 - 100 Hz range at 25 N, and 100 Hz at 50 N grip force. The level of vibration transmitted to wrist is considerably lower compared to the other two locations, irrespective of grip force. The vibration transmitted to the wrist decreases gradually with increasing frequency, and approaches to nearly 1 % at 500 Hz. The vibration transmissibility ratio tends to increase with an increase in the grip force in almost the entire frequency range.

Figure 7.5 illustrates the vibration transmissibility characteristics of the hand-arm system subject to constant acceleration excitation of 2.0 g peak. The results are similar to the data presented in Figure 7.4. The vibration transmissibility, measured at the wrist, is considerably lower than those measured at the finger and knuckle. The vibration transmissibility of the wrist approaches nearly 10 % at 200 Hz and almost 1 % at 500 Hz. A comparison of

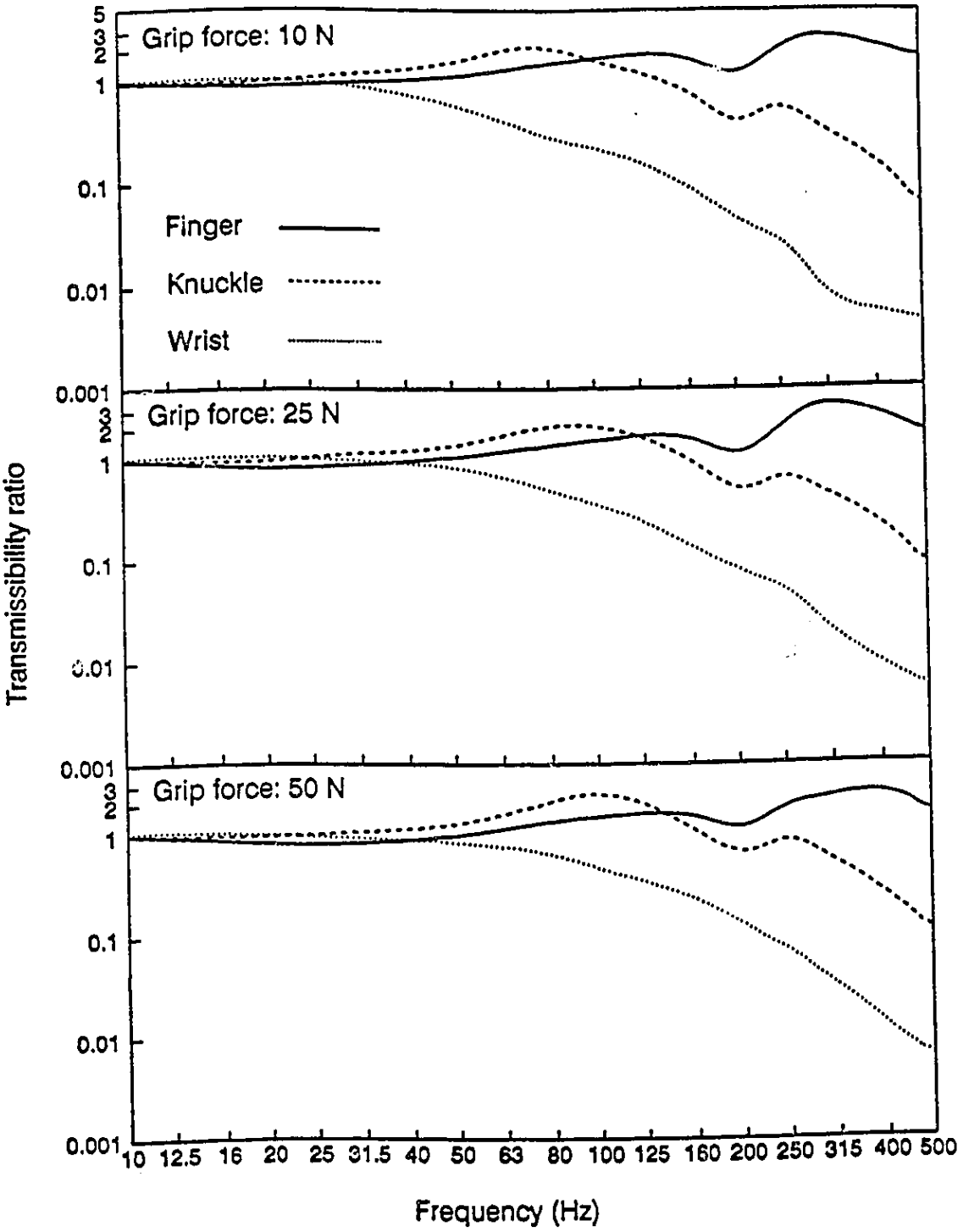

Figure 7.4: Vibration transmissibility of the hand-arm system (Excitation: 1.0 g peak acceleration).

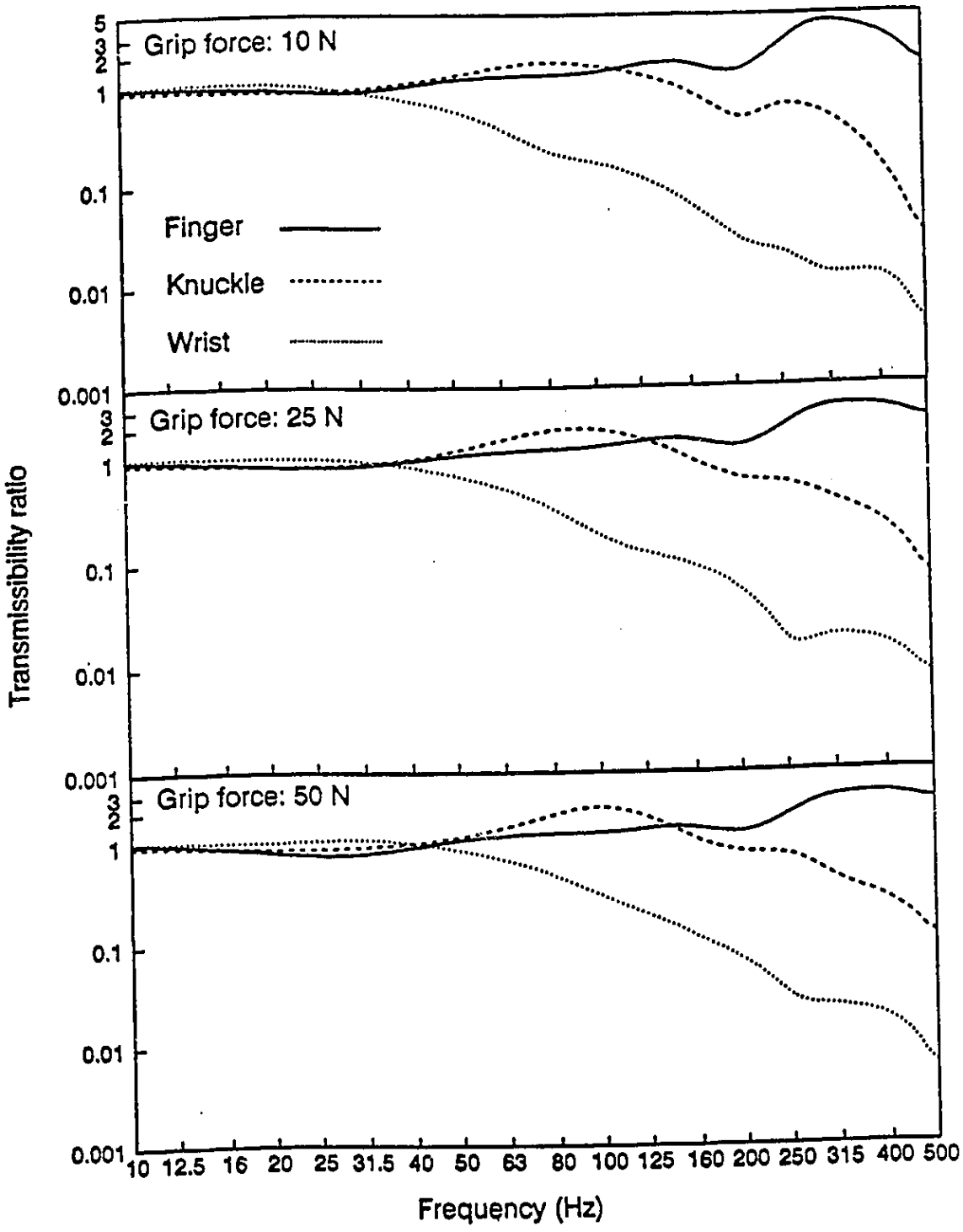

Figure 7.5: Vibration transmissibility of the hand-arm system (Excitation: 2.0 g peak acceleration).

Figure 7.5 and Figure 7.4 reveals that vibration transmissibility tend to increase slightly when amplitude of excitation is increased.

Figure 7.6 illustrate the mean values and the envelopes of vibration transmissibility characteristics measured on four subjects under different levels of grip forces and accelerations. The envelope and mean values of the transmissibility measured at the knuckle and wrist are compared to the results reported by *Reynolds et al. (1977)*, and *Abrams et al. (1969)*, to highlight similarities with the reported data. *Reynolds et al.* (1977) reported the mean knuckle transmissibility data for 8.9 N grip force under identical direction of vibration, type of grip and location of transducer. Although the measured data compare well with the reported data as shown in Figure 7.6 (a), the measured resonant frequency (near 100 Hz) is observed to be higher than that reported by *Reynolds et al. (1977)*. This discrepancy may be attributed to higher grip forces (10 N, 25 N and 50 N) used in the present study. The increase in fundamental resonant frequency with grip force may be related to an increase in hand stiffness caused by the increase in grip force.

The measured wrist transmissibility characteristics are compared to those reported by *Reynolds et al. (1977)* and *Abrams et al. (1969)*, as shown in Figure 7.6 (b). The data reported by *Reynolds et al. (1977)* were obtained using a grip force of 8.9 N and finger-type grip. The data reported by *Abrams et al. (1969)* were obtained from a cadaver arm by fixing accelerometers directly on the bone. Although the measured transmissibility characteristics correlate well with the published data, in a qualitative manner, considerable quantitative difference may be observed. The differences among the data may be attributed to the different experimental conditions employed in each study. At excitation frequencies

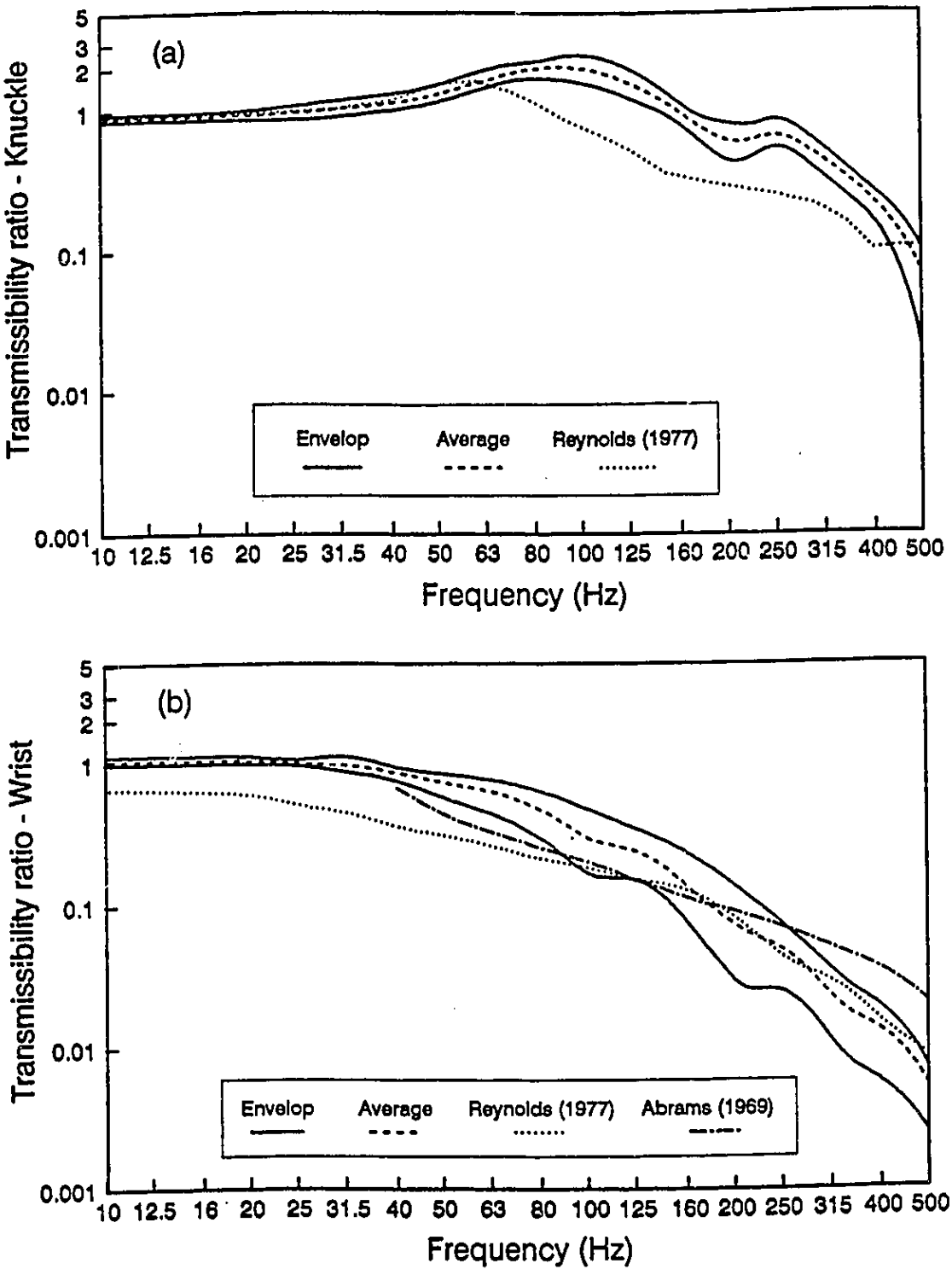

Figure 7.6: Vibration transmissibility of the hand-arm system compared, (a) Knuckle; (b) wrist.

above 300 Hz, the wrist transmissibility reported by *Abrams et al. (1969)* is larger than the measured values. This difference may be attributed to the location of the transducer, which was mounted directly on the bone of a cadaver arm. The difference may be further attributed to different visco-elastic properties of the cadaver and live hand-arm. At low excitation frequencies, the wrist transmissibility reported by *Reynolds et al. (1977)* is lower than those established from this study (≅ 1.0). The lower transmissibility at low frequencies may be attributed to difference in grip force, type of grip used. Further, errors due to mounting of accelerometer can not be discounted altogether.

7.5.2 TRANSMISSIBILITY CHARACTERISTICS OF GLOVES

The relative vibration transmission characteristics of the gloves are evaluated by comparing the knuckle transmissibility of the hand with and without the glove. Figure 7.7 illustrates the vibration transmissibility characteristics to the knuckle of the hand with and without the glove under a 10 N grip force and a constant excitation level of 1.0 g peak acceleration The vibration transmitted to the knuckle of the bare hand is shown by the continuous solid line. The vibration transmissibility of the selected nine gloves is presented by their respective glove number (# 1 to # 9) as described in Table 7.2. From the figure it is evident that gloves in-general provide slight attenuation of vibration at low frequencies and tend to amplify transmitted vibration at frequencies above 200 Hz. The glove # 1, an anti vibration and fingerless glove, yields vibration transmissibility identical to that of the bare hand in the 10 - 160 Hz excitation frequency range. The vibration transmissibility of the glove is more than that of the bare hand in the 160 - 250 Hz frequency range. The glove, however, attenuates the transmitted vibration at frequencies above 250 Hz. The vibration transmissibility of glove # 2 is greater than that of the bare hand in the 80 -160 Hz and above

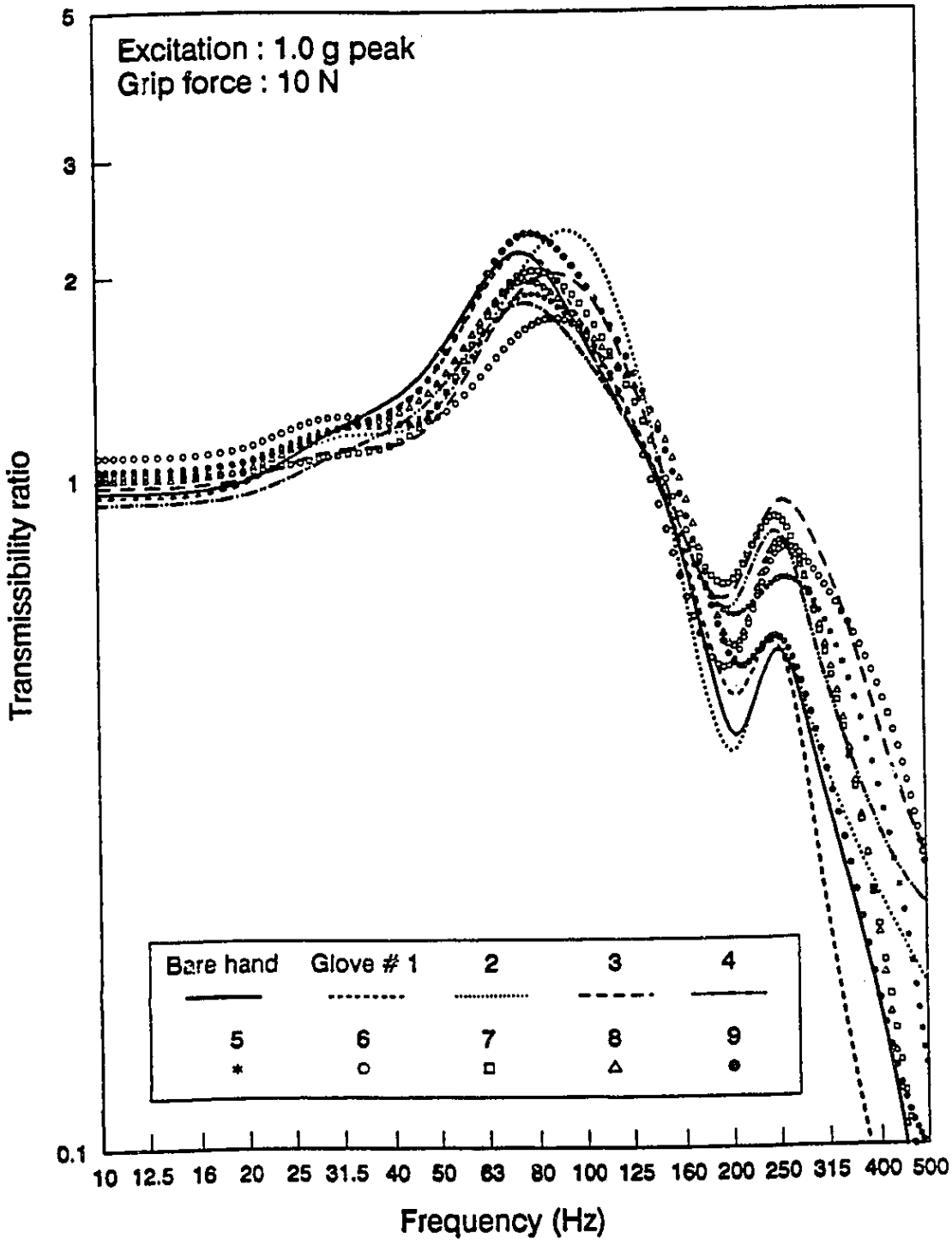

Figure 7.7: Vibration transmissibility of the hand, with and without glove.

250 Hz frequency bands, and slightly lower in 25 - 80 Hz and 160 - 250 Hz bands. The glove also tends to increase the fundamental resonant frequency of the hand. The vibration transmissibility characteristics of glove # 3 (a full antivibration glove) are higher than those of the bare hand in the entire frequency range, except in the 25 - 100 Hz band. The glove # 4, a general purpose glove, yields attenuation of transmitted vibration in the 10 - 125 Hz frequency range, and an amplification of transmitted vibration at excitation frequencies above 125 Hz. Glove # 5 and # 6, made by one manufacturer yield similar vibration transmissibility characteristics at different excitation frequency ranges. The glove # 5, an antivibration full glove made of Sorbothane, yields vibration transmissibility identical to that of the bare hand in the 80 - 160 Hz excitation frequency range. The vibration transmissibility of the glove is higher than that of the bare hand in the excitation frequency range of 10 - 30 Hz, and 160 - 500 Hz. The glove, however, attenuates the transmitted vibration in the frequency range of 30 - 80 Hz. The vibration transmissibility characteristics of glove # 6, an antivibration glove also made of Sorbothane, is identical to the transmissibility characteristics of glove # 5 in different frequency ranges as discussed earlier. Glove # 7 (an antivibration glove) slightly attenuates vibration in the narrow frequency band of 25 - 80 Hz, and amplify transmitted vibration at other frequencies. The vibration transmissibility characteristics of glove # 8 are similar to that of glove # 7 as the glove provides slight attenuation in the frequency band of 20 - 80 Hz. Glove # 9 was observed to amplify transmitted vibration at all excitation frequencies except in the band of 40 - 80 Hz.

Figures 7.8 to 7.12 present the vibration transmissibility characteristics of the hand with and without gloves under different magnitudes of grip forces and excitation levels. An examination of these figures reveals similar characteristics

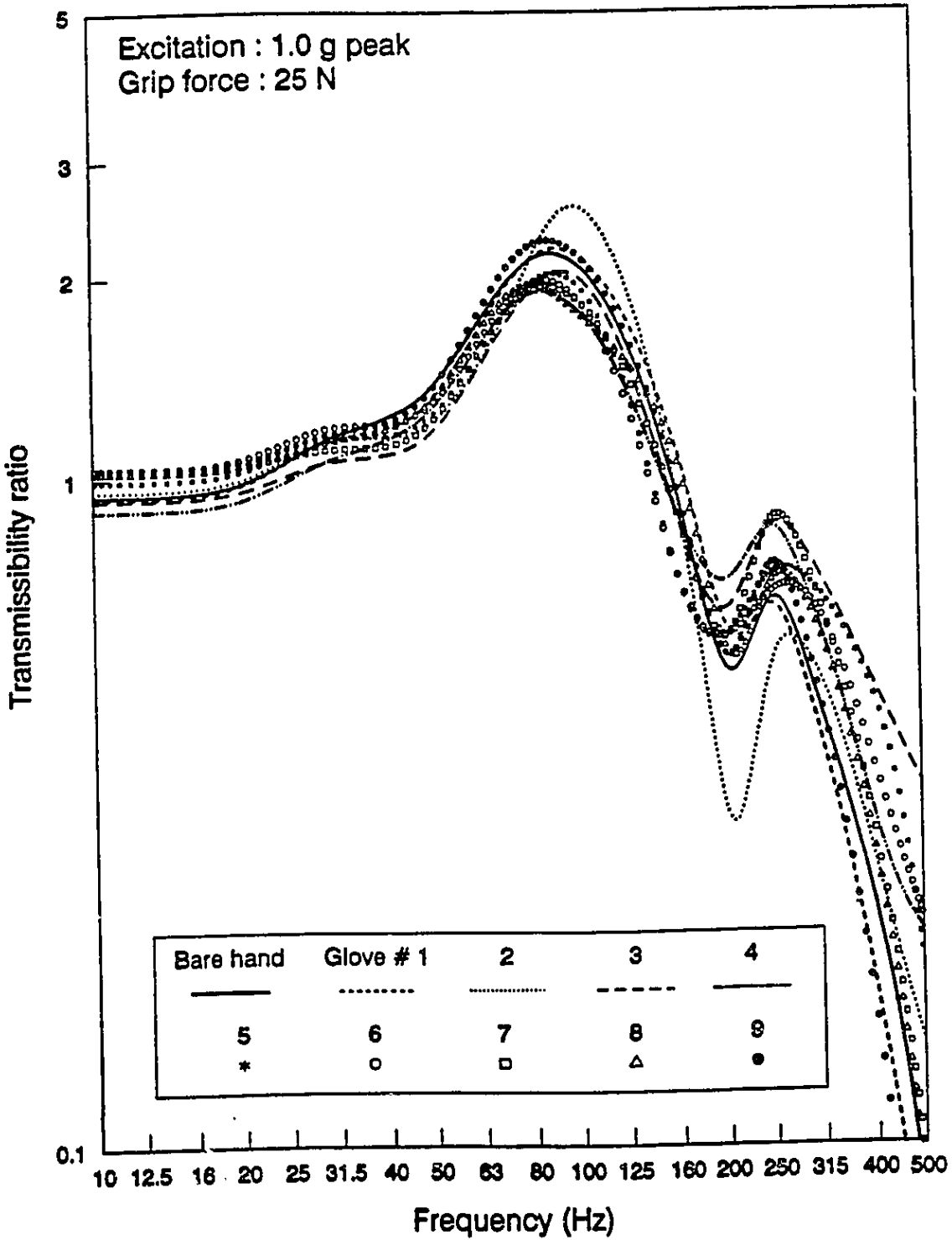

Figure 7.8: Vibration transmissibility of the hand, with and without glove.

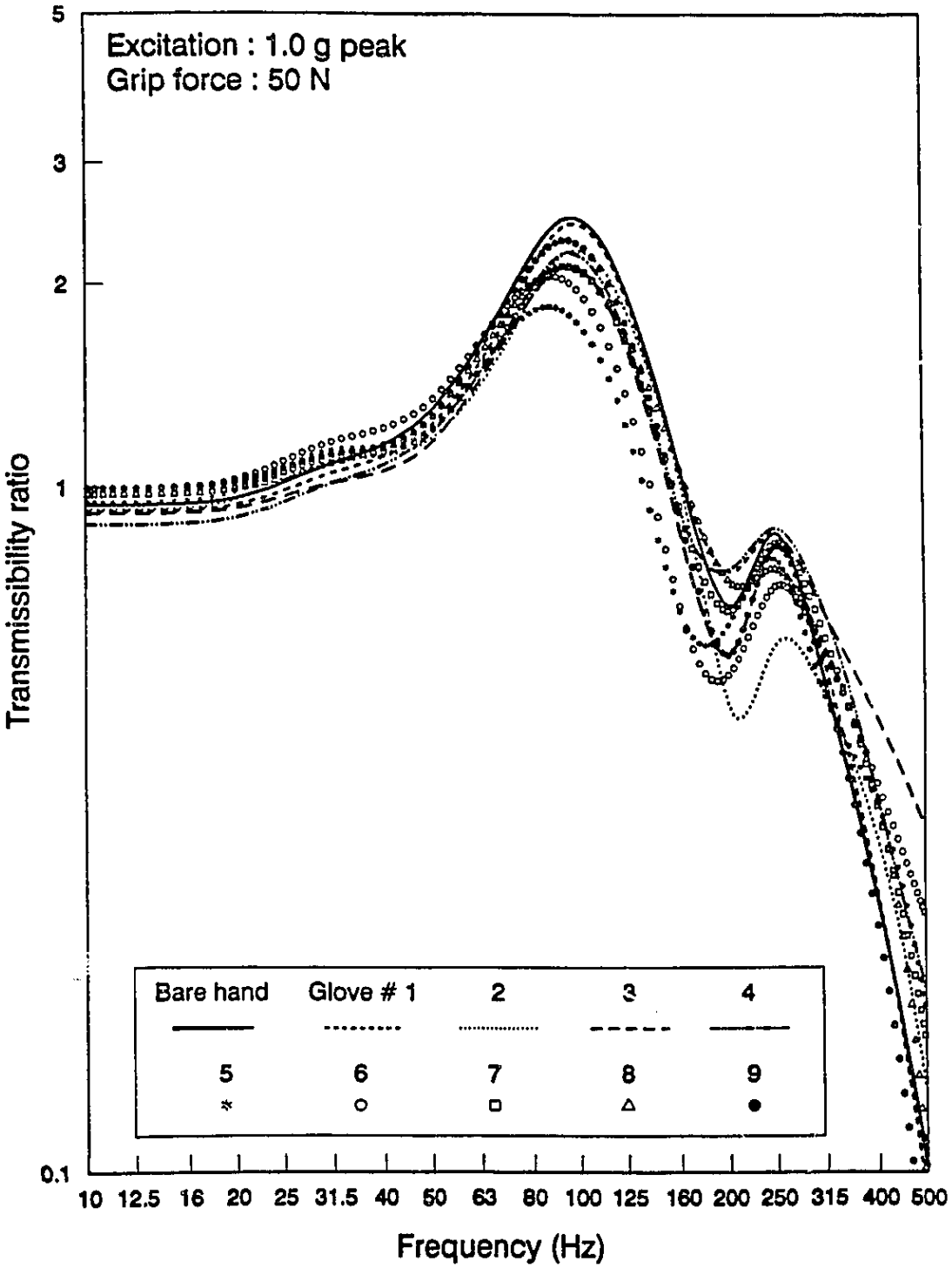

Figure 7.9: Vibration transmissibility of the hand, with and without glove.

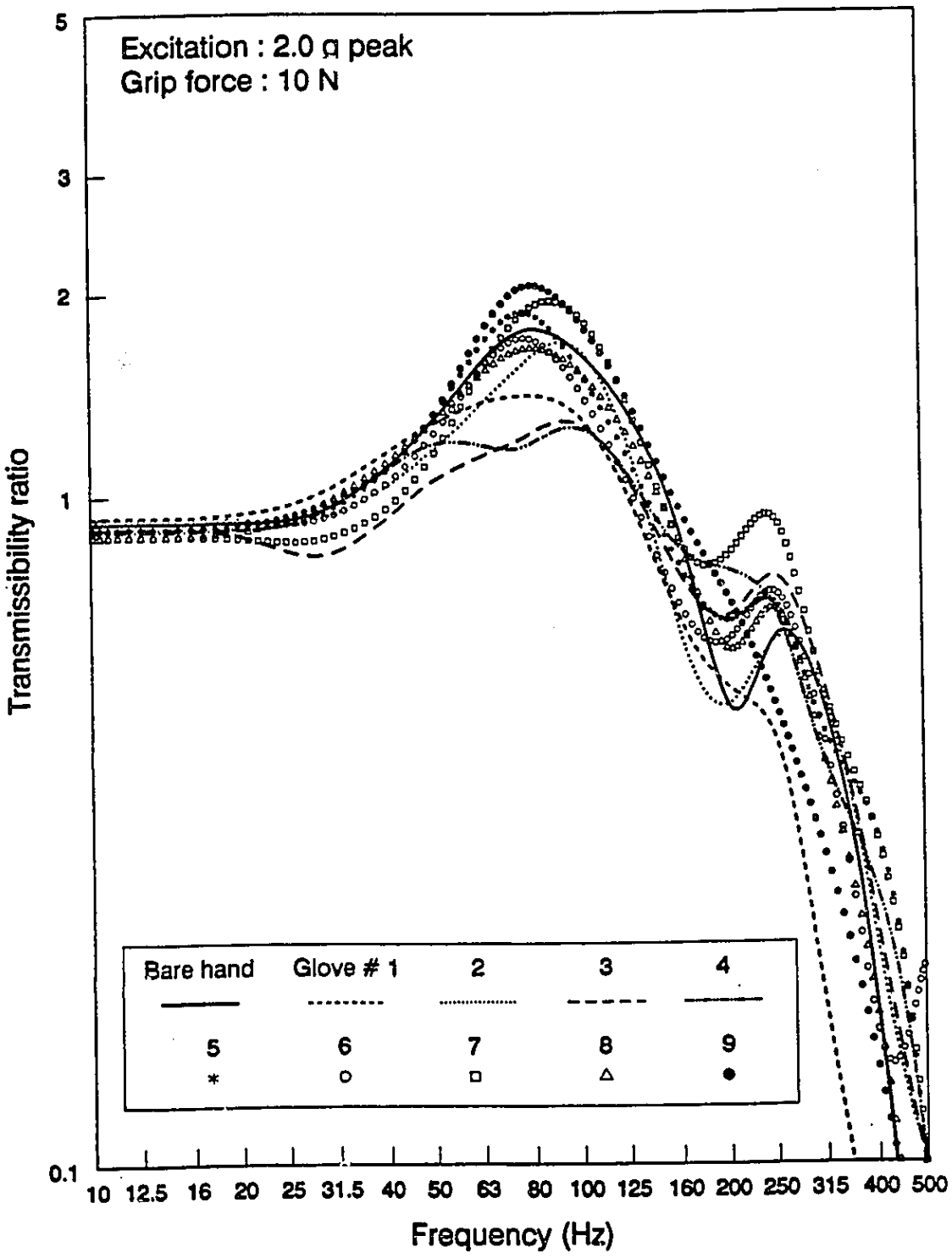

Figure 7.10: Vibration transmissibility of the hand, with and without glove.

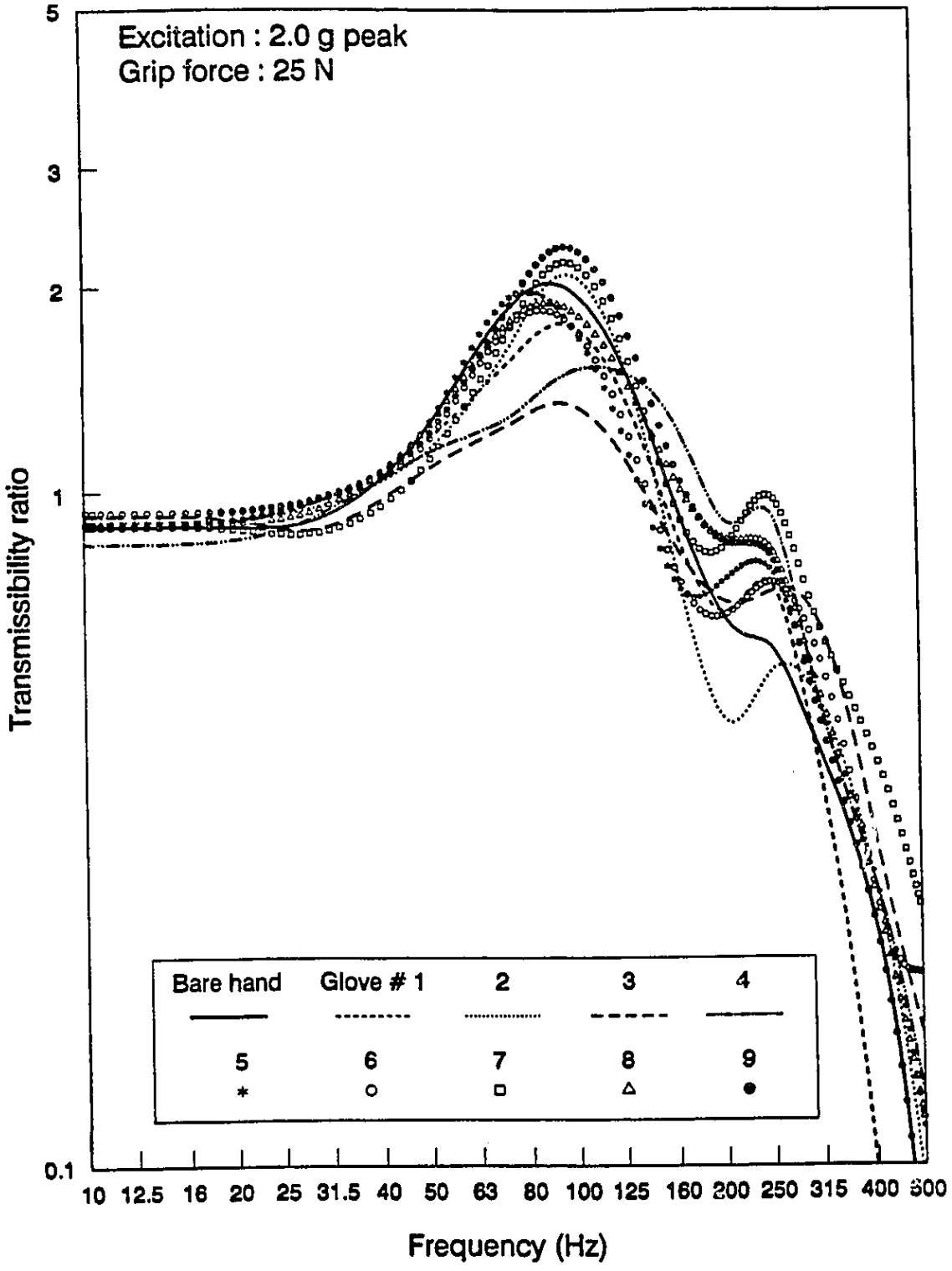

Figure 7.11: Vibration transmissibility of the hand, with and without glove.

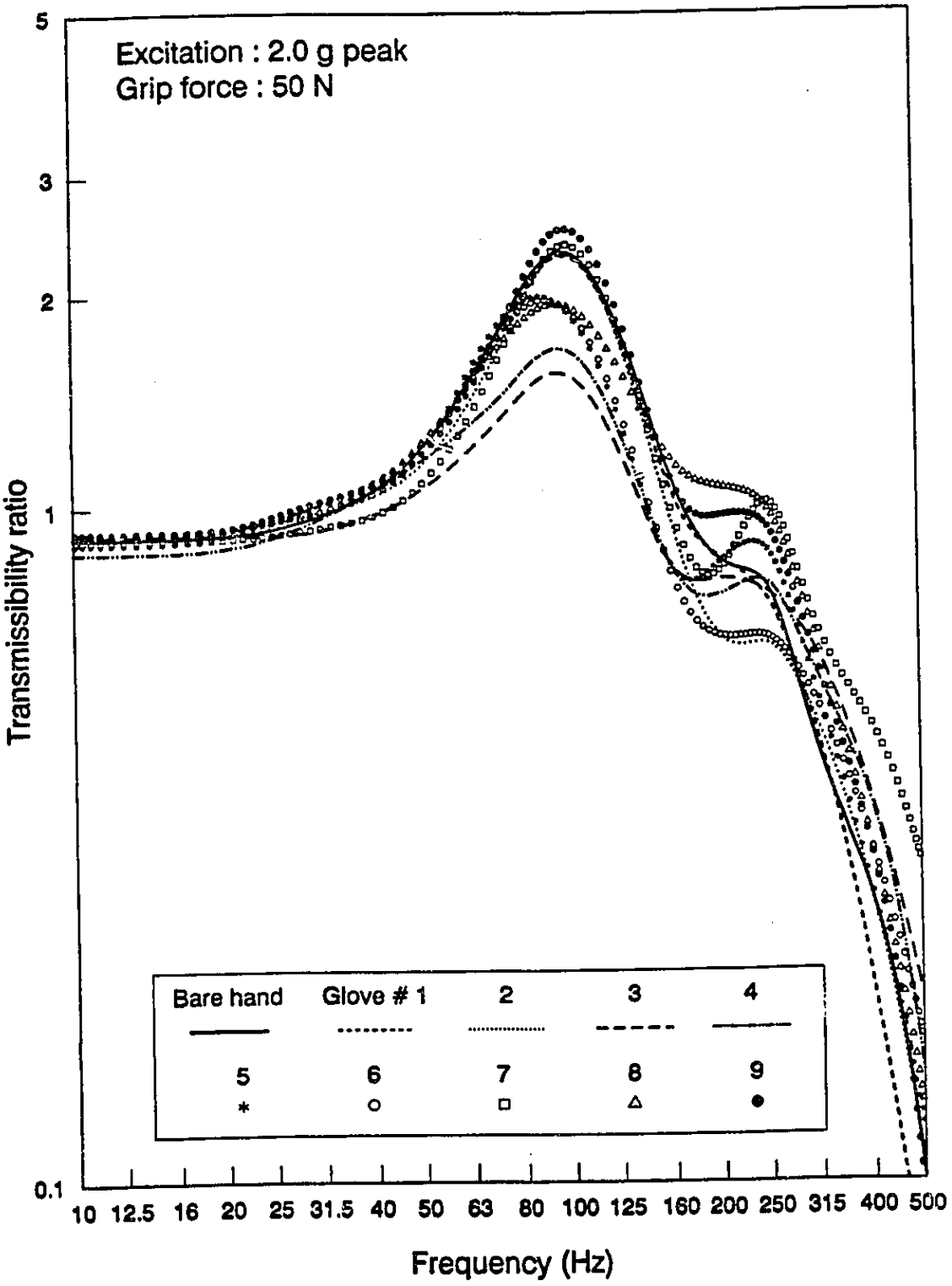

Figure 7.12: Vibration transmissibility of the hand, with and without glove.

of gloves as discussed above. A comparison of Figures 7.7 - 7.12 also indicates that the vibration transmissibility of the gloves changes with the change in grip force and excitation level, suggesting the non-linear behavior of the visco-elastic properties of the gloves. Further examination of these figures reveals that all the nine gloves transmitted different levels of vibration at different frequencies. Only one glove appears to provide modest vibration attenuation (glove # 1) in all the cases examined. This observation is further supported by the studies conducted by *Starck et al.* (*1990*) and *Christ* (*1982*). *Starck et al.* (*1990*) reported that the glove transmitted high levels of vibration in the entire selected frequency range of 40 Hz - 630 Hz, while *Christ* (*1982*) concluded that gloves provide only modest vibration attenuation in a limited frequency band. The results presented in Figures 7.7 to 7.12 clearly illustrate that the gloves are ineffective in isolating the impinging vibrations in the frequency range of interest (10 - 500 Hz).

7.5.3 HAND AND HAND-GLOVE MODELS

The transmissibility error function, described in Equation (7.4) is minimized using the optimization software, to derive the model parameters. The optimization is performed with several starting values of the parameters to ensure near uniqueness of the model parameters. The equations of motion for the linear models are solved to yield transmissibility characteristics of the hand and coupled hand-glove system. The vibration transmissibility characteristics of the two- DOF model are compared to the mean and envelope of the measured data as shown in Figure 7.13. The model response characteristics correlate well with the measured transmissibility characteristics in the entire frequency

TABLE 7.3
Parameters of the Analytical Transmissibility Models of the Hand and the Glove

m_1 (kg)	0.249
m_2 (kg)	0.129
m_g (kg)	0.125
K_1 (N/m)	15.00E5
K_2 (N/m)	02.29E4
K_g (N/m)	01.54E4
C_1 (Ns/m)	100.00
C_2 (Ns/m)	106.00
C_g (Ns/m)	048.70

range as shown in the figure. The model parameters derived using optimization software are listed in Table 7.3. The mass of the hand (m_1) is obtained as 0.249 kg, which coincides well with normal range of hand mass. The value of mass m_2, the coupled mass of the rest of the hand, however, is very low (0.129 kg). This low value of m_2 may be attributed to decoupling of the hand and arm at higher frequencies so that impinged vibrations remain confined to the hand alone. The model parameters thus obtained are used to extract the representative glove parameters by fitting the transmissibility data obtained with the gloves. During the optimization process, only the glove parameters were permitted to vary, while the parameters of the 2- DOF model were held constant. The parameters of glove, derived from optimization, are listed in Table 7.3. The vibration transmissibility characteristics, computed from the 3- DOF model of the hand-glove, are compared to the mean and envelope of the measured data as

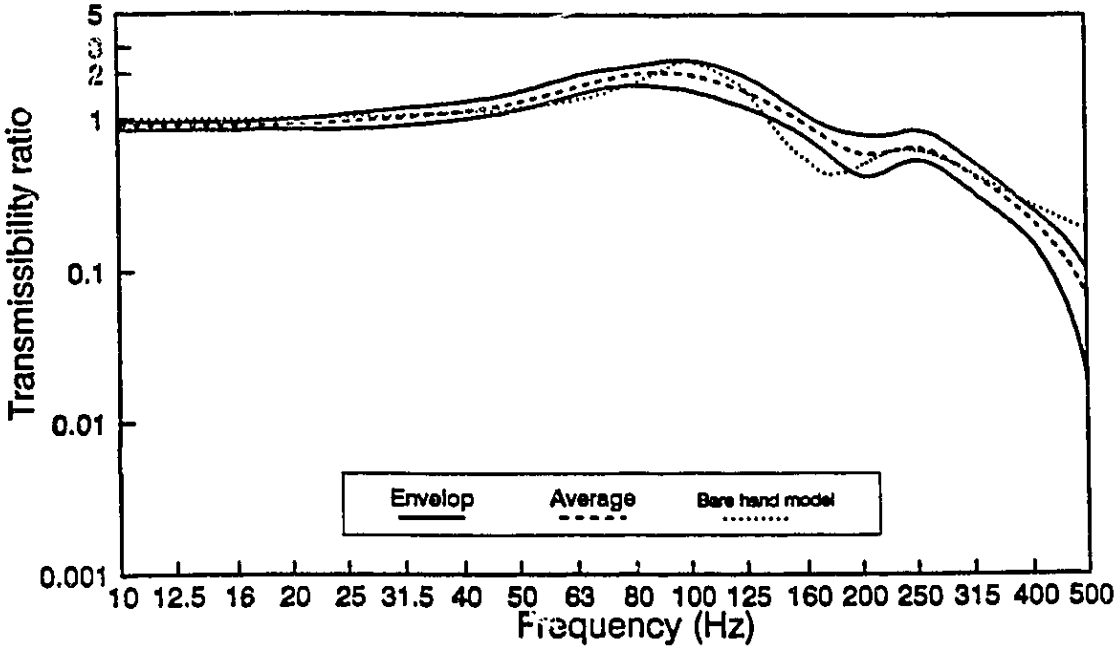

Figure 7.13: Vibration transmissibility of hand model compared with measured data.

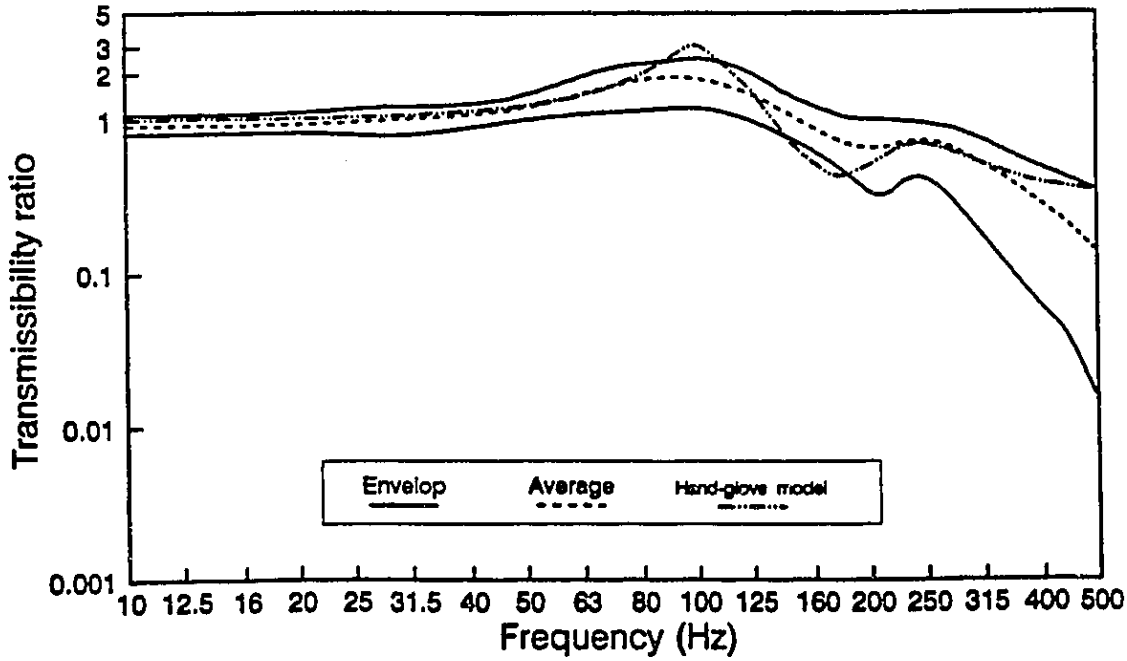

Figure 7.14: Vibration transmissibility of coupled hand-glove model compared with measured data.

shown in Figure 7.14. The model response correlates well with the measured response in the entire frequency range. The mass of the glove obtained as 0.125 kg, corresponds well with the average glove mass, as shown in Table 7.2.

7.6 Summary

A test methodology using a laser based vibration sensor is proposed to evaluate the vibration isolation performance of commercially available industrial hand gloves. The vibration transmissibility characteristics of the finger, knuckle and wrist were obtained in the 10 - 500 Hz frequency range, under different magnitudes of grip forces and excitations. The transmissibility characteristics, thus obtained, showed good agreement with the results reported in the published literature. The measured vibration transmissibility characteristics of the hand revealed that only 1 % of the vibration is transmitted to the wrist at high frequencies (500 Hz), and vibration transmitted to the hand increased with increase in the grip force. From the measurements performed on nine gloves it is concluded that the gloves do not attenuate hand-transmitted vibration in the entire frequency range of interest. Some gloves, however, yielded vibration attenuation in certain frequency bands. The vibration transmissibility of the glove changed with change in the grip force and excitation level, suggesting the nonlinear behavior of the glove materials. The hand transmissibility data were utilized to develop hand, and hand-glove mechanical models. The model transmissibility characteristics correlated well with the measured transmissibility data.

CHAPTER 8

CONCLUSIONS AND RECOMMENDATIONS FOR FUTURE WORK

8.1 General

Prolonged exposure to hand transmitted vibration is known to cause several diseases among the operators of power tools. The occurrence of vibration white finger (VWF) disease and rate of degeneration can be attributed to several physical and biodynamic factors such as acceleration, frequency, direction of vibration, duration of exposure, pattern of exposure, grip force and posture. Various epidemiological studies have reported high prevalence rates of VWF symptoms among operators of hand-held power tools. These high prevalence rates prompted several clinical studies to establish the cause-effect relationships, and engineering studies to improve work place vibration environment. These studies have primarily focused on dynamic response characterization of the hand-arm and development of mathematical models. In view of the complex nature of the hand-arm system, the influence of numerous intrinsic and extrinsic parameters, on the hand-arm vibration response characteristics is not yet fully understood. The primary focus of the thesis research was formulated to study various aspects of hand-arm vibration, which included: (i) Characterization of biodynamic response through driving point mechanical impedance measurement and analysis, (ii) Study of hand grip pressure distribution to enhance an understanding of a probable mechanism leading to VWF disease; (iii) Study of electromyography (EMG) of the finger flexor muscles under vibration; and (iv) Study of vibration transmissibility characteristics of the hand-arm and protective gloves. The results of the study have been discussed and compared with results reported in the literature, when available. The measured data were further utilized to derive the analytical

driving-point impedance and vibration transmissibility models of the hand-arm system.

8.2 Highlights of the Study

The major highlights of this investigation are summarized in the subsections below:

MECHANICAL IMPEDANCE OF THE HAND-ARM SYSTEM

The driving-point mechanical impedance has been extensively used to characterize the dynamic response of the hand-arm system. The reported hand-arm impedance data, however, differ considerably in magnitude as well as phase angle response. While attempts were made to enhance an understanding of these differences with variations in test parameters employed by different investigators, these discrepancies generally remained unexplained. An extensive study was thus undertaken to obtain the driving point impedance of the male human hand-arm system under varied, but nearly realistic test conditions. An instrumented handle fixture was fabricated and experiments were performed on four male subjects for a range of test conditions, under sinusoidal as well as stochastic excitations in the 10 - 1000 Hz frequency range. The influences of grip force and handle vibration on the impedance response of the hand-arm system are thoroughly examined and discussed. The measured impedance data were utilized to develop various linear and nonlinear hand-arm models with constant and grip force dependent parameters.

DEVELOPMENT OF HAND-ARM IMPEDANCE MODELS

A methodology to identify the parameters of hand-arm vibration (HAV) models, whether linear or nonlinear, using mechanical impedance data and

nonlinear programming based optimization technique, is proposed. Measured impedance data were utilized to develop three- and four-degrees-of-freedom (DOF) linear and nonlinear HAV models. The HAV models are analyzed to yield the impedance characteristics in the 10-1000 Hz frequency range. A local equivalent linearization algorithm, based upon the principle of energy similarity, is implemented to simulate the nonlinear HAV models. Optimization methods are employed to identify the model parameters, such that the magnitude and phase errors between the computed and measured impedance characteristics are minimum in the entire frequency range. The results of the study showed that for a selected grip force, the linear three - and four- DOF models correlate well with the measured response in the entire frequency range.

This study also proposed methods to develop HAV models with grip force dependent parameters such that the strong dependence of the impedance on the grip force may be effectively simulated. Although the linear three- and four-DOF models with grip force dependent restoring and dissipative components correlated well with the measured data at different grip forces in a qualitative manner, the model response deviated considerably from the measured response. The nonlinear three- and four- DOF models with grip force dependent restoring, and dissipative elements were subsequently developed and analyzed. The response characteristics of these models correlated well with the measured data in all the three directions of vibration.

SYNTHESIS OF THE IMPEDANCE DATA

A synthesis of the selected data was performed and envelope contours, encompassing the mean values of the selected data, were constructed. The mean values of the selected data sets, together with the smoothed envelopes,

were utilized to define the target and range of idealized values of impedance magnitude and phase in the X_h, Y_h and Z_h directions in the 10 to 1000 Hz frequency range. The impedance data that fall within the proposed range of idealized values are considered to provide acceptable representations of the human male hand-arm impedance. A pooling of results from different studies suggested that there is a notable dependence of the X_h component of impedance magnitude on the hand grip force. The corresponding dependence of the impedance phase, however, was observed to be small.

The synthesized values of impedance magnitude and phase angle were utilized to derive four-DOF lumped-parameter models of the hand-arm in all three orthogonal axes. The solution of the optimization problem revealed almost identical mass of the hand-arm in all the three orthogonal axis of vibration, and the model impedance correlated well with the mean values of the impedance. The model mass was observed to be concentrated near the fixed base of the system (close to the torso). The dynamic mass of the hand-arm in contact with the handle was found to be extremely small (4.3 to 19 grams) in all the three directions, which is compatible with that of a superficial component of the flesh or skin in the palm and fingers.

GRIP PRESSURE DISTRIBUTION

A method of measuring hand grip pressure distribution using flexible thin film pressure sensors is proposed to study the hand grip pressure distribution at the hand-handle interface under static and dynamic loading conditions. Measurements were performed to relate the occurrence of pressure peaks at the hand-handle interface with the magnitude of grip force, and vibration characteristics. The results of the study revealed a high concentration of

pressure at the tips of the index and middle fingers, and the base of the thumb under static grip forces. These pressure peaks shifted towards the middle of the fingers under application of dynamic loads, irrespective of the magnitude of the grip force, vibration frequency and acceleration level. The location of pressure peaks may be related to the probable impairment of the blood flow to the fingers, which is known to cause VWF disease.

ELECTROMYOGRAPHY OF FINGER FLEXOR MUSCLES

The vibration response of the hand-arm system is further investigated through electromyography (EMG) of the finger flexor muscles under varied test conditions. Surface electromyography tests were performed to study the influence of grip force, direction of vibration, frequency and magnitude of vibration excitation on the activities of finger flexor muscles. Dynamic measurements were performed at six discrete frequencies in the 20 - 1000 Hz range, and different levels of peak acceleration (0.5 g, 1.0 g, 2.0 g and 3.0 g). Grip forces of 25 N, 50 N, 75 N, 100 N, 125 N and 150 N were used for static loading, and 25, 50 and 100 N for dynamic loading. EMG recorded for different grip force levels, under static loading, revealed that the muscle activity increased with the grip force. EMG recorded during dynamic testing was influenced by the acceleration and was 150 - 600 % higher than the EMG level measured under corresponding static loading. EMG increased with increase in the acceleration, independent of the excitation frequency. However, the influence of frequency was not evident at frequencies above 50 Hz. The electrical activity of the finger flexor muscles increased considerably with the grip force under static as well as dynamic loads. The statistical analysis of the measured data clearly revealed that direction of vibration, excitation level and grip force have significant influence ($p < 0.001$) on the electrical activity of the finger flexor muscles, while

the influence of excitation frequency was insignificant ($p > 0.9$). Similarly, the interactions among the direction of vibration, grip force and excitation levels revealed significant influence ($p < 0.05$).

VIBRATION TRANSMISSION ANALYSIS

Miniature accelerometers and laser based vibration sensors were utilized to obtain vibration transmissibility characteristics of the wrist, knuckle and the finger under different grip forces. The measured data provided vibration transmission characteristics of the hand. The vibration transmissibility characteristics of the finger, knuckle and the wrist were obtained in the frequency range of 10 - 500 Hz using three grip forces and two excitation levels. The transmissibility characteristics thus obtained were observed to be in good agreement with the studies reported in the literature. The vibration transmissibility characteristics of the hand were analyzed to establish the grip force, acceleration levels and the excitation frequencies. At frequencies above 300 Hz, the vibration transmitted to the wrist was observed to be very low. The measured data further revealed that the vibration transmitted to the hand increased with increase in the grip force. A methodology is proposed to evaluate the vibration isolation performance of commercially available industrial hand gloves using laser based vibration sensor. The studies conducted on nine gloves indicated that the gloves do not attenuate vibration in the frequency range considered in the study (10 - 500 Hz). Certain gloves, however, provide modest vibration isolation in a few frequency bands. The vibration transmissibility characteristics of gloves changed with changes in the grip force and excitation level, suggesting a nonlinear behavior of the glove material. Further, the hand transmissibility data were utilized to develop lumped parameter linear models of the hand, and hand-glove systems. The

transmissibility characteristics of the analytical models were analyzed and compared with the measured data.

8.3 Conclusions

From the results of experimental and analytical studies on hand-arm vibration response, the following conclusions are drawn:

- The mechanical impedance of the hand-arm system can be measured accurately, with high degree of repeatability, using either deterministic or stochastic excitations.

- The driving point impedance of hand-arm system is dependent upon many tool-related factors, such as grip force, excitation frequency, and direction of vibration.

- The impedance of hand-arm system increases with increase in the grip force. The variations in impedance with change in the magnitude of vibration is relatively insignificant.

- At high excitation frequencies, above 500 Hz, the impedance magnitude increases independent of direction of vibration and excitation level.

- The human hand-arm impedance is strongly related to the direction of vibration. The impedance measured under excitation in Y_h- direction is lower than that measured under X_h- and Z_h- directions of vibration. In X_h- direction, the hand-arm impedance increases with increase in the excitation frequency

in the entire frequency range. Similar conclusions, however, couldn't be drawn in the Y_h- and Z_h- directions.

- The strong dependence of hand-arm impedance on the grip force, and frequency and direction of vibration can be best expressed by a describing function through a regression analysis. The function may be used to predict the hand-arm response for a range of grip forces and excitation frequencies in a given direction of vibration.

- The inter-subject variations in the measured impedance response for a specific direction of vibration and grip force are observed to be high compared to the intra-subject variations. The intra subject variations are very small (≅1.0%).

- In all the three orthogonal directions of vibration either three- or four-DOF linear lumped parameter models describe the dynamic response of hand-arm system for a pre-defined constant value of the grip force. The hand-arm vibration models with grip force dependent parameters, however, predict the biodynamic response of hand-arm system more accurately, for a wide range of grip forces.

- Idealized mechanical impedance envelope contours developed through synthesis of measured mean values may be considered to provide acceptable representation of the human male hand-arm impedance. Four-DOF lumped parameter models fit well with the idealized values in the entire frequency range of 10 - 1000 Hz.

- Flexible pressure sensors can be effectively used to measure the hand-handle interface pressure under static and dynamic loading conditions.

- Under static conditions grip forces yield concentration of high interface pressure peaks near the tips of the index and middle fingers. Under handle vibration, however, these peaks shift to the middle of the index and middle fingers, irrespective of the grip force, and frequency and magnitude of vibration.

- The hand-handle interface pressure on the lateral side of the hand is considerably higher than that on the medial side. The magnitudes of pressure peaks increases with increase in the grip force.

- The EMG of finger flexor muscles increases with increase in grip force under static and dynamic conditions.

- The EMG of the finger flexor under vibration is observed to be as high as 6 times the EMG measured under static condition. The statistical analysis of the data revealed that the magnitude and direction of vibration, and grip force influence the EMG of finger flexor muscles most significantly ($p < 0.001$). The effect of vibration frequency is observed to be insignificant ($p > 0.9$). The measured EMG data revealed that the influence of excitation frequency above 50 Hz is insignificant.

- The influence of excitation frequency on the finger flexor muscles is not clearly seen at high frequencies. This is related to the attenuation of high frequency vibrations in the palm of the hand. The vibration transmissibility

studies conducted on the hand-arm system reveal that high frequency excitations are primarily isolated in the palm of the hand.

- The vibration transmissibility studies of the hand-arm indicated that only 10 % and 1 % of impinged vibrations are transmitted to the wrist at excitation frequencies near 250 Hz and 500 Hz, respectively. The measured data compared well with reported data in the literature, notwithstanding the differences in the measurement procedures.

- The magnitude of hand-transmitted vibration increases with an increase in the grip force.

- The vibration transmissibility studies indicated identifiable finger resonances near 150 and 300 Hz, and knuckle resonances near 80 Hz and 225 Hz. The transmissibility measurements of the, wrist, however, do not exhibit clear peaks, suggesting that the wrist is a highly damped system.

- Laser based vibration sensors can be effectively used to evaluate the vibration attenuation performance of protective gloves.

- The performance evaluations of the commercially available anti-vibration and general purpose gloves revealed that gloves, in-general, do not provide effective vibration attenuation in the entire frequency range.

- The vibration transmissibility characteristics of gloves vary with variations in the excitation levels, grip force and excitation frequency, suggesting the nonlinear properties of the glove materials.

- The vibration transmissibility characteristics of the hand can be estimated through analysis of the two-degrees of freedom hand model proposed in the study.

8.4 Recommendations for Future Studies

- The results of the study suggest a strong need to attenuate hand transmitted vibration. The hand-arm models, developed in this study, may be utilized in conjunction with models of the power tools and field measured vibration data, to design effective vibration isolators.

- Concentration of high pressure peaks at middle of the fingers may be related to impairment of blood flow to the fingers. The VWF disease, related to impaired blood flow, is known to attack finger tips in the initial stages, and subsequently extending to the finger base and the rest of the hand. Further studies on measurement of finger blood flow can thus provide significant knowledge on the mechanism of VWF disease.

- A quantitative or qualitative measure of the blood flow to the fingers, under vibration, can perhaps provide significant knowledge on the mechanism leading to the onset of VWF disease at finger tips.

- Protective gloves or handle grips with composite stiffness characteristics should be investigated to minimize concentration of high pressures at the hand-handle interface.

- Further research investigations on the design of handles may be carried out to ensure more uniform pressure distribution in the hand.

- Further studies must be undertaken to determine the dynamic response of the muscles, and its relationship with the fatigue and stress experienced by the human operator. Such a study will permit identification of safer operating conditions.

- The hand-arm vibration models, proposed in this study, should be further validated through measurements on a large number of subjects under a wide range of tool-related factors.

- Although, few studies have reported the vibration transmissibility characteristics of the hand-arm system, only limited attempts have been made to analytically relate the impinging vibrations to the transmitted vibrations. Further research efforts to develop effective models are extremely desirable. These models can serve as a powerful tool to design vibration isolators.

- The idealized impedance values derived from the synthesis of the measured data, may be utilized to develop vibration isolation and protective devices, as these values are considered to represent the average impedance of human male hand-arm system.

- Studies must be undertaken to identify optimal glove parameters, such that effective attenuation of vibration may be realized.

- Investigation on reduction of tool vibration using either active or passive damping mechanisms are highly desirable to reduce the health risks posed by hand-transmitted vibration.

- Further studies may be conducted to study the grip pressure distribution under weight of the tool.

- The research efforts must be mounted to design hand-held power tools such that the handle vibration predominate only above 400 Hz, beyond the resonant frequencies of the human hand-arm.

REFERENCES

Aatola, S. 1989: Transmission of vibration to the wrist and comparison of frequency response function estimators, *Journal of Sound and Vibration*, 131(3), pp. 497-507.

Abrams, Jr., C.F. and Suggs, C.W. 1969: Chain saw vibration: Isolation and transmission through the human arm, *Transactions of the ASAE*, pp. 423-25.

Abrams, C.F. 1971: Modeling the vibrational characteristics of the human hand using driving point mechanical impedance method, *North Carolina State University*, Ph.D. thesis.

Agate, J.N., Druett, H.A. and Tombleson, J.B.L. 1946: Raynaud's phenomenon in grinders of small metal castings, *Brit J of Ind Med*, 3, pp. 167-174.

Agate, J.N. 1949: An outbreak of cases of Raynaud's phenomenon of occupational origin, *Brit J of Ind Med,* pp. 144-163.

Alaranta, H. and Seppalainen, A.M. 1977: Neuropathy and the automatic analysis of electomyographic signals from vibration exposed workers, *Scand. J. Work Envi. & Health*, 3 : pp. 128-34.

Armstrong, T.J., Chaffin, D.B. and Foulke, J.A. 1979: A methodology for documenting hand positions and forces during manual work, *Journal of Biomechanics*, 12, pp. 131-133.

Ashe, W.F., Cook, W.T. and Old, J.W. 1962: Raynaud's phenomenon of occupational origin, Archives of Environmental Health, 5, pp. 63-73.

Ayoub, M.M. and Presti, P.Lo. 1971: The determination of an optimum size cylindrical handle by use of electromyography, *Ergonomics*, 4, pp. 509-518.

BSI 6842 1987: British standard guide to the measurement and evaluation of human exposure to vibration transmitted to the hand, *British Standards Institution*, London, England.

Banister, P.A. and Smith, F.W. 1972: Vibration induced white fingers and manipulative dexterity, *Brit J of Ind Med,* 29, pp. 264-67.

Basmajian, J.V. 1978: Muscles Alive, Their Functions Revealed by Electromyography, Fourth Edition, *Williams & Wilkins*, Baltimore/London.

Basmajian, J.V. and Blumenstein, R. 1982: Electrode Placement in EMG Biofeedback, Reprinted, *Williams & Wilkins*, Baltimore/London, pp. 69.

Bednal, A.W. 1987: Hand-arm vibration in Great Britain, Proceedings of the fifth international conference on low frequency noise and vibration, *Multi-Science Publishing Co.*, Oxford, pp. 13-20.

Behrens, V., Taylor, W., Wilcox, T., Miday, R., Spaeth, S. and Burg, J. 1984: Vibration syndrome in chipping and grinding workers. III. Epidemiology, *J Occup Med* 26 (10), pp. 769 - 773.

Bernard, D. 1990: Etude de la Masse Apparente du Système Main-Bras et de l'Activité Musculaire Correspondante lors d'une Simulation de Brise-Bréton. Vandoeuvre-Les-Nancy: *Institut National de Recherche et de Sécurité* ,Report MAV-DT - 140/DB.

Berthoz, A. and Metral, S. 1970: Behaviour of a muscular group subjected to a sinusoidal and trapezoidal vibration of force, *Journal of Applied Physiology*, 29(3), pp. 378-384.

Boileau, P.-E., Boutin, J. and Drouin, P. 1992: Experimental validation of a wrist measurement method using laser interferometry; *Proceedings of 6th International conference on hand-arm vibration* (In press), Bonn, Germany.

Bovenzi, M., Petronio, L., and Di Marino, F. 1980: Epidemiological survey of shipyard workers exposed to Hand Arm Vibration, *Int. Arch. Occup. Envi. Health*, 46, pp. 251-256.

Brammer, A.J., and Taylor, W. (eds) 1982: Vibration effects on the hand and arm in industry, *John Wiley & Sons*, New York.

Brammer, A.J. 1982: Relations between vibration exposure and the development of the vibration syndrome, In: Brammer and Taylor (eds) Vibration effects on the hand and arm in industry. New York, *John Wiley & sons*, pp. 283-290.

Brammer, A.J. 1984: Exposure of the hand to vibration in industry, *NRCC Document* No. 22844, NRCC, Ottawa, Canada.

Brammer, A.J. 1986: Dose response relationships for hand transmitted vibration, *Scand J Work Envi & Health*, 12(4): pp. 284-88.

Brammer, A.J., Piercy, J.E. and Auger, P.L. 1987a: Assessment of impaired tactile sensation - A pilot study, *Scand. J. Work Envi. & Health*, 13, pp. 380-384.

Brammer, A.J., Taylor, W. and Lundborg, G. 1987b: Sensorineural stages of the hand-arm vibration syndrome, *Scand. J. of Work, Env. & Health*, 13, pp. 279-283.

Brammer, A. J. 1993: Personal Communications.

Brubaker, R.L., Mackenzie, C.J.G., and Bates, D.V. 1983: Vibration white finger disease among tree fellers in British Columbia. *J. of Occupational Medicine*, 25, pp. 403, 408.

Brubaker, R.L., Mackenzie, C.J.G. and Hutton, S.G. 1986: Vibration induced white finger among selected underground rock drillers in British Columbia, *Scand J of Work, Env & Health,* 12 (4), pp. 296-300.

Burstrom, L. 1990: Measurement of the impedance of the hand and arm; *Int. Arch of Occup Environ Health*, 62, pp. 431-439.

Burstrom, L. and Lundstrom, R. 1992: Determination of the mechanical energy absorption in the human hand-arm whilst exposed to vibration, *Proceedings of 6th International conference on hand-arm vibration* (In press), Bonn, Germany.

CEN 1992: Hand-arm vibration- Method for the measurement and evaluation of the vibration transmissibility of gloves, *Comité Européen de Normalisation* CEN/231/3 N 46.

Chaffin, D.B. and Anderson, B.J. 1984: Occupational Biomechanics, *John Wiley & Sons*, New York.

Chatterjee, D.S., Petrie, A. and Taylor, W. 1978: Prevalence of vibration induced white finger in fluorsparmines in Weardale, *Brit J of Ind Med*, 35, pp. 208-218.

Christ, E. 1982: Anti-vibration gloves; Performance tests, *Die Berufsgenossenschaft.*

Daikoku, M. And Ishikawa, F. 1989: Mechanical impedance and vibration model of hand-arm system, *Proceedings of the Fifth Int. Conference on Hand-Arm Vibration*, Kanazawa, Japan, pp. 167-171.

Dieckmann, D. 1959: Ein schwingungmechanisches modell for das schwingungserregte hand-arm system des menschen, *VDI-Zeitung* 101, pp. 23-26.

Dobry, M.W., Barczewski, R. and Stammers, C.W. 1992: A pneumatic tool vibration isolator, *Journal of Sound and Vibration* 153, pp. 171-175.

Dupuis, H. and Jansen, G. 1979: Immediate effects of vibration transmitted to the hand, *International Symposium Man under Vibration Suffering and Protection*, Udine (Italy), pp. 76-86.

Dupuis, H. and Schafer, N. 1986: Effects of impulse vibration on the hand-arm system, *Scand. J. of Work Env. & Health*, 12, pp. 320-322.

Engstrom, K.and Dandanell, R. 1986: Exposure conditions and Raynaud's phenomenon among riveters in the aircraft industry, *Scand J of Work Env & Health*, 12(4), pp. 293-295.

EMED 1989: EMED is a trade mark of *NOVEL gmbh*, Beichstrabe 8, 8000 Munich 40, Germany.

Farkkila, M. 1978: Grip force in vibration disease, *Scand. J. Work Env. & Health* 4, pp. 159-66.

Farkkila, M., Pyykkö, I., Kprhonen, O. and Stark, J. 1979: Hand grip forces during chain saw operation and vibration white finger in lumberjacks. *Brit J of Ind Med*, 36: pp. 336-41.

Farkkila, M., Pyykko, I., Korhonen, O. and Starck, J. 1980: Vibration induced decrease in the muscle force in lumberjacks, *European Journal of Applied Physiology*, 43, pp. 1-9.

Farkkila, M., 1982: Hand grip force and muscle fatigue in the etiology of the vibration syndrome. In : Brammer and Taylor (eds), *Vibration effects one the hand and arm in industry*, New York, John Wiley & Sons, pp. 45-50.

Fellows, G.L. and Freivalds, A. 1991: Ergonomics evaluation of a foam rubber grip for tool handles, *Applied Ergonomics*, pp. 225-230.

Folkow, B. 1972: Cardiovascular response to acute mental stress in spontaneously hypertensive rats. *Acta Physiol. Scand.*, pp. 7-8

Fritz, M. 1987: Simulation of hand arm vibration by means of a biomechanical model, In: *International Series on Biomechanics*, Volume 7-A, Free university press, Amsterdam, pp. 456-46.

Fuatsuka, M., Ueno, T. 1985: Vibration exposure and vibration induced white finger due to chain saw operation. *J Occup Med* 27(4): pp. 257-264.

Gemne G. and Saraste, H. 1987: Bone and joint pathology in workers using hand-held vibrating tools: An overview, *Scand. J. of Work, Env. & Health* 13, pp. 290-300.

Gemne, G., Pyykko, I., Taylor W. and Pelmear P.L. 1987: The Stockholm workshop scale for the classification of cold-induced Raynaud's phenomenon in

the hand-arm vibration syndrome, *Scand. J. of Work, Env. & Health* 13, pp. 275-278.

Goel, V.K. and Rim Kwan 1987: Role of gloves in reducing vibration: Analysis for pneumatic chipping hammer, *Amer. Ind. Hyg. Asso. J.*, 48(1), pp. 9-14.

Griffin, M.J. 1974: Some problems associated with the formulation of human response to vibration. In : Taylor, W. (ed), *The vibration syndrome*, Academic press, London.

Griffin, M.J. 1980: Vibration injuries of the hand and arm; Their occurrence and the evaluation of standards and limits, *Health and safety executive*, research paper No. 9, London, England.

Griffin, M.J., Macfarlane, C.R. and C. D. Norman 1982: The transmission of vibration to the hand and the influence of gloves, In: *Vibration Effects on the Hand and Arm in Industry*, A. J. Brammer and W. Taylor, (eds), John Wiley & Sons, New York, pp. 103-116.

Griffin, M.J. 1990: Handbook of Human Vibration. *Academic Press*, London.

Habu, K. 1984: An objective testing method for the diagnosis of Vibration related disorders, their evaluation, and the reversibility and non reversibility of finger function, *Jpn. J. Trauma Occup. Med.*, 29 (5): pp. 479-491.

Harada, N. and Matsumoto, T. 1982: Various function tests on the upper extremities and the vibration syndrome. In Brammer and Taylor (eds): *Vibration effects in industry*. John Wiley & Sons, New York, pp. 71-76.

Harrison, R.T., and Murphy, W.A. 1982 : Motor cycle handlebar vibration, In Brammer and Taylor (eds): *Vibration effects on the hand and arm in industry*, John Wiley & Sons, New York, pp. 239-244.

Hellstrom, B., and Andersen, K.A. 1972: Vibration injuries in Norwegian forest workers, *Brit J Ind Med*, 29, pp. 255-263.

Hempstock, T.I. and O'connor, D.E. 1975: The measurement of hand vibration, In Taylor and Pelmear (eds): Vibration white finger in industry, Academic press, London, pp. 111-122.

Hempstock, T.I. and O'connor, D.E. 1989: Measurement of impedance of hand-arm system, *Proc. Inst. of Acoustics*, Vol. 11 Part 9, pp. 483-490.

Hempstock, T.I. 1992: Personal Communications.

Hesse M. 1989: Die antwort des hand-arm-systems auf stochastiche erregung und ihre anwendung in schwingungsschutz, *Universität Dortmund*, Dissertation.

Holley, L.K. 1979: A new pressure measuring system for cushions and beds with a review of the literature, *Paraplegia*, 17, pp. 461-474.

IDEAS 1990: IDEAS is a trade mark of *Structural Dynamics Research Corporation*, Ohio, USA.

IMSL 1988: IMSL is a trade mark of *IMSL, Inc.*, Texas, USA.

ISO 5349, 1986: Guidelines for the measurement and the assessment of human exposure to hand transmitted vibration.

ISO 1988: Mechanical input impedance and vibration model of the human hand-arm system, ISO/TC 108/SC 4/WG 5 N 53.

ISO 1992 Hand-arm vibration- Method for the measurement and evaluation of the vibration transmissibility of gloves, International Standards Organization ISO/108/4/3 N65.

Iwata, H. 1968: Effects of rock drills on operators (parts I and II), *Ind Health*, 6, pp. 28-46.

Iwata, H., Dupuis, H. and Hartung, E. 1972: Ubertragung von horizontalen sinussch wingungen auf die oberen extremitaten bei halbpronationsstellung und reaktion des m biceps, *Int. Arch. Arbeitsmed*, 30, pp. 313-327.

Jahn, R. and Hesse, M. 1986: Applications of hand-arm models in the investigation of the interaction between man and machine, *Scand. J. Work, Env. and Health*, 12, pp. 343-346.

James, P.B., Yates, J.R., and Pearson, J.C.G. 1975: An investigation of the prevalence of bone cysts in hands exposed to vibration. Vibration White Finger in Industry, *Academic Press*, London, 1975.

Janda, D.H., Geiringer, S.R., Hankin, F.M. and Barry D.T. 1987: Objective evaluation of grip strength, *Journal of Occupational Medicine*, 29, pp. 569-571.

Jandak Z. 1989: Energy transfer to hand-arm system at exposure to vibration, *Proc. of 5 Int. Conf on Hand-Arm Vib.*, Kawasaki, Japan, pp. 49-54.

Klimkova-Deutschova, E. 1966: Neurological aspekte der vib. skrankheit. Arch. Gewerbepath. *Gewerbehyg*. 22, pp. 297-305.

Krause, P., Orban, A., Panzke, K.J. and Popov, K. 1979: Critical assessment of common methods to determine vibrational stress of hand-arm system, *International Symposium Man under Vibration Suffering and Protection*, Udine (Italy), pp. 261-274.

Kumlin, T. Wiikeri, M. AND Sumari, P. 1973: Radiological changes in carpal and metacarpal bones and phalanges caused by chain saw vibration, *Brit. Journal of Indus. Medic.*, 30, pp. 71-73.

Linden, O., Greenway, R.M. and Piazza, J.M. 1965: Pressure distribution on the surface of the human body: I. Evaluation in lying and sitting positions using a bed of springs and nails, *Arch. of Phys. Med. & Rehab.*, pp. 378-385.

Lundstrom, R. 1986: Responses of mechnoreceptive afferent units in the globrous skin of the human hand to vibration, *Scand. J. Work Envi. & Health*, 12(4), pp. 413-16.

Lundstrom, R. and Burstrom, L. 1989: Mechanical impedance of the human hand-arm system, *Int. Journal of Industrial Ergonomics*, 3, pp. 235-242.

Matsumato, T., Yamada, S. and Harada, N. 1979: A comparative study of vibration hazards among operators of vibrating tools in certain industries, *Arh Hig Rada Toksikol* 30, pp. 701-707.

Matsumato, T., Harada, N., Yamada, S. and Kobayashi, S. 1981: On vibration hazards of chipping hammer operators in an iron foundry, *Jap J Ind Health* 23, pp. 51-60.

Meltzer, G. 1979: A vibration model for the human hand-arm system, *Proceedings of Int. Symposium Man under Vibration Suffering and Protection*, Udine, Italy, pp. 210-221.

MINITAB 1988: MINITAB is a registered trade mark of Minitab, Inc., State College, PA, USA.

Mishoe, J.W. and Suggs, C.W., 1974: Hand-arm vibration. Part II. Vibrational responses of the human hand, *J. of Sound and Vibration*, 53, pp. 545-558.

Mishoe, J.W. and Suggs, C.W. 1977: Hand arm vibration part II: Vibrational responses of the human hand, *J. of Sound and Vibration*, 53, pp. 545-558.

Miyashita, K. Shiomi, S., Itoh, N., Kasamatsu, T., and Iwata, H. 1983: Epidemiological study of vibration syndrome in response to total hand-tool operating time: *Brit J. Ind Med*, 40, pp. 92-98.

Miwa, T., Yonekawa, Y., Nara, A., Kanada, K. and Baba, K. 1979: Vibration isolators for portable vibrating tools part 1. A grinder, *Industrial Health*, 17, pp. 85-122.

Nerem, R.M. 1977: Vibration enhancement of blood-arterial wall macromolecule transport, *Proceedings of the International Hand-Arm Vibration Conference*, pp. 37-41.

NIOSH 1990: Criteria for a recommended standard , Occupational exposure to hand arm vibration, Ohio, USA.

Oliver, T.P., Pethybridge, R.J. and Lumley, K.P.S. 1979: Vibration white finger in dockyard workers, *Arch Hig Rada Tokksikol* 30, 683-693.

Pelmear, P.L., Taylor, W. and Pearson, J.C.G. 1975: Raynaud's phenomenon in grinders, In: Taylor, W. and Pelmear, P.L. (eds), *The vibration White Finger in Industry*, Academic press, London, pp. 21-30.

Pelmear, P.L., Leong, D., Taylor, W., Nagalingam, M. and Fung, D. 1989: Measurement of vibration of hand-held tools: weighted or unweighted?, *J of Occupational Medicine*, 31, pp. 902-908.

Pelmear, P.L., Taylor, W. and Wasserman, D.E. 1992: Hand-Arm Vibration: A Comprehensive Guide for Occupational Health Professionals, *Van Norstrand Reinhold*, New York.

Pelnar, P.V., Gibbs, G.W. and Pathak, B.P. 1982: A pilot investigation of the vibration syndrome in forestry workers of eastern Canada. In Brammer and Taylor (eds): *Vibration effects on the hand and arm in industry*, John Wiley & Sons, New York.

Piché, A., Rakheja, S., Gouw, G.J. and Sankar, T.S. 1988: Development of an elastic human-seat interface pressure sensing system, *ICAAR7* 88, Montreal, pp. 118-119.

Pokorny, C.K. and Gerald, C.F. 1989: Computer graphics - The principles behind the art and science, Franklin, Beedle & Associates, California, USA, pp. 258-265.

Pyykkö, I. 1974: A physiological study of the vasoconstrictor reflex in traumatic vasospastic disease, *Scand. J. Work, Env. & Health*, 11, pp. 170-186.

Pyykkö, I. 1975: Vibration Syndrome a review, *Vibration and work*, Proceedings of the Finnish-Soviet-Scand. symposium, pp. 1-24.

Pyykkö, I., Färkkilä, M., Toivanen, J. Korhonen, O. and Hyvärinen, J. 1976: Transmission of vibration in the hand-arm system with special reference to changes in compression force and acceleration; *Scand. j. of work, env. & health*, 2, pp. 87-95

Pyykkö, I. 1986: Clinical aspects of the hand arm vibration syndrome. *Scand. J. Work Envi. & Health*, 12(4), pp. 439-47.

Radwin, R. 1986: Neuromuscular effects of vibrating hand tools on grip exertions, tactility, discomfort, and fatigue, Ph.D. thesis, *The Univ. of Michigan*, Michigan, USA.

Radwin, R., Armstrong, T.J. and Chaffin, D.B. 1987: Power hand tool vibration effects on grip exertions, *Ergonomics*, 30, pp. 833-855.

Rakheja, S., Van Vliet, M. and Sankar, S. 1985: A discrete harmonic linearization technique for simulating non-linear mechanical systems, *J. of Sound and Vibration*, 100, pp. 511-526.

Rakheja, S. and Sankar, S. 1986: Local equivalent constant representation of non-linear damping mechanisms, *Engineering Computations*, 3, pp. 11-17.

Rens, G., Dubrulle, P. and Maichaire, J. 1987: Efficiency of conventional gloves against vibration, *Ann. Occup. Hyg.*, 31(2), pp. 249-54.

Reynolds, D.D. 1977: Hand-arm vibration: A review of three year's research, *Proceedings of the 3rd International Hand-Arm Vibration Conference*, Ohio, USA, pp. 99-129.

Reynolds, D.D. and Soedal, W. 1977a: Dynamic response of the hand-arm system to a sinusoidal input, *J. of Sound and Vibration*, 21, pp. 339-353.

Reynolds, D.D. And Angevine E.N. 1977b: Hand-arm vibration, Part II: Vibration transmission characteristics of the hand and arm; *Journal of sound and vibration*; 51(2), pp. 255-65.

Reynolds, D.D, Wasserman, D.E., Basel, R., Taylor, W., Doyle, T.E. and Asburry, W. 1982: Vibration acceleration measured on pneumatic tools used in chipping and grinding operations. In Brammer and Taylor (eds), Vibration effects on the hand and arm in industry, John Wiley & Sons, New York, pp. 211-224.

Reynolds, D.D. and Falkenberg, R.J. 1984: A study of hand vibration on chipping and grinding operators, part II: Four-degree-of-freedom lumped parameter model of the vibration response of the human hand, *J Sound and Vibration*, 95, pp. 499-514.

Robert, J., Mereau, P. Cavelier, C. and Chameaud, J. 1977: Occupational angioneurotic problems caused by hand tool vibrations, *Arch Mal Prof* 38, pp. 437-455.

Roberts, J. 1981: Response of nonlinear mechanical systems to random excitations, Part 2: Equivalent linearization and other methods, *Shock and Vibration Digest*, 13, pp. 15-29.

Roddie, I.C. and Shepphard, I.T. 1957: Evidence for critical closure of digital resistance vessels with reduced transmural pressure and passive dilation with increased venous pressure, *Journal of Physio*, London. 136, pp. 496-506.

Sakurai, T. 1990: Suspected vibration magnitude on the body of chain saw users among national forest workers in Kyusyu, from 1956 to 1984, *The kurume medical journal*, 37, pp. s13-s22.

Schittkowski, K. 1986: NLPQL - A Fortran subroutine for solving constrained non-linear programming problems, *Annals of Oper. Res.*, 5, pp. 485-500.

Seitz, P. 1990: Personal communications on MICROEMED system developed by *NOVEL gmbh*, Germany.

Starck, J.P., Farkkila, M.A. Aatola, S., Pyykkö, I. and Markonen, O. 1983: Vibration syndrome and vibration in pedestal grinders, *Brit J Ind Med*, 40, 426-433.

Strack, J., Pekkarinen, J. and Chun Chang, L. 1990: Transmission of vibration from tool handle to wrist and to head; *The kurume medical journal*, 37, pp. s1-s11.

Stewart, A and Goda, D.F. 1970: Vibration syndrome, *Brit J Ind Med*, 27, pp. 19-27.

Suggs, C.W. 1974: Modeling of the dynamic characteristic of the hand-arm system, In: Taylor, W. and Pelmear, P.L. (eds), *The vibration syndrome* , Academic press, London, pp. 169-186.

Suggs, C.W. and Mishoe, J.W. 1977: Hand-arm vibration: Implications drawn from lumped parameter models, *Proceedings of the 3rd International Hand-Arm Vibration Conference*, Ohio, USA, pp. 136-141.

Taylor, W., Pearson, J., Kell, R.L. and Keighley, G.D. 1971: Vibration syndrome in forestry commission chain saw operators, *Brit J Ind Med*, 28, pp. 83-89.

Taylor, W., Pelmear, P.L. (eds) 1975: Vibration white finger in industry, *Academic press,* London.

Taylor, W. And Brammer, A.J. 1982: Vibration effects on the hand and arm in industry: An introduction and review, *Vibration effects on the hand and arm in industry (Edited by Brammer, A.J. and Taylor, W.), John Wiley & Sons*, New York, pp. 1-12.

Taylor, W., Wilcox, T. and Wasserman, D. 1981: Health hazard evaluation report, Neenah Foundry Company, Neenah, Wisconsin, *NIOSH report,* HHE 80-189-870.

Taylor, W., Wasserman, D., Behrens, V., Reynolds, D.D. and Samueloff S. 1984: Effect of air hammer on the hands of stonecutters. The limestone quarries of Bedford, Indiana, revisited. British Journal of Industrial Medicine, 41: pp. 289-295.

Teleky L. 1938: Pneumatic tools., *Occ. Health*, 1, 1-12.

Thomson, W.T. 1965: Vibration Theory and Applications, *Prentice-Hall*, Englewood Cliffs, NJ, USA.

Vainio, K. 1950: Om Vibrations syndrome, sarskit hos maskinoborrare, *Nord. Hyg. J.*, 31, pp. 249-265.

Wasserman, D., Badger, D., Doyle,T.E. and Margolies, L. 1974: Industrial Vibration - An overview, *Journal of American Society of Safety Engineers*, 19, pp. 38-43.

Wasserman, D.E., Taylor, W. and Curry, M.G. (eds) 1977: *Proceedings of the international occupational hand-arm conference*, Cincinnati, Ohio, USA.

Wasserman, D.E., Reynolds, D.D., Behrens, V., Samueloff, S. and Basel, R., 1982: Vibration white finger disease in U.S. workers using pneumatic chipping and grinding hand-tools - Vol. II - Engineering testing, *NIOSH Publication* No. 82-101.

Wasserman D.E. 1988: Human aspects of occupational vibration, *J. Env. Sci.* 26: pp. 58-62.

Weiss, B.E., and Clarke, N.P. 1964: Mechanical Impedance as a tool in research on human response to acceleration, *Aerospace Medicine*, pp. 945-950.

Witte, A.F. And Rodeman, R. 1976: Dual specifications in random vibration testing, An application of mechanical impedance: *Shock & Vibration bulletin* No.41, pp. 109-118.

Wood, L.A., Suggs, C.W. and Abrams, C.F. 1978: Hand arm vibration part III: A distributed parameter dynamic model of the human hand-arm system, *J of Sound and Vibration*, 57, pp. 157-169.

Yodaiken, R.E., Jones, E. and Kunicki, R. 1985: The Raynaud phenomenon of occupational origin, Adv. Microcirc., 12, pp. 6-33.

APPENDIX - I

Driving Point Mechanical Impedance of Hand-Arm System

TABLE A1
Driving Point Mechanical Impedance of Hand-Arm System

Direction: X_h	Excitation: 1.0 g peak - sine sweep					
Frequency (Hz)	Grip force					
	10 N		25 N		50 N	
	Magnitude (Ns/m)	Phase (degrees)	Magnitude (Ns/m)	Phase (degrees)	Magnitude (Ns/m)	Phase (degrees)
10	31.0	57.5	37.0	51.5	42.5	46.5
12.5	32.5	57.0	38.5	51.2	43.5	46.1
16	34.5	56.4	41.0	50.5	45.5	45.5
20	37.2	55.5	44.2	50.0	48.5	45.0
25	41.5	53.7	49.4	48.5	54.5	43.7
31.5	48.0	51.0	57.5	47.1	64.5	42.0
40	57.0	48.0	69.0	44.7	78.2	40.3
50	68.1	45.1	81.5	43.0	92.0	38.7
63	83.5	40.5	99.5	40.1	111.3	36.5
80	102.2	37.5	120.0	38.5	135.0	34.5
100	125.0	35.5	147.5	37.4	160.5	33.5
125	150.5	35.0	175.0	37.2	194.0	33.5
160	180.0	35.7	215.0	40.0	236.0	36.0
200	197.0	36.1	222.5	41.1	243.5	37.3
250	199.0	36.5	222.1	42.5	239.0	39.7
315	201.0	37.0	217.0	43.0	225.0	40.0
400	265.0	37.5	275.0	43.4	285.0	39.1
500	382.5	38.0	394.5	43.9	416.0	39.7
630	475.0	38.3	490.0	44.4	525.0	40.5
800	580.0	38.7	605.0	44.8	644.0	40.8
1000	700.0	39.1	735.0	45.2	785.0	40.8

TABLE A2
Driving Point Mechanical Impedance of Hand-Arm System

Direction: X_h			Excitation: 2.0 g peak - sine sweep			
Frequency (Hz)	Grip force					
	10 N		25 N		50 N	
	Magnitude (Ns/m)	Phase (degrees)	Magnitude (Ns/m)	Phase (degrees)	Magnitude (Ns/m)	Phase (degrees)
10	28.0	74.5	31.2	62.0	33.5	58.2
12.5	29.4	74.1	32.3	61.5	35.6	57.5
16	31.0	73.0	34.4	60.8	39.5	56.4
20	33.8	71.8	37.5	59.5	44.2	55.0
25	37.5	69.2	42.5	58.5	51.0	53.5
31.5	42.2	65.3	50.5	56.2	63.5	51.5
40	49.5	60.1	60.5	53.4	75.0	49.3
50	58.0	55.0	72.9	50.0	91.2	47.1
63	66.5	50.1	89.5	46.3	110.5	44.4
80	84.5	42.8	108.6	42.7	134.5	42.0
100	101.0	39.1	128.5	40.2	155.0	40.1
125	122.5	37.5	151.8	38.5	180.2	39.1
160	148.5	38.2	179.5	38.2	201.5	39.0
200	170.0	40.3	199.0	38.8	218.0	39.5
250	188.0	41.5	211.5	40.0	223.0	39.9
315	205.4	41.9	220.6	41.6	222.6	40.0
400	284.0	42.2	296.5	43.7	296.0	40.2
500	425.5	42.5	444.0	45.7	455.2	40.5
630	531.5	42.7	548.5	47.2	559.1	40.6
800	642.0	43.0	655.0	49.0	661.5	40.8
1000	775.0	43.3	780.0	50.9	782.1	41.0

TABLE A3
Driving Point Mechanical Impedance of Hand-Arm System

Direction: X_h	Excitation : 3.0 g peak - sine sweep					
Frequency (Hz)	Grip force					
	10 N		25 N		50 N	
	Magnitude (Ns/m)	Phase (degrees)	Magnitude (Ns/m)	Phase (degrees)	Magnitude (Ns/m)	Phase (degrees)
10	33.8	72.8	35.5	70.7	39.6	59.5
12.5	34.5	72.5	36.4	70.1	40.5	58.5
16	36.1	72.0	38.0	69.3	42.5	57.8
20	37.9	70.9	40.4	68.2	45.2	56.8
25	41.1	68.6	44.6	66.2	50.4	55.0
31.5	45.9	64.2	52.3	62.5	60.9	52.4
40	52.5	59.4	62.1	58.1	71.5	49.2
50	61.4	54.3	72.6	53.7	84.9	46.4
63	72.1	47.2	89.1	47.4	104.5	42.5
80	86.5	42.3	106.5	42.6	124.7	39.2
100	100.5	39.1	123.5	38.6	145.4	37.1
125	122.4	38.2	145.5	37.3	166.5	36.1
160	150.6	40.3	169.5	38.5	188.5	36.9
200	177.1	43.4	185.4	41.7	201.0	38.6
250	205.2	45.2	194.2	45.2	203.2	40.2
315	230.4	45.8	209.6	46.5	207.2	40.5
400	309.5	46.2	300.5	46.7	303.5	41.2
500	453.2	46.4	461.1	47.2	464.8	41.5
630	564.2	46.7	584.4	47.4	598.2	41.8
800	675.8	47.3	709.7	47.9	733.7	42.2
1000	810.0	47.6	860.0	48.2	895.0	42.5

TABLE A4
Driving Point Mechanical Impedance of Hand-Arm System

Direction: X_h			Excitation: 0.2 m/s² *rms* - random			
Frequency (Hz)	Grip force					
	10 N		25 N		50 N	
	Magnitude (Ns/m)	Phase (degrees)	Magnitude (Ns/m)	Phase (degrees)	Magnitude (Ns/m)	Phase (degrees)
10	47.8	37.6	62.4	46.7	69.6	54.6
12.5	51.5	37.1	65.6	46.2	72.0	54.1
16	56.5	36.4	70.5	45.6	75.5	53.4
20	61.6	35.4	75.6	44.5	79.7	52.3
25	67.5	34.0	82.4	43.1	86.2	50.5
31.5	74.5	32.1	92.0	41.0	96.5	47.8
40	83.8	30.2	103.6	38.5	109.5	45.0
50	95.1	28.4	118.3	36.5	126.5	42.1
63	112.9	26.7	140.5	34.5	153.4	39.3
80	139.0	26.4	172.1	33.6	188.5	37.0
100	172.4	28.3	212.0	35.0	235.6	37.2
125	210.5	32.5	255.5	38.3	284.3	39.4
160	238.4	39.7	286.2	43.5	318.9	43.1
200	225.5	46.5	270.9	47.9	300.1	47.6
250	154.3	53.6	185.7	51.5	206.6	51.3
315	100.3	57.5	116.5	53.1	125.5	53.4
400	174.5	59.4	175.2	53.6	178.4	54.2
500	308.5	59.9	297.5	54.1	299.5	54.6
630	420.3	60.1	402.4	54.5	402.5	54.8
800	549.8	60.5	520.7	54.8	516.4	55.3
1000	698.0	61.0	660.0	55.4	650.0	55.8

TABLE A5
Driving Point Mechanical Impedance of Hand-Arm System

Direction: X_h	Excitation: 0.5 m/s² *rms* - random					
Frequency (Hz)	Grip force					
	10 N		25 N		50 N	
	Magnitude (Ns/m)	Phase (degrees)	Magnitude (Ns/m)	Phase (degrees)	Magnitude (Ns/m)	Phase (degrees)
10	56.5	34.5	53.2	49.5	65.5	52.2
12.5	58.6	33.7	57.5	48.2	67.4	50.6
16	61.5	32.6	62.5	47.1	70.5	49.4
20	65.6	31.3	69.5	45.1	75.2	47.4
25	69.5	30.3	75.7	43.3	81.5	45.8
31.5	75.6	28.5	85.6	41.0	92.3	43.2
40	84.3	27.2	98.7	39.1	105.6	41.3
50	96.5	26.1	114.5	40.0	124.2	38.9
63	112.7	24.8	135.6	35.4	150.5	37.4
80	136.9	24.4	164.8	34.8	185.0	36.8
100	170.3	25.1	203.4	35.6	227.6	37.9
125	207.5	26.8	240.5	38.2	270.1	40.5
160	228.5	28.9	265.9	41.4	297.5	43.9
200	209.8	30.8	242.1	43.9	272.9	46.7
250	135.1	32.7	155.5	46.8	174.4	49.4
315	87.9	34.9	95.1	49.7	99.2	52.7
400	180.6	37.3	179.8	52.2	175.5	55.2
500	336.5	38.9	340.2	52.1	320.4	55.1
630	460.3	39.9	440.2	51.3	418.5	54.3
800	607.0	41.2	550.5	50.2	556.8	53.0
1000	770.0	42.5	680.0	48.4	705.0	51.2

TABLE A6
Driving Point Mechanical Impedance of Hand-Arm System

Direction: X_h	Excitation: 0.7 m/s² *rms* - random					
Frequency (Hz)	Grip force					
	10 N		25 N		50 N	
	Magnitude (Ns/m)	Phase (degrees)	Magnitude (Ns/m)	Phase (degrees)	Magnitude (Ns/m)	Phase (degrees)
10	37.5	36.3	48.9	46.7	61.2	49.6
12.5	40.5	35.4	52.6	45.4	62.6	49.2
16	45.5	34.3	58.0	43.8	65.1	48.4
20	50.1	33.2	63.6	42.6	69.1	47.5
25	57.1	31.6	71.5	40.0	75.6	46.4
31.5	67.5	30.3	83.4	37.5	86.5	44.6
40	78.2	28.6	96.4	35.6	101.1	42.3
50	91.9	27.9	110.5	34.3	119.5	39.9
63	109.5	27.6	135.3	33.1	138.5	38.5
80	137.5	28.5	165.5	33.2	180.2	37.8
100	168.2	31.7	201.1	35.7	220.4	39.3
125	204.5	36.8	238.5	40.3	260.2	43.1
160	225.2	44.1	263.1	46.8	286.1	48.5
200	208.2	51.3	241.8	52.8	263.5	53.5
250	144.5	57.2	165.3	57.5	178.4	57.0
315	110.8	59.6	121.5	61.4	126.4	62.6
400	230.2	62.5	231.5	64.3	239.4	69.1
500	390.0	66.4	415.0	64.8	439.0	66.5
630	475.0	62.5	530.0	63.2	580.0	60.9
800	587.0	56.3	635.2	59.0	714.0	54.6
1000	725.0	50.0	750.0	53.0	850.0	48.0

TABLE A7
Driving Point Mechanical Impedance of Hand-Arm System

Direction: Y_h			Excitation: 1.0 g peak sine sweep			
Frequency (Hz)	Grip force					
	10 N		25 N		50 N	
	Magnitude (Ns/m)	Phase (degrees)	Magnitude (Ns/m)	Phase (degrees)	Magnitude (Ns/m)	Phase (degrees)
10	17.5	53.8	20.5	55.1	26.2	49.4
12.5	20.7	51.3	23.5	54.2	32.5	48.6
16	24.2	48.1	30.0	51.3	39.6	47.6
20	27.5	45.0	35.1	48.9	46.7	46.2
25	31.1	41.1	40.6	45.7	54.9	44.2
31.5	35.5	35.4	48.5	40.8	66.5	40.9
40	39.2	30.7	55.7	35.5	77.4	37.0
50	42.5	23.5	62.5	30.0	87.5	33.3
63	46.9	15.5	71.4	22.5	101.0	26.1
80	48.7	8.5	77.2	13.6	109.1	17.5
100	48.9	1.5	80.1	5.5	115.3	9.5
125	47.6	-3.5	80.5	-2.7	117.9	1.4
160	44.5	-6.6	75.5	-10.6	114.5	-7.5
200	41.3	-4.2	68.1	-13.7	105.9	-12.5
250	40.3	4.8	60.3	-10.1	95.7	-13.3
315	45.0	18.0	56.3	3.1	85.3	-8.5
400	54.3	19.4	63.8	11.2	83.2	-3.2
500	60.7	16.9	72.5	13.0	84.4	2.3
630	70.5	17.3	84.6	16.5	94.0	10.1
800	97.8	18.5	115.5	19.7	126.0	16.2
1000	148.0	26.0	163.0	27.0	180.0	23.0

TABLE A8
Driving Point Mechanical Impedance of Hand-Arm System

Direction: Y_h	Excitation: 2.0 g peak sine sweep					
Frequency (Hz)	Grip force					
	10 N		25 N		50 N	
	Magnitude (Ns/m)	Phase (degrees)	Magnitude (Ns/m)	Phase (degrees)	Magnitude (Ns/m)	Phase (degrees)
10	20.0	44.1	24.5	41.1	32.8	37.1
12.5	21.8	42.8	26.7	39.8	34.4	35.8
16	24.4	41.0	30.0	38.0	37.1	34.0
20	27.5	39.1	33.7	36.0	40.5	31.8
25	31.6	36.1	39.5	33.1	45.1	28.9
31.5	37.4	32.5	46.0	29.6	51.5	25.3
40	44.8	28.0	54.2	25.0	60.4	20.4
50	51.9	23.7	61.6	20.8	70.1	15.0
63	58.6	18.1	69.3	15.5	83.0	9.7
80	61.9	12.6	74.1	10.4	101.2	4.3
100	63.0	7.8	75.6	5.8	113.8	-0.7
125	63.0	4.0	75.2	2.2	115.6	-4.7
160	62.0	0.2	72.7	-1.0	109.3	-8.0
200	60.1	-1.0	68.5	-2.1	98.1	-9.1
250	57.8	1.2	63.0	0.3	84.0	-7.0
315	57.0	7.3	61.5	6.6	73.1	-0.8
400	59.5	13.7	67.3	13.3	71.8	6.6
500	65.6	16.8	77.2	17.5	81.2	14.0
630	78.0	17.4	92.5	18.8	100.6	18.3
800	103.5	19.5	115.5	17.4	134.4	18.2
1000	132.0	24.0	140.0	15.0	175.0	16.0

TABLE A9
Driving Point Mechanical Impedance of Hand-Arm System

Direction: Y_h	Excitation : 3.0 g peak sine sweep					
Frequency (Hz)	Grip force					
	10 N		25 N		50 N	
	Magnitude (Ns/m)	Phase (degrees)	Magnitude (Ns/m)	Phase (degrees)	Magnitude (Ns/m)	Phase (degrees)
10	25.5	36.3	41.4	25.4	63.5	60.5
12.5	27.5	35.5	43.6	25.7	66.6	58.5
16	29.4	34.2	45.9	25.5	69.9	55.4
20	31.0	32.4	47.1	25.2	71.4	54.2
25	32.7	30.5	50.5	23.7	76.7	49.5
31.5	34.6	27.1	53.9	22.0	82.1	44.2
40	37.1	23.1	58.0	19.6	88.1	38.4
50	39.4	18.9	61.9	16.8	93.9	32.2
63	41.3	13.5	66.1	12.6	99.7	23.6
80	42.1	7.6	69.1	7.4	104.5	15.3
100	41.8	0.7	70.6	1.0	108.3	6.5
125	40.9	-2.5	70.9	-5.4	109.4	-1.0
160	38.8	-4.1	66.5	-10.7	105.4	-8.3
200	36.9	1.0	58.5	-12.1	95.5	-12.0
250	39.4	11.0	52.8	-5.8	87.6	-10.5
315	46.9	21.1	53.2	8.5	82.5	-4.0
400	56.4	19.7	63.0	16.8	80.4	3.0
500	61.6	16.0	72.3	16.7	83.9	8.4
630	70.7	18.1	85.1	18.0	98.8	16.3
800	96.8	20.8	115.7	22.3	136.6	22.5
1000	135.0	32.0	160.0	33.3	185.0	31.5

TABLE A10
Driving Point Mechanical Impedance of Hand-Arm System

Direction: Y_h	Excitation: 0.2 m/s² *rms* - random					
Frequency (Hz)	Grip force					
	10 N		25 N		50 N	
	Magnitude (Ns/m)	Phase (degrees)	Magnitude (Ns/m)	Phase (degrees)	Magnitude (Ns/m)	Phase (degrees)
10	76.3	24.5	92.3	37.8	101.2	49.6
12.5	74.9	20.2	93.8	33.7	106.0	46.1
16	73.1	15.5	95.4	29.2	110.6	42.2
20	70.3	10.1	95.6	24.7	114.7	38.4
25	68.2	6.0	95.4	19.3	118.8	32.1
31.5	64.1	0.6	93.2	12.2	121.0	25.3
40	59.4	-4.1	90.6	7.5	121.9	18.1
50	54.2	-7.8	86.5	2.2	121.2	10.4
63	48.2	-10.6	80.4	-3.5	117.2	3.3
80	43.1	-9.7	73.5	-7.0	109.5	-3.4
100	38.1	-7.3	66.8	-8.9	100.2	-8.1
125	34.6	-2.8	59.7	-9.5	92.4	-10.5
160	31.5	2.2	52.6	-7.7	84.1	-12.7
200	30.4	7.5	46.4	-1.3	74.8	-12.1
250	31.6	18.9	41.7	13.0	61.3	-2.4
315	35.2	36.1	42.1	30.4	52.2	10.8
400	41.3	53.1	50.6	45.4	49.4	27.2
500	54.2	64.5	62.1	61.5	58.6	51.0
630	77.8	65.5	87.6	66.4	87.7	62.9
800	102.5	64.4	125.1	66.4	130.4	66.5
1000	135.0	68.5	158.0	71.7	168.0	70.1

TABLE A11
Driving Point Mechanical Impedance of Hand-Arm System

Direction: Y_h	Excitation: 0.5 m/s² *rms* - random					
Frequency (Hz)	Grip force					
	10 N		25 N		50 N	
	Magnitude (Ns/m)	Phase (degrees)	Magnitude (Ns/m)	Phase (degrees)	Magnitude (Ns/m)	Phase (degrees)
10	58.8	17.8	77.0	28.4	78.0	45.0
12.5	57.4	17.6	76.4	24.9	81.4	42.1
16	55.4	16.9	75.4	20.0	86.0	38.0
20	53.7	16.0	74.4	16.2	89.1	34.5
25	51.8	14.6	73.0	12.0	92.1	30.4
31.5	48.5	12.3	70.6	6.5	95.3	24.3
40	45.3	9.1	67.7	1.0	98.0	17.9
50	41.1	5.3	63.7	-5.0	99.5	10.0
63	37.6	2.1	59.6	-9.4	98.2	3.0
80	34.2	-0.5	55.1	-12.4	92.6	-4.3
100	31.5	-2.0	49.5	-14.0	85.2	-9.5
125	29.5	-1.3	45.1	-13.6	78.8	-12.7
160	27.2	3.4	38.5	-10.3	70.0	-14.6
200	27.0	10.4	34.2	-3.5	62.9	-14.2
250	29.3	21.8	32.8	9.0	52.1	-11.3
315	34.5	34.1	35.5	28.5	43.4	-0.4
400	42.8	49.5	42.7	54.6	45.5	36.8
500	53.3	62.1	61.1	68.2	62.8	62.4
630	74.8	61.5	99.5	69.3	99.1	68.3
800	101.5	52.3	136.9	60.0	143.2	61.3
1000	126.0	57.6	164.0	64.7	175.4	66.7

TABLE A12
Driving Point Mechanical Impedance of Hand-Arm System

Direction: Y_h	Excitation: 0.7 m/s² *rms* - random					
Frequency (Hz)	Grip force					
	10 N		25 N		50 N	
	Magnitude (Ns/m)	Phase (degrees)	Magnitude (Ns/m)	Phase (degrees)	Magnitude (Ns/m)	Phase (degrees)
10	49.3	25.5	75.9	27.6	83.8	41.4
12.5	48.2	24.6	75.4	23.8	86.6	38.3
16	46.8	23.2	74.6	18.9	89.5	34.5
20	45.2	21.5	73.5	14.5	92.2	29.9
25	43.6	19.4	72.2	10.1	94.1	25.5
31.5	41.2	16.3	70.1	4.8	95.4	19.4
40	38.4	12.4	67.2	-1.9	96.1	12.7
50	35.2	7.8	63.4	-8.3	95.2	4.9
63	32.5	4.1	59.4	-13.0	92.3	-1.5
80	30.7	1.5	55.7	-15.4	87.5	-6.4
100	28.7	-0.1	49.4	-16.1	77.8	-11.4
125	28.3	0.5	45.1	-14.3	69.2	-13.5
160	27.7	4.0	39.7	-10.8	62.6	-13.7
200	25.8	7.6	36.0	-5.4	55.4	-13.3
250	24.9	14.1	31.9	3.2	46.7	-10.5
315	24.9	26.5	28.6	19.6	39.1	-1.5
400	30.8	50.1	34.2	51.5	38.8	36.5
500	47.7	60.1	55.7	66.1	61.4	64.1
630	71.4	57.7	91.9	68.7	97.7	65.6
800	94.5	46.9	131.5	57.8	144.6	57.8
1000	115.0	47.8	157.0	62.6	168.8	62.4

TABLE A13
Driving Point Mechanical Impedance of Hand-Arm System

Direction: Z_h	Excitation: 1.0 g peak sine sweep					
Frequency (Hz)	Grip force					
	10 N		25 N		50 N	
	Magnitude (Ns/m)	Phase (degrees)	Magnitude (Ns/m)	Phase (degrees)	Magnitude (Ns/m)	Phase (degrees)
10	195.0	68.5	242.0	58.5	277.0	57.5
12.5	198.7	68.3	243.7	58.1	279.5	57.3
16	201.3	67.5	246.0	57.7	282.0	56.7
20	204.5	66.8	249.2	57.2	284.6	56.1
25	208.7	65.8	253.4	56.5	287.2	55.2
31.5	214.5	64.5	259.0	55.8	289.5	54.2
40	222.1	63.0	265.8	55.0	291.3	52.8
50	231.5	61.1	275.3	54.2	293.4	51.4
63	245.5	59.0	288.7	53.1	296.2	49.2
80	260.1	56.6	304.4	51.8	302.7	47.8
100	280.0	54.2	330.1	50.0	316.3	46.0
125	301.2	52.2	358.4	48.1	330.5	45.1
160	318.5	50.0	383.7	45.1	350.8	42.8
200	314.4	44.7	383.3	39.3	350.2	38.1
250	280.2	42.4	360.6	36.9	334.9	36.5
315	249.5	45.1	311.9	40.5	293.5	40.8
400	210.6	54.2	240.5	51.1	218.9	51.1
500	148.0	58.9	166.9	56.6	139.8	53.3
630	190.3	60.0	254.1	59.3	255.9	57.7
800	470.0	62.5	515.0	61.4	555.8	59.7
1000	890.0	64.5	875.0	65.0	960.0	60.0

TABLE A14
Driving Point Mechanical Impedance of Hand-Arm System

Direction: Z_h	Excitation: 2.0 g peak sine sweep					
Frequency (Hz)	Grip force					
	10 N		25 N		50 N	
	Magnitude (Ns/m)	Phase (degrees)	Magnitude (Ns/m)	Phase (degrees)	Magnitude (Ns/m)	Phase (degrees)
10	130.0	68.5	155.0	65.5	179.0	61.0
12.5	136.1	68.2	159.1	64.5	182.5	60.1
16	140.4	67.7	161.8	63.5	187.5	59.0
20	145.1	67.0	165.2	62.1	193.7	57.8
25	150.5	66.0	169.6	60.7	200.6	56.5
31.5	156.7	64.8	175.0	59.2	208.7	55.2
40	163.5	65.2	181.5	57.8	217.9	53.2
50	172.0	61.4	189.4	56.3	228.1	52.7
63	183.2	59.0	203.5	53.8	244.5	50.6
80	198.8	56.7	218.8	51.9	258.7	48.8
100	220.5	54.2	245.5	48.3	280.5	45.5
125	250.4	52.1	273.8	44.1	301.7	41.6
160	275.6	49.6	305.6	38.5	320.2	37.2
200	282.5	46.1	310.5	35.2	515.5	35.1
250	260.3	42.2	286.1	32.2	278.7	35.7
315	235.7	45.1	259.0	35.5	249.3	41.3
400	201.4	54.4	221.4	43.7	213.6	52.4
500	146.7	62.0	160.5	50.4	148.5	63.2
630	163.2	64.5	180.2	54.7	193.3	62.9
800	287.7	58.0	314.9	51.7	449.2	58.8
1000	570.0	60.0	626.0	63.7	778.0	66.4

TABLE A15
Driving Point Mechanical Impedance of Hand-Arm System

Direction: Z_h	Excitation: 3.0 g peak sine sweep					
Frequency (Hz)	Grip force					
	10 N		25 N		50 N	
	Magnitude (Ns/m)	Phase (degrees)	Magnitude (Ns/m)	Phase (degrees)	Magnitude (Ns/m)	Phase (degrees)
10	50.1	30.0	75.1	20.2	81.7	11.3
12.5	52.0	30.6	77.2	20.3	83.1	12.3
16	53.4	30.9	79.9	20.5	85.3	13.7
20	55.7	31.3	83.7	20.6	86.8	14.4
25	59.1	31.7	88.9	21.1	94.3	16.8
31.5	64.1	32.0	95.7	21.5	102.3	18.4
40	70.9	32.2	104.4	22.1	113.1	19.8
50	79.7	32.3	115.1	22.8	126.7	21.2
63	95.0	32.5	132.3	23.6	145.6	22.7
80	115.1	32.6	154.4	24.6	172.9	24.0
100	142.3	32.7	188.7	25.8	208.8	25.2
125	186.5	33.1	228.5	27.0	248.2	26.1
160	230.6	33.7	270.4	28.9	295.5	26.8
200	271.7	35.2	302.7	32.1	325.4	26.8
250	295.1	37.4	312.3	36.1	342.1	26.7
315	310.1	43.0	317.9	43.2	352.6	28.7
400	314.5	50.9	321.1	51.8	356.4	36.6
500	323.3	56.0	329.9	57.4	366.2	47.4
630	387.6	59.2	401.1	59.5	445.2	55.7
800	470.0	61.6	494.0	62.5	548.3	59.5
1000	734.0	59.0	770.0	65.3	852.0	62.9

TABLE A16
Driving Point Mechanical Impedance of Hand-Arm System

Direction: Z_h	Excitation: 0.2 m/s² *rms* - random					
Frequency (Hz)	Grip force					
	10 N		25 N		50 N	
	Magnitude (Ns/m)	Phase (degrees)	Magnitude (Ns/m)	Phase (degrees)	Magnitude (Ns/m)	Phase (degrees)
10	75.0	23.1	115.0	24.5	128.1	22.4
12.5	78.9	23.8	118.7	24.9	130.9	22.7
16	81.4	24.3	121.0	25.5	134.2	23.1
20	84.9	25.0	124.2	26.3	138.8	23.8
25	89.8	25.9	128.5	27.4	144.7	24.6
31.5	96.5	27.0	134.1	28.6	151.9	25.7
40	105.1	28.4	141.1	30.2	160.6	27.1
50	116.2	30.0	150.2	32.0	171.3	28.7
63	130.3	31.5	165.5	34.5	188.6	30.9
80	155.4	34.9	185.5	37.2	211.6	33.5
100	190.0	38.0	218.0	40.6	249.0	36.5
125	230.2	41.3	260.3	44.2	292.2	39.7
160	275.5	46.8	304.1	49.2	337.4	43.7
200	292.7	51.5	316.0	52.8	349.5	47.1
250	281.5	57.4	295.5	59.9	322.2	53.1
315	259.3	59.7	265.8	63.4	287.1	56.6
400	256.2	62.0	260.0	68.1	280.0	62.0
500	316.5	69.4	320.6	76.6	355.0	69.0
630	428.9	73.9	423.6	80.2	493.4	68.4
800	537.1	73.4	538.3	78.3	626.5	70.4
1000	620.0	76.8	640.7	80.9	740.0	73.8

TABLE A17
Driving Point Mechanical Impedance of Hand-Arm System

Direction: Z_h	Excitation: 0.5 m/s² *rms* - random					
Frequency (Hz)	Grip force					
	10 N		25 N		50 N	
	Magnitude (Ns/m)	Phase (degrees)	Magnitude (Ns/m)	Phase (degrees)	Magnitude (Ns/m)	Phase (degrees)
10	100.2	33.5	110.3	12.6	120.5	16.7
12.5	104.5	33.2	112.7	13.2	124.1	17.3
16	107.6	32.8	113.4	14.0	126.8	18.2
20	112.1	32.3	114.7	15.1	130.7	19.4
25	117.7	31.7	117.1	16.4	136.2	21.1
31.5	125.1	31.1	120.9	18.3	143.6	23.3
40	134.7	30.5	126.4	20.5	153.2	26.1
50	146.7	29.9	133.7	23.2	165.1	29.4
63	165.2	29.2	150.2	27.2	187.7	34.7
80	185.2	29.4	157.4	28.9	196.6	36.4
100	215.6	30.4	197.4	34.3	240.1	42.5
125	250.1	32.3	234.7	38.0	276.9	46.1
160	286.1	36.3	273.6	42.9	314.1	50.6
200	285.6	40.9	279.2	48.2	320.0	55.1
250	247.7	46.8	249.7	54.3	294.7	60.3
315	200.3	50.2	205.8	56.9	262.2	64.0
400	173.8	57.4	177.0	63.4	256.1	69.4
500	217.4	72.2	218.6	78.9	318.8	78.2
630	291.6	69.8	290.4	76.3	424.7	79.3
800	425.2	66.1	419.0	77.3	560.8	80.1
1000	625.0	69.4	646.5	78.4	698.0	82.7

TABLE A18
Driving Point Mechanical Impedance of Hand-Arm System

Direction: Z_h			Excitation: 0.7 m/s² *rms* - random			
Frequency (Hz)	Grip force					
	10 N		25 N		50 N	
	Magnitude (Ns/m)	Phase (degrees)	Magnitude (Ns/m)	Phase (degrees)	Magnitude (Ns/m)	Phase (degrees)
10	68.4	27.7	109.1	20.4	132.6	34.8
12.5	68.7	27.4	110.6	20.7	135.4	34.5
16	71.3	27.1	113.6	21.2	138.6	34.1
20	73.5	26.7	117.0	21.8	143.1	33.6
25	76.8	26.2	121.8	22.7	149.5	33.0
31.5	81.7	25.6	128.6	23.7	158.2	32.1
40	83.3	24.8	137.4	25.1	169.3	31.1
50	97.7	24.1	148.4	26.7	183.4	30.0
63	114.1	23.4	169.2	29.4	211.4	28.7
80	129.7	23.5	186.3	31.3	235.7	28.3
100	156.6	25.1	215.9	34.2	282.4	29.2
125	190.1	28.1	247.5	37.2	335.2	31.3
160	229.2	33.5	279.3	41.3	390.7	35.1
200	241.5	39.1	283.4	45.1	402.8	38.1
250	231.6	47.5	255.7	50.4	367.6	41.1
315	203.6	56.1	216.4	54.0	311.5	45.0
400	187.5	69.3	193.5	55.7	277.1	53.1
500	230.5	80.4	238.4	56.3	332.7	60.4
630	303.7	65.6	307.0	57.1	451.1	49.1
800	456.3	73.9	475.8	58.1	690.8	55.4
1000	595.0	82.8	720.0	58.5	910.0	65.3

TABLE A19
Mean Values of Driving Point Mechanical Impedance of Hand-Arm System

Grip force: 25 N					Excitation: Sine sweep	
Frequency (Hz)	Direction					
	X_h		Y_h		Z_h	
	Magnitude (Ns/m)	Phase (degrees)	Magnitude (Ns/m)	Phase (degrees)	Magnitude (Ns/m)	Phase (degrees)
10	34.6	61.4	28.8	40.5	157.4	48.1
12.5	35.7	60.9	31.3	39.9	160.0	47.6
16	37.8	60.2	35.3	38.3	162.6	47.2
20	40.7	59.4	38.6	36.7	166.0	46.6
25	45.5	57.7	43.5	34.2	170.6	46.1
31.5	53.4	55.3	49.5	30.8	176.6	45.5
40	63.9	52.1	56.0	26.7	183.9	45.0
50	75.7	48.9	62.0	22.5	193.3	44.4
63	92.7	44.6	68.9	16.9	208.2	43.5
80	111.7	41.3	73.5	10.5	225.9	42.8
100	133.2	38.7	75.4	4.1	254.7	41.4
125	157.4	37.7	75.5	-2.0	286.9	39.7
160	188.0	38.9	71.6	-7.4	319.9	37.5
200	202.3	40.5	64.1	-9.3	332.2	35.5
250	209.3	42.6	58.7	-5.2	319.7	35.1
315	215.7	43.7	57.0	6.1	296.3	39.7
400	290.7	44.6	64.7	13.8	261.0	48.9
500	433.2	45.6	74.0	15.7	219.1	54.8
630	541.0	46.3	87.4	17.8	278.5	57.8
800	656.6	47.2	115.6	19.8	441.3	58.5
1000	791.7	48.1	154.3	25.1	757.0	64.7